ADSORPTION AND PHOTOCATALYTIC ACTIVITY OF GRAPHENE-BASED NANOMATERIALS

Bayisa Meka Chufa

A Dissertation Submitted to the Department of Applied Chemistry, School of Applied Natural Science

Presented in Fulfillment of the Requirement for the Degree of Doctor of Philosophy in Applied Chemistry (Materials Chemistry)

Office of Graduate Studies
Adama Science and Technology University

April, 2022
Adama, Ethiopia

ADSORPTION AND PHOTOCATALYTIC ACTIVITY OF GRAPHENE-BASED NANOMATERIALS

By Bayisa Meka Chufa

Supervisors

Prof. Teketel Yohannes

Dr. Bedasa Abdisa

A dissertation Submitted to Department of Applied Chemistry, School of Applied Natural Science

Presented in Fulfillment of the Requirement for the Degree of Doctor of Philosophy in Applied Chemistry (Materials Chemistry)

Office of Graduate Studies

Adama Science and Technology University

April, 2022

Adama, Ethiopia

Declaration and Recommendation

Declaration

I hereby declare that this Dissertation entitled Adsorption and photocatalytic activity of graphene-based nanomaterials" is my original work. That is, it has not been submitted for the award of any academic degree, diploma, or certificate in any other university. All sources of materials used for this thesis have been duly acknowledged through appropriate citations.

Bayisa Meka Chufa	_____	10/04/2022
Name of Student	Signature	Date

Recommendation

I/we, the supervisor(s) of this dissertation, hereby certify that I/we have read and revised the dissertation entitled "Adsorption and photocatalytic activity of graphene-based nanomaterials" prepared under my/our guidance by Bayisa Meka Chufa submitted in partial fulfillment of the requirements for the degree of Doctor of Philosophy in Materials Chemistry. Therefore, I/we recommend the submission of the final draft of the dissertation to the department for final defense.

Teketel Yohannes Anshebo	_____	10/04/2022
Major Supervisor	Signature	Date
Bedasa Abdisa Gonfa	_____	10/04/2022
Co-supervisor	Signature	Date

Approval Page of Ph.D. Dissertation

I/we hereby certify that the recommendations and suggestions made by the board of examiners are appropriately incorporated into the final version of the dissertation entitled "Adsorption and photocatalytic activity of graphene-based nanomaterials" by Bayisa Meka Chufa.

Teketel Yohannes Anshebo _____ _____

Major Supervisor Signature Date

Bedasa Abdisa Gonfa _____ _____

Co-supervisor Signature Date

We, the undersigned, members of the Board of Examiners of the dissertation open defense by Bayisa Meka Chufa have read and evaluated the dissertation entitled "Nanoadsorption and photocatalytic activity of graphene-based nanomaterials" and examined the candidate during open defense. This is, therefore, to certify that the dissertation is accepted for partial fulfillment of the requirement of the degree of Doctor of Philosophy in Materials Chemistry.

Chairperson	Signature	Date
Internal Examiner	Signature	Date
External Examiner 1	Signature	Date
External Examiner 2	Signature	Date

Finally, approval and acceptance of the dissertation is contingent upon submission of its final copy to the Office of Postgraduate Studies (OPGS) through the candidate's Department Graduate Council (DGC) and School Graduate Committee (SGC).

Department Head	Signature	Date
School Dean	Signature	Date
Office of Postgraduate Studies,	Dean Signature	Date

Acknowledgments

First of all, I would like to acknowledge my Advisors Prof. Teketel Yohannes and Dr. Bedasa Abdisa for their valuable and constructive comment, ideas and tireless follow-up and guidance throughout the entire work. I particularly appreciate Prof. Guttena Veerabhadram, my previous advisor, for his encouragement and support by providing quality flake graphite for free which I can`t afford otherwise. Without the support of prof. Veerabhadram, the realization of this work was questionable. He has also provided me with basic guidelines to follow on the dissertation work. From the very beginning to this moment, he has continuously guided me moving forward. Prof. Veerabhadram has given me intellectual and emotional support throughout this journey.

I also would like to thank Chemistry Department head Dr. Fedlu Kedir and later Dr. Aschalew Taddese for their support and motivation toward the realization of this work. I would also like to thank the department secretary, Mrs Abonesh Agdew for her unreserved support from the start to the end. All Chemistry department members are appreciated for their support in one or another way towards the accomplishment of the dissertation work.

I would like to send my appreciation to Adama Science and Technology University for the opportunity provide to me to do my PhD degree and provision of the lab space to execute the research work.

Lastly I would like to thank Bizunesh Kefyalew, Iticha Abdisa, Guta Amenu, Demeke Tesfaye and Bontu Gudeta for their unreserved support and unlimited generosity during the course of my laboratory work.

Contents

List of Figures

List of Tables

List of Acronyms and Abbreviations

Ab/Ac	Full Name	Ab/Ac	Full Name
2D	Two dimensional	GBNs	Graphene based nanomaterials
TPa	Terra Pascal	SDBS	Sodium dodecyl benzene sulphonate
GPa	Giga Pascal	GIC	Graphite intercalation compounds
SSA	Specific surface area	HOPG	Highly oriented pyrolytic graphite
G	Graphene	DGU	Density gradient ultracentrifugation
GO	Graphene oxide	GICs	Graphite intercalation compounds
rGO	Reduced graphene oxide	DMF	Dimethylformamide
MS	Metal sulfide	TBA	Tetrabutylammonium
SA	Surface area	CVD	Chemical vapor deposition
GBNs	Graphene based nanomaterials	PECVD	Plasma enhanced chemical vapor deposition
MS	Metal sulfide	UHV	Ultrahigh vacuum
NM	Nanomaterial	FLG	Few-layer graphene
VA	Vernonia Amygdalina	ATRP	Atom transfer radical polymerization
CNTs	Carbon nanotubes	PAHs	Planar polycyclic aromatic hydrocarbons
TBA	Tetra butyl ammonium	PECVD	plasma enhanced chemical vapour deposition
GFET	Graphene effect transistor	GPN	Graphene based plasmonic nanomaterials
FET	Field effect transistor	LED	Light emitting diodes
FRET	Fluorescence resonance energy transfer	FTO	Fluorine doped tin oxide
ITO	Indium doped tin oxide	TEA	Triethanolamine
COD	Chemical oxygen demand	TBA	Tetrabutylammonium
TAA	Thioacetamide	DXR	Doxorubicin hydrochloride
EPA	Environmental protection agency	PECVD	Plasma enhanced chemical vapour deposition

Abstract

The world population is growing at an alarming rate and this has resulted in the intensification of industrial activities causing contamination of air, soil and aquatic ecosystems. The demand for pure drinking water is growing with population and people still have insufficient access to it. In most African rural communities, ground water is the primary source for drinking purpose. However, if beyond permissible level, F^- is a toxicant chemical in ground water sources with tremendous health disorder. Thus, this work presents green a synthesis method of graphene based nanomaterials, characterizations of the synthesized nanomaterials, and its application in nano-adsorption of F^- and photocatalysis of methylene blue (MB) for environmental protection. The synthesized products were characterized by GC-MS, UV-Vis, XRD, FT-IR, DTA, TGA, HR-TEM and EDAX. Solvent extraction method was used to obtain the phytochemical compounds from Vernonia Amygdalina (VA) plant leaves. The UV-Vis analysis of VA leaf extract revealed different peaks in water, methanol and ethanol extracts. The GC-MS records displayed a number of complex compounds of which six of them were common to all solvents five of them were common to two solvents and the rest were unique to their corresponding extracting solvents. UV-Vis records of reduced graphene oxide (rGO) revealed major peaks at 262, 252, 297 nm and XRD records showed different peaks at $2\Theta = 24^0$, 21.3^0, 19.8^0 in methanol, ethanol and water extracts respectively. Methanol extraction of VA was the preferred method for the large scale production of graphene based materials. The fast, non-explosive two step method in the absence of ice bath were used to obtain graphene oxide (GO). rGO-Bi_2S_3 was synthesized using a single step refluxed method for the degradation of methylene blue (MB). The comparative degradability degree of the dye under visible light irradiation with and without catalyst was studied. The performance tests showed 99% degradation of MB with and 7% without catalyst under the same condition within 25 minutes. The durability and reusability tests for the catalyst were also studied for five cycles. The maximum loss of capacity of the catalyst within 25 minutes was 0.5%. Hence, rGO-Bi_2S_3 was found to be the ideal material for the degradation of MB. The adsorption of F^- from ground water by GO under specific conditions such as: agitation rate of 120 rpm, contact time of 90 minutes, adsorbent dosage of 0.42 mg/L, initial F^- concentration of 10 mg/L and pH of 6.8 was investigated. The results obtained showed 99.3% F^- removal from NaF prepared solution and 91.6% fluoride removal from real sample. The retained properties of GO after adsorption observed by UV-Vis analysis confirmed the recyclability of the adsorbent. The results obtained also showed that the adsorption kinetics with the coefficient of determination (R^2) for pseudo- first-order (SFO) and pseudo-second-order (SSO) were 0.96 and 0.99 respectively. Based on these results, the adsorption of F^- onto GO is a pseudo-second-order kinetics type. Furthermore, according to the adsorption isotherm study, Freundlich isotherm model showed a good fit to the experiments with R^2 (0.99). The adsorption capacity of the adsorbent was found to be 301.43 mg/g. Hence, this study showed that GO is the preferred and effective adsorbent material for the removal of F^- from ground water.

Keywords: *Adsorption; Photocatalysis; Fluoridated Ground water; Graphene based nanomaterials; Methylene blue;*

Chapter One

1. Background

1.1 Introduction

The 21st century has been termed as the century of the environment (Perreault, Fonseca De Faria, et al., 2015). The world population is growing at an alarming rate and this has resulted in the intensification of agriculture and industrial activities which in turn have resulted in the contamination of air, soils and aquatic ecosystems and that brought about global climate change. Consequently, this world is under stress with the worst extremes of human activities but still is striving to defend itself through its natural web-net process. However, the scholars predicted that the battle field would most probably be finalized at some point with the limited and nonrenewable resources routed by the unlimited and ever perpetuating act of human beings. Hence environmental issues are becoming a major focus of political and scientific attention. For instance, Ethiopia has embarked on a transformational journey of becoming a low middle-income carbon neutral economy by 2025. This is to be achieved by shifting economic activities from agriculture-led to industrial-led sectors and the pursuit for industrialization is the most feasible option for ensuring the intended structural transformation. This, on the other hand has resulted in the large emission of industrial byproducts pollutants to the environment. On the first hand, this motivated us to focus on the concrete current issue, the environmental pollution, which will also be, sustained in the future in the world if not given due attention (Suggs & Neic, 2010).

Pollutants such as organic and inorganic compounds in soil, air and water produced by human activities, backfired and severely hurting and further threatening ecological balance and human health. In addition to the huge environmental pollutant discharge from the developed countries, many developing countries are transforming their economy from less or none polluting traditional agricultural activities to more polluting modern agricultural activities and/or industrialization. Mining and leather industries are the sources of heavy metal pollutants. Textile industries are also the main sources of organic pollutants and dyes (Carmen & Daniela, 2016). Therefore, the modernization of agriculture without pollutant mitigation strategy and intensification of industries without pollutant discharge monitoring strategies are the deadly threating acts of human being to the environment. Hence this work is intended to alleviate the pollution problem using adsorption and photocatalysis.

Recently, many effective photocatalysts (Azeez et al., 2018; Yildirim & Ozturk, 2018) and nano-adsorbents (Kariuki et al., 2015; Zhang & De, 2011) materials based on their size, especially of carbonaceous materials have been designed due to their high efficiency and ease of fabrication. Here we proposed a novel experimental ways of studying the mechanism by which adsorbates are continuously adsorbed without saturation of the active surface and stabilization of e^--h pair of the semiconductor by graphene based scaffolds. Hence the core point of this dissertation work is the preparation of graphene based nanomaterials; study its application in nano-adsorption and photocatalysis.

There are three predominant allotropes of carbon material: diamond, graphite, fullerene, and amorphous carbon called carbon black (Shabalin, 2014). The degree of crystallinity and the types of hybridization of carbon atoms in their structure is used to categorize these allotropes under anyone of the above classes. Carbon atoms in diamond are all sp^3 hybridized and arranged in cubic structure which comprises of two interpenetrating face-centered cubic (fcc) lattices (Vajtai, 2013). Graphite is a naturally occurring form of crystalline carbon composed of stacked sheets of carbon atoms called graphene. Unlike diamond, graphite exists in a hexagonal crystal structure. Graphite occurs naturally in the earth's crust when carbon is subjected to pressure and temperature around 750 ^{0}C to compress into graphite (Zhang et al., 2018). It is extremely soft and breaks into thin flexible flakes that easily slide over one another, resulting in a greasy feel. It has low specific gravity but has high electrical and thermal conductivity. It is extremely resistant to heat and nearly inert in contact with almost any other material; making it highly resistant to corrosion (Diego, 2015). Graphite are primarily (80-85% of total demand) used as a conductive electrode used to refine iron in an electric arc furnace or alumina in an aluminum smelter. Other markets include the battery anode sector and brake linings which both compete with natural graphite for market share (Bafekrpour et al., 2012). Generally, graphite is available in its two broad categories; synthetic and natural graphite (Trammell & Pappano, 2011).

Synthetic graphite is a manmade substance manufactured by the high temperature processing of amorphous carbon materials. The types of amorphous carbon used as precursors to give graphite are many, and can be derived from petroleum, coal, or natural and synthetic organic materials. In some cases, graphite can even be manufactured by the direct precipitation of graphitic carbon from pyrolysis of a carbonaceous gas such as acetylene (pyrolytic graphite). One important commonality between all graphite

precursors is that they must contain carbon. It is a specific form of carbon, so it can only be derived from other carbon containing substances (März et al., 2018a). Only certain types of carbonaceous feeds are suitable for the production of synthetic graphite to ensure a high quality graphitic carbon. The dry raw materials are mixed and moulded into desired shapes and baked or carbonised at 800 – 1300 ^{0}C over several weeks and then further processed at temperatures of 2,600-3,000 ^{0}C for graphitisation.

The main types of natural graphite are flake, amorphous and vein (Simandl et al., 2015); so that the source of our graphene and its derivatives for this dissertation work is microcrystalline graphite. Microcrystalline graphite (commercially called amorphous) occurs in metamorphic anthracite coal beds or in carbonaceous sedimentary rocks in form of extremely fine crystalline grains. Suppliers of microcrystalline (”amorphous”) graphite are China, Mexico, Korea, and Zimbabwe. Vein graphite (crystalline lump graphite) occurs as filling fissure (cracks in rocks) in veins in metamorphic or igneous (formed from molten magma or lava) rocks. Vein graphite may have various forms and dimensions from fine powder to lumps of 10 cm size. Vein graphite structure has high crystallinity, which provides excellent electrical conductivity of the material. Current supplier of vein graphite is Sri Lanka (Magampa et al., 2013).

Flake graphite occurs as isolated, flat, plate like particles with hexagonal edges with a distinctive flake formation. Flake graphite is formed at convergent plate boundaries when organic rich shales and limestones are subjected to the heat and pressure of regional metamorphism. This produces marble, schist, and gneiss that contain tiny crystals and flakes of graphite. These rocks are mined, crushed to a particle size that liberates the graphite flakes, and processed by specific gravity separation or froth flotation to remove the low-density graphite. This mineral is abundant in the southern Oromia, Guji and Borena zone of Ethiopia. Flake graphite is subdivided into coarse (large and medium) and fine sizes with flake graphite purity varies from 85-95% fixed carbon content after processing. Natural flake has the widest range of use and accounts for about 49% of natural graphite consumption. The primary use includes brake linings, batteries and fuel cells. According to literatures; China, Mozambique and Brazil are the largest producers of flake graphite (Desai & Njuguna, 2012).

The crystalline structure of graphite consists of hexagonal rings forming thin parallel plates (graphene). Each carbon atom is covalently bonded to three other atoms in the plate

where the angle between two bonds is 120°. The outermost electron shell of a carbon atom has four valence electrons, three of which are used by the covalent bonds. The fourth valence electron does not take part in covalent bonds and may be easily displaced from the electron shell by an electric field. These electrons provide electrical conductivity of graphite (Pietronero, 1980).

The graphene layers are bonded to each other in graphite structure by weak Van der Waals forces as shown in Figure 1. The layered structure of graphite allows sliding movement of the parallel graphene plates. Weak bonding between the plates determines softness and self-lubricating properties of graphite.

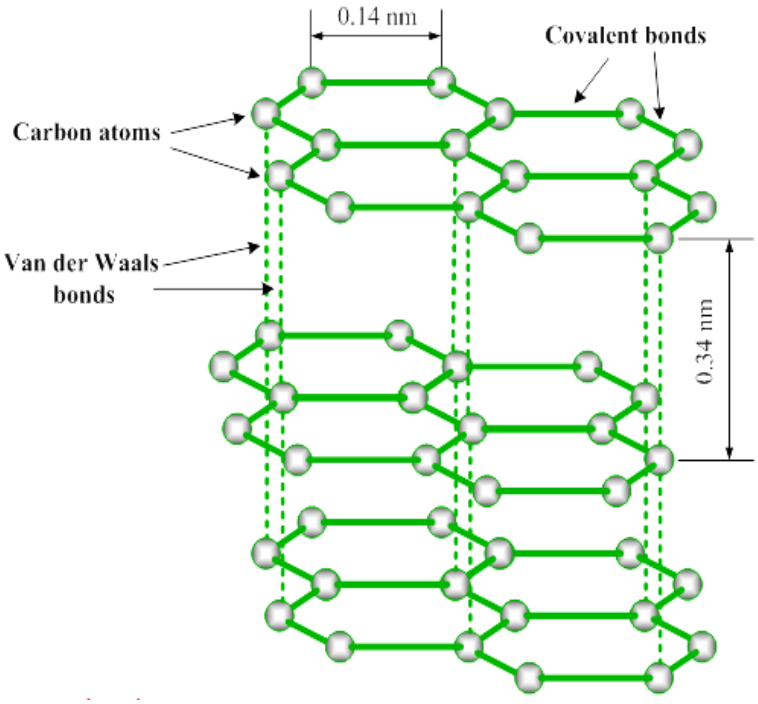

Figure 1: Structure of graphite (Simandl et al., 2015).

Graphene is a single layer of atoms in graphite with a two-dimensional hexagonal lattice in which one atom forms each vertex. It is the basic structural element of other allotropes, including graphite, charcoal, carbon nanotubes and fullerenes. It can also be considered as an indefinitely large aromatic molecule, the ultimate case of the family of flat polycyclic aromatic hydrocarbons (Mikhailov & Pietronero, Strassler, 2012). It has special properties which set it apart from other allotropes of carbon. In proportion to its thickness, it is about 100 times stronger than the strongest steel. Yet its density is dramatically lower than any steel, with a surface mass of 0.763 mg per square meter. It conducts heat and electricity very efficiently and is nearly transparent (Kumar et al., 2013). A single graphene sheet is

a planar monolayer of sp^2-bonded carbon atoms arranged on a two-dimensional honeycomb lattice made of hexagonal rings. Planar polycyclic aromatic hydrocarbons (PAHs) with only benzenoid hexagonal rings can be viewed as fragments of a graphene sheet with the peripheral atoms saturated with hydrogen, and thus provide molecular models of graphene segments. Graphene segments are of paramount importance both from scientific and technological perspectives.

Moreover, the PAHs or graphene segments themselves are of great research interest, since they are widely found in the residues of domestic and natural combustion of coal, wood, and other organic materials and their unique electronic properties provide opportunities for novel functionalized nanomaterials and nanodevices. Understanding the mechanism of formation of graphene, segments are necessary to control its formation and in turn, to meet its application requirements. Graphene materials are endowed with a number of properties, including luminescence; which has been frequently reported in various chemical vapour deposition (CVD) of Diamond or a-C:H films (Zhang & De, 2011).

In the past decades, there has been a growing interest in the screening of plants for varieties of purposes such as medical applications, R&D and nutritional values (Ajani et al., 2019; Ekaluo et al., 2015; Mk et al., 2019). The green synthesis of nanomaterial, for instance reduction of silver to silver nanoparticles was one of the most researched area of application of bitter leaf (Amechi, 2018; Ariffinisa Lintang Widyaningtyas, Yoki Yulizar, 2019; Nzekekwu, Ak; Abosede, 2019; Pandurangan et al., 2018). Bitter leaf (*Vernonia Amygdalina*, VA) is a soft wood shrub tree commonly found naturally in tropical Africa and Asia. It is a promising plant in research and development and often used as a traditional medicine and nutritional purposes (Alara et al., 2019a; Oseni et al., 2014). The medicinal value of this plant studied and reported so far includes antidiabetics properties, anthelmintic activity, antimutagenicity and effects on CD4+ cell count (HIV/AIDS), antipyretic activities, anti-inflammatory, analgesic activity, hepatoprotective, antimalarial, antiplatelet and anticoagulant, antimicrobial, antifertility, abortifacient, hypolipidemic and anticancer activity, anti-allergic activity, cathartic effect and antioxidant properties (Achuba, 2018).

The secondary metabolites obtained from this plant leaf extract contain reducing sugar, polyphenolics, terpenoids, flavonoids, saponins, anti-fungi, antileukemia, alkaloids,

cardiac glycosides, steroids/triterpenes, and anthraquinone (Achuba, 2018; Ilondu, 2010; Momoh & Polytechnic, 2020).

Alkaloids, flavonoids, terpenoids, ketones, amides, aldehydes, polyphenols and carboxylic acids exists in bitter leaf (*Vernonia Amygdalina*) plant extracts are good agents for bioreduction of metal ions into nanostructures. However, the previous works showed that the reducing phytochemicals in the leaf extract contains mainly of the reducing components called terpenoids. In addition to reducing activities, terpenoids are also serving as the capping and stabilizing agents (Altemimi et al., 2017; B.S. Audu, P.C. Ofojekwu, A. Ujah, 2014; Malik & Ahmed, 2018). Hence, this abundantly and locally available, safe (eco-friendly) and economically viable plant contains an extraordinary nontoxic chemical compounds (extracts) within it. Therefore, a better extraction method or/and extracting solvents that may use to obtain the optimum value of such important compound (reducing agents) in bitter leaf (*Vernonia Amygdalina*) should be well known.

Most of the research work, on the method of extraction to isolate bioactive compounds from the plant matrix and reported in the past includes ultra-sound assisted extraction, solvent extraction, supercritical fluid extraction, pressurized solvent extraction, Soxhlet extraction; hydrodistillation, decoction, maceration and micro-wave assisted extraction (Alara et al., 2019a). Amongst these methods we the solvent extraction method was preferred for this work purpose due to its efficiency and effectiveness, low cost, shortened extraction time and simple method compared to the others. Many works have been reported on the use of solvents such as methanol, ethanol and water for VA extraction. However, it should be clearly known which one of the three solvents shall specifically and preferably be used for the green synthesis of graphene or (rGO). Hence, in this study we intended to extract the bio-reducing agent in bitter leaf (*Vernonia Amygdalina*) using three different solvents methanol, ethanol and water and to identify the best solvent extraction method for the application of green synthesis of graphene based nanomaterials. The objective also includes the characterization of the extracted phytochemical compounds in plant matrix using GC-MS and UV-VIS spectroscopy to identify the existence of reducing and capping agent in the plant extract.

Graphene, a two dimensional, only one atom thick and densely packed crystalline material, is the thinnest, lightest and strongest material on earth and the best conductor of heat and electricity known to man (Kopelevich & Luk'yanchuk, 2010; Mao et al., 2013;

Torrisi et al., 2012). This material has been identified and analyzed by mechanical exfoliation of pyrolytic graphite a decade ago by Manchester University physists Geim and Novoselov, because of which they won the noble prize in 2010 for their record breaking work (Geim, 2011; Zainuddin et al., 2018). Even if the above method and epitaxial chemical vapor depositions are more preferable to produce precise pristine graphene, they are less effective for large scale manufacturing (Deng et al., 2019; Dong et al., 2019). The interest of scientists to investigate this material began 70 years ago, when Wallace explained some of the physical properties of graphite through the band theory of solids (Morichi et al., 2008). The carbon atoms are connected in a hexagonal honeycomb lattice in graphene and can be seen with the naked eye because it absorbs about 2.3% of light (Perreault, Fonseca De Faria, et al., 2015). Recent studies showed that graphene is not only strongest material ever measured but also the stiffest and its current density is a million times that of copper (Chen & Cheung, 2016a). This new material has shown a number of unique properties so that it is much more than just a scientific interests; it boasts a growing list of real world applications (Hakimi & Alimard, 2012; Kumar et al., 2013; Yildirim & Ozturk, 2018).

Hence, the large scale production method of graphene and its family should be pronounced by researchers. The most popular approach to produce large scale graphene to date is the use of strong oxidizing agent to obtain graphene oxide (GO) (Ghanem & Rehim, 2018; Yenny Hernandez, Mustafa Lotya, Valeria Nicolosi, Fiona M Blighe Sukanta De & Duesberg, 2009). GO is the oxidized analogy of graphene from which we can only synthesize graphene in a large scale (Pachauri et al., 2017). It is a non-stoichiometric chemical compound of carbon, hydrogen and oxygen in variable ratios which largely depend on the processing methodologies (Gürünlü et al., 2020; Hessain & Hassan, 2020; Joshi et al., 2020). GO possesses large amount of oxygen functional groups that are presented to carbon skeleton in the form of epoxide & hydroxyl across the basal plane, hydroxyl, carbonyl & carboxyl at the edge during chemical oxidation from the oxidizing agent (Mahendran et al., 2020; Rawal et al., 2020; N. Singh et al., 2020). These deliberate insertion of oxygen containing functional group into graphite is reflected by the increment of interlayer distance from 0.34nm in graphite to 0.63nm in GO (Feng et al., 2020). Then this product, firstly graphite oxide and later on graphene oxide (after exfoliation by addition of distilled water and ultrasonication) reveal the following special properties such as easy functionalization, hydrophilicity, ability to convert to graphene (for

large scale production) and prevent the restoration of Van Der Waals interaction between graphene layer in graphite leading to exfoliation upon sonication (Çıplak et al., 2020; Haghighi & Tabrizi, 2013; Jilani, Othman, et al., 2018; Ying ying Liu et al., 2020; Nazarpour et al., 2020). Therefore, chemical exfoliation method is the most popular method to prepare GO, reduced graphene oxide (rGO) and graphene. GO is highly polar and hydrophilic but is nonconductor of electricity because of the presence of large amount of oxygen at its edge and basal plane (Xiaofeng Liu et al., 2014; Manchala et al., 2019).

In this study, graphene oxide was synthesized by the novel modification of the improved method which later on used as a precursor for the synthesis of reduced graphene oxide by the simplest green method. Solvent extracted compounds of *vernonia amygdalina* (VA) plant were used to synthesize rGO. This method is cheap that the reducing agent is abundantly locally available, ecofriendly that it does not discharge any gas and toxic substances to the environment unlike the antioxidant chemicals such as hydrazine hydrate and ascorbic acid and furthermore the synthesizes method is easy and scalable. In our preceding study, we identified the optimum condition and effective solvent extraction method to be used to extract compounds from VA for the synthesis rGO.

Hence the objective of this study was to synthesis reduced graphene oxide using abundantly available plant extracts of *vernonia amygdalina* as reducing and capping agent. The objective also includes the large scale synthesis of this recently significant attention captured; graphene based material, at nanoscale.

Nanosized materials are materials exhibiting unique physical, chemical, mechanical, electrical, biological and thermal properties than their bulk counter parts due to their high surface area, small particle size and possible quantum confinement effects (Khan et al., 2019; Q. Wu et al., 2020; Zhu & Liu, 2009). Semiconductor materials are solid materials having energy band gap lying in between conductor and insulator. Semiconductor materials manufactured to the nanoscale shares the above described property. The development of these materials necessitates the progress of sciences: chemistry, physics engineering and technology of the materials (Gupta & Gupta, 2015; Matyushkin et al., 2016). Bismuth sulfide nanostructure (Bi_2S_3) is a semiconductor material with unique features such as favorable energy band gap, high absorption coefficient and environmentally friendly elemental composition than the other known semiconductors (Liao et al., 2001; Zhang Liu et al., 2012; H. Wang et al., 2002). Bi_2S_3 has a direct narrow

band gap energy of 1.34eV and finds application in photodiodes arrays, photovoltaic convertor and thermoelectric cooling devices based on peltier effects (Boulouz et al., 2014; Ge et al., 2017; Liu et al., 2013; Matyushkin et al., 2016; Yuan et al., 2019; Zou et al., 2002).

The world population is growing at a fastest rate and this resulted in the intensification of industrial activities which in turn resulted in the contamination of environment. For instance, textile industries are the main sources of dyes, which are the top pollutants of water bodies (Carmen & Daniel, 2012a; Le Marechal et al., 2012; Luongo, 2015) and Bi_2S_3 has been attracting significant attention of researchers owing to its interesting band gap in the photocatalysis application for water purification (Nassar et al., 2011; Piras et al., 2014; Wu et al., 2010). However, the small band gap of Bi_2S_3 is subjected to the risk of charge carrier recombination and its light response range but still very effective and efficient if composited with a platform which stabilize the band gap and optimize its light absorption range (Ghanbari et al., 2014; Huang et al., 2013; Zhao et al., 2017). Different synthesis method of Bi_2S_3 has been reported so far, however many of them are chemical method that discharges hazardous pollutants to the environment (Piras et al., 2014; Stavila et al., 2009). Because of its non-toxicity, energy band gap, light absorption potential and ease of fabrication, Bi_2S_3 has been the preferred and widely used semiconductor (Ai et al., 2011; Chen et al., 2013; Hu et al., 2014). Hence the safe, cheap and simple synthesis method of Bi_2S_3 semiconductor should be devised by researchers.

As indicated in many recent research works, different approaches such as constructing heterostructured photocatalysts for the charge separation efficiency and extending the light response range by coupling the suitable band gap structure was the most promising approach to promote photocatalytic efficiency of Bi_2S_3 (Ayodhya & Veerabhadram, 2018; Luan et al., 2015). Owing to their unique electronic properties for application of photovoltaic devices, graphene has attracted interest of researchers recently (Luan et al., 2015). Graphene possesses properties such as high specific surface area (2600 m^2g^{-1}), electrical conductivity (550 S cm^{-1}), electron mobility at room temperature (200,000 $cm^2v^{-1}s^{-1}$), and current density up to six orders of magnitude higher than copper (Matte et al., 2011) which are important for the application of a photocatalytic activities.

In this section, a cheap, simple and green synthesis method of Bi_2S_3 was presented using methanol extracted compounds of vernonia amygdalina at low temperature below 100 ^{0}C.

The plant extract was used as a capping agent for the stabilization of the product nanostructure. Graphene oxide (GO) was synthesized using improved method with a slight modification and it was reduced to produce reduced graphene oxide (rGO) by green synthesis method. The rGO-Bi_2S_3 composite was synthesized from the mixture of rGO and Bi_2S_3 under single step refluxed hydrothermal method. The enhanced photocatalytic activity of Bi_2S_3 using rGO for the degradation of methylene blue (MB) was studied thoroughly. The durability and reusability of the heterogeneous catalyst was also explored exhaustively.

The demand for pure drinking water supply is growing rapidly as the result of continuous increase of world population (Peres & Cury, 2011). Most people living in the rural areas are using ground water as the main source for drinking. Usually, ground water have agonized high concentration of fluoride due to dissolution of some mineral ores (Chandrawat, 2020; Ki et al., 2020; Lin et al., 2020). Although ground water possess good microbiological and biological properties, it is contaminated with some toxic chemicals which may pose serious health effects on living organisms (Thole, 2013). Besides its advantages at its permissible concentration, fluoride causes significant health problem (Pratap & Singh, 2013). World health organization (WHO) set the recommended upper limit of fluoride ion concentration to be consumed in food stuff should not be more than 1.5 mg/L (Cay Butler, 2006). However, fluoride ion concentrations in some African rift valleys ground water were recorded to be greater than this limit by far. Most of the east Africans regions which extend from Jordan valley down through Sudan, Ethiopia, Kenya, Uganda and Tanzania were reported to have maximum fluoride ion concentration (Datturi et al., 2015; Mandefro Ararso, 2017; Sara Datturi, Assefa Kumsa, Seifu Kebede, 2017).

Reports showed that Ethiopian rift valley ground water contains fluoride concentration which is much higher than the allowable level (Alemu et al., 2015; Travi, 1998). The concentration of fluoride ion in Ethiopian rift valley lakes, such as Lake Shala and Lake Abijata were recorded to be 264 mg/L and 202.4 mg/L, respectively (Mandefro Ararso, 2017). The increase in the concentration of fluoride ion in ground water along the course of the river flow is due to the existence of the acidic rocks lengthways across and the existence of recent volcanic hot eruption (Ghanbarian et al., 2020; Medellin-castillo et al., 2007; Sahu et al., 2021). The landforms of Ethiopian rift valley exist in a variety of terrain that is significantly important to the enrichment of fluoride into ground water (Kair & Faj, 2014). If beyond the permissible values, fluoride causes a significant health disorder.

According to some research findings, the ingestion of fluoride with concentration 1.5-3 mg/L cause dental fluorosis, 3.5-9 mg/L cause skeletal fluorosis, and longtime ingestion of fluoride with concentration greater than 10 mg/L cause an irreversible damage to the bone called bone immobility or crippling fluorosis (Aggeborn & Öhman, 2017; Kosik-bogacka et al., 2015; Q Xiang, Y Liang, L Chen, C Wang, B Chen, X Chen, 2003).

Although defluoridation of water is difficult and expensive, a number of methods have been applied (Ayalew, 2020). The most common defluoridation techniques reported were ion-exchange, precipitation, nanofiltration, electrochemical methods, reverse osmosis and adsorption (Karthikeyan, 2019; Malakootian et al., 2011). Among these, adsorption is quite effective and efficient methods because of the ease of operations, less time and space consumption, ease of material availability, ecofriendly and cost effective methods (Collivignarelli et al., 2020; Perreault, Faria, et al., 2015; Publishing & Supply, 2020). The ground water sources serving as a drinking water supply for a community living in "Dugda-Bora district of Oromia regional state, Ethiopia" contain high concentration of fluoride which caused a tremendous health effects and death (Fito et al., 2019; Ku et al., 2002). The above mentioned defluoridation techniques have been applied (Aigbe & Onyancha, 2020; Tan et al., 2020) but the problem were not yet resolved.

Activated carbon has been used as adsorbent due to its excellent adsorption capacity for a wide range of contaminants; however its application is restricted recently due to the high production cost and difficulties in recyclability (Tefera et al., 2020; Xu et al., 2020). Carbon nanotubes (CNTs) and graphene based materials (GBMs) have been developed as an alternative to conventional adsorbents (Meijiao et al., 2013). Researchers used CNTs to build new adsorbents because of their high surface area, non-corrosive, presence of oxygen-containing functional groups, tunable surface chemistry, and scalable production(Yang et al., 2015). However, graphene-based nanomaterials were found to be more advantages than CNTs in adsorption activities due to:

1. The availability of two basal planes of single layered graphene materials for pollutant adsorption whereas the inner wall of CNTs is not accessible by the adsorbates

2. The ease of synthesis of graphene based materials by simple chemical exfoliation of graphite without using complex apparatus or metallic catalysts and the produced graphene based materials is free of catalyst residues so that no further purification steps are needed (Xing Li et al., 2014)

3. The as-prepared GO possesses a large number of oxygen-containing functional groups which are likely responsible for the adsorption of ionic pollutants and no additional acid treatments needed to impart a hydrophilic character and reactivity unlike CNTs.

In this work, the application of graphene based nanomaterial as adsorbents for the removal of fluoride ion from aqueous solution were explored. Besides, we described key adsorption mechanisms performed by GO. A novel experimental method of studying the mechanisms by which adsorbent was continuously adsorbing adsorbate without saturation of the active site was also described. Based on the recent discoveries that the graphene oxide surface can be modulated by molecules assembled on its surface and pH optimization we have made fluoride adsorption study using GO by optimizing pH.

1.1.1 Objectives of the Study

1.1.1.1 General Objective

The purpose of the study is to synthesis and characterizes graphene-based nanomaterials for environmental protection applications.

1.1.1.2 Specific Objectives

- To extract *vernonia amygdalina* leaf using methanol, ethanol and water.
- To identify the best plant extract for the reduction of graphene oxide.
- To synthesis GO nanostructures using simple reflux method.
- To synthesis rGO nanostructure using *vernonia amygdalina* plant extract.
- To synthesis Bi_2S_3 nanostructure semiconductor.
- To synthesis rGO - Bi_2S_3 nanocomposite.
- To characterize the synthesized nanostructures and nanocomposite.
- To optimize graphene oxide nanoadsorbent for F^- remediation.
- To study the photocatalytic activity of rGO - Bi_2S_3 nanocomposite for degradation of methylene blue dye

1.1.2 Statement of the problem

The world population is growing at an alarming rate and this resulted in the intensification of agriculture and industrial activities which in turn resulted in contamination of air, soils and aquatic ecosystems that brought about global climate change. Consequently, this world is under stress with the worst extremes of human activities. For instance Ethiopia has embarked on a transformational journey of becoming a low middle-income carbon neutral economy by 2025. This is to be achieved by shifting economic activities from

agriculture-led to industrial-led sectors. This, on the other hand resulted in the large emission of industrial byproducts pollutants to the environment. Moreover, the demand for pure drinking water supply is also growing rapidly as the result of continuous increase of world population. Most people living in the rural areas are using ground water as the main source for drinking. Usually, ground water have agonized high concentration of fluoride due to dissolution of some mineral ores. Besides its advantages at its permissible concentration, fluoride causes significant health problem if its concentration in food stuff is beyond the permissible level. World health organization (WHO) set the recommended upper limit of fluoride ion concentration to be consumed in food stuff should not be more than 1.5 mg/L (Cay Butler, 2006). However, fluoride ion concentrations in some African/Ethiopian rift valleys ground water were recorded to be greater than this limit by far. This work is provoked due to the concrete current issue, the environmental pollution, and the effects of fluoride on human health.

1.1.3 Research Questions

We planned to develop graphene oxide-metal sulfide nanocomposite heterogeneous photocatalyst for the decomposition of organic pollutant and also planned to develop graphene based nanomaterials for the adsorption of inorganic pollutant on the carbon lattice surface. Therefore the graphene-based material prepared along the course of the proposed research was confirmed to be accurate, long lasting, inexpensive and sensitive material to effectively decompose and adsorb the target pollutants and answered the following questions.

- What is the best solvent for the green synthesis of graphene
- What is the optimum design for graphene oxide to adsorbent fluoride ion?
- What is the optimum design for rGO-Bi_2S_3 nanocomposite for organic dyes degradations?

1.1.4 Innovation

The idea of studying fluoride ion adsorption from aqueous solution by graphene oxide through functionalization and pH optimization is new. This work was planned and assumed to be based on the recent discovery that the graphene surface can be modulated by molecules assembled on its surface and pH optimization. With this method and specific nanoadsorbent design, a high level of target ion detection was achieved. Moreover, the proposed experiments allowed characterizing of the processes of stabilizing the active site of semiconductor and increasing the surface area for photolytic activities of graphene based material.

1.1.5 Significance of Study

Graphene based nanomaterials have a big potential for practical applications in environmental fields. The possible application of graphene-based nanomaterials as nanoadsorbent for fluoride ion in drinking water is new idea. Confidentially, the technique; photocatalytically degradation of organic pollutant; innovate the material research on the ionic level and will find its place in future industrial applications. The sensitivity of graphene based nanomaterials to ions of different charges in liquid environment could potentially make graphene based nanomaterial an alternative material for the nanoadsorption for environmental applications.

Chapter Two

2. Literature Review

2.1 Photocatalysis

Researchers worldwide prefer plenty and clean energy sources, the sunlight, for energy production, environmental protection and water purification, having photocatalysis as the promising method in mind. This method works based on the production of electron-hole pairs by illumination with light of suitable energy on a semiconductor material such as metal sulfide nanostructures dispersed in an aqueous medium (Nengjie Huo, Alberto Figueroba, Yujue Yang, Sotirios Christodoulou, Alexandros Stavrinadis, César Magén, n.d.). The band gap of metal sulfide nanoparticles can be delicately tuned by simply controlling their particle sizes without altering the chemical compositions of metal sulfide, which is the reality of binary metal sulfide nanoparticles (Wu et al., 2010).

Based on this, during the last decades, there are a number of novel techniques that have been developed for band gap tuning of binary metal sulfide through simple artificial size control (Yuan et al., 2019). This semiconductor material doubles their efficiency when they are manufactured to some nanoscale size. Nanoparticles applications are versatile and range from industrial and environmental goods to everyday products derived from food, textile and cosmetic industries. The photocatalyst material activated by light plays a decisive role to perform an efficient photocatalytic reaction, and therefore its selection should be done carefully to fulfill both, the appropriate electronic structure and reasonable energy of light for its photoactivation because the rate of the photocatalytic reaction is independent of the active site (Chen et al., 2013).

In this regard, application of photocatalysis, especially photocatalysis using semiconductor particulate system, appears to be the most appealing means than the more conventional chemical oxidation methods for decomposition of toxic compounds to nonhazardous products. This is because of the fact that semiconductors are inexpensive, non-toxic, having high surface area, broad absorption spectra with high absorption coefficients, exhibiting tunable properties which can be modified by size reduction, doping, sensors, etc., affording facility for multielectron transfer process and capable of extended use without substantial loss of photocatalytic activity (Yuan et al., 2019).

The tendency of photoactivation is achieved by the unique photophysical and photochemical properties of these nano-sized photocatalysts. The photocatalytic

degradation of the toxic compounds (dyes, pesticides, phenolic compounds, etc.) using the photoactive materials in an aqueous medium mainly depends on the band gap, surface area, amount of catalyst, and generation of an electron-hole pair. It has been observed that the surface area plays a major role in among all factors in the photocatalytic degradation of dyes, by providing a higher surface area, which leads to the higher adsorption of dye molecule on the surface of photocatalyst and enhances the photocatalytic activity (Nyangiwe, 2012b).

In the past few decades, high efficiency and stable graphene oxide photocatalysts have been extensively studied for the degradation of organic pollutants and their potential applications to environmental remediation (Luan et al., 2015). Currently, considerable attention has been paid to semiconductor and graphene/semiconductor-based photocatalysis for the degradation of pollutants owing to its low energy input, easy operation, cleanness and high efficiency due to large surface area. Some of the recent reports has been done for the comparison of photocatalytic activity of organic dyes using rGO, GO and GO based semiconductor composites, the degradation activity of dyes using semiconductors like TiO_2, NiO, CdS, ZnS, CeO_2/SnO_2, g-C_3N_4 and Ag_3PO_4 coupled with GO exhibited greater efficiency than the other catalysts such as semiconductors in the absence of GO and pure GO (Gupta & Gupta, 2015).

The improved photocatalytic activity of these GO composites was observed due to the efficient separation of photo-generated electron-hole pairs. The enhanced photocatalytic activity of GO incorporated semiconductor photocatalysts is highly related to the number of separated photo-generated charge carriers. In addition, graphene acted as an ideal catalyst and facilitates charge transfer to suppress the recombination of electron-hole pairs in the nanocomposites. Generally, photocatalytic enhancement in the graphene-semiconductor composites can be explained in terms of some mechanisms due to unique properties of graphene, such as: extension of the wavelength of the absorbed light due to the chemical bonds which narrow the band gap of semiconductor and transparency of graphene, suppression of the recombination of photogenerated electron hole pairs by accepting the excited electron from the conduction band due to its long π-conjugation structure and increasing absorptivity of pollutants. Therefore, the photocatalytic activity of GO based semiconductor composite is higher than that of pure semiconductors (Perreault, Fonseca De Faria, et al., 2015).

2.1.1 Synthesis of Graphene

To realize the full potential of graphene in a broad range of its applications, a scientifically consistent understanding of the various methods for graphene synthesis is crucial. The size and quality of the graphene produced depends on the techniques used and the next sub-sections are devoted to some of the commonly used synthesis methods; their merits and demerits.

i. Exfoliation and Cleavage

It was reported that the excellent properties of graphene related materials are highly dependent on the exfoliation of the graphite down to single graphene sheet in the matrices. However, aggregation is the main problem in the synthesis and processing of bulk graphene sheets. Unless well separated, graphene tends to form irreversible agglomerates or even restack to form graphite through interactions with Van der Waals.

a. Mechanical Exfoliation

Mechanical exfoliation in solution is a simple flaking process in which a commercially available highly focused pyrolytic graphite (HOPG) sheet was dryly etched to several 5 μm deep mesa in oxygen plasma. The mesas were then stuck onto a photoresist and were peeled off layers by a scotch tape. The thin flakes left on the photoresist were washed off in acetone and transferred to a silicon wafer. It was found that these thin flakes were composed of monolayer or a few layers of graphene (Bekyarova et al., 2012; Reeves, 2010). On the other hand, although chemical oxidation of graphite and the subsequent exfoliation provide large amount of graphite oxide monolayer, the invasive chemical treatment inevitably generates structural defects as indicated by Raman spectroscopic studies (März et al., 2018b). These structural defects disrupted the electronic structure of graphene and changed it to semi-conductive. Therefore, physical exfoliation approaches are desirable where it is required to maintain the graphene structure. Keeling and Wallace demonstrated that graphite could be exfoliated in N-methyl-pyrrolidone to produce defect-free monolayer graphene (Forrester & Kusmartsev, 2014). The disadvantage of this process is the high cost of the solvent and the high boiling point of the solvent that makes the following graphene deposition difficult (Keeling, 2017; Morichi et al., 2008). A surfactant sodium dodecyl benzene sulfonate, SDBS have been used to exfoliate graphite in water to produce graphene (Sciences, 2015). The graphene monolayers are stabilized against aggregation by a relatively large potential barrier caused by the Coulomb repulsion between surfactant-coated sheets (Yenny Hernandez, Mustafa Lotya, Valeria Nicolosi,

Fiona M Blighe Sukanta De & Duesberg, 2009). On the other way, sodium chlorate have been used as a surfactant to exfoliate graphite and moved further to isolate the resultant graphene sheets with controlled thickness using density gradient ultracentrifugation (DGU) (Cai et al., 2012).

b. Intercalation of Small Molecules by Mechanical Exfoliation

Graphite agglomeration can be greatly reduced by adding small molecules between the graphite layers or by applying non-covalently molecules or polymers to the surfaces, producing compounds for graphite intercalation. In graphite intercalation compounds (GICs), the graphite layers remains unaltered with guest molecules located in the interlayer galleries. When the layers of graphite interact with the guest molecules by charge transfer, the in-plane electrical conductivity generally increases but when the molecules form covalent bonds with the graphite layers as in fluorides or oxides the conductivity decreases as the conjugated sp^2 system is disrupted.

Acetic acid, acetic acid anhydride, concentrated sulphuric acid and hydrogen peroxide are sources of some ultrasonic solvents. Of all these, concentrated sulfuric acid was proven to be the best ultrasonic solvent to provide the optimal environment for ultrasonic irradiation preparation of the expandable graphite. Such sulfuric acid intercalated graphite compound consisted of layers of hexagonal carbon structure within which H_2SO_4 was intercalated. Expandable graphite could be prepared either by oxidation with a chemical reagent or electrochemically in the intercalating acid (Hacker et al., 2013). Graphite could expand up to a hundred times in volume at high temperature due to the thermal expansion of the evolved gases trapped between the graphene sheets. So it was reasonably assumed that oxidants and other molecules could enter in the interlayer space of expandable graphite more easily compared to natural graphite. Commercial expandable graphite was subjected to brief heating (60s) at 1000 °C in forming CO_2 gas. It was then grounded with NaCl crystals and reintercalated with oleum. The exfoliated graphite was then dispersed in N, N-dimethylformamide (DMF) and treated with tetrabutylammonium (TBA). TBA could insert into and increase the distance between adjacent layers of graphite facilitating the separation of graphene sheets in surfactant solutions (Xiaolin Li et al., 2008).

ii. Chemical Vapor Deposition (CVD)

a. Thermal CVD

In addition to mechanical exfoliation and chemical sheet reduction methods, several promising approaches have been published, including SiC epitaxial growth and chemical vapor deposition (CVD) on metal surfaces. Among them, the CVD growth was concluded to be the most promising technique for large-scale production of graphene films so far. A CVD process which uses Ni as a substrate involves dissolving carbon into the nickel substrate followed by a precipitation of carbon on the substrate by cooling the nickel. The Ni substrate is placed in a CVD chamber at a vacuum of 10^{-3} Torr and temperature below 1000°C with a diluted hydrocarbon gas. The deposition process starts with the incorporation of a limited quantity of carbon atoms into the Ni substrate at relatively low temperature, similar to the carburization process. The subsequent rapid quenching of the substrate caused the incorporated carbon atoms to out-diffuse onto the surface of the Ni substrate and form graphene layers. Therefore, the thickness and crystalline ordering of the precipitated carbon (graphene layers) is controlled by the cooling rate and the concentration of carbon dissolved in the nickel which is determined by the type and concentration of the carbonaceous gas in the CVD, and the thickness of the nickel layer (Deng et al., 2019; Seah et al., 2014).

On the other hand the graphene growth on low carbon solubility (<0.001 atomic %) substrate like Cu mainly happens on the surface through the following four-step process (Vinet & Zhedanov, 2011). First: catalytic decomposition of methane on Cu to form CxHy upon the exposure of Cu to methane and hydrogen. Depending on temperature, methane density, methane flow and partial hydrogen pressure, the Cu surface is undersaturated, saturated or supersaturated with CxHy organisms in this phase. Second: Nuclei formation as a result of local CxHy supersaturation where the undersaturated Cu surface does not form a nuclear one. Third: Nuclei expand to form graphene islands saturated on Cu surface, or super-saturated with CxHy species. Finally full Cu surface coverage by graphene under certain temperature (T), methane flow rate (JMe), and methane partial pressure (PMe). An interesting feature of the CVD approach to synthesize graphene is the possibility for substitutional doping by introducing other gases, such as NH_3, during the growth. The nitrogen atoms can be doped into graphene as pyridinic, graphitic and pyrrolic forms. These nitrogen doped graphene (N-graphene) layers have demonstrated interesting properties (Lv et al., 2015).

b. Plasma Enhanced CVD

Plasma enhanced chemical vapor deposition (PECVD) provides another graphene synthesis path at a lower temperature than thermal CVD. Thick graphite structures were observed during the fabrication of nanostructured graphite-like carbon using a dc discharge Plasma enhanced chemical vapor deposition. The first report of the production of mono- and few layer of graphene by Plasma enhanced chemical vapor deposition involved a radio frequency Plasma enhanced chemical vapor deposition system to synthesize graphene on a various substrates where graphene sheets were produced from a gas mixture of 5–100% CH_4 in H_2 (total pressure 12 Pa), at 900W power and 680 °C substrate temperature. The advantages of the plasma deposition include very short deposition time (<5 min) and a lower growth temperature of 650 °C compared to the thermal CVD approach (1000 °C) (Bo et al., 2013; J. Sun et al., 2015).

c. Thermal Decomposition On SiC and Other Substrates

The development of graphite by ultra-high vacuum (UHV) annealing of the SiC surface was an attractive approach particularly for the semiconductor industry, as the products are obtained on SiC substrates and do not require transfer before processing devices (Çelebi et al., 2012; De Heer et al., 2011). When SiC substrate is heated under UHV, silicon atoms sublimate from the substrate. The removal of Si leaves surface carbon atoms to rearrange into graphene layers. The thickness of graphene layers depends on the annealing time and temperature. The formation of few-layer graphene (FLG) typically requires few minutes annealing of the SiC surface at temperature around 1200 °C. More recently, vapor phase annealing has been used to produce FLG on SiC. At the expense of a higher temperature typically 400 °C above UHV temperature, this method leads to the formation of FLG on SiC with improved thickness homogeneity. Another uncertainty involves the different epitaxial growth patterns on different SiC polar face (i.e. Si-face or C-face). Unusual rotational graphene stacking were observed in multilayers graphene grown on the C-face surface but not on Si-face surface. Such mismatch of graphene growth process has profound effects on the physical and electronic properties of epitaxial graphene. On the C-face, the twisted interface leads to the decoupling between different layers of graphene, each of which behaves as a single layer (Milenov et al., 2017; Yazdi et al., 2016; Yu et al., 2011).

2.1.2 Graphene Derivatives

Graphene oxide is an oxidized form of graphene known as the only intermediate or predecessor to the large-scale development of graphene. It was named after the English chemist, Sir Brodie; first recorded oxidation of graphite a centuries ago (Feicht et al., 2019). About thirty years ago, the term graphene was officially claimed to define the single atom-thin carbon layer of graphite, which structurally comprises sp^2 hybridized carbon atoms arranged in a honeycomb lattice, rendering itself large surface area and some promising properties in terms of mechanical, electrical, and others. Despite these extraordinary properties, purely single-layer graphene remains very limited success in practical applications due to the difficulties in the large-scale formation of specifically organized structures. But the precursor GO has advanced much in both academics and industries in the last decades because of its readiness by exfoliating bulk graphite oxide facilely prepared from the oxidation of graphite. This bottom-down chemical strategy features the upmost flexibility and effectiveness thereby arousing the greatest interest in practical applications.

Now it is seemingly clear that GO is a non-stoichiometric chemical compound of carbon, oxygen, and hydrogen in variable ratios which largely yet partly depend on the processing methodologies. GO possesses abundant oxygen functional groups that are introduced to the flat carbon grid during chemical exfoliation, evidenced as oxygen epoxide groups (bridging oxygen atoms), carbonyl (C=O), hydroxyl (-OH), phenol, and even organosulfate groups (impurity of Sulphur). In other word, these defects of various kinds are brought into the naturally intact graphene structure, further categorized into on-plane functionalization defects and in-plane lattice defects (vacancy defects and hole defects) which are semi-randomly distributed in GO's σ-framework of the hexagonal lattice. Such a defect-rich structure leads to a set of unique properties of GO and render it availability and scalability of consequent applications via post treatments, e.g. chemically-derived graphene-like materials, functionalized graphene-based polymer composites, sensors, photovoltaics, membranes and purification materials. On the detailed structure of GO, however, it remains some ambiguous and literature reports are still in argument (Eigler & Hirsch, 2014). In addition, methods in regard to synthesis of GO has been massively researched in the past few years. The effectiveness and environmental benignity was core driven force for the continuous evolvement (Jilani, Othman, et al., 2018; J. Li et al., 2014).

GO and rGO have different characteristics as compared to graphite and graphene. GO is the oxide form of graphene, where oxygen is introduced to graphene through chemical oxidation. Moreover, GO is described as heavily oxygenated, with the presence of many oxygen-containing functional groups such as epoxide, hydroxyl, carbonyl and carboxyl groups on its basal plane. Thus, with the presence of these functional groups, GO becomes hydrophilic which allows better interfacial interaction with polar polymer matrices for improvement of mechanical and electrical properties for various applications. However, the oxygen functionalization on GO reduced the electrical conductivity and therefore, GO becomes less preferable for conductive polymer-based composites. Besides, rGO contains fewer amounts of oxygen functionalized groups as compared to GO which can be synthesized in chemical and thermal reduction. However, the thermal reduction requires high cost since the reduction is conducted at high temperatures, thus, the chemical reduction is preferable by most researchers. There are plenty of reducing agents such as hydrazine hydrate, ascorbic acid and others (Hidayah et al., 2017; Zainuddin et al., 2018). However, in this work rGO was synthesized using green synthesis method.

2.1.2.1 Synthesis of Graphene Oxide

There are two general synthetic approaches of graphene oxides i.e., dry or wet medium approaches. The dry medium synthetic approach consists of an oxidation reaction of graphene through atomic oxygen in ultrahigh vacuum conditions or by exposure to molecular oxygen and treating with ozone under ultraviolet light. But a suitable and large scale production approach consists of wet synthesis in which graphite is typically used as graphene source, due to its natural abundance and inexpensive cost. There are many wet synthesis methods reported and the most commonly used so far are the following three methods.

a) Brodie Method.: British Chemist, B.C. Brodie was the first researcher that discovers properties of graphite oxide and since then, many interesting researches have been done by researchers all over the world. However due to limitation of data, research about graphite oxide is still on going by researchers. In Brodie`s method, ratio of 1:3 of graphite and potassium chlorate ($KClO_3$) were mixed and reacted with fuming nitric acid (HNO_3) in 3 or 4 days at 60^oC.

b) Staudenmaier Method: The Brodie's reaction was improved by Staudenmaier by adding sulfuric acid, to the reactant to increase the acidity of the mixture, and several

aliquots of solid $KClO_3$, over the course of reaction. Even if both methods generates ClO_2, toxic gas which rapidly decomposes in air giving explosions, these modifications led to a more oxidized graphitic material and a simplification of the reaction time.

c) Hummers Method: This group proposed an alternative way to improving the safe operational conditions with a drastic reducing production time, from several days to a few hours. In this case, the oxidation of graphite was achieved by harsh treatment of one equal weight of graphite powders in a concentrated H_2SO_4 solution containing three equal weights of $KMnO_4$ and 0.5 equal weight of $NaNO_3$. The three improvement made by Hummers are: the reaction can be completed within a few hours, $KClO_3$ was replaced by $KMnO_4$ to improve the reaction safety, avoiding the evolution of explosive ClO_2 and the use of $NaNO_3$ instead of fuming HNO_3 eliminates the formation of acid fog. Hummer's method has been paid the most intensive attention because of its high efficiency and satisfying reaction safety. However still it has the following two faults: the oxidation procedure releases toxic gasses such as NO_2 and N_2O_4 and the residual Na^+ and NO_3^- ions which are difficult to remove from the waste water formed from the processes of synthesizing and purifying GO. Tour and co-workers improved the Hummers method by excluding $NaNO_3$, increasing the amount of $KMnO_4$, and performing the reaction in a 9:1 by volume mixture of H_2SO_4/H_3PO_4. This modification is successful in increasing the reaction yield and reducing toxic gas evolution, while using twice as much $KMnO_4$ and 5.2 times as much H_2SO_4 as those required by Hummers method and also introducing a new component of H_3PO_4 to the reaction system (Kianpour et al., 2017). A comparison of the improved, conventional and modified Hummer's, respectively procedures of graphene oxide synthesis from expanded graphite is shown in Figure 2.

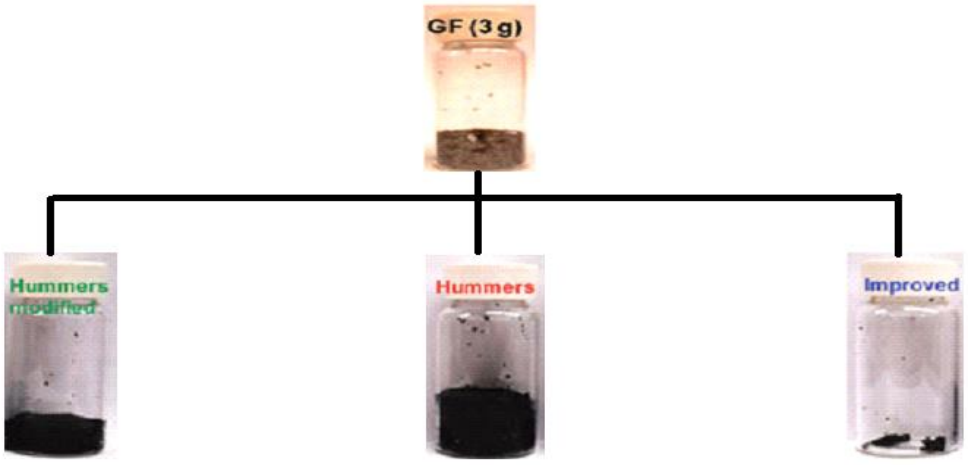

Figure 2: Procedure scheme for Tour method (Dideikin & Vul', 2019).

2.1.2.2 Synthesis of Reduced Graphene Oxide

The chemical structure of graphene oxide such as the type and distribution of oxygen-containing functional groups have been studied using NMR 13C-labelled graphene oxide suggesting that the basal plane of the sheet is decorated with hydroxyl and epoxy (1,2-ether) functional groups with small amount of lactol, ester, acid and ketone carbonyl groups at the edge (Cai et al., 2008; Yan & Chou, 2010). Chemical reduction of graphene oxide sheets has been performed with several reducing agents including hydrazine, and sodium borohydrate. Hydrazine hydrate, unlike other strong reductants, does not react with water and was found to be the best one in producing very thin and fine graphite-like sheets. During the reduction process, the brown colored dispersion of graphene oxide in water turned black and the reduced sheets aggregated and precipitated as shown in Figure 3. Hydrazine takes part in ring-opening reaction with epoxides and forms hydrazino alcohols (Thakur et al., 2015; Vorrada et al., 2013).

The carboxylic acid groups were unlikely to be reduced by hydrazine and thus remained intact after hydroxyl reduction. The adjustment of pH with ammonia solution deprotonated the carboxylic acid groups and thus the electrostatic repulsion among the charged groups on reduced graphene oxide enabled the formation of well-dispersed graphene colloids in water without any stabilizers. But, unless stabilized by selected surfactants, reduced graphene in organic solvent tend to agglomerate due to their hydrophobic nature. Another possible route to reduce GO was using sodium borohydride ($NaBH_4$) in aqueous solution where sodium borohydride is more effective than hydrazine as a reductant of graphene oxide although it can be slowly hydrolyzed by water. The $NaBH_4$ treatment eliminated all the parent oxygen containing groups and the resultant solid became IR inactive like pure graphite (Dreyer et al., 2010; Hakimi & Alimard, 2012).

Other chemical reduction routes including using hydroquinone, gaseous hydrogen (after thermal expansion)], and strongly alkaline solutions have also been investigated. Thermal reduction is another approach to reduce GO to reduced graphene oxide that utilizes the heat treatment to remove the oxide functional groups from graphene oxide surfaces (Habte et al., 2019).

2.1.3 Surface Functionalization of Graphene Oxide (GO)

The surface functionalization follows two approaches: covalent functionalization and non-covalent functionalization.

In covalent functionalization, oxygen functional groups on graphene oxide surfaces, including carboxylic acid groups at the edge and epoxy/hydroxyl groups on the basal plane can be utilized to change the surface functionality of graphene oxide. Graphene oxide had been treated with organic isocyanates to give a number of chemically modified GO. Treatment of isocyanates reduced the hydrophilicity of graphene oxide by forming amide and carbamate esters from the carboxyl and hydroxyl groups of graphene oxide. The subsequent addition of nucleophilic species, such as amines or alcohols, produced covalently attached functional groups on graphene oxide via the formation of amides or esters. The resultant amine functionalized graphene oxide has demonstrated various applications in optoelectronics, drug-delivery materials, biodevices, and polymer composites. The attachment of hydrophobic long, aliphatic amine groups on hydrophilic graphene oxide improved the dispersability of modified graphene oxide in organic solvents, while porphyrin-functionalized primary amines and fullerene-functionalized secondary amines introduced interesting nonlinear optical properties. The amine groups and hydroxyl groups on the basal plane of graphene oxide have also been used to attach polymers through either grafting-onto or grafting-from approaches. To grow a polymer from graphene oxide, an atom transfer radical polymerization (ATRP) initiator was attached to graphene surfaces (Bottari et al., 2017). Besides the carboxylic acid groups, the epoxy groups on graphene oxide can be used to attach different functional groups through a ring-opening reaction.

The non-covalent functionalization of graphene oxide utilizes the weak interactions (i.e. p–p interaction, Van der Waals interactions and electrostatic interaction) between the graphene oxide and target molecules. The sp^2 network on graphene oxide provides p–p interactions with conjugated polymers and aromatic compounds that can stabilize reduced graphene oxide resulted from chemical reduction and produce functional composite materials (Bilalis et al., 2014). During the chemical reduction of graphene oxide, reduced graphene oxide nanosheets are stabilized via the p–p interaction between aromatic molecules and reduced graphene oxide nanosheets. Aromatic molecules have large aromatic plane and can anchor onto the reduced graphene oxide surface without disturbing its electronic conjugation, providing stability for reduced graphene oxide. Dye-labeled DNA has also been used to functionalize graphene oxide to detect proteins and DNA. In the presence of a target, the binding between the dye-labeled DNA and target molecule will alter the conformation of dye labeled DNA, and disturb the interaction between the

dye-labeled DNA and graphene oxide. Such interactions releases the dye-labeled DNA from the GO, restoring of dye fluorescence (Zhenbao Liu et al., 2014; X. Wu et al., 2018).

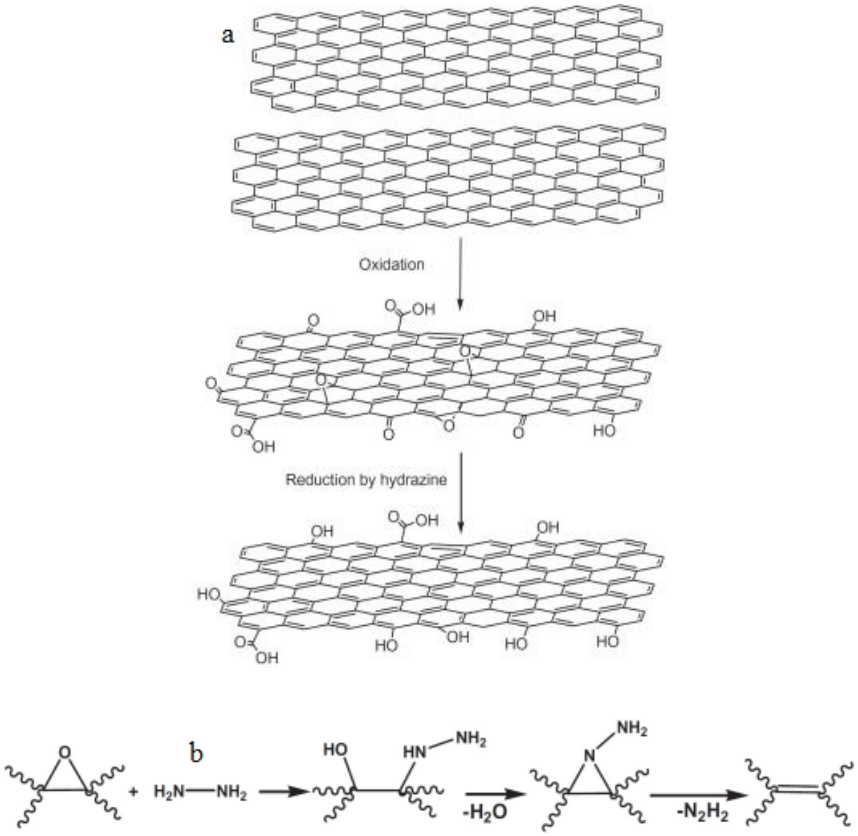

Figure 3: (a) Oxidation of graphene to GO and rGO. (b) A proposed reaction pathway for epoxy reduction by hydrazine (Petersen, 2015).

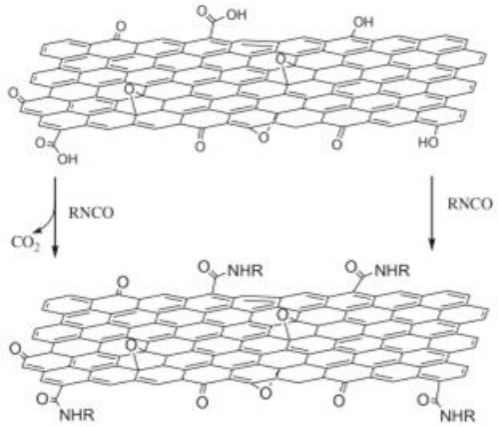

Figure 4: Isocyanate treatment of GO where organic isocyanate reacts with the hydroxyl and carboxyl groups of the graphene oxide sheets (Pei & Cheng, 2012).

2.1.4 Properties of Graphene and its Derivatives

Graphene was theoretically described 70 years ago (Morichi et al., 2008). However it is only in 2004 that a stable 2D sheet of carbon atoms; graphene, was successfully isolated

by mechanical exfoliation of highly oriented pyrolytic graphite sample (Geim, 2011). Graphene can be rolled up to form some carbon allotropies such as carbon nanotubes, fullerenes and overlapped to form graphite as shown in Figure 5.

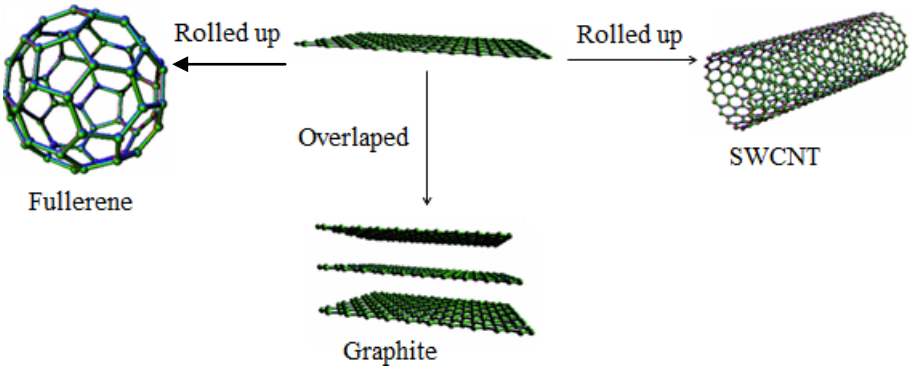

Figure 5: Theoretical relationship between allotropes of carbon.

Owing to their unique chemical, thermal, electronic, and mechanical properties, graphene has attracted great interest among scientists. Some of the unique properties includes high specific surface area (SSA) of 2600 m^2 g^{-1}, excellent thermal conductivities of 5000 W m^{-1} K^{-1}, good electrical conductivity of 550 S cm^{-1}, high-speed electron mobility at room temperature of 200,000 cm^2 V^{-1} s^{-1}, a current densities up to six orders of magnitude higher than copper, high stiffness and strength with Young's modulus of 1 TPa and intrinsic strength of 130 GPa in its primeval form (Chen & Cheung, 2016a), extraordinary electrocatalytic activity and optical properties (Matte et al., 2011). Besides all this advantages, there are also many factors which hinder the electronic properties of graphene such as the presence of defects, impurities, functional groups, the size and flatness of the sheet, and the nature of the precursor (Perreault, Fonseca De Faria, et al., 2015).

The charge carrying fermions of graphene is another sources of uniqueness of its electronic properties and because of the symmetry of the honeycomb lattice, the electrons in graphene generally obey the relativistic Dirac equation (De & Mayado, 2016a). But the speed of light that is used in this equation is replaced by the Fermi velocity of electron which is about 10^6 m/s (Veligura, 2007a). Because of this, the solution of the Dirac equation gives a linear dispersion relation for the fermions. Therefore the fermions could be considered as massless particles inside the structure of graphene. Hence the interaction between fermions and the honeycomb lattice (Fuchs, 2013) causes electrons effectively to obey the relativistic Dirac equation; which is distributed in a conical spectrum shown in Figure 6.

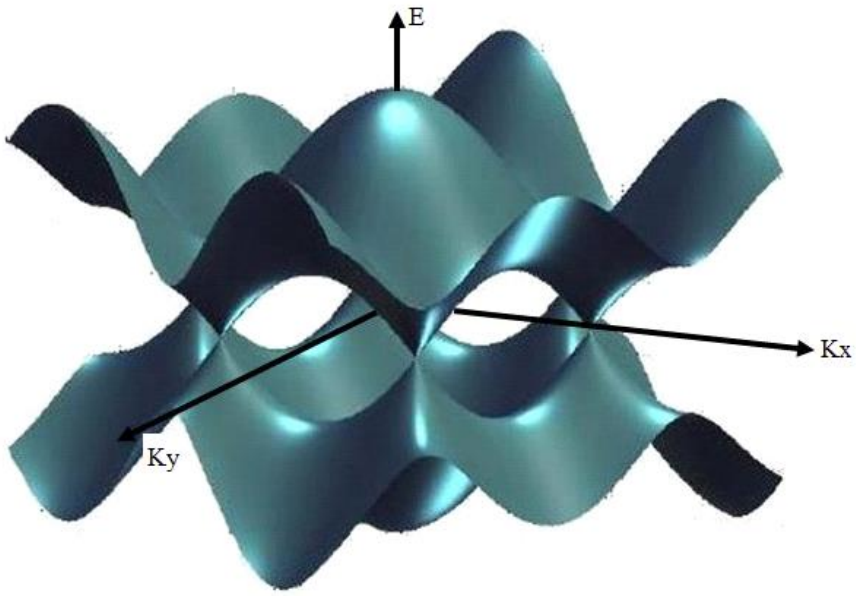

Figure 6: Band structure of graphene; energy *versus* particle momentum (Sadurní et al., 2015).

Generally there are some basic operational principles of graphene based on its electronic properties. These mainly depending on five different molecular interactions such as: electrostatic interaction, hydrophobic effect, π–π bonding, hydrogen bonding, and covalent bonding. The change in electrical conductivity of graphene is associated with adsorption of chemical substances on its surface (Varghese et al., 2015). Graphene and its derivatives, possess special intrinsic properties such as a two dimensional material with maximum surface to volume ratio, highly conductive in case of pristine graphene and reduced graphene oxide. Pristine graphene has few crystal defects with low level of noise and they allow four probe measurements (Tian et al., 2017). All of these features contribute to make a unique combination that maximizes the intended nanoadsorption and photocatalytic activities with some moderate functionalization.

The distinctive electronic, thermal and mechanical properties of graphene make it a very promising candidate for a wide range of applications in nanoscience and nanotechnology. The versatile properties of graphene are very well documented in the exponentially growing scientific literature (Seekaew et al., 2019). Some of its interesting properties and its technological implications are discussed hereafter.

2.1.4.1 Electronic Properties

Graphene has immense potential for electronics for an extraordinarily high mobility of its charge carriers at room temperature. When Si-based technology is approaching its

fundamental limits, graphene seems to be an ideal candidate to take over from silicon (Ghori et al., 2018). Yet, graphene is semi-metallic with no band gap, which severely limits its applications in electronics due to its high leakage current in many applications. The electronic band gap plays a central role in modern device physics and technology and controls the performance of semiconductor devices (Castro Neto et al., 2009). Moreover, it is a property inherent to semiconductors and insulators which considerably govern their transport and optical properties. It has been possible to open and tune the band gap of graphene bilayers by applying an electric field or by doping. These results have profound implications for potential utilization of graphene in electronics. The structure of graphene can be tailored to change its electronic properties (spectrum) by several means (Molitor et al., 2011). The structural manipulation may induce optical properties (i.e. band-gap opening), which in turn gets incorporated into it, resulting in its potential for opto-electronic applications.

One of the most useful properties of graphene is that it is a zero-overlap semimetal (with both holes and electrons as charge carriers) with very high electrical conductivity Zhen & Zhu, 2018). Carbon atoms have a total of 6 electrons; 2 in the inner shell and 4 in the outer shell. The 4 outer shell electrons in an individual carbon atom are available for chemical bonding, but in graphene, each atom is connected to 3 other carbon atoms on the two dimensional plane, leaving 1 electron freely available in the third dimension for electronic conduction. These highly-mobile electrons are called pi (π) electrons and are located above and below the graphene sheet. These pi orbitals overlap and help to enhance the carbon to carbon bonds in graphene. Fundamentally, the electronic properties of graphene are dictated by the bonding and anti-bonding (the valance and conduction bands) of these pi orbitals.

Combined research over the last 50 years has proved that at the Dirac point in graphene, electrons and holes have zero effective mass. This occurs because the energy – movement relation (the spectrum for excitations) is linear for low energies near the 6 individual corners of the Brillouin zone. These electrons and holes are known as Dirac fermions, or Graphinos, and the 6 corners of the Brillouin zone are known as the Dirac points. Due to the zero density of states at the Dirac points, electronic conductivity is actually quite low. However, the Fermi level can be changed by doping (with electrons or holes) to create a material that is potentially better at conducting electricity than, for example, copper at room temperature (De & Mayado, 2016b; Veligura, 2007b).

Tests have shown that the electronic mobility of graphene is very high, with previously reported results above 15,000 $cm^2V^{-1}s^{-1}$ and theoretically potential limits of 200,000 $cm^2V^{-1}s^{-1}$ (limited by the scattering of graphene's acoustic photons). It is reported that graphene electrons act very much like photons in their mobility due to their lack of mass. These charge carriers are able to travel sub-micrometer distances without scattering; a phenomenon known as ballistic transport. However, the quality of the graphene and the substrate that is used will be the limiting factors. With silicon dioxide as the substrate, for example, mobility is potentially limited to 40,000 $cm^2V^{-1}s^{-1}$ (Castro Neto et al., 2009).

2.1.4.2 Optical Properties

The interaction of graphene with electromagnetic radiation is fascinating due to the two-dimensional confinement of electrons and the exceptional band structure of graphene. Graphene has a simple band structure with zero band-gap, but its optical response is nontrivial (Falkovsky, 2008). The band structure of graphene consists of completely filled conduction band and empty valence band which cross linearly at the Dirac point. The optical absorption of pristine graphene is attributed to the interband and intraband transitions. For single-layer graphene, absorption in the visible spectral region is negligibly small and also frequency independent (Kavitha & Jaiswal, 2016). However, this negligibly small absorption must be seen in light of the single-atom thickness of the absorbing layer. With this thickness is taken into account, it is not difficult to see that the light-matter interaction in graphene is rather extraordinarily large. On substrates with low roughness, graphene can be visualized under white light illumination, despite being a single atom thick layer. The Fermi-level can be easily tuned by electrostatic gating or equivalently by electron/hole chemical doping, which brings about large control over its optical properties. In the far infrared region absorption can be explained within a Drude model and it can be tuned over a broad terahertz frequency range by tailoring graphene nanostructures and electrostatic gating (Chiu et al., 2016). When illuminated with ordinary light, the photogenerated charge carriers thermalize, and subsequently cool down non-radiatively to form a non-equilibrium distribution near the Dirac point; this gives rise to hot luminescence. When it is illuminated with ultra-short laser pulses, larger concentrations of thermalized electrons are obtained and this saturates further absorption of light due to Pauli blocking (Bennaceur et al., 2011). Graphene's ability to absorb a rather large 2.3% of white light is also a unique and interesting property, especially considering that it is only 1 atom thick. This is due to its aforementioned electronic

properties; the electrons acting like massless charge carriers with very high mobility. A few years ago, it was proved that the amount of white light absorbed is based on the Fine Structure Constant, rather than being dictated by material specifics. Adding another layer of graphene increases the amount of white light absorbed by approximately the same value (2.3%). Graphene's opacity of $\pi\alpha \approx 2.3\%$ equates to a universal dynamic conductivity value of $G=e^2/4\hbar$ (±2-3%) over the visible frequency range.

2.1.4.3 Mechanical Properties

Another of graphene's stand-out properties is its inherent strength. Due to the strength of its 0.142 Nm-long carbon bonds, graphene is the strongest material ever discovered, with an ultimate tensile strength of 130,000,000,000 Pascals (or 130 giga pascals), compared to 400,000,000 for A36 structural steel, or 375,700,000 for Aramid (Kevlar). Not only is graphene extraordinarily strong, it is also very light at 0.77 milligrams per square meter (for comparison purposes, 1 square meter of paper is roughly 1000 times heavier). It is often said that a single sheet of graphene (being only 1 atom thick), sufficient in size enough to cover a whole football field, would weigh under 1 single gram (Chen & Cheung, 2016b).

What makes this particularly special is that graphene also contains elastic properties, being able to retain its initial size after strain. In 2007, Atomic force microscopic (AFM) tests were carried out on graphene sheets that were suspended over silicone dioxide cavities. These tests showed that graphene sheets (with thicknesses of between 2 and 8 Nm) had spring constants in the region of 1-5 N/m and a Young's modulus (different to that of three-dimensional graphite) of 0.5 TPa. Again, these superlative figures are based on theoretical prospects using graphene that is unflawed containing no imperfections whatsoever and currently very expensive and difficult to artificially reproduce, though production techniques are steadily improving, ultimately reducing costs and complexity (Lu et al., 2016; Papageorgiou et al., 2017).

2.1.4.4 Thermal Properties

Thermal transport in graphene is a thriving area of research, thanks to graphene's extraordinary heat conductivity properties and its potential for use in thermal management applications. The measured thermal conductivity of graphene is in the range 3000 - 5000 W/mK at room temperature, an exceptional figure compared with the thermal conductivity of pyrolytic graphite of approximately 2000 $W \cdot m^{-1} \cdot K^{-1}$ at room temperature. There are,

however, other researches that estimate that this number is exaggerated, and that the in-plane thermal conductivity of graphene at room temperature is about 2000–4000 $W \cdot m^{-1} \cdot K^{-1}$ for freely suspended samples (Fu et al., 2020). This number is still among the highest of any known material. Graphene is considered an excellent heat conductor, and several studies have found it to have unlimited potential for heat conduction based on the size of the sample, contradicting the law of thermal conduction (Fourier's law) in the micrometer scale. In both computer simulations and experiments, the researchers found that the larger the segments of graphene, the more heat it could transfer (Zhang et al., 2018). Theoretically, graphene could absorb an unlimited amount of heat. The thermal conductivity increases logarithmically, and researchers believe that this might be due to the stable bonding pattern as well as being a 2D material. As graphene is considerably more resistant to tearing than steel and is also lightweight and flexible, its conductivity could have some attractive real-world applications. Some of the potential applications for graphene-enabled thermal management include electronics, which could greatly benefit from graphene's ability to dissipate heat and optimize electronic function. In micro- and nano-electronics, heat is often a limiting factor for smaller and more efficient components. Therefore, graphene and similar materials with exceptional thermal conductivity may hold an enormous potential for this kind of applications (Balandin, 2011).

2.1.5 Characterization of Graphene and Its Derivatives

The unique chemical, mechanical, optical, structural thermal and electronic properties of graphene are some of the reasons why it can be readily characterized by a wide variety of experimental techniques. Tunneling electron microscopy (TEM) images are formed by the electron interaction with materials when an electron beam is transmitted through a material specimen. TEM is one of the techniques widely used to study structural quality and the layer number of graphene. An example is shown in Figure 7. The layer number of graphene in dimethyl sulfoxide (DMSO) solution can be clearly seen from the TEM image. Three, four, five, and six layers of graphene can be observed as three, four, five, and six dark fringes, respectively.

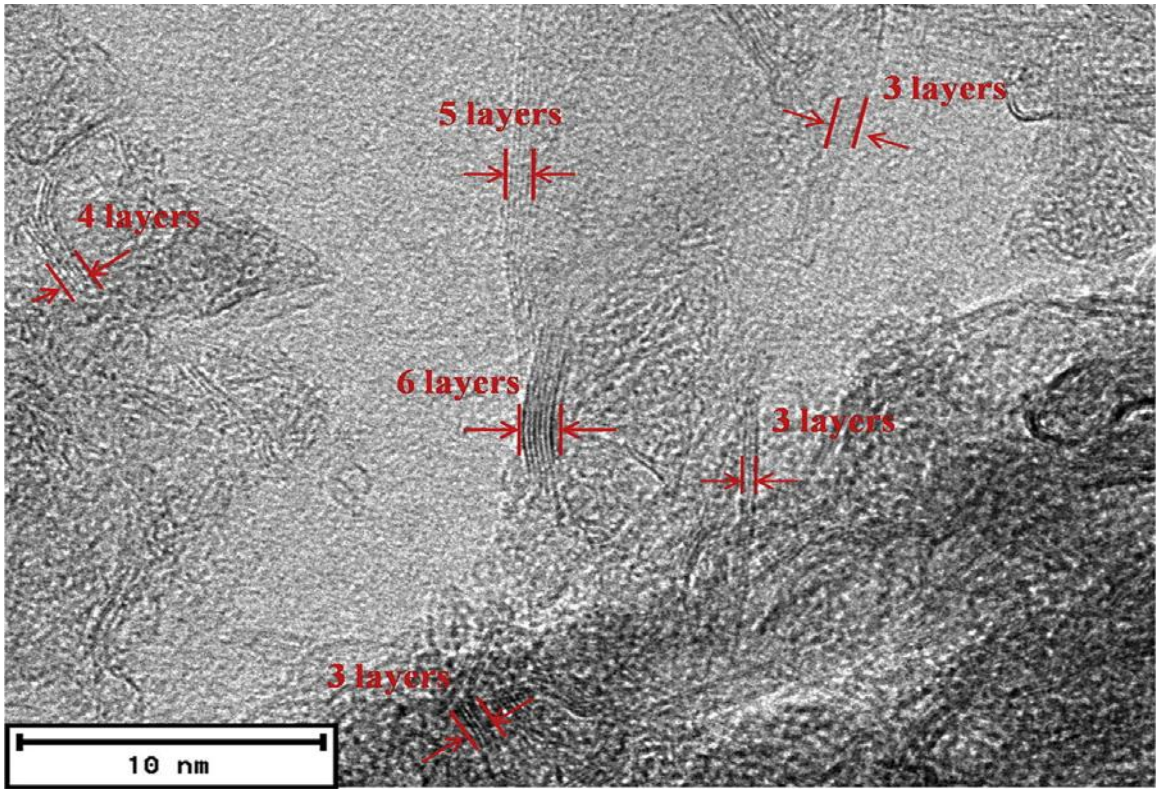

Figure 7: A Tunneling electron microscopy image of graphene in dimethyl sulfoxide (Sur et al., 2016).

Morphology of graphene is mostly studied using scanning electron microscopy (SEM) images. SEM imaging has some advantages for detecting impurities, folds, and discontinuities of synthesized graphene on different substrates. The difficulty of graphene study by SEM is resolution limitation of ultrathin graphene layer imaging. Figure 8 shows SEM images of graphene films with different numbers of layers on the alumina substrate. In the case of monolayer and bilayer graphene, the porous alumina surface behind the sheets can be seen through. However, the porous alumina surface cannot be obviously seen from the SEM image if the number of graphene layers is more than three.

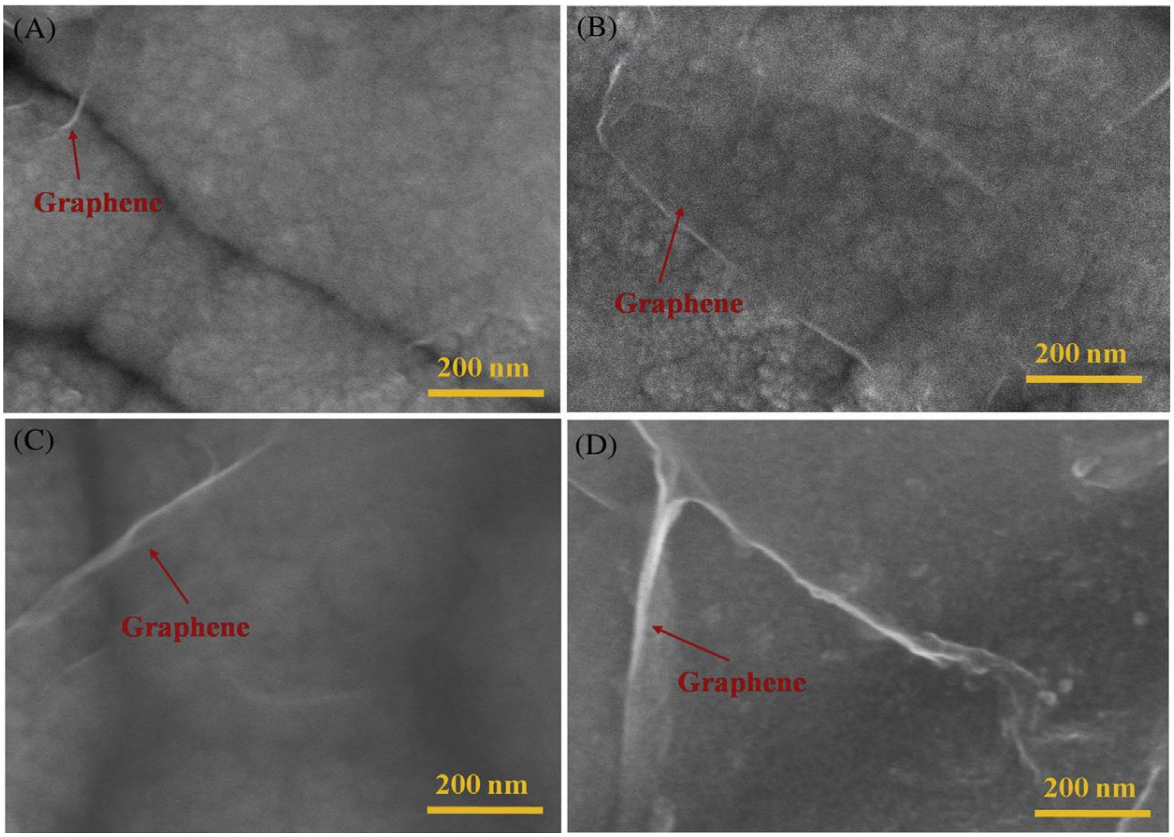

Figure 8: Scanning electron microscopy (SEM) images of (A) monolayer, (B) bilayer, (C) three-layer, and (D) multilayer graphene films on alumina substrate (Sur et al., 2016).

The oxygen functionalities are very obvious in the furrier transform infrared spectroscopy (FTIR) spectrum of GO and rGO since multiple peaks at 3400 cm^{-1} (O-H stretching vibrations), at 1720 cm^{-1} (C=O stretching vibrations) and at 1060 cm^{-1} (C-O stretching vibrations) amongst others, can be seen in Figure 9. The weak band displayed at 1359 cm^{-1} corresponds to the stretching vibration result of C-OH of carboxyl originating from carboxylic acids. The bands for the C-H symmetric and asymmetric stretching frequencies were observed at 2863 and 2923 cm^{-1} respectively in both GO and rGO. The FT-IR spectral record of rGO is shown in Figure 9. As the oxygen containing functional groups were removed by the reducing agent, the characteristic absorption peaks of oxide groups decreased significantly and the CO_2 peak at 2340 cm^{-1} vanished indicating the successful reduction of GO. The sharp band formed at 1570 cm^{-1} was attributed to (C=C) stretching.

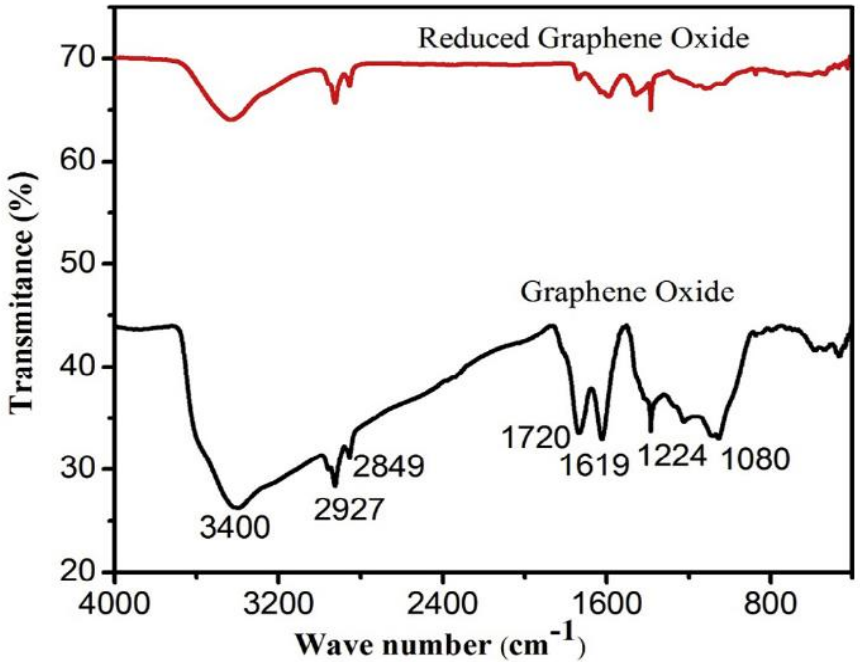

Figure 9: Furrier transforms infrared spectroscopy spectra of GO and rGO (Reeves, 2010).

The ^{13}C NMR spectrum of bulk GO has been used to study its structure and gives three characteristic peaks at 60, 70 and130 ppm, assigned to C-OH, C-O-C and C=C groups. The structural model that is most widely accepted is the one of Lerf, who used ^{13}C NMR to characterize the material in detail. Fully-oxidized GO exhibits an atomic C to O ratio of around 2:1, while it can form stable solutions. Alcohols and epoxides are its main functional groups, while carboxylic and ketone groups can be found on the edges of GO. Rourke et al. have shown that GO that is prepared by the popular Hummers method, contains functional graphene sheets which consist of strongly-bound oxidative debris. The removal of the oxidative debris can be performed with a simple base wash, while the debris with higher levels of functionalization can be dissolved fully into water, leaving a suspension of functionalized graphene sheets. This process also enables deoxygenation, since it increases the C/O ratio (Casabianca et al., 2010).

The Raman spectrum of GO is also different from that of graphene, since a strong D band that is not present in graphene can be seen in GO, indicating the formation of the sp^3 bonds as shown in Figure 10. There is also the broadening of the G band, compared to graphene. Moreover, the relative intensities of the G and D bands can be used for the evaluation of the defects that are formed during the reduction of GO.

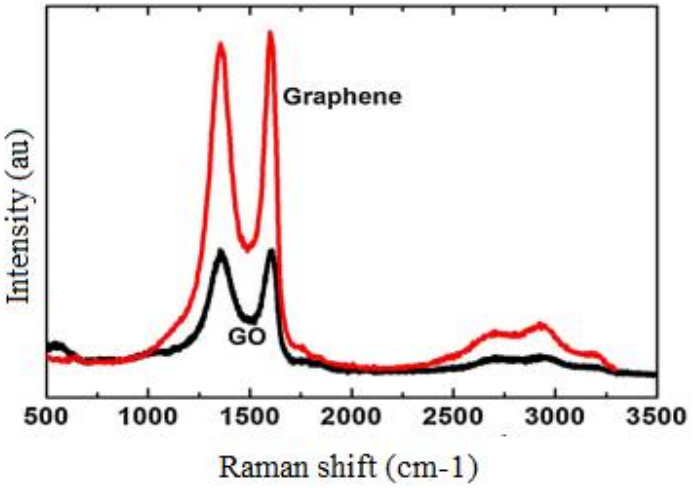

Figure 10: Raman spectra of graphene oxide and graphene (Reeves, 2010).

UV–VIS spectroscopy can be also used for the evaluation of the GO dispersion and of the reaction process. The electronic conjugation of GO can be assessed from the shifting of the characteristic peak at 230 nm towards higher wavelengths 262 nm in rGO and the increasing of the intensity of absorbance, indicating the restoration of the conjugation as shown in Figure 11.

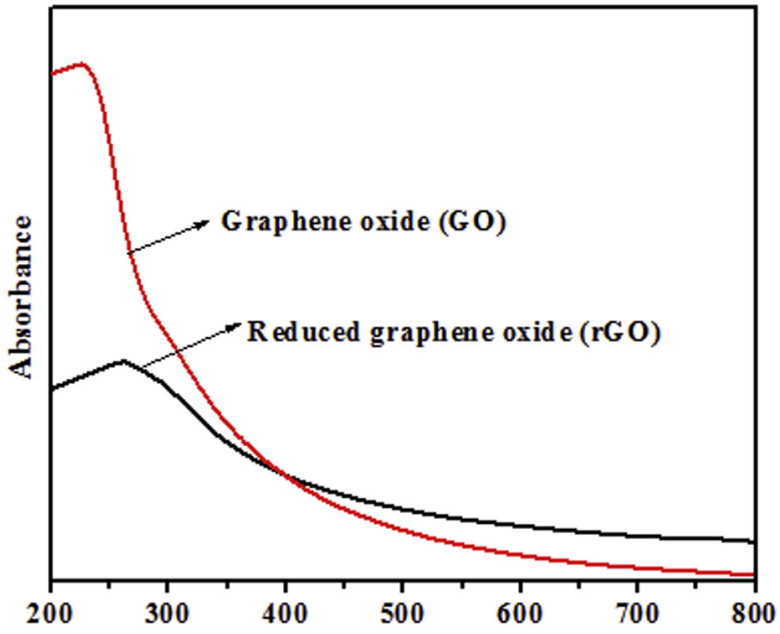

Figure 11: UV-Vis absorbance spectra of graphene oxide and reduced graphene oxide (MM et al., 2017).

Photoluminescence (PL) measurements are also important for the characterization of solutions of GO and especially base-washed GO. As shown in Figure 12 (a) GO and (b) rGO the oxidative debris of as-produced GO fluoresces much more intensely than the as-produced rGO with a dispersive emission profile shifting to lower wavelength as the

excitation wavelength is decreased and behaving as an ensemble of nano meter sized fluorophores.

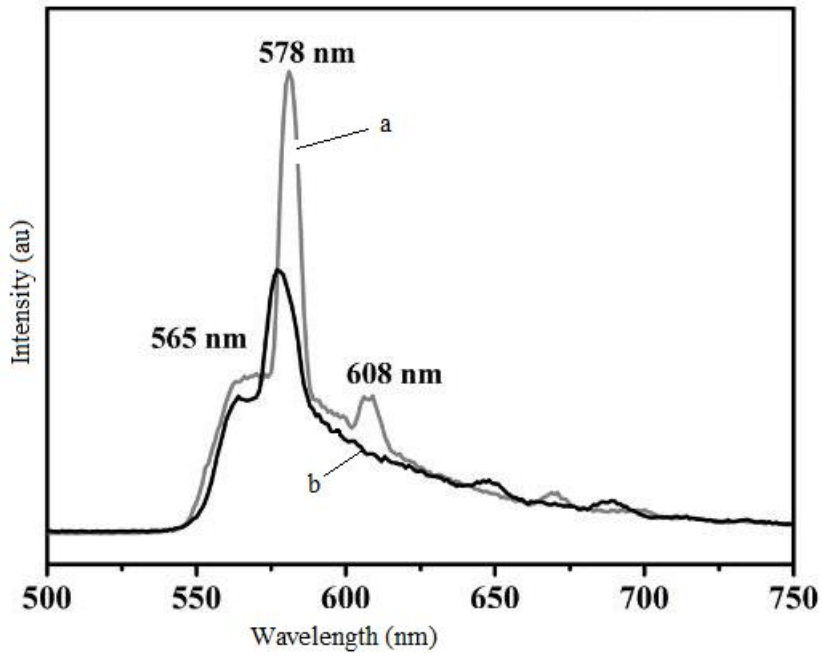

Figure 12: Photoluminescence spectra of GO (a) and rGO (b) paper (MM et al., 2017).

X-ray diffraction can be used to monitor the transformation from graphite to GO since the strong Bragg peak of graphite at (2θ=26°) disappears after the conversion procedure and a new peak appears at lower angles as shown in Figure 13. Moreover, the inter-layer distance can be calculated with the use of Bragg's law and generally ranges from 0.6 to 1.0 nm, depending on the preparation method.

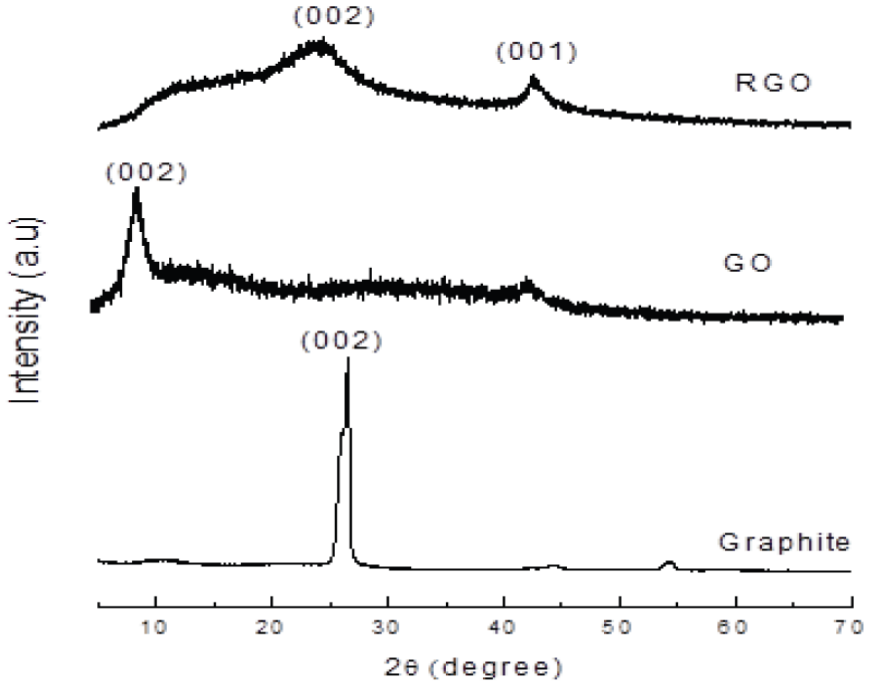

Figure 13: X-ray diffraction spectra of graphite, GO, and rGO (Allen et al., 2010).

Thermogravimetric analysis is also useful since the presence of oxygen functionalities in GO enable the decomposition of the material at lower temperatures and in general, in three steps as shown in Figure 14; the first one corresponds to the removal of moisture, the second one corresponds to the pyrolysis of the oxygen-containing groups and the third one is attributed to the decomposition of the more stable oxygen functionalities such as the carbonyls and phenols.

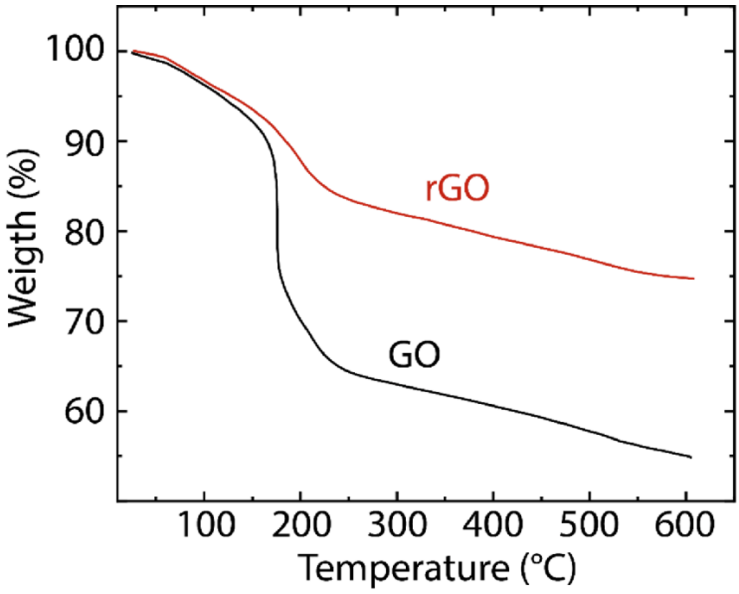

Figure 14: Thermogravimetric (TGA) analysis of GO and rGO (Allen et al., 2010).

2.1.6 Applications of Graphene and Its Derivatives

Graphene and its derivate recently gained science and engineering awareness due to its numerous applications. The discovery of graphene is rightly regarded as a milestone in the world of material science; as can be seen in the worldwide attention, the material has received in the fields of electronics, photonics, capacitors/supercapacitors, biosensing, etc. They are used in numerous applications as illustrated below. In this section, applications of graphene and its derivatives are discussed in detail. These applications include photocatalysis, electronics, gas sensing, graphene-based heterogeneous electrodes for energy storage devices, adsorption, sound devices etc.

Graphene membranes have been used for water filtration, gas separation and desalination projects (Jilani, Hafiz, et al., 2018). If used on food and pharmaceutical packages, the transfer of water and oxygen can be stopped and perishable goods preserved for longer time by Graphene coatings (Nyangiwe, 2012a). Graphene-based composites for instance paint combined with graphene could possibly stop rust. Graphene batteries have been

confirmed that it increases the lifespan of batteries and ensure quicker charging capacity. Graphene supercapacitors provide huge amounts of power using much less energy (Mao et al., 2013). It could potentially be used in the storage of solar and wind power. In a Medical science it has been successfully used in tissue engineering, biomicrorobotics and, due to the atomic thickness and modifiable chemistry, it makes an excellent candidate for mammalian and diagnosis devices (Hakimi & Alimard, 2012). Graphene sensors have a superior capacity to detect objects on a molecular level. The use of graphene could mean unbreakable touch screens, flexible and wearable technology and speedy graphene circuits and computer chips (Kumar et al., 2013).

GO were used in electronic fabrications as initial materials (P. Kumar et al., 2013). Electronic devices such as graphene effect transistors (GFETs) and field effect transistors (FETs) are graphene-based (Sadurn´ı, E. Rivera-Moci˜nos, 2015). Reduced graphene oxides (rGO) are used as chemical sensors. Functionalized graphene oxide in conjunction with glucose oxidase deposited on electrode material is used as an electrochemical glucose sensor. They are widely used in the manufacturing of electronic devices like light-emitting diodes (LEDs) and solar cells. Reduced graphene oxide dispersed in a solvent can be used in the production of the transparent electrode, which is an alternative transparent electrode like FTO and ITO. Reduced graphene oxide nanocomposites have a high surface area and good conductivity, which suited them for use in supercapacitors and lithium-ion batteries with good energy storage capacity. GO-based supercapacitors and lithium-ion batteries possess high-energy storage capacity, long life span, and good cycle stability. As far, back as the 1960s, scientists have started studying graphite oxide usage in desalination of water. In 2011, some group of researchers employed the principle of reverse osmosis using GO to achieve the same goal. It was discovered that graphite allows water to pass through but retain some larger ions. Its narrow mono- or bilayer capillaries allow water but restrain heavy ions (Díez-Pascual, 2021).

Moreover, in the year 2015, a group of scientists also purified water using graphene tea by removing 95% of heavy metal ions in water solution. It was reported that in 2006, engineers fabricated graphene-based thin film powered by solar energy that possesses the quality of filtering dirty and salty water. These films are non-heavy and can be easily produced on a large scale. Graphite and its derivative like GO are widely used in the biomedical field as a constituent in the drug delivery system. Magnetite stacked with GO

and doxorubicin hydrochloride (DXR) drug adsorbed onto the system is used as anticancer treatment by targeting it to a specific site to kill cancer cells. Graphene oxide and reduced graphene oxide have been incorporated into many gadgets. These GO-/rGO-based gadgets are fabricated with the quality to identify biologically significant molecules. GO/rGO uses fluorescence resonance energy transfer (FRET) characteristics to work effectively as a biosensor. All elements that form part of GO or rGO functional groups can be effectively stored in their sheets and extracted later for use and are also being explored for their applications in hydrogen storage (Abdel Maksoud et al., 2021).

Recently, the science of plasmonics discovered that near field infrared optical microscopy and infrared spectroscopy of graphene provide accommodations for plasmonic surface mode. Scientists recently found out that graphene lubricants perform better than regularly used graphite lubricants. A graphene lubricant applied to a ball and bearing roller or steel ball and steel disc lasted for 6500 cycles, while our usually used graphite lubricants lasted only for 1000 cycles. A heavenly crammed graphene layer deposited on glass substrates absorbs radio waves of the wavelength range of 125–165 GHz bandwidth by 90%. In our modern houses, graphene serves as roof, door, and window coatings to safeguard houses from radio wave interference. A nanoantenna called graphene-based plasmonic nanoantenna (GPN) operates on a wavelength of millimeter within the radio wavelength range. This nanoantenna is better than our conventional antennas because its operational surface plasmon polaritons wavelength is much smaller compared to the wavelength of electromagnetic waves propagating at the same frequency. Our conventional antenna operational frequencies range from 100 to 1000, which is very huge compared to GPNs. Graphene, has been predicted as a good candidate for the manufacturing of electrostatic audio microphones and speakers due to their lightweight, which provides moderately good frequency response. In 2015 an A model audio ultrasonic microphone and the speaker was fabricated; it operates at a frequency range of 20–500 kHz. Its performance operation was up to 99% efficiency, good and uniform frequency output throughout the audible range (Huang, 2016).

2.1.7 Organic Dyes.

The dyes are natural and synthetic compounds that make the world more beautiful through coloured products. The textile dyes represent a category of organic compounds, generally considered as pollutants, presented into wastewaters resulting mainly from processes of chemical textile finishing. The textile coloration industry is characterized by a very large

number of dispersed dye houses of small and medium size that use a very wide range of textile dyes (Carmen & Daniel, 2012a).

The nature and origin are firstly considered as criteria for the general classification in natural and synthetic textile dyes. The natural textile dyes were mainly used in textile processing until 1856, beginning in 2600 BC when was mentioned the use of dyestuff in China, based on dyes extracted from vegetable and animal resources. It is also known that the Phoenicians were used Tyrian purple produced from certain species of crushed sea snails in the 15th century BC, and indigo dye produced from the well-known indigo plant since 3000 BC. The dyes from madder plants were used for wrapping and dyeing of Egyptian mummies clothes and also of Incas fine textures in South America (Marechal et al., 2012).

The synthetic dyes were firstly discovered in 1856, beginning with ‚mauve ‘dye (aniline), a brilliant fuchsia colour synthezed by W.H. Perkin (UK), and some azo dyes synthezed by diazotization reaction discovered in 1958 by Gries (Germany) (Luongo, 2015). These dyes are aromatic compounds produced by chemical synthesis, and having into their structure aromatic rings that contain delocated electrons and also different functional groups. Their color is due to the chromogene-chromophore structure (acceptor of electrons), and the dyeing capacity is due to auxochrome groups (donor of electrons).

The chromogene is constituted from an aromatic structure normally based on rings of benzene, naphthaline or antracene, from which binding chromofores that contain double conjugated links with delocated electrons are obtained (Saini, 2017). The chromofore configurations are represented by the azo group (-N=N-), ethylene group (-C=C-), methine group ($-CH_3$), carbonyl group (-C=O), carbon-nitrogen (-C=NH; -CH=N-), carbon-sulphur (-C=S; -C≡S-S-C≡), nitro ($-NO_2$; -NO-OH), nitrozo (-N=O; =N-OH) or chinoid groups. The auxochrome groups are ionizable groups that confer to the dyes the binding capacity onto the textile material. The usual auxochrome groups are: $-NH_2$ (amino), -COOH (carboxyl), $-SO_3H$ (sulphonate) and -OH (hydroxyl) (Mustereț & Teodosiu, 2007). Five examples of textile dyes are presented in Figure 15**.**

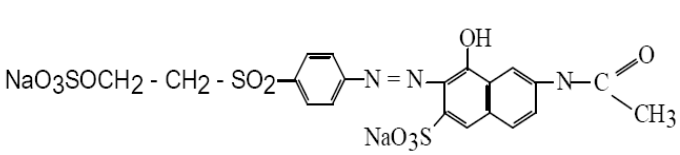

Reactive Orange 16
C.I. 18097
Anionic monoazo reactive dye;
MW = 617.54 g/mol;
λ_{max} = 495 nm

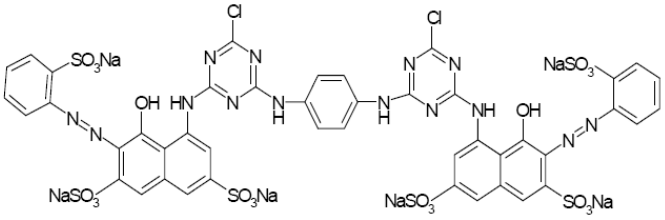

Brilliant Red HE-3B
(Reactive Red 120)
C.I. 25810
Anionic, bifunctional
azo reactive dye;
MW = 1463 g/mol;
λ_{max} = 530 nm

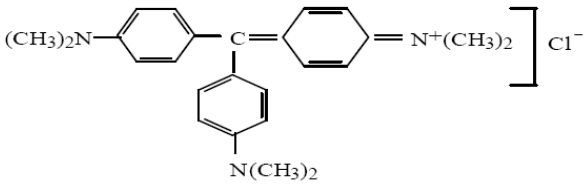

Crystal Violet
(Basic Violet 3)
C.I. 42555
Cationic triphenylmethane dye;
MW = 407.99 g/mol;
λ_{max} = 590 nm

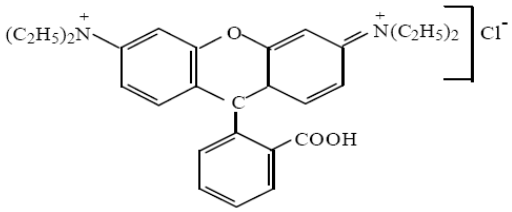

Rhodamine B
(Basic Violet 10)
C.I. 45170
Cationic, Xantenic dye;
MW =479.2 g/mol;
λ_{max} = 550 nm

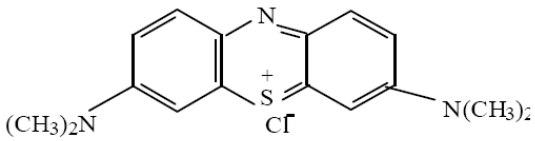

Methylene Blue
(Basic Blue 9)
C.I. 52015
Cationic, phenothiazine dye;
MW =319.85 g/mol;
λ_{max}= 660 nm

Figure 15: Chemical structure and principal characteristics of different textile dyes (Carmen & Daniel, 2012a).

The major textile dyes can be included in the two high classes: azo and anthraquinone. These two classes of dyes comprises about 65-75% of the total textile dyes. The azo dyes are characterized by reactive groups that form covalent bonds with HO^-, HN^-, or HS^- groups in fibres such as cotton, wool, silk, nylon. Azo dyes are mostly used for yellow, orange and red colors. Anthraquinone dyes constitute the second most important class of textile dyes, after azo dyes, and have a wide range of colors in almost the whole visible spectrum, but they are most commonly used for violet, blue and green colors (Mustereţ & Teodosiu, 2007).

2.1.8 Polluting effects of organic dyes

The environmental issues associated with residual dye content or residual colour in treated textile effluents are always a concern for each textile operator that directly discharges, both sewage treatment works and commercial textile operations, in terms of respecting the colour and residual dye requirements placed on treated effluent discharge. Dye concentrations in watercourses higher than 1 mg/L caused by the direct discharges of textile effluents, treated or not, can give rise to public compliant. High concentrations of textile dyes in water bodies stop the reoxygenation capacity of the receiving water and cutoff sunlight, thereby upsetting biological activity in aquatic life and also the photosynthesis process of aquatic plants or algae. The colour in watercourses is accepted as an aesthetic problem rather than an eco-toxic hazard. Therefore, the public seems to accept blue, green or brown colour of rivers but the 'non-natural' colour as red and purple usually cause most concern (Mustereţ & Teodosiu, 2007).

The polluting effects of dyes against aquatic environment can be also the result of toxic effects due to their long time presence in environment (i.e. half-life time of several years), accumulation in sediments but especially in fishes or other aquatic life forms, decomposition of pollutants in carcinogenic or mutagenic compounds but also low aerobic biodegradability. Due to their synthetic nature and structure mainly aromatic, most of dyes are non-biodegradable, having carcinogenic action or causing allergies, dermatitis, skin irritation or different tissular changes. Moreover, various azo dyes, mainly aromatic compounds, show both acute and chronic toxicity. High potential health risk is caused by adsorption of azo dyes and their breakdown products (toxic amines) through the gastrointestinal tract, skin, lungs, and also formation of hemoglobin adducts and disturbance of blood formation (Pereira & Alves, 2012).

Several azo dyes cause damage of DNA that can lead to the genesis of malignant tumors. Electron-donating substituents in ortho and para position can increase the carcinogenic potential. The toxicity diminished essentially with the protonation of aminic groups. Some of the best known azo dyes such as Direct Black 38 azo dye, precursor for benzidine; azodisalicylate, precursor for 4-phenylenediamine and their breakdown derivatives inducing cancer in humans and animals are benzidine and its derivatives, and also a large number of anilines including 2-nitroaniline, 4-chloroaniline, 4, 4'-dimethylendianiline, 4-phenylenediamine, etc (Description, 2007).

In different toxicological studies are indicated that 98% of dyes has a lethal concentration value (LC50) for fishes higher than 1 mg/L, and 59% have an LC50 value higher than 100 mg/L (i.e. 31% of 100-500 mg/L and 28% higher than 500 mg/L). Other ecotoxicological studies indicated that over 18% of 200 dyes tested in England showed significant inhibition of the respiration rate of the biomass (i.e. wastewater bacteria) from sewage, and these were all basic dyes. The bioaccumulation potential of dyes in fish was also an important measure estimating the bioconcentration factor (dye concentration in fish/dye concentration in water). No bioaccumulation is expected for dyes with solubility in water higher than 2000 mg/L. Dyes are not biodegradable in aerobic wastewater treatment processes and some of them may be intactly adsorbed by the sludge at wastewater biological treatment (i.e. bioelimination by adsorptive removal of dyes) (Pereira & Alves, 2012).

2.1.9 Removal of dyes from industrial wastewater

The textile organic dyes must be separated and eliminated (if necessary) from water but especially from industrial wastewaters by effective and viable treatments at sewage treatment works or on site following two different treatment concepts as:

1. Separation of organic pollutants from water environment, or
2. The partial or complete mineralization or decomposition of organic pollutants. Separation processes are based on fluid mechanics (sedimentation, centrifugation, filtration and flotation) or on synthetic membranes (micro-, ultra- and nanofiltration, reverse osmosis). Additionally, physico-chemical processes (i.e. adsorption, chemical precipitation, coagulation-flocculation, and ionic exchange) can be used to separate dissolved, emulsified and solid-separating compounds from water environment (Assmuth et al., 2011).

2.1.10 Adsorption

One of the most effective and proven treatment with potential application in textile wastewater treatment is adsorption. This process consists in the transfer of soluble organic dyes (solutes) from wastewater to the surface of solid, highly porous, and particles (the adsorbent). The adsorbent has a finite capacity for each compound to be removed, and when is ‘spent’ must be replaced by fresh material (the spent adsorbent must be either regenerated or incinerated).

Adsorption is an economically feasible process for dyes removal and/or decolourization of textile effluents being the result of two mechanisms: adsorption and ion exchange. The principal influencing factors in dye adsorption are: dye/adsorbent interaction, adsorbent surface area, particle size, temperature, pH, and contact time. Adsorbents which contain amino nitrogen tend to have a significantly larger adsorption capacity in acid dyes.

The most used adsorbent is activated carbon, and also other commercial inorganic adsorbents. Some 'low cost' adsorbents of industrial or agricultural wastes (i.e. peat, coal ashes, refused derived coal fuel, clay, bentonite and modified bentonite, red soil, bauxite, ebark, rice husk, tree barks, neem leaf powder, wood chips, ground nut shell powder, rice hulls, bagasse pith, wood sawdust, grounded sunflower seed shells, other ligno-cellulosic wastes, etc.) are also used for removal of dye and organic coloured matter from textile effluents. The use of these materials is advantageous mainly due to their widespread availability and cheapness. Sometimes the regeneration is not necessary and the 'spent' material is conventionally burnt although there is potential for solid state fermentation (SSF) for protein enrichment. The use of 'low cost' adsorbents for textile dye removal is profitable but requires huge quantity of adsorbents, being lower efficient than activated carbon (Assmuth et al., 2011).

2.1.11 Irradiation

The irradiation treatment is a simple and efficient procedure for eliminating a wide variety of organic contaminants, and as well disinfecting harmful microorganism using gamma rays or electron beams (e.g., source for irradiation can be a monochromatic UV lamps working under 253.7 nm). A high quantity of dissolved oxygen is required for an organic dye to be effectively broken down by irradiation. The dissolved oxygen is consumed very rapidly and so a constant and adequate supply is required. Irradiation treatment of a secondary effluent from sewage treatment plant reduced COD, TOC and colour up to 64%, 34% and 88% respectively, at a dose of 15 K Gy gamma-rays. The efficiency of irradiation treatment increases when used catalyst is titanium dioxide. A lot of data are reported with the practical results obtained at the simple exposure of different dye solutions or dispersions and dye-containing textile wastewaters to sunlight for a period of a half, one or two months (direct photolysis with natural sunlight into open basins). All these reports indicated high removals of colour (>84%), dye destruction by photooxidation following first order kinetics at treatment of some vat dye effluents. But the direct photolysis of textile organic dye in the natural aquatic environment has proven difficult

due to strong dependence of the decay rates on dye reactivity and photosensitivity. Most of all commercial dyes are usually designed to be light resistant.

Therefore, the recent researches have been directed towards investigation of organic dye photodegradation by sensitizers or catalysts in aqueous/dispersion systems by UV irradiation. Moreover, there are reported high removal of indigo-colour when is initiated a laser fading process for indigo coloured denim textile mainly based on basic interaction of laser beam with indigo-coloured textile (Assmuth et al., 2011).

2.1.12 Membrane processes

The increasing of water cost and necessity of reduction of water consumption implies treatment process which is integrated with in-plant water circuits rather than subsequent treatment. From this point of view, membrane filtration offers potential application in combination with other textile effluent treatments.

Membrane processes for wastewater treatment are pressure-driven processes, capable to clarify, concentrate, and most importantly separate dye discontinuously from effluent. These are new technologies, which can restrict organic contaminants and microorganisms presented in wastewater (i.e. color removal, BOD reduction, salt reduction, Polyvinyl Acetate (PVA) recovery, and latex recovery). The common membrane filtration types are: micro-filtration (MF), ultra-filtration (UF), nano-filtration (NF), and reverse osmosis (RO). The choice of the membrane process must be guided by the required quality of the final effluent (Pinto, 2020).

2.1.13 Oxidative processes

Chemical oxidation represents the conversion or transformation of pollutants by chemical oxidation agents other than oxygen/air or bacteria to similar but less harmful or hazardous compounds and/or to short-chained and easily biodegradable organic components (aromatic rings cleavage of dye molecules). The modern textile dyes are resistant to mild oxidation conditions such those existing in biological treatment systems. Therefore, efficient dye and colour removal must be accomplished by more powerful oxidizing agents such as chlorines, ozone, Fenton reagents, UV/peroxide, UV/ozone, or other oxidizing procedures or combinations (Lellis et al., 2019).

2.1.14 Coagulation-flocculation and precipitation

It is clearly known that the coloured colloid particles from textile effluents cannot be separated by simple gravitational means, and some chemicals (e.g., ferrous sulphate, ferric

sulphate, ferric chloride, lime, polyaluminium chloride, polyaluminium sulphate, cationic organic polymers, etc.) are added to cause the solids to settle. These chemicals cause destabilisation of colloidal and small suspended particles (e.g. dyes, clay, heavy metals, organic solids, oil in wastewater) and emulsions entrapping solids (coagulation) and/or the agglomeration of these particles to flocs large enough to settle (flocculation) or highly improve further filtration. In the case of flocculation, anionic and non-ionic polymers are also used. The mechanism by which synthetic organic polymer removes dissolved residual dyes from effluents is best described in terms of the electrostatic attraction between the oppositely charged soluble dye and polymer molecules (Iwuozor, 2019). Many of the most problematic dye types, such as reactive dyes, carry a residual negative charge in their hydrolyzed dissolved form, and so positively charged groups on the polymers provide the necessary counter for the interaction and subsequent precipitation to occur. The immediate result of this coprecipitation is the almost instantaneous production of very small coloured particles, having little strength and breaking down at any significant disturbances. The agglomeration of the coloured precipitates by using appropriate high polyelectrolyte flocculants produces stable flocs. The main disadvantages of this treatment are the process control that is a little difficult, the potential affection of precipitation rate and floc size by impurities such as non-ionic detergents remaining in the effluent, and the sludge production which has to be settled, dewatered and pressed into a cake for subsequent landfilling tipping (Sun et al., 2019).

There are reports on the very effective chemical coagulation-flocculation (C-F) and precipitation of textile wastewater which reduced the load on the biological treatment, working with polyaluminium chloride along with an organic polymer (Lin & Chen, 1997) or ferrous/ferric chloride and a commercial organic coagulant aid at pH of 6.7-8.3 (colour removal > 80%) or alum at pH=8.2 (54-81% colour removal) with addition of bentonite (3 g/L) for Remazol Violet dye-containing effluent. Other efficient textile treatments mentioned by different textile operators consist in coagulation-flocculation followed by membrane technology (especially for recycling textile effluents) (Abdelrasoul et al., 2013; Ji & Zhao, 2017; Yao et al., 2020).

2.1.15 Biological treatments

Biological treatments are considered reproduction, artificially or otherwise, of selfpurification phenomena existing in natural environment. There are different biological treatments, performed in aerobic or anaerobic or combined anaerobic/aerobic conditions.

The processing, quality, adaptability of microorganisms and the reactor type are decisive parameters for removal efficiency. Biological treatment process for decolorization of industrial effluents is ambiguous, different and divergent. Dyes themselves are not biologically degradable since microorganisms do not use the coloured constituents as a source of food. The most currently used biodegradation involve aerobic microorganisms, which utilize molecular oxygen as reducing equivalent acceptor during the respiration process. But biodegradation in anaerobic environment conditions (anoxic and hypoxic environments) also occurs, and survival of microorganisms is possible by using sulphate, nitrates and carbon dioxide as electron acceptors (Carmen & Daniel, 2012b).

Research data indicates that certain dyes are susceptible to anoxic/anaerobic decolourization, and also that an anaerobic step followed by an aerobic step may represent a significant advancement in biological decolourization treatment in future. The treatment plant that receives dye-containing effluents has high potential to form toxic biodegradation products such as toxic amines, benzidine and its derivates, etc. To avoid that risk, anaerobic/aerobic sequential reactor systems seem to be an efficient procedure (i.e. efficient colour removal takes place during the anaerobic treatment, and high reduction of aromatic amines and other organic compounds occurs during the subsequent aerobic treatment). Under aerobic conditions, most of the azo dye metabolites are quickly degraded by oxidation of the substituents or of the side branches (Sandhya, 2010).

However, some of them are still rather recalcitrant. Successful removal of poorly degradable amines was often achieved by adaptation of microorganisms (i.e. acclimatization of biological sludge to nitroaniline containing wastewaters; after gradual adaptation, the microorganisms are able to eliminate 3- and 4-nitroaniline simultaneously). Difficult to be biodegraded are also the aromatic amines containing sulfo substituents in metha position (e.g., 3- aminobenzenesulfonate) that can be treated with good efficiencies with flow-through bioreactors within 28 days. Contrarily, some experimental results found anaerobic mineralization to be efficient for aromatic amines. The main advantage of biological treatment in comparison with certain physico-chemical treatments is that over 70% of organic matter expressed by COD-Cr may be converted to biosolids (Singh & Arora, 2011).

TiO_2 and ZnO have conventionally been used as a photocatalyst material for the photodegradation of harmful organic dyes. But, their practical applications are limited by

the absorption of only 3-4% of the solar spectrum. Recently, metal chalcogenides having formula $A_2^vB_3^{vI}$ (where, A = As, Sb, Bi and B = S, Se, Te) found wider applications in thermoelectric, electronic and optoelectronic devices3. Among them, bismuth sulfide (Bi_2S_3) a direct band gap (Eg ~1.3 eV) visible-NIR region active semiconductor has been emerged out as an efficient photocatalyst material. It consists of layered structure which is interconnected by Bi-S bonds. Owing to its narrow band gap and layered structure, it can be proven to be a very promising material in photocatalysis (Sharma & Khare, 2017).

2.1.16 Synthesis of Bi_2S_3

In many previous researches, three most common synthesis methods were used to produce Bi_2S_3. These methods were hydrothermal, microwave and sonochemical methods which were discussed thoroughly in this dissertation works. Hydrothermal is a unique method for fabricating nanostructures with specific and controlled morphologies, while predominant morphology in other methods like sol-gel, sonochemical is nanoparticle. Hydrothermal method provides preferred orientation morphology. In this method, because of some particular conditions such as high temperature and pressure, the nanoparticles grow insitu and form nanostructure shape. The synthesis of metal sulfide nanostructures using thioglycolic acid via hydrothermal method was reported repeatedly in recent years. It is revealed that thioglycolic acid acts as the oriented growth reactant during above process (Ghanbari et al., 2014; Liao et al., 2001; Wang et al., 2002).

As a representative of good semiconductors, bismuth sulfide (Bi_2S_3) has been attracting a considerable interest owing to its potential application in thermoelectric, electronic and optoelectronic devices and IR spectroscopy. In addition, it has an energy band gap of 1.3 to 1.7 eV, which is suitable for making photodiode arrays and photovoltaics. A band gap can be tuned depending on the size of the subcomponents. Bi_2S_3 nanowhiskers were synthesized using bismuth nitrate, thiourea, poly (N-vinyl-2-pyrrolidone) and N, N-dimethylformamide by microwave heating, but the products were not well crystallized. Bi_2S_3 nanorods were synthesized by microwave heating using bismuth nitrate, thioacetamide and formaldehyde. A single-crystalline Bi_2S_3 nanocrystals with urchin like and rod-like morphologies can be synthesized using Bi_2O_3, HCl, $Na_2S_2O_3$ and ethylene glycol (EG) by a simple and fast microwave heating method (Chen et al., 2013).

Crystallized bismuth sulfide has been prepared by thermal decomposition of bismuth dithiocarbamate complexes, metal ethylxanthate, Bi–thiourea complex, and

thiosulfatobismuth. However, high temperature is required, and the final products contain some impurities. Bi_2S_3 nanorods and Bi (Se, S) nanowires have been prepared by the hydrothermal and solvothermal preparation techniques, but those techniques need longer reaction time, higher temperature, and higher pressure. Conventionally, bismuth sulfide is prepared by direct element reaction in a quartz vessel at high temperature. The chemical deposition methods have been applied to prepare Bi_2S_3 through a reaction of bismuth salt complexed by triethanolamine (TEA) or ethylenediaminetetraacetic acid (EDTA) in an aqueous solution containing a sulfur source such as thioacetamide (TAA), thiourea, sodium thiosulfate, or gaseous H_2S. The powders obtained through this route are mostly amorphous or poorly crystallized. The chemical deposition of Bi_2S_3 in nonaqueous solution has also been reported. Colloidal suspensions of bismuth sulfide have been prepared in water at room temperature with a solution of $Bi(NO_3)_3$ and $Na_2S.9H_2O$ as the starting materials, but sodium hexametaphosphate is needed to stabilize Bi^{3+} and only colloidal particles can be obtained (Yuan et al., 2019).

Crystallized bismuth sulfide has been prepared by thermal decomposition of various precursors such as bismuth dithiocarbamate complexes, metal ethylxanthate, bismuth-thiourea complex, and thiosulfatobismuth. However, high temperature is required and the final products contain some impurities. The size and morphology of the products can be controlled by applying different reaction conditions including temperature, reaction time, and solvents. However, this method requires relatively high pressure, and it takes a long time for the reaction to be completed. However, the precursor compound $Bi\{S_2CN(CH_3)(C_6H_{13})\}_3$ must be prepared first. Ultrasound has become an important tool in chemistry in recent years. It has been extensively used to generate novel materials with unusual properties, because it causes the formation of particles with a much smaller size and higher surface area than those reported by other methods (Piras et al., 2014).

When solutions are exposed to strong ultrasound irradiation, bubbles are implosively collapsed by acoustic fields in the solution. High-temperature and high-pressure fields are produced at the centers of the bubbles. This effect is known as acoustic cavitation. The temperature is estimated to be 5000 K, the pressure reaches over 1800 atm, and the cooling rate is over 1010 K/s when the bubbles implode, which enables many chemical reactions to occur. Ultrasound offers a very attractive method for the preparation of nanosized materials. It has shown very rapid growth in its application to materials science due to its unique reaction effects. The advantages of this method include a rapid reaction

rate, the controllable reaction conditions, and the ability to form nanoparticles with uniform shapes, narrow size distributions, and high purities. The sonochemical method has been successfully applied to the preparation of various nanosized materials including metals, metal carbides, metal oxides and metal chalcogenides (Ai et al., 2011).

2.1.17 Synthesis of rGO-Bi_2S_3/GO-Bi_2S_3 composite

Recently, graphene sheets, a new two dimensional carbon material, due to their extraordinary electronic transport properties, large surface area and mechanical flexibility have been considered as a matrix material to improve electrochemical performance of metal sulfides. Herein, the a facile strategy to prepare Bi_2S_3/RGO composites, based on an oxidation–reduction reaction between graphene oxide and $Bi(NO_3)_3$. $5H_2O$ were used. Most often the Bi_2S_3/RGO composites were synthesized by a one pot hydrothermal route. First, the Graphene oxide GO, prepared by a modified Hummers method, was dispersed in ultrapure water with vigorous ultrasonic agitation to form a homogeneous solution. Then, $Bi(NO_3)_3 \cdot 5H_2O$ and l-cysteine were mixed with the above dispersion as it can be seen in Figure 16, after continues stirring, the solution was transferred to Teflon-lined stainless steel autoclave and then heated in an electric oven at 180^0C for 12 h. Eventually, the autoclave was allowed to cool down to room temperature naturally. The resulting black precipitate was collected by centrifugation, washed several times with ultrapure water and absolute ethanol, and dried at 60◦C in vacuum overnight. As prepared Bi_2S_3/RGO composite which is used as a material for lithium storage, exhibits high specific capacity and enhanced cycling performance compared to pure Bi_2S_3 nanoparticles (Ayodhya & Veerabhadram, 2018).

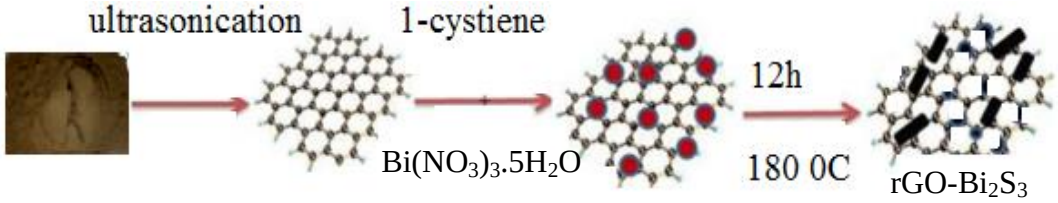

Figure 16: Schematic illustration for the synthesis of Bi_2S_3-rGO NSs (Ayodhya & Veerabhadram, 2018).

Herein, GO-Bi_2S_3 nano-structures have synthesized via a stable and cost effective sonochemical method from $Bi(NO_3)_3.5H_2O$ and $Na_2S.9H_2O$ as a raw materials, GO used as a capping agent. The Bi^{3+} solution was added into the GO solution in round bottom flask, followed by adding an equal amount of S^{2-} solution under magnetic stirring. Then, the black precipitates were formed and the total reaction mixture was kept in the ultrasonic

bath for 1 h at room temperature. Finally, the black colored solution was filtered and washed with distilled water and ethanol several times to remove ionic residue, and then dried in an oven at 100 ^{0}C for 8 h. The synthetic procedure of GO-Bi_2S_3 NSs by the sonochemical method is shown in Figure 17.

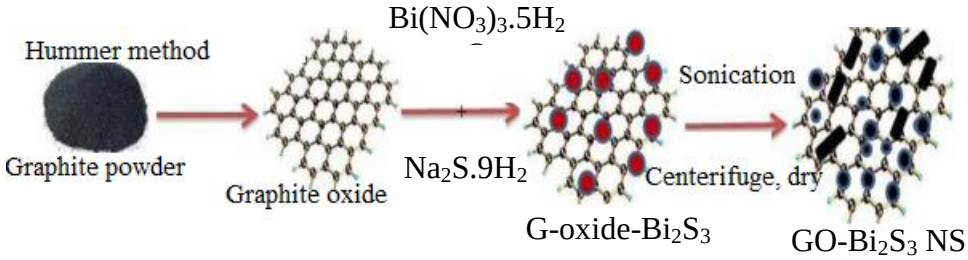

Figure 17: Schematic illustration for the synthesis of GO-Bi_2S_3 NSs (Ayodhya & Veerabhadram, 2018).

2.2 Adsorption.

Water pollution and water scarcity are among the most challenging problems facing mankind nowadays. With rapid population growth, steadily improving life standards, fast industrialization and modernization of developing countries, these challenges will persist, if not worsen, in the years to come. Conventional water treatment technologies, including adsorption, chemical treatment, membrane-based separation, and biological treatment, are generally designed on the basis of bulk water chemistry and without any doubt, these technologies have made critical contributions to sustaining human society in the past century. However, the ever increasing demand for safe and clean water is gradually pushing them to their limits (Liu et al., 2015).

With population expansion and industrialization, heavy metals have become some of the most hazardous and widespread water pollutants, which is a serious problem for human society today. Substantial amounts of various toxic metals are released into water systems by many types of industries such as mining, electroplating, electrolysis, tanning, photography, metal surface treating and others. Conventional methods such as chemical precipitation, filtration, ion exchange, electrochemical treatment, membrane technologies, adsorption on activated carbon, evaporation, etc., are applied to remove metal ions from aqueous solutions (Li et al., 2015). However, these methods are far from effective, efficient and practical enough to solve the problem. The removal of metal ions by chemical precipitation or electrochemical treatment when ion concentration is between 1 and 100 mg/L, or when ion product is lower than Ksp is usually inefficient. For example, the limit of copper in drinking water recommended by WHO is 2 mg/L, which is not

possible to achieve by precipitation. Besides, it is inevitable that new chemicals must be introduced into water systems, including acid and base (pH adjustment), flocculating agents, coagulants, etc., which usually generates new problems. Other conventional methods like ion exchange, membrane technologies, activated carbon adsorption or evaporation are not economical due to substantial energy consumption, especially when treating large amounts of water containing heavy metals at low concentration Kumar & Vijaya, 2017).

According to reports, samples taken from all corners of Ethiopian landforms, almost all of the samples taken from the rift valley region were found to contain the fluoride ion concentration greater than the WHO standard level (Kebede, 2013). For instance, the concentration of fluoride ion recorded for rift valley lakes such as lake Shala is (246 mg/l), and lake Abijata is (204 mg/l) (Demelash et al., 2019) on the other hand, high land lakes and springs contain insignificant level of fluoride ion concentration. Several literatures show that the enrichment of fluoride ion in ground water along the course of the river flow was accountable to the existence of acidic rocks initiated by heat differences generated lengthways across a river flow and the recent volcanic hot eruption centers. Rift ward flowing groundwater from plateau may increase the fluoride concentration in the aquifer systems of the rift if the flowing groundwater encounters acidic rocks with heat difference along the flow path. Generally, the landforms of Ethiopian rift valley exist in a variety of terrain that is significant importance to the enrichment of fluoride into groundwater occurrence and movement (Kebede, 2013).

2.2.1 Fluoride Occurrence

Significant amount of fluoride occurs in some classes of igneous rock such as granites and pegmatite. The order of abundance of fluoride in sedimentary rock in decreasing order is shale, carbonate rocks, sandstone, respectively, but deep sea clay found to have richest accumulations of fluorine. The most common source of fluoride in the rift valley region is originated from the volcanic rocks exist at lower pH such as pumice, obsidian, pyroclastic deposits, ignimbrite and rhyolite. The deposition of volcanic ash and the falling of pumice volcanic rock (Peccerillo et al., 2007) are the most common potential reservoirs of the fluoride ion enrichment into Ethiopian rift valley groundwater.

There are several factors that control the concentration of fluoride in the rift valley ground water includes lithology, thermal gradient, hydraulic gradient, groundwater water velocity,

mean residence time, and depletion of calcium due to evaporation and cation exchange. Accordingly, as shown in Figure 18, the concentration of fluoride ion in the rift valley region was found to vary from place to place. For example, the fluoride concentration of rift valley lake (Ansari et al., 2011) is about 2 mg/l to 250 mg/l, for spring is about 2 to 150 mg/l and for thermal groundwater is about 2 to 68 mg/l and from non-detectable to 6.4 mg/l for cold groundwater.

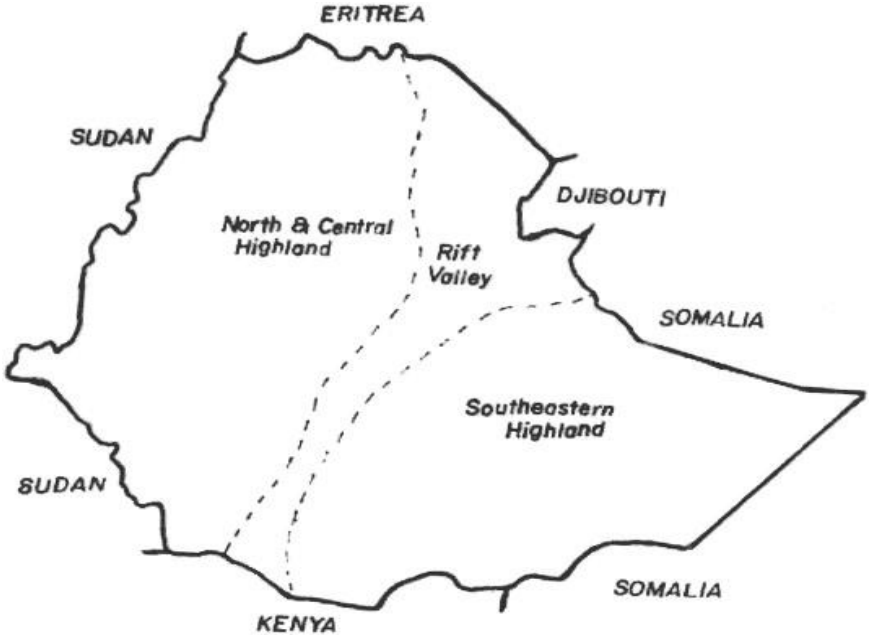

Figure 18: Fluoride distribution in Ethiopia (Ministry of Water Resources, 2013).

The ingestion of fluoride is essential for human health provided that the concentration not beyond the upper level 1.5 mg/l set by WHO in drinking water. The consumption of fluoride ion in food stuff with limit to the standard value is very important to keep skeletal and dental health. However, the consumption of this mineral above the labeled concentration brings about tremendous health effects. According to the findings (Thole, 2011) the ingestion of fluoride with the concentration between 1.5 to 3 mg/l cause browning and smears of colors of teeth which is commonly called dental fluorosis. This is the onset of the problem which makes the teeth very strong and brittle. Ingestion of fluoride with the concentration between 3.5 to 9 mg/l is resulted in the skeletal fluorosis this indicates the worsening of the situations. However, the ingestion of fluoride in the food stuff for a long time with the concentration greater than 10 mg/l brings about the crippling fluorosis and this is an irreversible damage to the bone causing immobility.

It is reported in the literature that excessive ingestion of fluoride ion has many other health effects including muscle fiber degeneration, reducing the level of hemoglobin,

deformation of red blood cells, excessive thirst, headache, skin rashes, depression, gastrointestinal problems, malfunction of urinary tracts, nausea, abdominal pains, tingling sensation in fingers and toes, reduced immunity and neurological manifestations similar to pathological changes that occur in Alzheimer`s disease patients. Nearly all foodstuffs contain at least traces of fluoride and all vegetables contain fluoride which was absorbed from soil and water. However, the ingestion of fluoride from water is much larger than its ingestion from foodstuffs and air. Therefore, great attention should be given to control fluoride concentrations in drinking water supply. According to world health organization recommendation (Sara Datturi, Assefa Kumsa, Seifu Kebede, 2017) the procedure for the mitigation of fluorosis in endemic area should be prioritized as follows.

- It is advisable to search for alternative sources of water for drinking with low fluoride concentration.
- Diluting the water containing high fluoride concentration with water containing low/non fluoride concentration until the fluoride concentration is lowered to 1.5 mg/l or below.
- Consume diet containing large amount of calcium, magnesium and vitamin C.

When all the above listed mitigation strategies are not feasible, remove fluoride ion from water to meet WHO upper limit level 1.5 mg/l.

The ion exchange reaction between hydroxide and fluoride in hydroxyapatite is the center of the fluorosis phenomenon occurrence (Premathilaka & Liyanagedera, 2019). The lattice size of the two crystals OH^- and F^- is comparable that the displacement reaction is feasible. The displacement of hydroxide ion from hydroxyapatite by fluoride ion is resulted in the formation of more acidic resistant structure known as fluoroapatite as shown below. There is also expected decomposition reaction of hydroxyapatite (1) to produce CaF_2 and dissolution of calcium and phosphorus in to the matrix phase but this is rare case.

$$Ca_5(PO_4)_3OH + F^- \longrightarrow Ca_5(PO_4)_3F + OH^- \qquad (1)$$

The early formed fluoroapatite material from the exposure of hydroxyapatite to fluoride ion concentration greater than 1.5 mg/l is more resistant to acidic attack than hydroxyapatite, offers a protective layer to the tooth enamel against acids from the foodstuffs and prevents dental carries. However, the excessive fluoride intake aggravates the reaction beyond the replacement of hydroxide by fluoride so that it results in the

decomposition of hydroxyapatite and leads to the formation of another compound called calcium decafluoride as shown by equation (2) (Huber & Mosler, 2013).

$$Ca_5(PO_4)_3F + 9F^- \longrightarrow Ca_5F_{10} + 3PO^{3-}_4 \quad (2)$$

This compound is very hard and brittle which is not appropriate for the functions of skeletal structure where an optimum flexibility is mandatory (Neel et al., 2016). There are some defluoridation practices as shown in the Table 1, which have been implemented in Ethiopia so far but the problem of dental fluorosis, skeletal crippling and other complicated health effects are persisted to till date.

Table 1: Fluoride remediation experience in Ethiopia(Fito et al., 2019)

Method	Advantage	Disadvantage	Remark	Reference
$Al_2(SO_4)_3$ with CaO	❖ High availability ❖ Easily obtained ❖ Easily synthesized ❖ Easily applied ❖ Easy to operate ❖ Efficient ❖ Less costly	❖ Mud production ❖ Non-recyclable ❖ High initial cost ❖ Less feasible for F^- >10 mg/l and F^-< 3mg/l ❖ Less applicable in rural area	Almost accepted by all	(Kowalchuk, 2012)
Bon Char	❖ Readily available ❖ Cheap ❖ Remove F^- easily	❖ Bad color, odor, taste ❖ Unpleasant ❖ Cultural conflict ❖ Scarcity of raw bones	Almost rejected by all	(Rojas-Mayorga et al., 2013)
Natural Clay	❖ Readily available ❖ Cheap	❖ Inefficient ❖ Easily operated ❖ Less manpower	Less preferred	(Nabbou et al., 2019)
Activated Alumina	❖ Effective	❖ Expensive ❖ Difficult to operate	Practiced	(Jing, 2014)

Consequently, the more efficient, effective and low cost water treatment technologies applicable for use in the rural and urban area is needed. Hence membrane filtration technology is among the advanced water treatment technologies which are being

employed in the treatment of ultra-pure water and carbon nanotube membrane is the potential material for the efficient and effective filtration technology (Saththasivam et al., 2018).

2.2.2 Nanoadsorption Activity

Owing to their nanodimension, nanomaterials revealed the highest capacity toward pollutant adsorption. Their nanoscale sizes further provide them the largest surface area to volume ratio which is considered as the top requirement of the material to be used as an adsorbate of pollutant (L. Ma et al., 2017). Heavy metal, organic dyes and anionic pollutants are the most common threatening pollutants that can uncontrollably enters the environment mainly the surface and ground water body from human activities. These provoked the environmental researchers all around the world to give due attention and work over preventing the pollution problem (W. Ma et al., 2008). Many technologies have been employed so far for pollutant removal and remediation from water supplies such as membrane filtration technology, ultraviolet irradiation technology, advanced oxidation technology, ion exchange technology and nanoadsorption technology. Conventional and technologically advanced materials having a various ranges of adsorption capacities, functional tunability, regenerability (recyclability), availability, stability under different working condition and cost of preparation have also been applied for pollutant removal. Mainly due to cost, complexity of the process and efficiency of the techniques adsorption is preferred to the above technologies, and due to surface tunability and stability under ambient condition graphene based nanomaterial is preferred to any of the material used for the adsorption of pollutants (Ji & Zhao, 2017).

Metals, the common pollutants that can enter into the water body from anthropogenic activities and its adsorption by GBNs was studied very extensively. But there is no significant report on the adsorption of nonmetallic anion by GBNs. Fluorine, the lightest of the halogen elements, belongs to group VII of the periodic table along with Cl, Br and I, and is one of most reactive of all nonmetallic elements. It accumulates in soil, water, plants and human bodies for a long period of time without degradation so that fluoride is non-biodegradable pollutants. The level of fluoride ion (F^-) in water bodies is of great environmental concern worldwide because of the vast ranges of health problem it causes such as osteoporosis, arthritis, brittle bones, cancer, infertility, brain damage, alzheimer syndrome, and thyroid disorder (Rashid & Ralph, 2017). Besides these problem, the concentration of fluoride in drinking water beyond the WHO standard limit 1.5 mg/L

cause dental fluorosis however if the concentration is higher than 3.5 mg/L leads to non-curable skeletal crippling fluorosis. A high level of fluoride which is equals to 264.0 mg/L in ground water have been reported in Ethiopian lake Shala and was reported to be resulted from the idea of acidic rocks and aggravated by heat anomaly generated along regional faults or from recent hot eruption centers favor high fluoride incorporation into the groundwater (Mandefro Ararso, 2017). The principle of fluorosis is by the displacement reaction of hydroxide ion by fluoride ion from hydroxyapatite which is resulted in the formation of more acid resistant structure called fluoroapatite which basically prevents dental carries.

$$Ca_5(PO_4)_3)OH + F^- \rightleftharpoons Ca_5(PO_4)_3F + OH^- \quad (3)$$

However the excessive fluoride intake enhances the reaction to go beyond replacement of hydroxide ion by fluoride ion and favors the formation of calcium decafluoride by distraction of the outer enamel cover as given below. This is resulted in the formation of small extent health effect; dental carries which will gradually aggravated to skeletal crippling and complete paralysis (Nelson & Higuchi, 1970).

$$Ca_5(PO_4)_3F + 9F^- \rightleftharpoons CaF_{10} + 3PO_4^{3-} \quad (4)$$

The health effect of fluoride ion (Das et al., 2014; Huber & Mosler, 2013) on people in the Dugda Bora district, East Shoa, Oromiyaa, Ethiopia is as shown in Figure 19.

Figure 19: Photos taken from “Dugda Bora District, East Shewa” Oromia.

2.2.3 Graphene materials for contaminant adsorption

Rapid population growth and intensification of agricultural and industrial activities have resulted in a dramatic increase in the number of contaminants released into the environment. These contaminants, which are very diverse in nature, represent a major environmental and public health concern. As a consequence; a global effort exists to develop robust technologies to effectively remove contaminants from both air and water. Among these technologies, adsorption is a fast, inexpensive, and effective method for

removal of contaminants from aquatic environments. Adsorption is a process where the pollutant (adsorbate) is captured by the nanomaterial (adsorbent) via physicochemical interactions (Ersan et al., 2017). Herein, we reviewed the application of graphene-based materials as adsorbents for the removal of inorganic, organic, and gaseous contaminants. In addition, we delineate key adsorption mechanisms and advantages/disadvantages of applying graphene materials as adsorbents for decontamination.

2.2.4 Metal ion adsorption

Metals are common pollutants that can undesirably enter aquatic environments and drinking water supplies from anthropogenic activities, such as mining and industrial wastes, or from the corrosion of pipes, soldered joints, and plumbing materials. Hence, there is a growing interest in controlling the concentration of toxic metals in water. For example, according to the United States Environmental Protection Agency (EPA), the allowed concentrations of copper (Cu) and lead (Pb) in drinking water are, respectively, 1.3 ppm and 15 ppb (Tyagi et al., 2020).

Conventionally, activated carbon has been used as adsorbent due to its excellent adsorption capacity for a wide range of contaminants. However, the wide use of activated carbon has been restricted because of its high production cost and the difficulty in regenerating it. Carbonaceous adsorbents based on CNTs and graphene materials have been developed as an alternative to conventional adsorbents. Carbon nanomaterials have been chosen as a platform to build new adsorbents, mostly because of their high surface area, non-corrosive property, and presence of oxygen-containing functional groups, tunable surface chemistry, and scalable production. For CNTs, the sorption capacity is mainly determined by the chemical nature of CNTs, the surface area, and the number of oxygen functional groups (Bhatnagar & Minocha, 2006). The mechanism of metal ion sorption on CNT surface has been related to electrostatic interactions and sorption–precipitation between metal ions and the oxygen-containing groups. These oxygenated groups provide a negative residual charge to the surface of CNTs. Thus, depending on the solution pH, the oxygen atoms hold a lone electron pair that is responsible for ion-exchange and electrostatic interaction with metal ions (Speranza, 2019).

Compared to CNTs, the utilization of graphene-based materials as adsorbents may offer several advantages. First, single-layered graphene materials possess two basal planes available for pollutant adsorption (Ali et al., 2019). In contrast, the inner walls in CNTs

are not accessible by the adsorbates. Second, GO and rGO can be easily synthesized through chemical exfoliation of graphite, without using complex apparatus or metallic catalysts. The resulting graphene material is free of catalyst residues, and no further purification steps are needed. In the specific case of GO, the as-prepared material already possesses a large number of oxygen-containing functional groups and no additional acid treatments are required to impart a hydrophilic character and reactivity to GO. This is a significant advantage, since those functional groups are likely responsible for the adsorption of metal ions by GO sheets (Aliyev et al., 2019).

A variety of studies have described the application of graphene based materials as adsorbents for the removal of inorganic species from aqueous solutions. Most of these studies have employed GO as a model adsorbent for remediation of metal ions in water. GO is preferable to pristine graphene for metal ion adsorption due to GO's high content of oxygen groups available to interact with metal ions. The importance of these oxygen-containing functional groups was demonstrated by comparing the Pb(II) adsorption performance of pristine and oxidized graphene sheets. Pristine graphene was first prepared through a vacuum-promoted low-temperature exfoliation and submitted to heat treatments at 500 and 700 1C (GNS500 and GNS700) to introduce oxygen functional groups. GNS500 and GNS700 revealed a higher adsorption capacity for Pb(II) compared to pristine graphene, which underscores the importance of carboxyl groups in the adsorption mechanism of Pb(II) (Verma & Kim, 2022).

Numerous factors, such as ionic strength, pH, number of oxygen-containing groups of GO, and presence of natural organic matter were found to influence the adsorption capacity of GO. For instance, the influence of ionic strength on the adsorption capacity may be due to competition between electrolytes (NaCl, KCl, and $NaClO_4$) and the metal ions for the GO surface. In fact, the introduction of electrolytes may affect the electrical double layer of hydrated particles, thus changing the way metal ions bind to the GO sheets. Wang et al. demonstrated that the adsorption ability towards Zn(II) was decreased after addition of $NaNO_3$, NaCl, and KCl to GO suspension. Conversely, the sorption capacity of GO for Cd(II) and Co(II) was weakly dependent on $NaClO_4$ concentration, while the adsorption of Pb(II) was not affected by changes in ionic strength (Perreault, Fonseca De Faria, et al., 2015).

The adsorption of metal ions on GO is also greatly affected by pH, with the adsorption capacity decreasing at lower pH. The behavior of GO in aqueous solution is governed by its pHpzc (pzc: point of zero charge). When solution pH is higher than pH_{pzc} ($pH > pH_{pzc}$), the GO surface is negatively charged because of the deprotonation of carboxyl and hydroxyl groups. When the GO surface is negatively charged, the electrostatic interaction with metal ions (positively charged) is favorable, leading to improvement in adsorption capacity. In contrast, when pH o pHpzc, GO becomes positively charged and electrostatic interactions are weakened due to charge repulsion (Ouyang et al., 2019).

In a similar way, pH also influences the charged nature of the adsorbates. Depending on the pH, metallic ions can form hydroxide species: $Me(OH)^{+}$, $Me(OH)_2$, and $Me(OH)_3^{-}$.The practical implications of these hydroxides are: (i) due to a lower residual charge, $Me(OH)^{+}$ species have less affinity to the GO surface compared to its counterpart M^{+2}; and (ii) at higher solution pH, precipitation of $Me(OH)_2$ or electrostatic repulsion of negative species by the negatively charged surface of GO can prevent the adsorption of metals on the graphene surface. In practical terms, the ideal procedure is to establish a pH condition where the metal maintains its Me^{+2} form, while the GO surface is negatively charged. This optimal pH range might be different according to each metal species and graphene sample. Sitko et al., for example, demonstrated the removal of Cu(II), Zn(II), Cd(II), and Pb(II) ions at pH 5.0, while Zhao et al. showed that Co(II) and Cd(II) were effectively adsorbed by GO sheets at pH 6.0 (Lee et al., 2017).

Even though electrostatic interaction between oxygenated groups and metal ions has been considered the major adsorption mechanism, a second type of interaction may occur. Huang et al. suggested that the delocalized p-electrons in the sp^2 network of graphene can act as Lewis bases donating electrons to metal ions. In this context, p-electrons on the graphene aromatic plane can be classified as the base (electron donors), while the metal species are the acid (electron acceptors). The same mechanism was previously proposed to explain the adsorption of Pb(II) ions on graphene (Ma et al., 2020).

Due to its large surface area and chemical stability, graphene has also become a versatile candidate for building adsorbent nanocomposites with inorganic nanomaterials. Of particular interest is the conjugation of graphene with magnetic nanoparticles (e.g., iron or iron oxide), which has been the most common approach to prepare graphene-based composites for the removal of metal ions. Although the high adsorption capacity and

magnetic property of iron oxide nanoparticles have stimulated their use as adsorbents, their application in continuous flow systems is difficult because of their small size and susceptibility to oxidation/dissolution. To overcome this drawback, graphene sheets can be used as a physical support to stabilize magnetic nanoparticles, facilitating their recycling and reuse. In addition, immobilizing magnetic nanoparticles on graphene sheets also prevents their aggregation, thus reducing the associated losses in surface area and adsorption capabilities. Also, the graphene–magnetic nanoparticle composites can be rapidly and efficiently separated from aqueous solutions using a simple magnet (Handayani et al., 2021).

Graphene–magnetic nanoparticle composites were highlighted as having improved adsorption performance. The high sorption capacity of magnetite–graphene composites may be attributed to a combined effect of metal complexation on the nanoparticles and on the adsorption sites on graphene aromatic layer. Beyond that, the decoration of graphene sheets with magnetic nanoparticles increases the surface area of the material, improving the number of binding sites for metal ions. The adsorption capacity of magnetic–graphene materials, like GO, is affected by changes in pH conditions and adsorbent dosage, time of contact, temperature, and presence of natural organic matter such as fulvic acid (Wang et al., 2014).

New adsorbents have also been prepared by modifying graphene materials with organic molecules that possess a natural ability to capture metal ions. As the intrinsic functional groups located on GO sheets are limited, the number of adsorption sites can be improved by grafting compounds such as ethylenediamine triacetic acid (EDTA) and chitosan. Most of these functionalization procedures have been performed taking advantage of the oxygenated functional groups on GO or rGO (Xiaolu Liu et al., 2021). For example, carboxyl groups were used to graft poly- (acrylamide) (PAM) chains on the surface of rGO sheets. The dispersibility and adsorption capacity of rGO for Pb(II) was remarkably improved after grafting with PAM, increasing from 500 mg g^{-1} to 1000 mg g^{-1}. In another study, chelating groups were also introduced to the GO surface through reaction of EDTA–silane with C–OH groups of graphene. After modification, the adsorption capability towards Pb(II) was enhanced due to the intrinsic complexation property of EDTA. The anchoring of EDTA molecules also resulted in improvement of surface area and numbers of functional groups on the original GO sheets (da Silva Alves et al., 2021).

In addition to increasing the adsorption capacity, functionalization of graphene materials with organic molecules can also be used to enhance the material recovery process. Thermo-responsive properties were imparted to graphene-based adsorbent materials using a non-covalent assembly of graphene-based adsorbent material with poly(N-isopropylacrylamide). The low critical solution temperature of poly(N-isopropylacrylamide) (32 ^{0}C) results in a nanocomposite material that undergoes rapid aggregation and sedimentation at temperatures higher than 36 ^{0}C. This aggregation is reversible and the nanocomposites can be resuspended upon decreasing the temperature below 34 ^{0}C. Compared to magnetic graphene-based composites, thermo-responsive materials allow for an increased material recovery without the requirement of a strong magnetic field (Seo et al., 2016).

Even though most studies report on the adsorption of cationic metal ions, graphene-based materials have also been explored for the removal of anionic pollutants from aqueous solutions, such as phosphate (PO_4^-), perchlorate (ClO_4^-), and fluoride (F^-).Unlike the immobilization of cationic metal species, the mechanism of anion (F^-, Cl^-, and Br^-) adsorption was previously attributed to anion–π interactions. This anion–π association is based on the interaction between the negatively charged anion (or lone electron pair) with an electron-deficient aromatic ring on graphene layer (Perreault, Fonseca De Faria, et al., 2015).

Table 2 depicts the most common adsorption mechanisms as well as advantages and disadvantage of using graphene materials and their derivatives as adsorbents for remediation and sequestration of metal ions from aqueous solutions.

Table 2: Specific mechanisms of interaction and possible advantages/disadvantages of using graphene materials as adsorbents to remove metal ions from aqueous solutions

Graphene-based materials	Mechanisms involved in the adsorption of metal ions	Advantages (A) and disadvantages (D)	Reference
Graphene oxide (GO)	Electrostatic interactions Ion exchange	(A) High dispersibility in water; good colloidal stability; abundant presence of oxygenated functional groups (D) Limited amount of sorption sites	(Ji et al., 2020)
Reduced GO (rGO) and Pristine graphene	Electrostatic interactions Lewis-base–acid mechanism	(A) Reestablishment of sp2 domains; better electron-transport property (D) Low density of oxygen-containing functional groups; lower colloidal stability	(Morais et al., 2015)
Magnetic graphene nanocomposites	Electrostatic interactions with graphene Interactions with the surface of the particles Magnetic properties of the nanoparticles	(A) Larger surface area compared to the pristine forms; increased amount of binding sites compared to pristine graphene; easy recovery from aqueous solutions (D) Co-reduction of GO during the attachment of the particles reduces the	(Jin et al., 2015)

		colloidal stability	
Graphene materials modified with organic molecules	Electrostatic interactions Complexation with organic molecules	(A) Larger surface area compared to pristine forms; good colloidal stability; improved amount of functional groups ($–NH_2$, –OH) (D) The stability of the loaded molecules varies according to the modification strategy (physical or chemical attachment)	(Yan et al., 2012)

Chapter Three

3. Materials and Methods

3.1 Chemicals and Reagents

All the chemicals and reagents used throughout this study were of analytical grade. Fresh leaves of VA were obtained from premises of Adama Science and Technology University (ASTU), and were authenticated at Jimma University, College of Agriculture, with authentication number 10031, Ethiopia. The leaves were washed thoroughly, and air dried in an open space for about ten days. After drying, the sample was blended using a Panasonic blender (Model: Pana-Mix-901shg, Malaysia) and sieved using standard sieve of 110 mm mesh size and stored in an airtight, polyethylene bag until required. Ethanol, methanol and distilled water used for extraction were obtained from the local market and were used directly without further purifications. Raw graphite powder (G, 97%, 100 micron, Vietnam), Sulfuric acid (H_2SO_4, 98%, Sigma-Aldrich), sodium hydroxide (NaOH, 98%, Oxford Lab Fine Chem ULP), Phosphoric acid (H_3PO_4, 75%, Sigma-Aldrich), Hydrogen peroxide (H_2O_2, 30%, Sigma-Aldrich), Hydrochloric acid, (HCl, 35%, Sigma-Aldrich), Thiourea (CH_4N_2S, 97%, Sigma-Aldrich), and potassium permanganate ($KMnO_4$ 98%, Sigma-Aldrich), methylene blue dye (MB, 95%, Sigma-Aldrich) were of analytical grade and used as purchased.

3.2 Preparation of plant extract

The leaf extracts were prepared by taking 10g of the grounded powder and dissolved in a 100 mL of three different solvents; water, ethanol and methanol (Alara et al., 2019b). Then the extract was filtered using Whatman number 1 filter paper. The resulting filtrate were further concentrated over a water bath at 40-50 ^{0}C. Each mixture solution was heated on a heater with magnetic stirrer to boil at their corresponding boiling points for five minutes for solvent removal. The stock solutions of each extracts were taken and desired working concentrations were prepared by appropriate techniques. The extracts were made ready and stored in a refrigerator at 4 ^{0}C for further use.

3.3 Synthesis of Graphene Oxide (GO)

GO was synthesized by making a slight modification to improved method (Marcano et al., 2010). A mixture of H_2SO_4/H_3PO_4 in a volume ratio of 9:1 was prepared. A second mixture of graphite/$KMnO_4$ in a mass ratio of 1:6 was prepared. The H_2SO_4/H_3PO_4 acid mixture were poured into the beaker containing graphite-$KMnO_4$ mixture slowly at room

temperature while continuous stirring. A deep green color solution was formed due to the production of highly oxidizing dimanganese heptoxide, Mn_2O_7. Under controlled temperature of the water bath at 80 ^{0}C, the solution was heated while string using a magnetic stirrer for six hours. The hot and slightly brown solution was taken off the water bath and added into 400 ml distilled ice water to terminate the reaction. Then 5 ml of H_2O_2 was added drop wise because of which a yellowish colored solution was formed. The purpose of addition of H_2O_2 was to stop the oxidation reaction by directly reacting with the excess of $KMnO_4$. The reaction product was washed with 1 liter of 5% HCl aqueous solution and distilled water four times each until the pH_{pzc} was obtained. The complete removal of SO_4^{-2} ion from the solution was checked by addition of $BaCl_2$ to the supernatant. Its presence produces a white precipitate of $BaSO_4$. The resulting paste was dried in an oven at 60 ^{0}C for 8 hours to obtain the brown graphene oxide powder sample.

3.4 Synthesis of Reduced Graphene Oxide (rGO)

Reducing capacity of three solvent extracted *Vernonia Amygdalina* (locally called "dhebicha") was studied. The extract was prepared using three different solvents such as methanol, ethanol and water. 10 mL of each of the extracts was added into a washed and dried clean 1000 mL beaker and 100 mL of the brown solution of graphene oxide was added into each of the extracts. The mixture was then heated using a heater with a magnetic stirrer in a water bath at 50 ^{0}C for an hour. Then the black suspension was taken off the heater cooled and centrifuged at 2000 rpm. Then the black residue was collected and oven dried at 80 ^{0}C for 12h to obtain a black powder rGO.

3.5 Synthesis of Bi_2S_3

1.5 g of bismuth chloride ($BiCl_3$) and 1.2g of thiourea (CH_4N_2S) was dissolved in 50 ml of distilled water each separately and mixed while continuous stirring using heater with magnetic stirrer at 100 ^{0}C. After 5 minutes of heating the mixture, 10 ml of methanol extracted compounds of *vernonia amygdalina* was added into the solution. And the mixture was set on the indirect heating using water bath under continuous stirring for six hours. Finally the obtained black paste was washed using distilled water and ethanol several times and oven dry at 60 ^{0}C for 12 hours to obtain a black powder Bi_2S_3.

3.6 Synthesis of Bi_2S_3-rGO composite

All reagents used in this experiment were analytical grade and used directly without further purification. A simple reflux method was used to synthesis rGO-Bi_2S_3. 1.43 g of

Bi_2S_3 powder was thoroughly dissolved in 50 ml of distilled water and 2 g of rGO was dissolved in the same volume of distilled water in a separate flask. Both mixture were poured into a 500 ml beaker and sonicated for two hours at room temperature. And then the mixture was heated under reflux at 100 ^{0}C for 12 hours. The black precipitate was filtered by using whatman number 1 filter paper and purified by washing several times with distilled water and ethanol respectively. The black paste was dried into a black powder in an oven under 120 ^{0}C for 18 hours.

3.7 Characterization techniques

Optical absorption properties of the samples were examined by ultraviolet-visible spectroscopy, UV-Vis (SM, UV-1600 Maadab-India). Double beam UV-Vis spectrophotometer ranged from 200-800 nm was used to determine the Optical properties of the samples.

An Agilent technology 7890B GC system equipped with mass spectrometric detector; 5977B GC/MSD GC-MS was used for analysis. The column used is HP-5MS Agilent technology, length of the column is 30 m, and internal diameter is 0.320 mm. The GC-MS was operated at an initial oven and the injection temperature of 80 ^{0}C and 250 ^{0}C respectively. The initial temperature was hold for two minutes at 10 ^{0}C/min and the final temperature was hold at the same temperature for six minutes. The injection was split mode. Helium gas was used as a mobile phase. The obtained chromatogram was recorded and the identifications of components were made by database of national institute of standards and technology (NIST).

The X-ray diffraction of the results were recorded on a panalytical PW 3040 X` Pert MPD X-ray diffractometer (XRD, Shimadzu, XRD-7000) with a continuous scanning rate of 1^0 per minute in a range of 2θ from 5(10) to 80^0 with a Cu-Kα X-ray diffraction source. This was performed to analyze the crystallinity and purity of the materials and also to characterize the interlayer spacing at 40 keV and 30 mA.

The confirmations of the formation of reduced graphene oxide from graphene oxide and the spectral positions of rGO-Bi_2S_3 were determined by Fourier transform infrared spectroscopy (Perkin Elmer FT-IR, Spectrum 65). The presences of oxygen containing functional groups on the basal plane or edge of the carbon framework in GO, rGO were determined by FT-IR. GO and rGO pellet were prepared using KBr as a mulling agent and the sample was analyzed in the range between 400 cm^{-1} 4000 cm^{-1}.

The morphology of the samples was analyzed using scanning electron microscopy, SEM (JEOL, JSM 6460LV).

High resolution transmission electron microscopy, HR-TEM (JEOL TEM 2100 HRTEM) was used to determine the morphology, measure the size of the particles.

EDAX was used to determine the elemental composition.

The differential thermal graphimetric DTG (DTG- 60H, Beijing, China) comprising thermal graphimetric analyzer (TGA) and differential thermal analyzer (DTA) was performed. These tests were operated under nitrogen atmosphere with platinum cell at 50 ml/min flow rate.

3.8 Photocatalysis Study

Before illumination, the mixture solution was stirred continuously in the dark for 30 min to create the adsorption/desorption equilibrium of MB on the NCs. The degradation experiment was carried out in the ~177 cm^2 circular glass reactor. A medium-pressure mercury vapor lamp (Hg lamp) was used as light source with a maximum wavelength 365 nm and corresponding power of 125 W. The samples were irradiated directly by focusing light into the reaction mixture at a distance of 20 cm. For the homogeneity of the solution; a magnetic stirring at a speed of 120 rpm was applied. The temperature of the overall reactor was controlled by jacket water circulation. 125 mL of methylene blue and 5 mg of the catalyst rGO-Bi_2S_3 were placed in a glass cup reactor (250 mL). Then, after at a fixed time interval of irradiation, 5 mL of reaction mixtures liquid was taken out and placed in centrifuge tubes which were later centrifuged to remove any residual catalyst. The photocatalytic degradation efficiency in percent was calculated using equation 5. The pseudo-first-order kinetic equation, equation 7 was used to study reaction dynamics (Revellame et al., 2020). The centrifugation and washing of the reaction liquid were done repeatedly using ethanol and water. The UV-Vis spectroscopy analyses were done against the concentrations of residual MB to evaluate the performance of the catalyst.

3.9 Adsorption study

All the chemicals and reagents used throughout this study were of analytical grade. 5 borosilicate glasses of 150 mL containing 50 mL of known concentration of fluoride solution (10 mg/L) at different pH, contact time, and adsorbent dosage were prepared at room temperature. This work was repeated for the real sample too. The filtrate was

collected by filtering the solution by using Whatman filter paper and was stored for the residual fluoride analysis using photometer measurement.

3.9.1 Reusability Study

The adsorbent was washed repeatedly using doubly distilled water and was used to check the recyclability and reusability test. The stock solution of fluoride was obtained by dissolving 2.21 g of NaF salt in 1 L of distilled water. 0.1 N of NaOH and H_2SO_4 were used to adjust the pH of the sample. The fluoride concentration was measured by (HACH photometer instrument, Model Number DR6000; USA). The equilibration for the adsorption experiment was maintained by continuous shaking of the mixtures using rotary shaker.

The percentage adsorption (A), percentage degradation (Φ) and adsorption capacity at equilibrium $q_{e,\ exp}$ (mg/g) were calculated as:

$$A = \frac{C_0 - C_t}{C_0} * 100,\ \Phi = \frac{C_0 - C_t}{C_0} * 100 \quad (5)$$

$$q_{e,\ exp} = \frac{(C_0 - C_t)V}{W} \quad (6)$$

Where C_0 and C_t are F^- concentration before and after adsorption, V(L) volume of F^- solution taken and W (g) is the weight of adsorbent used.

3.9.2 Study of Adsorption Kinetics

The following Equations were used to study fluoride adsorption kinetics and rate controlling steps. Pseudo-first-order (SFO) and pseudo-second-order (SSO) equations were denoted by (7) and (8) respectively.

$$\log(q_e - q_t) = \log qe^{-\frac{k_f t}{2.303}} \quad (7)$$

$$\frac{t}{q_t} = \frac{1}{q_e^2 k_s} + \frac{t}{q_e} \quad (8)$$

Where k_f – SFO rate constant (g/mg, min), k_s – SSO rate constant (g/mg, min)

3.9.3 Diffusion Studies

The adsorption mechanisms were thoroughly explained by using models – an intraparticle diffusion model which employs Weber Morris plot i.e. q_t versus t shown in equation 9, and

a particle diffusion model based on Chanda plot i.e. *ln(1-Ct/Ce)* versus *t* as shown in equation 10.

$$qt = k_{id} t^{0.5} + C_i \quad (9)$$

Where k_{id} ($mgg^{-1}min^{0.5}$) is the rate constant of stage *i* and C_i is the thickness of the boundary layer, it constant.

$$\ln(1 - \frac{C_t}{C_e}) = -k_p t \quad (10)$$

Where k_p ($mgg^{-1}min^{-1}$) is the rate constant

These two models are used to evaluate either the retention process is controlled by an intraparticle diffusion model or a particle diffusion model. The precision of adsorption kinetics model fitting was checked by standard deviation (SD), coefficient of determination (R^2) and non-linear chi-square (χ^2), equation 11.

$$\chi^2 = \sum \frac{(q_{e,\exp} - q_{e,\ cal})^2}{q_{e,\ cal}^2} \quad (11)$$

3.9.4 Adsorption Isotherm

In this work, four adsorption isotherm models (Langmuir, Freundlich, Tempkin and Dubinin-Radushkevich, D-R) were used to analyze the equilibrium relationship between the adsorbent and the adsorbate. The following equations 12, 13, 14 and 15 describe the Langmuir, Freundlich, Temkin and Dubinin-Radushkevich, D-R isotherm models respectively.

$$q_e = \frac{C_e * K_L * q_m}{1 + K_L * C_e}, \quad (12)$$

The Langmuir constant shows the free energy (ΔG) for the process of adsorption which can be obtained from:

$$\Delta G = -RTlnK_L$$

The Langmuir equilibrium parameter R_L is described as:

$R_L = \frac{1}{1+(1+K_L C_0)}$, C_0 is the initial adsorbate concentration. If $R_L > 1$ it is unfavorable process, if $R_L < 1$ the process is favorable and if $R_L = 0$, the adsorption process is irreversible.

$$q_e = K_F * C_e^{\frac{1}{n_F}} \quad (13)$$

Where q_e is the amount of fluoride adsorbed per unit mass of the adsorbent (mg/g), C_e equilibrium concentration (mg/L), q_m maximum adsorption capacity of the adsorbent(mg/g), K_L& K_F are Langmuir and Freundlich adsorption rate constants (L/mg) and $(mg/g(L/mg)^{1/nF})$ respectively. 1/n is the adsorption intensity.

The Temkin model which takes into account the interactions of the adjacent adsorbate ions and assumes the heat of adsorption decreases linearly with increasing covered surface is expressed as:

$$q_e = \frac{RT}{b} lnk_T + \frac{RT}{b} lnC_e \quad (14)$$

Where b is heat of sorption (in Joules per mole) and K_T is Tempkin equilibrium constant (in litter per milligram), R is universal gas constant and T is absolute temperature.

The other isotherm model which relates the adsorption characteristics with the available porosity and applied only to porous materials is D-R model. This model is usually applied to solution containing intermediate to high range concentration and is expressed as:

$$lnqe = lnqs - K_{DR}\mathcal{E}^2 \quad (15)$$

Where q_s is the theoretical adsorption saturation capacity (in milligram per gram), K_{DR} is the D-R isotherm constant (in $mole^2$ per $joule^2$), and the term Ɛ is obtained from the expression:

$$\mathcal{E} = RTln[1 + \frac{1}{C_e}]$$

The mean free energy (E) for adsorption can be calculated as:

$$E = \frac{1}{\sqrt{2K_{DR}}}$$

Chapter Four

4. Results and discussion

4.1 Characterization

4.1.1 Visual Observation

As shown below in Figure 20a, b, c and d, four main different colors were observed during the stepwise synthesis of rGO. The mixing of the two mixtures (mixture of graphite/$KMnO_4$ and H_2SO_4/H_3PO_4) were resulted in the formation of a dark green colored; thick solution as shown in Figure 20a. This color was due to the formation of the high oxidizing agent dimanganese heptoxide (Mn_2O_7) (Fentaw & Worku, 2017; Marcano et al., 2010) from the reaction of MnO^+_3 and MnO^-_4 and in the meanwhile the temperature of the solution were increased to 45^0C. The thick slurry solution observed in Figure 20b was due to prolonged reaction under heating and stirring. The presence of unreacted potassium peroxide was observed by the formation of yellowish color by the addition of H_2O_2 which was disappeared later by intensive washing. The brown color as indicated below in Figure 20c was obtained which is one of the confirmations of formation of graphene oxide nanostructure. The dark black suspension formed as shown in Figure 20d is the sign of GO reduction to produce rGO. The image of powders depicted in Figure 21e and 21f below are GO and rGO respectively. The brown powder on the left hand side (e) is GO and the black powder on the right hand side (f) is the reduced form of GO called rGO.

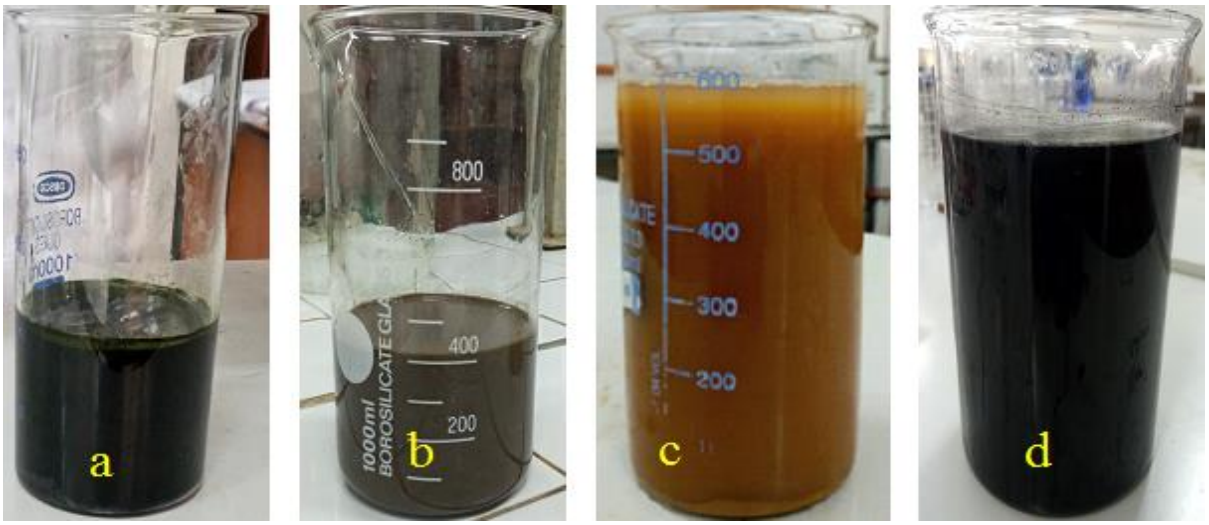

Figure 20: The color change observed during the stepwise synthesis of reduced graphene oxide by using methanol extracted VA, indicated from a-d.

The reduction was done by using *Vernonia Amygdalina* plant extract and this result confirmed that bitter leaf extract is eco-friendly and excellent reducing agent for the nanosynthesis of rGO.

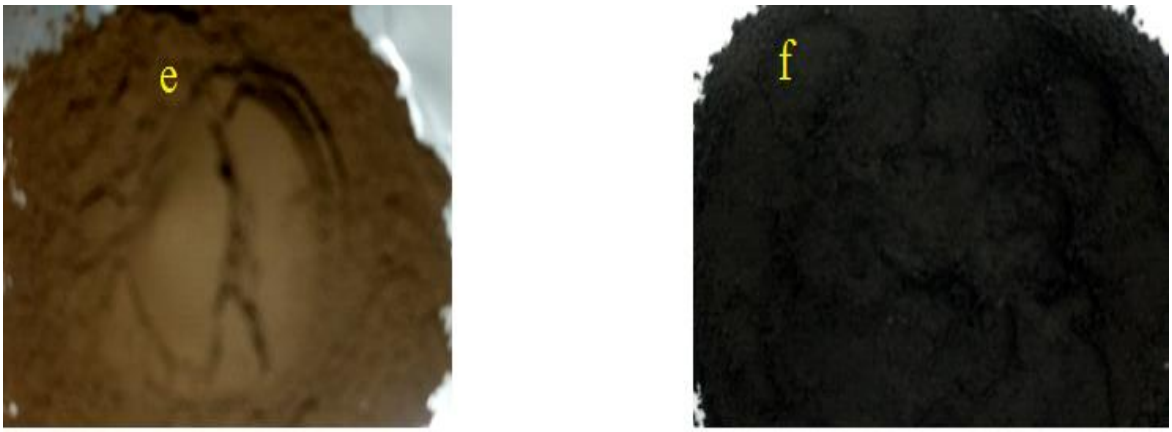

Figure 21: The powder of GO (e) and rGO (f).

Mechanisms of GO reduction:

$KMnO_4$ donates a large number of oxygen to the precursor graphite to produce GO in the presence of chopping and intercalating agent H_2SO_4/H_3PO_4. Hence GO possesses large amount of oxygen containing functional group at its basal plane (epoxy and hydroxyl) and at its edge (carboxyl, carbonyl and hydroxyl). GO make use of these active sites to react with the other active site on the alkaloids, polyphenols, carboxylic of the *Vernonia amygdalina* extract. In this study the hydroxyl of methanol extracted polyphenols were reacted with the hydroxyl and epoxy group on the GO favoring a ring formation which was followed by ring opening that facilitates the reduction of GO. Besides, the hydroxyl group on the polyphenols of plant extract was reacted with the carboxylic group of the GO and generating an ester in the condensation process. In each of this process a cleavage of bonds were occurred and reduction of GO were progressed. In the meanwhile the long chain methanol extracted compounds such as the carbonyl; hydroxyl and esters were involved in the capping agent of the synthesized rGO through π-π* stacking interaction principle (Mahendran et al., 2020). The nucleophilic substitution reactions were happened simultaneously as in the case of SN_2 principle (Manchala et al., 2019).

As can be seen in Figure 22, three different colors (a, b, c) were dominantly displayed during the stepwise synthesis of bismuth sulfide. Immediately as the solutions of white crystalline salt $BiCl_3$ and the white fine powder CH_4N_2S were mixed, a corn yellow colored solution was formed as indicated in Figure 22a. This is the initial step and

indication of the generation of sulfide ion as a result of hydrolysis reaction by the action of OH^- in aqueous solution as shown by equation 17 (Walker et al., 1956).

$$(NH_2)_2CS + 2H_2O \xrightarrow{\Delta} 2NH_3 + 2CO_3^{2-} + S^{2-} + 2H_2O \quad (17)$$

Upon the addition of *vernonia amygdalina* plant leaves extract and heating under continuous stirring, the deep black color was formed as shown in Figure 22c, through the royal yellow color solution, Figure 22b. The brown oily supernatant (Figure 22d) was decanted and a black past was collected from which the black powder was obtained by oven drying at 100 ^{0}C overnight as depicted in Figure 22d.

Figure 22: The color change observed during the stepwise synthesis of bismuth sulfide by using methanol extracted VA, indicated from a-e.

4.1.2 UV-Vis analysis

The diluted solution of different solvent extracted *Vernonia Amygdalina* as shown in Figure 23 was analyzed using UV-Vis spectrophotometer.

Figure 23: Extracts solutions of *Vernonia Amygdalina* using ethanol (EE), water (WE), and methanol (ME) solvents.

As it can be seen from Figure 24, the total peaks of UV-Vis record for the three extracted solutions were found between 220 to 700 nm and the numbers of major peaks observed when methanol and ethanol used were almost identical. The presence of the peak at (319 nm) on water extracted leaf indicates the existence of alkaloids (N. G. Vinokurova, N. F. Zelenkova, B. P. Baskunov, 2014). In this study, terpenoids were also observed in the wavelength range of 235 to 375 nm in both methanol and ethanol extracts which is consistent with the works of Malik and Ahmed (Malik & Ahmed, 2018). Total Phenolic compounds are observed on all the three extracts between 250 and 420nm specifically at 319 nm on water, 334 nm on both methanol and ethanol (Kocsis & Hideg, 2013). This crude extract also showed an absorbance peak at around the wavelength of 242 nm which shows the presence of tannins (Naczk et al., 2001). As shown in Figure 24, saponins has a maximum peak absorption at 235 nm which is in agreement with other reports (C. Yuan et al., 2018).

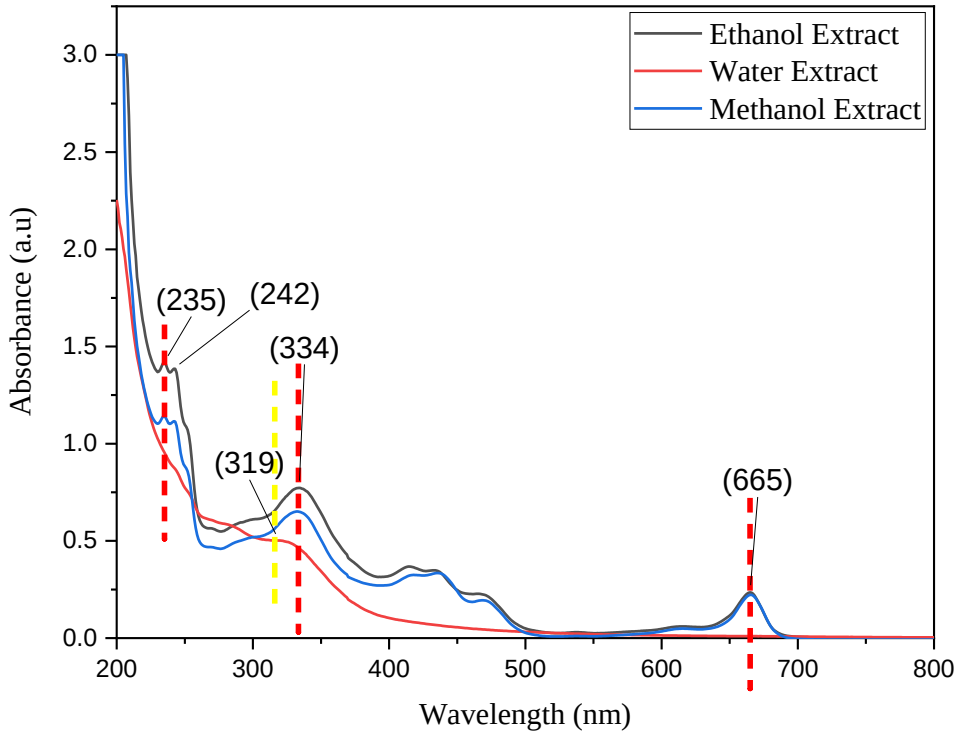

Figure 24: UV-visible absorbance spectra record of bitter leaf extracts of *Vernonia Amygdalina* in methanol, ethanol and water.

The UV-Vis records of the resulting reduced graphene oxide were shown in Figure 26. As it can be clearly seen from the Figure, rGO was successfully formed from GO by using VA plant extract as reducing and capping agent.

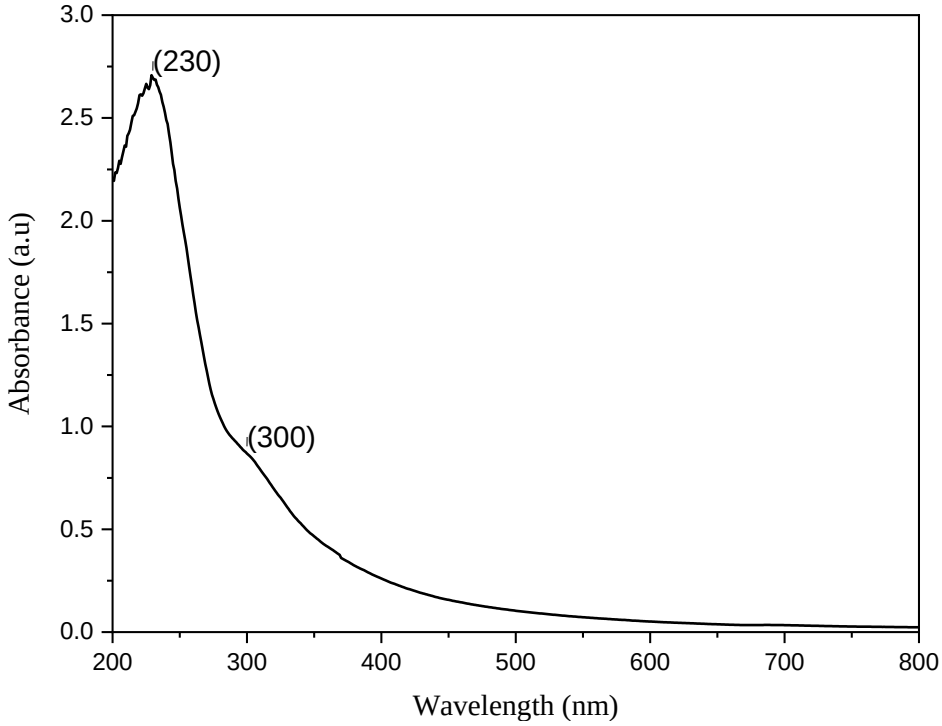

Figure 25: UV-visible absorbance spectral record of GO synthesized by modifying the tour improved method.

The confirmation of the formation of rGO was shown by the increment of the wave length from 230 nm for GO (Figure 25) to an absorption peak greater than 250 nm in the case of rGO (Dideikin & Vul', 2019; Fentaw & Worku, 2017; MM et al., 2017).

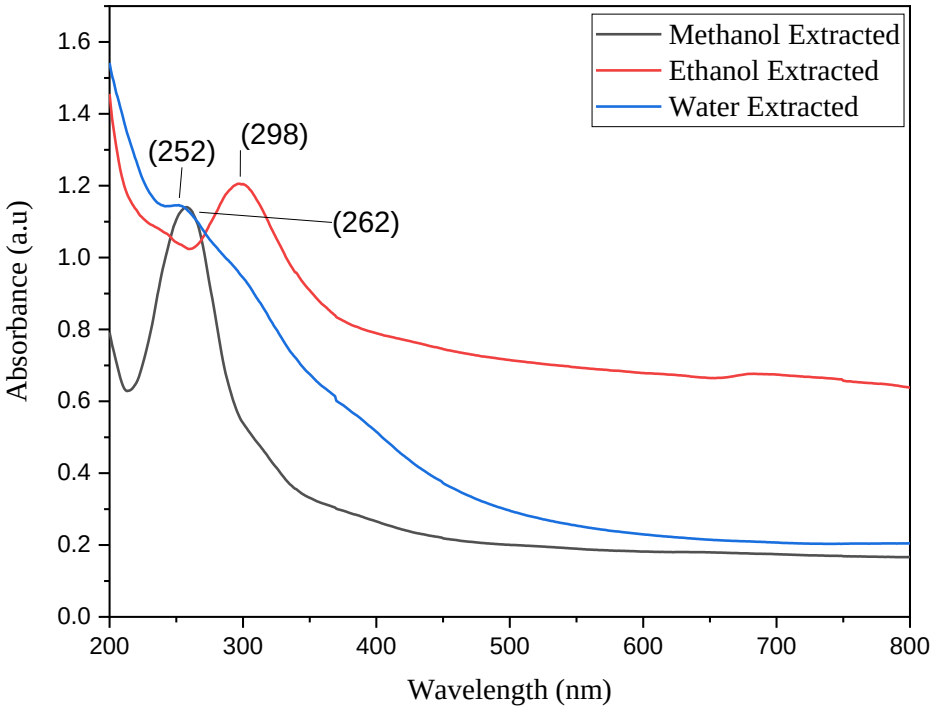

Figure 26: UV-visible absorbance spectra record of rGO reduced with methanol, ethanol and water.

The increase in the wavelength or the red shift was occurred probably due to the increase in the concentration of electron at the edge and basal plane of the graphene material which in turn confirms the restoration of the electronic conjugation. As shown in Figure 26, the UV-Vis spectral values of rGO obtained using methanol, ethanol and water extracted compounds of VA was 262, 298 and 252 nm, respectively. Even if the three solvent extracted compounds from VA plant were capable to reduce GO to rGO, based on the analysis made on peak position, the intensity and clarity of absorption peak and the previously reported UV-Vis absorption peak value of rGO, the one recorded when methanol used as a solvent for extraction was the best method for the green synthesis of reduced graphene oxide.

As shown in Figure 27, the π-π* transition λ_{max} values for GO is observed at 230 nm and for rGO was at 262 nm which means a peak at larger wavelength was recorded for rGO. This specify that most of oxygen functionalities were removed from the surface of GO and conjugations C=C remains restored. This indicates that there are a large number of -C=C- free conjugations in rGO.

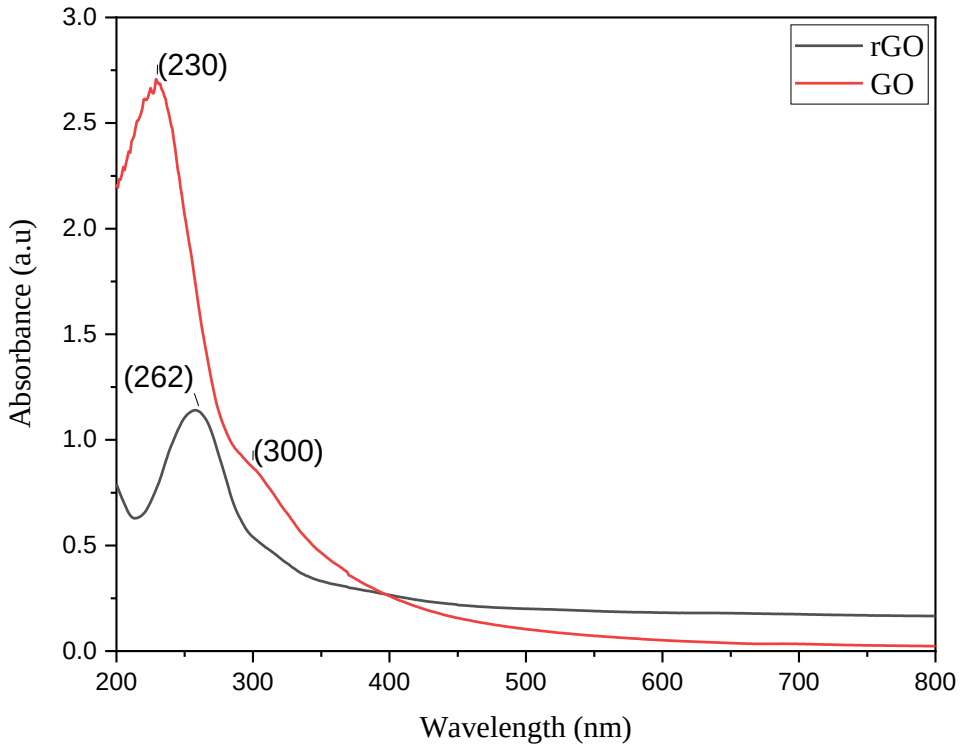

Figure 27: UV-Vis absorbance spectra record of GO and rGO.

In this case a small amount of energy is required to remove its electron. As the absorption peak decreases, there must be decrease in the delocalization of electron which means on the other hand decrease in the degree of conjugation. In this case large amount of energy

that is required to remove electron is needed because of their strong attachment to the parent in the localized bond. Here more electronegative oxygen atom is occupied either at the basal plane or at the edge so that less delocalization effect was observed. A shoulder peak was also observed at 300 nm as shown in Figure 27 which was attributed to n-π* transition. The n-π* transition is a transition occurred from either hydroxyl or carboxyl or carbonyl group in the structure of GO and rGO. As a result of reduction reaction, GO is deoxygenated and converted into rGO with a less number of attached oxygen and there must be a greater number of n-π* transition in GO than rGO. The higher the intensity of n-π* transition the higher is the degree of oxidation (Feng et al., 2020).

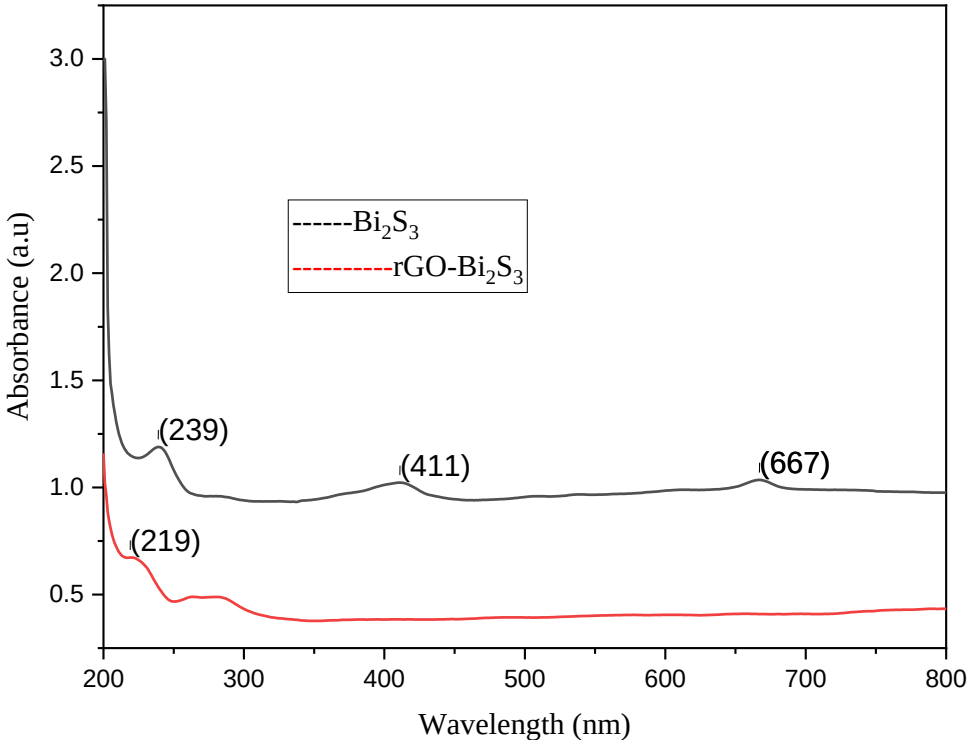

Figure 28: UV-Vis absorbance spectra record of Bi_2S_3 and rGO-Bi_2S_3 composite.

In UV-Vis analysis of Bi_2S_3 and rGO-Bi_2S_3 as shown in Figure 28, peak observed at around 400 and 680 on bismuth sulfide was disappeared in the case of the heterostructure composite.

4.1.3 GC-MS analysis

The chromatograph profile of the yields of extracts in the three solvents recorded by GC-MS is shown in Figures 29a, b, c for methanol, ethanol and water respectively. It revealed a complex mixture of compounds. However, similar to UV-Vis analysis, the major mother components of the extracts identified by GC-MS were terpenoids, fatty acids and their esters. Terpenoids are a family of asteraceae and fatty acids including their methyl and

ethyl esters occur in different abundance in the extracts of *Vernonia Amygdalina* (Abirami & Rajendran, 2012; Igwe & Ijeh, 2015). The major peaks with the largest area observed in each solvent were 10 for methanol, 7 for ethanol and 6 for water. This analysis revealed almost similar constituents in all the three extracts; however it displays many additional compounds in water extracts. The overall retention time in case of methanol ranges from 3 to 23.56 minutes, in case of ethanol ranges from 3 to 20 minutes and in case of water it ranges from 3 to 23.90 minutes. Retention time – or maybe more accurately, retention volume – is to analytical chemists almost the most important feature of the chromatogram since it is the key to separate, identify and to quantify the analyte of interest from any complex media. In fact, peak identification is initially accomplished by comparing the retention time of the unknown component to that of a standard. As a consequence of this prime consideration, great efforts have been dedicated to develop standard chromatographic methods that allow the identification of mixture components based on their retention times. Gas chromatographic elution, however, shows a significant variation from run-to-run in the time domain due to uncontrollable fluctuations in temperature and pressure, and from sample to sample due to matrix effects and column degradation(Etxebarria et al., 2009). Therefore, GC-MS gives a uniform identification of mixture components.

The interpretation of the GC-MS spectrum was done based on the NIST library and the fragmentation patterns given in Figures 29a, b, c have helped in the identification of a particular class of compounds.

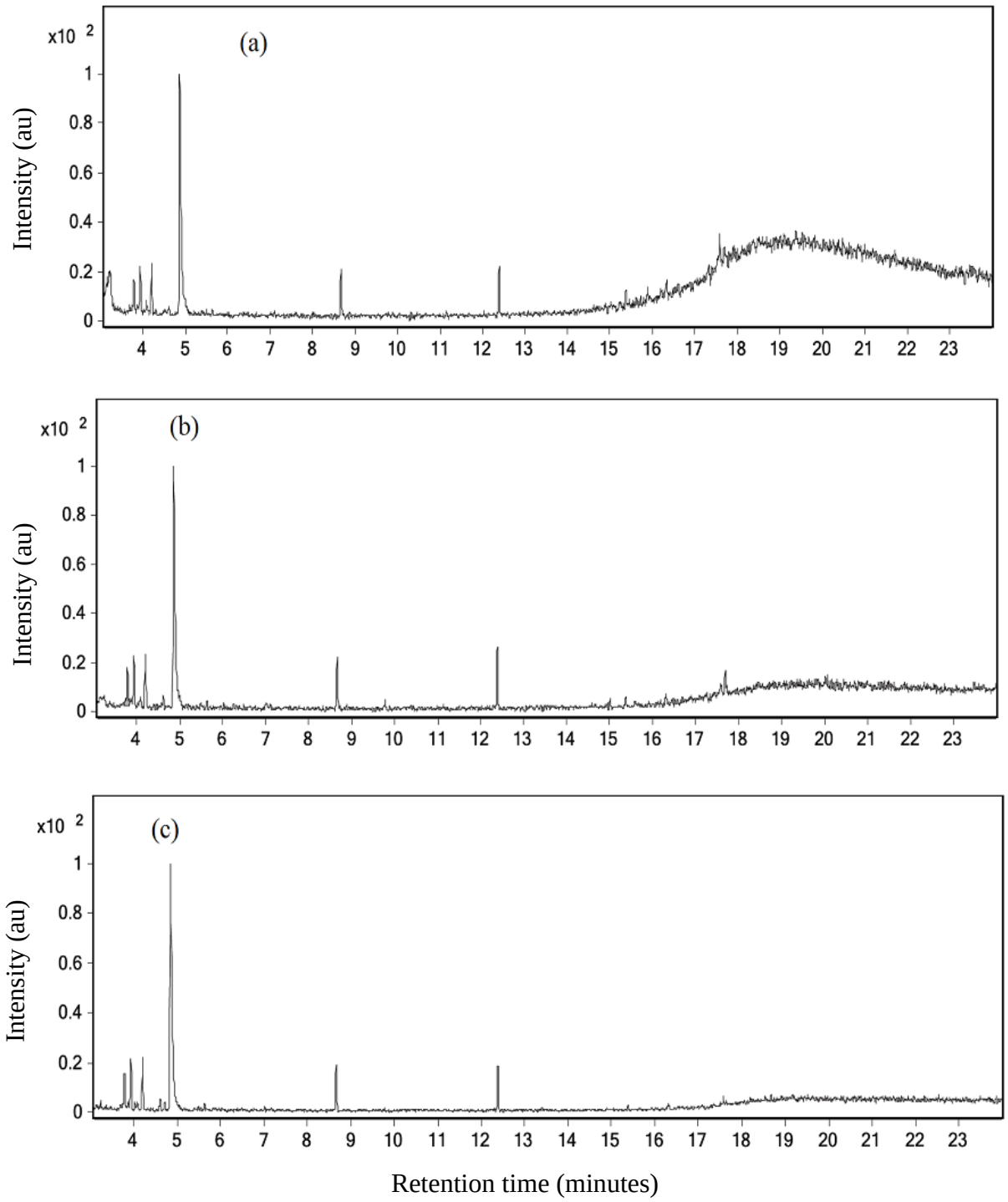

Figure 29: GC-MS chromatogram of bitter leaf extracts in (a) methanol (b) ethanol (c) water.

In this study, about six common compounds were extracted using the three solvents and these compounds were used as a reducing agent and/or capping agent in the green synthesis of reduced graphene oxide. However there were also some compounds which were specific and they are unique to their corresponding extracting solvents. The comparative study of reduction capacity of the three solvent extracted compounds based

on whether the common compound or unique compounds are involved in the reduction reaction process was elaborated. If only one of the solvent extracted compound i.e. which is not found in common in the two or three solvent cases reduce GO to rGO then the reducing agent is a finger print to the specific solvents. The following Tables (Tables 3, 4, and 5) describe the compounds which are common to two of the three or to all the three solvents and compounds which are specific to each solvent respectively.

Table 3: GC-MS identified antioxidant/capping compounds common to all solvent extraction.

S. No	Compound Name	Retention time (in minutes.)			Molecular formula
		M	E	W	
1	1,2,3-tri(t-Butyl) cyclo propenylium tribromide	15.8	15.0	7.12	$C_{15}H_{27}Br_3$
2	1,2,3-tri(t-Butyl) cyclo propenylium hydrogen dichloride	9.87	16.3	4.40	$C_{15}H_{28}C_{l2}$
3	2-(4-oxa-5-azaspiro [2,4]hept-5-en-6-yl methyl) cyclo hexanone	10.8	8.88	15.7	$C_{12}H_{17}NO_2$
4	1,1`-(1-(4-chlorophenyl)-5-methyl-1H-pyrozole-3,4-diyl)-bis(3-(furan-2-yl) prop-2-en-1-one	11.1	20.1	23.9	$C_{24}H_{17}ClN_2O_4$
5	(4Z)-4-octene	8.67	8.67	8.67	C_8H_{16}
6	5-methyl-6-oxa-1-aza-bicyclo [3.1.0] hexene	4.86	4.86	4.86	C_5H_9NO

Note: M = Methanol, E = Ethanol, W = Water

The mass spectrum allows us to identify the compounds from millions of potential chemicals. As sample molecules exit the GC column and enter into the mass spectrophotometer, they encounter an energy source. This energy removes a single electron from the sample molecule and the products were moving through the mass spectrometer, where the detector is only sensitive to positively charged molecules. The detector transforms the number of molecules into an electrical signal and integrator translates this individual signal peaks into a bar graph. The abundance is plotted as a function of molecules mass to charge ratio (m/z) on a bar graph as shown below in Figures

30a, b, c. Here the base and the molecular ion peaks were only given due attention for the selection.

Table 4: GC-MS identified antioxidant/capping compounds common to two of the solvent extraction.

S. No	Name of the compounds	Retention time		Molecular Formula	Solvent	
1	2-[(1-methylbutyl)-1-(phenyl methyl)] Benz imidazole	3.69	3.69	$C_{19}H_{22}N_2O_2S$	M	W
2	[2,4-dimethyl-6-nitro-2-(3-nitrophenyl)-3,4-dihydro-2H-1-benzopyran-3-yl] phenyl methanone	3.79	3.79	$C_{24}H_{20}N_2O_6$	M	W
3	3.alpha.-methyl-3.beta-formyl-5.alpha.H, 7.alpha.H, 6.beta.H, 11.beta.H-eudesman-6,12-olide	15.4	16.3	$C_{15}H_{22}O_3$	E	W
4	Phenyl-4- [bis (ethoxycarbonyl) but-3-ynyl]-2,3,4-trideoxy-.alpha.,L-glycero-pent-2-enopyranoside	4.09	23.9	$C_{21}H_{26}O_6$	E	W
5	(E)-methyl-5-(6-fluoro pyridin-3-yl)-5-hydroxypent-2-enoate	12.4	12.4	$C_{11}H_{12}FNO_3$	M	W

Note: M = Methanol, E = Ethanol, W = Water

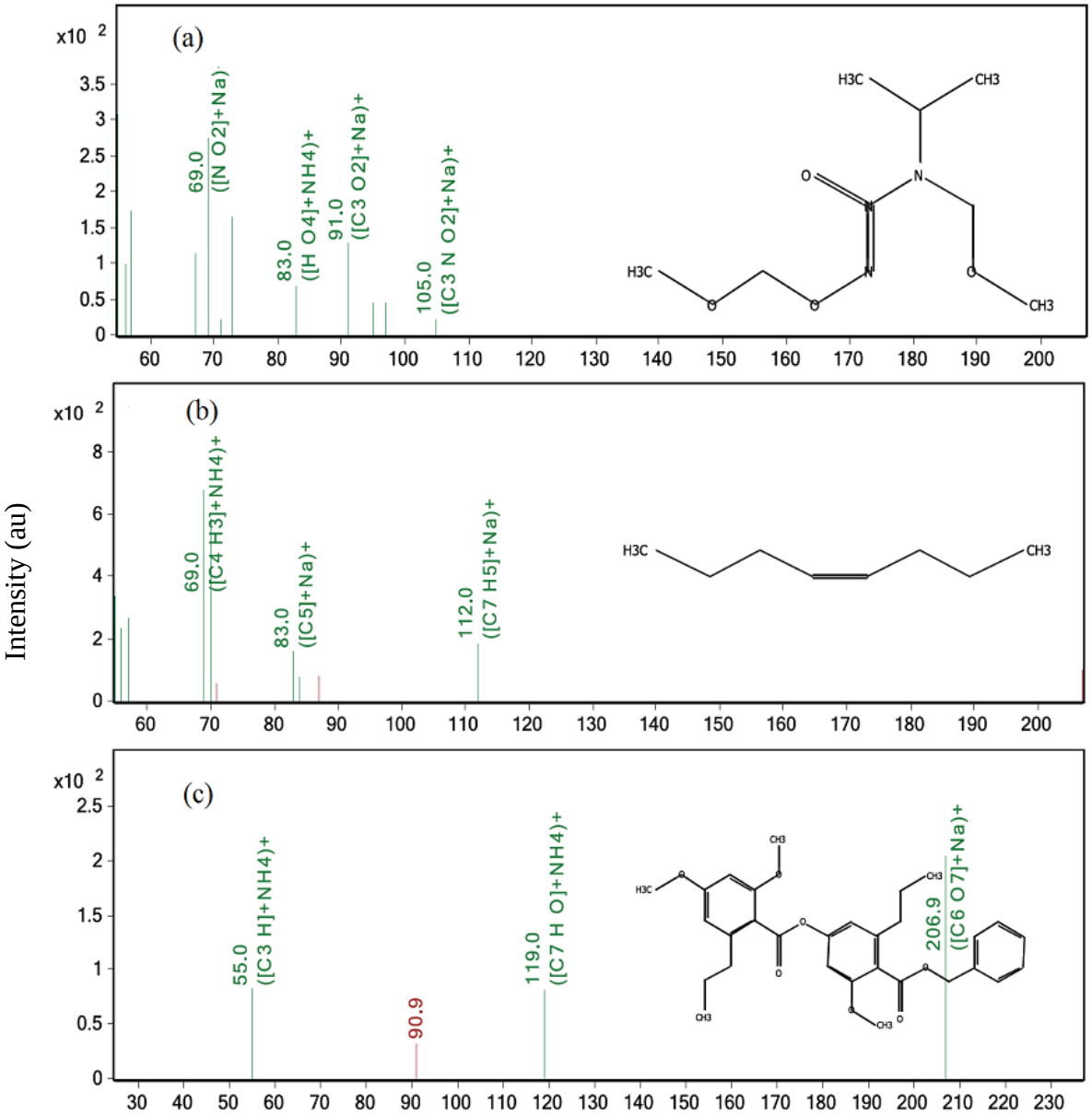

Figure 30: the structure of extracted compounds of *Vernonia Amygdalina* and its corresponding mass spectrum in (a) methanol (b) ethanol (c) water**.**

Table 5: GC-MS identified antioxidant/capping compounds specific to one solvent extraction.

S. No	Name of the compounds	Retention time (in minutes)	Molecular Formula	Solvent
1	7,9-(p-methoxyphenylidene dioxy)-5-methoxy-2,4,6,8-tetra methylnonan-1,3-diol	17.6	$C_{22}H_{36}O_6$	W
2	5-(4-aminophenyl)-10,15,20-triphenylprophirin	15.4	$C_{44}H_{31}N_5$	W
3	Ethanone, 2-[(1-methyl-2-prpenyl)oxy]-1-phenyl	3.78	$C_{12}H_{14}O_2$	E
4	2-propanoic acid, 2-methyl-, butyl ester	3.94	$C_8H_{14}O_2$	E
5	(S)-(E)-(-)-4-Acetoxy-1-one	23.6	$C_{20}H_{28}O_3$	M
6	14.alpha.-cheilanth-13(14)-enic methyl ester	20.5	$C_{26}H_{42}O_2$	M

Note: M = Methanol, E = Ethanol, W = Water

4.1.4 XRD Analysis

Figure 31 shows the XRD patterns and characteristic parameters of reduced graphene oxide. Many previous studies shows that the diffraction peak of rGO powder was formed at $2\theta = 24^0$ and corresponding layer to layer distance of 0.37 nm (MM et al., 2017; Romero et al., 2018).

In this study rGO was synthesized by a green method using solvent extraction. Antioxidant compounds extracted from plant *Vernonia Amygdalina* using solvents such as methanol, ethanol and water were used to reduce GO to rGO. The X-ray diffraction patterns of as synthesized rGO was recorded as shown in Figure 31.

From the pattern, the peak characterizing rGO obtained by a compound extracted by ethanol was located at $2\theta = 19.8^0$ with the corresponding d-spacing value of 0.44 nm. The peak characteristic obtained from water extracted compound was located at $2\theta = 21.3^0$ and d-spacing of 0.41 nm. In both cases we observed the maximum interlayer distance that deviates from the literature values which might be the result of the lower reducing capacity or the presence interfering impurities, in compounds extracted by these solvents.

The XRD patter also shows a perfect peak at $2\theta = 24^0$ with the d-spacing of 0.37 nm. This peak depicted the formation of graphene with few layers or the appropriate reduction of graphene oxide to reduced graphene oxide. This peak corresponds to the reduction of GO by methanol extracted compounds of *Vernonia Amygdalina*. Thus there must be methanol extracted compounds (methanol finger print) that were not common to the other solvent participated in the reduction process. There are compounds such as cheilanth-enic methyl ester and acetoxy-one in Table 5 which was supposed to be the most effective compounds found only in methanol extracted VA to act as a reducing and capping agent. There is also a peak at around $2\theta = 43^0$ on all of the three solvent extracted peak which is because of the turbostratic disorder exhibited by molecules of graphene based materials (Fentaw & Worku, 2017).

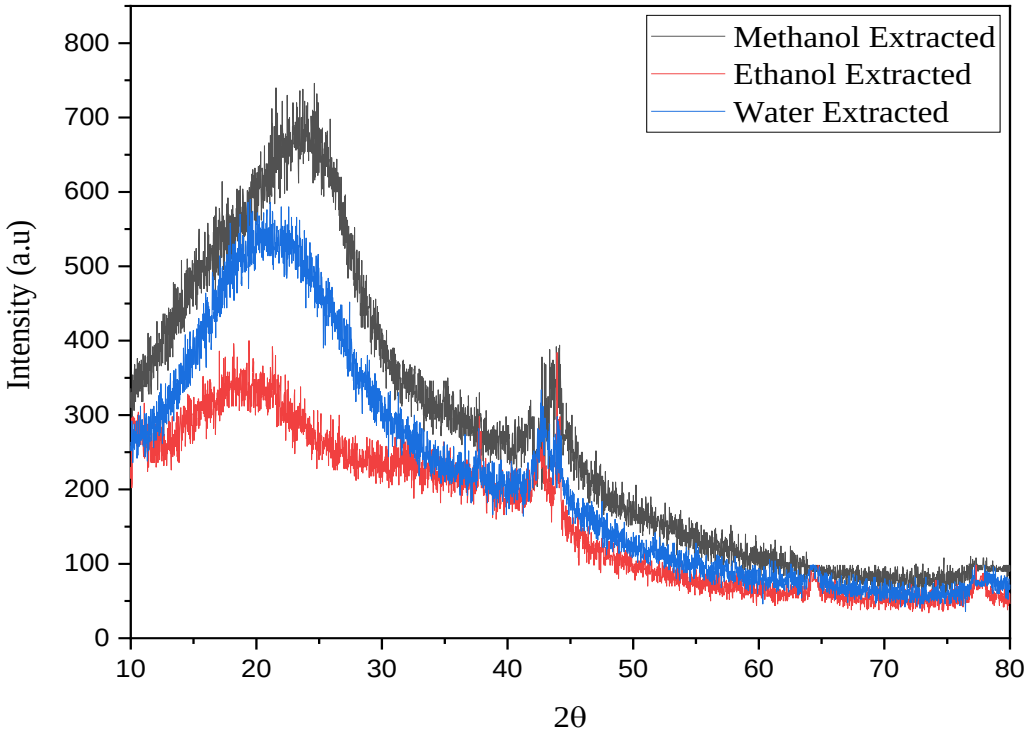

Figure 31: XRD diffraction pattern of rGO reduced with methanol, ethanol and water.

The changes in the crystal structure of graphite followed by its oxidation to produce GO and subsequent reduction to produce rGO was evaluated by XRD patterns as shown in Figure 32. Besides to structural arrangement, this characterization technique used to monitor the extent of oxidation and purity of the material under examination. The interlayer spacing and its corresponding sharp peak at 2θ value of graphite is 0.34 nm and 26.4^0, respectively which is in a good agreement with a graphitic nature and exactly matches with the literature values (Fentaw & Worku, 2017; MM et al., 2017). Regarding GO; the 2θ value was shifted to 10^0 and the d-spacing to 0.88 nm as a result of the

intercalation of oxygen containing functional group from the oxidizing agent $KMnO_4$ using the intercalating agent H_2SO_4. This insertion of oxygen containing functional group in the form of hydroxyl and epoxy across the basal plane and carbonyl and carboxyl at the edge of graphitic structure increases the interlayer distance significantly. Thus the bond between the layers became so weak that they can simply disintegrate to pieces of layers called graphene or rGO by introducing reducing and chopping agents.

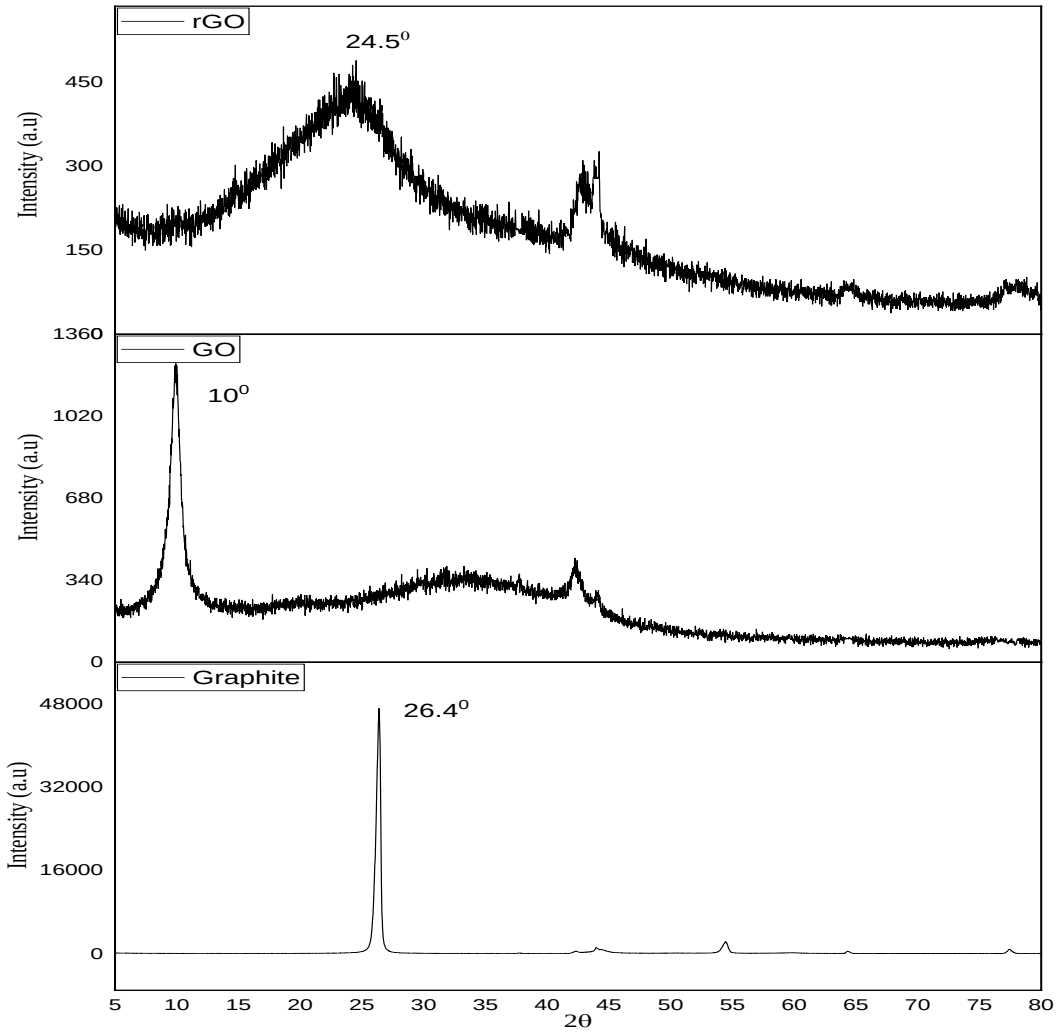

Figure 32: XRD diffraction patterns of graphite, GO and rGO.

Furthermore, peaks were observed at around $2\theta = 43^0$ in GO and rGO which were resulted due to slipping out of the alignments of crystal structure from basal planes. With the green reduction using methanol extracts of *Vernonia Amygdalina* (Dhebicha) of GO to produce graphene/ (rGO), there was a shift in the d-spacing and 2θ values to 0.36 nm and 24.5^0 respectively and this result confirmed the successful reduction of GO to graphene.

With the green reduction using methanol extracts of *Vernonia Amygdalina* (in Afaan Oromo called - Dhebicha) of GO to produce graphene/ (rGO), there was a shift in the d-spacing and 2θ values to 0.37 nm and 24.5^0 respectively and this result confirmed the successful reduction of GO to graphene/rGO separately.

The average crystalline structural properties of GO was also determined by using XRD techniques (Chufa et al., 2021; Fentaw & Worku, 2017). The XRD patterns showed the larger d-spacing for GO (0.88 nm) than graphite (0.34 nm) (Hessain & Hassan, 2020) and this is attributed to the insertion of a large number of oxygen containing functional group between the precursor graphite during oxidation process.

Figure 33 shows the XRD patterns of the as-synthesized Bi_2S_3 and rGO-Bi_2S_3 nanostructure. All the reflections in the diffraction peaks can be indexed as the orthorhombic structured Bi_2S_3 with lattice constants (of standard data) a = 11.150 A, b = 11.303 A, and c = 3.981 A (JCPDS No. 17-0320). The intensities and positions of the peaks are in a good agreement with literature values (F. Chen et al., 2013; Liao et al., 2001; H. Wang et al., 2002).

Here, the powder X-ray diffraction (XRD) is also used to determine the phase structure of the as-prepared rGO-Bi_2S_3 composite. The result obtained for rGO-Bi_2S_3 is slightly different from the XRD pattern of Bi_2S_3 which implies that the weak XRD spectra of rGO at $2\theta = 24.5^0$ is shielded by the strong peak intensities of Bi_2S_3 at around $2\theta = 25^0$. The peaks observed at $2\theta > 40^0$ in Bi_2S_3 is disappeared in the case of composites but get relatively narrower which is attributed to the degree of crystallinity and purity of rGO-Bi_2S_3. As it was determined from TGA analysis the amount of rGO in the composite is lower and as a result its peak is dominated by the peak of Bi_2S_3.

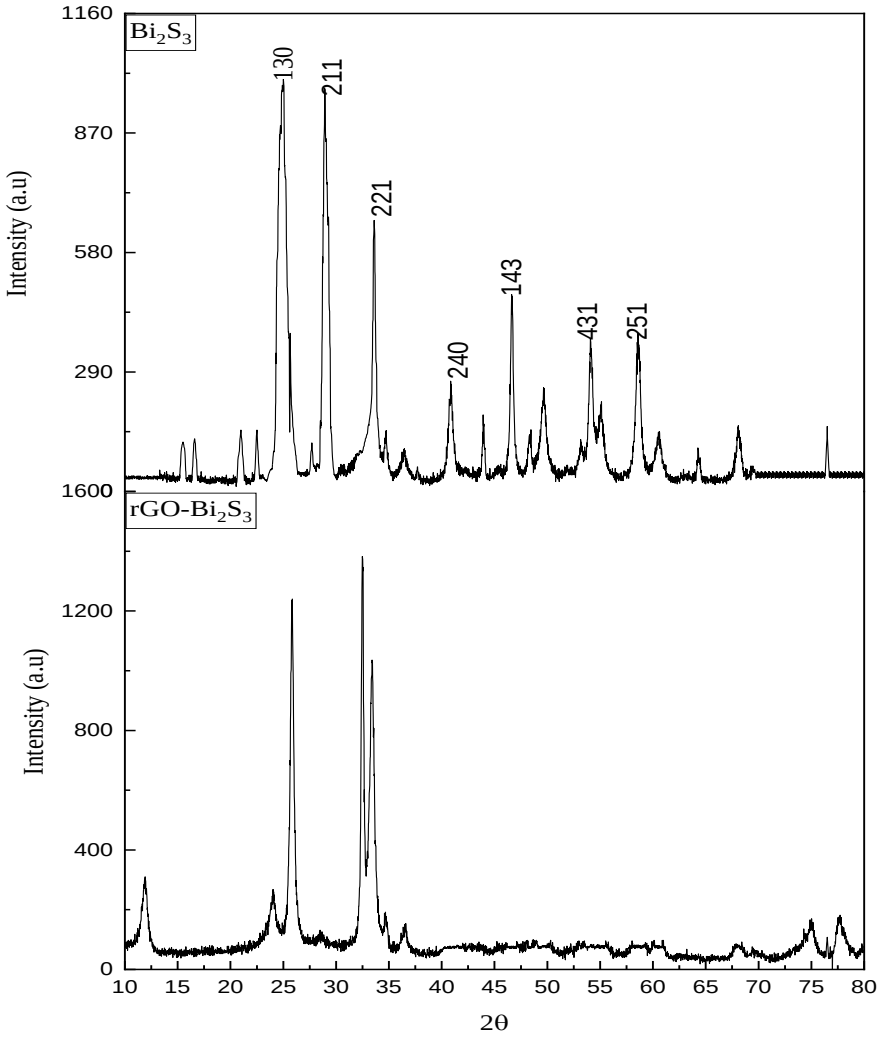

Figure 33: XRD diffraction pattern of as synthesized Bi_2S_3 and rGO-Bi_2S_3.

4.1.5 Fourier-transform Infrared spectroscopy (FTIR)

The functional groups and structure of GO was determined from its FT-IR spectral analysis as shown in Figure 34. The absorption peaks recorded were associated with their corresponding functional groups in the basal plane and edge of the mother GO structure. The broad band observed at 3400 $cm^{-1}$was for hydroxide groups, the bands at 2850 and 2920 cm^{-1} were for the C – H symmetric and asymmetric stretching frequencies respectively, the band at 1735 cm^{-1} was for the C = O carboxyl group, the band at 1623 cm^{-1} was for the C = C of aromatic rings, the band at 1378 cm^{-1} was for the stretching of the C – OH of the carboxylic acids, the band at 1226 cm^{-1} corresponds to the epoxide (C – O) functional groups and the one at 1051cm^{-1} was for alkoxy C–OH. Therefore, the presences of these oxygen containing functional groups in the structure of GO confirmed the successful oxidation of the precursor graphite to produce graphene oxide whereas the

sharp absorption band observed at 1623 cm-1 depicted the retaining of C = C in the aromatic ring in GO.

The structure of the prepared rGO was characterized using FT-IR spectroscopy. The FT-IR record displayed a broad stretching peak at 3408 cm^{-1} which was attributed to the ^{-}OH of the intercalated residual water molecules and the peak at 1634 cm^{-1} by the same molecules but due to bending vibration (Fentaw & Worku, 2017) is disappeared in rGO. As the oxygen containing functional groups were removed by the reducing agent, the characteristic absorption peaks of oxide groups decreased significantly and the CO_2 peak at around 2340 cm^{-1} vanished indicating the successful reduction of GO. The compounds obtained from *Vernonia amygdalina* (VA) by solvent extraction using methanol as a solvent was used to reduce GO to rGO. Most of the peaks related to carbonyl, carboxyl, and hydroxyl of water are disappeared in the spectra of rGO. The sharp band formed at 1570 cm^{-1} was attributed to (C=C) stretching. The absorption peak formed at 1222 and 1051 cm^{-1} as a result of stretching vibration of epoxide and alkoxy (C-O) group, respectively in GO is not observed in rGO which is also the indicator of the successful reduction of GO. Hence, the FT-IR spectra record confirms the complete reduction of GO to rGO and the rGO synthesized was used to prepare rGO-Bi_2S_3 nanostructure composite for the decomposition of methylene blue in the presence of visible light irradiation.

As the oxygen containing functional groups were removed by the reducing agent, the characteristic absorption peaks of oxide groups decreased significantly and the CO_2 peak at 2340 cm^{-1} vanished indicating the successful reduction of GO. The sharp band formed at 1570 cm^{-1} was attributed to (C=C) stretching.

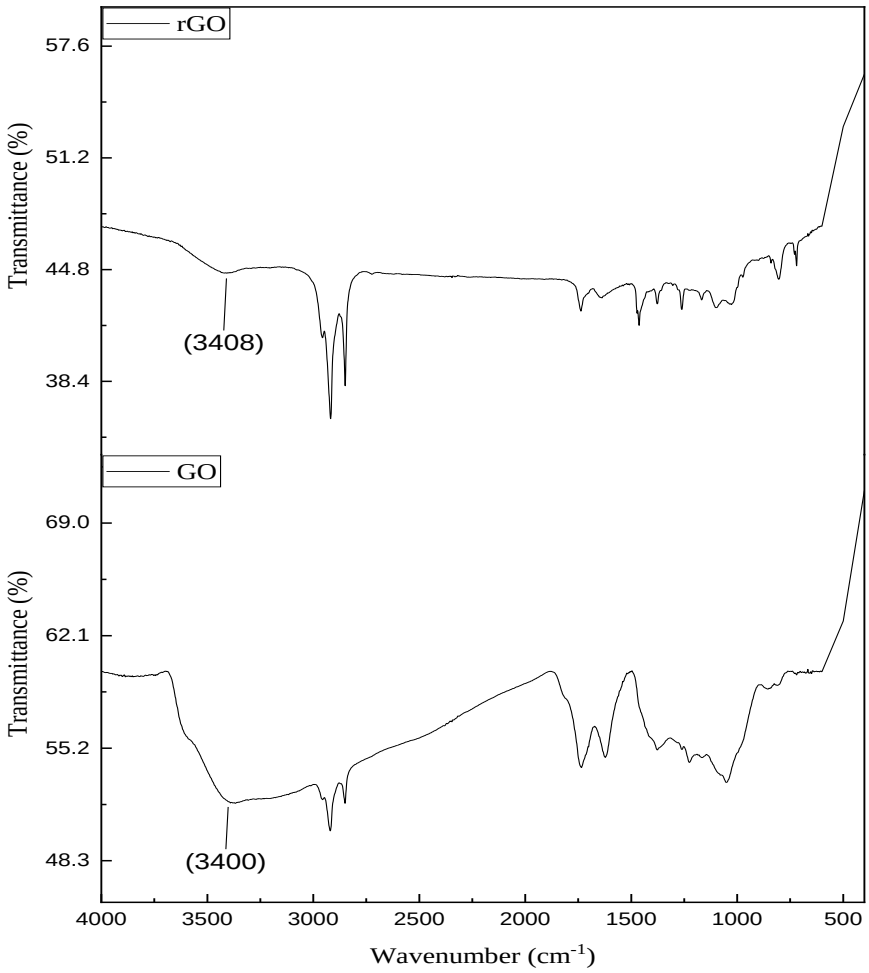

Figure 34: FT-IR absorbance spectra of GO and rGO.

The structural information of the rGO-Bi_2S_3 nanocomposite was further characterized by FT-IR spectroscopy as shown in Figure 35. Upon oxidation of graphite to GO, the observed representative peaks of rGO were significantly confirmed above. However, most of these absorption peaks related to the oxidized groups vanished in the FT-IR spectrum of the rGO-Bi_2S_3 nanocomposite, and a new absorption peak at about 1570 cm^{-1} appeared (corresponding to the aromatic skeletal C=C stretching vibration of graphene sheets), indicating the reduction of the functional groups and restoration of the π-conjugation structure of graphene during the reduction process. In addition, the additional peak at ~518 cm^{-1} could be due to the stretching vibration of Bi–S, suggesting that Bi_2S_3 NSs were successfully anchored on the surface of graphene. The new peaks at 2960 and 2864 cm^{-1} were attributed to the asymmetric and symmetric stretching vibrations of $–CH_2–$ groups, respectively.

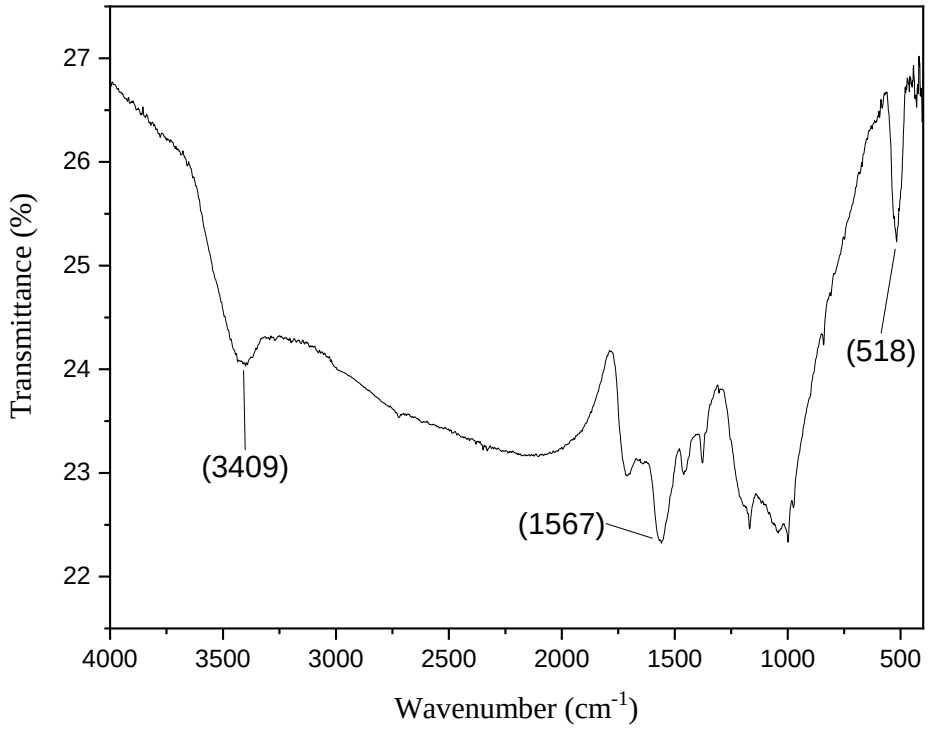

Figure 35: FT-IR absorbance spectra of rGO-Bi_2S_3 composite.

The relatively smaller band unlike that of broad peak in GO formed at 3409 cm^{-1} in Figure 37 is attributed to the O-H functional group of the residual water stretching and the band observed at 1567 cm^{-1} is due to the bending vibration of the same group(Z. Zhang et al., 2013). The relatively wide absorption peak formed at 1090 cm^{-1} is attributed to the interaction between rGO and Bi_2S_3 nanostructure composite(L. Zhang et al., 2015)

4.1.6 Scanning electron microscopy (SEM)

SEM is a powerful technique in providing informative data for characterizing microstructure such as corrosion, fracture, grains and grain boundaries(Choudhary, O.P. and Choudhary, 2017). Figures 36a, b, c show the micrographs for Graphite, GO and rGO at a magnifications of 17,000X, 18,000X and 18,000X respectively. Figure 36a shows the graphite micrograph which depicts the existence of platelet like crystalline structure of carbon. The graphite micrograph shown below appears to be ordered and compact stack with properly aligned edge because of the existence of Van der Waals forces which bonded its layer together. The SEM morphology of modified tour method synthesized GO in this work clearly shows a two dimensional sheet like structure. As indicated in Figure 36b, SEM image of GO showed smooth, wrinkled folded at its surface due to the expansion of layer because of insertion of oxygen containing functional group during oxidation. The layered flakes observed were the confirmation of complete oxidation of

graphite to GO. This is resulted in the destroying of the laminated structure in graphite so that the structure of GO is delaminated and disordered. Unlike graphite, GO sheets were thicker at the edge than at the basal planes because of the highly combination of oxygen containing functional group at the edge. As it can be observed from the SEM image of GO, its layers were independently suspended in the matrix and there is no sign of bending observed.

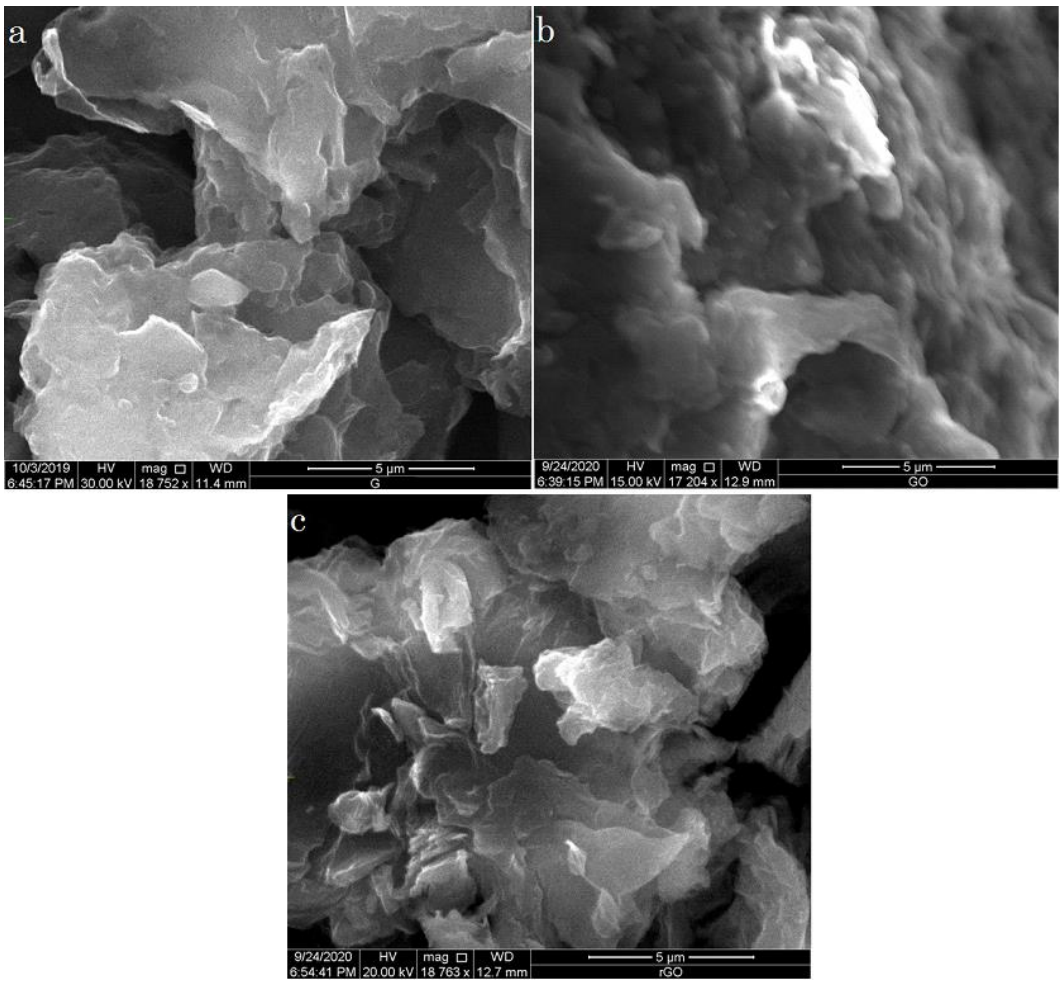

Figure 36: SEM image of a) Graphite, b) GO and c) rGO at the same magnification.

Figure 36c shows the micrograph of rGO obtained by the green reduction of GO using bitter leaf extracts. An improvement in the surface morphology of rGO was observed when compared with the surface morphology of GO because of the removal of wrinkled and folds. After the reduction of GO different forms of transparent and thin layers structure of rGO were obtained. SEM image of rGO demonstrate individual sheet like structure by means of self-assembly techniques which indicated the successful reduction of GO into rGO by using solvent extracted *Vernonia Amygdalina*.

The SEM images recorded under different magnification of the same sample of GO synthesized by slight modification to the improved method was shown in Figure 37 (a-d).It is evident from these micrographs that the GO showed more wrinkled and folded at its edges agglomerates with two dimensional sheets like structure shown in Figure 37 (b & c). In the GO morphologies given below because of the layer expansion due to the insertion of oxygen containing functional groups visible layer arrangements were recorded in Figure 38a, which was also reported in literatures (Choudhary, O.P. and Choudhary, 2017; Chufa et al., 2021). The multiple lamellar layer structures and independent individual sheets of GO were also observed in the micrographs as shown in Figure 38d. The thickness of GO observed at the edge is due to the combination of the oxygen containing functional group concentrated at the edge than at the middle portion.

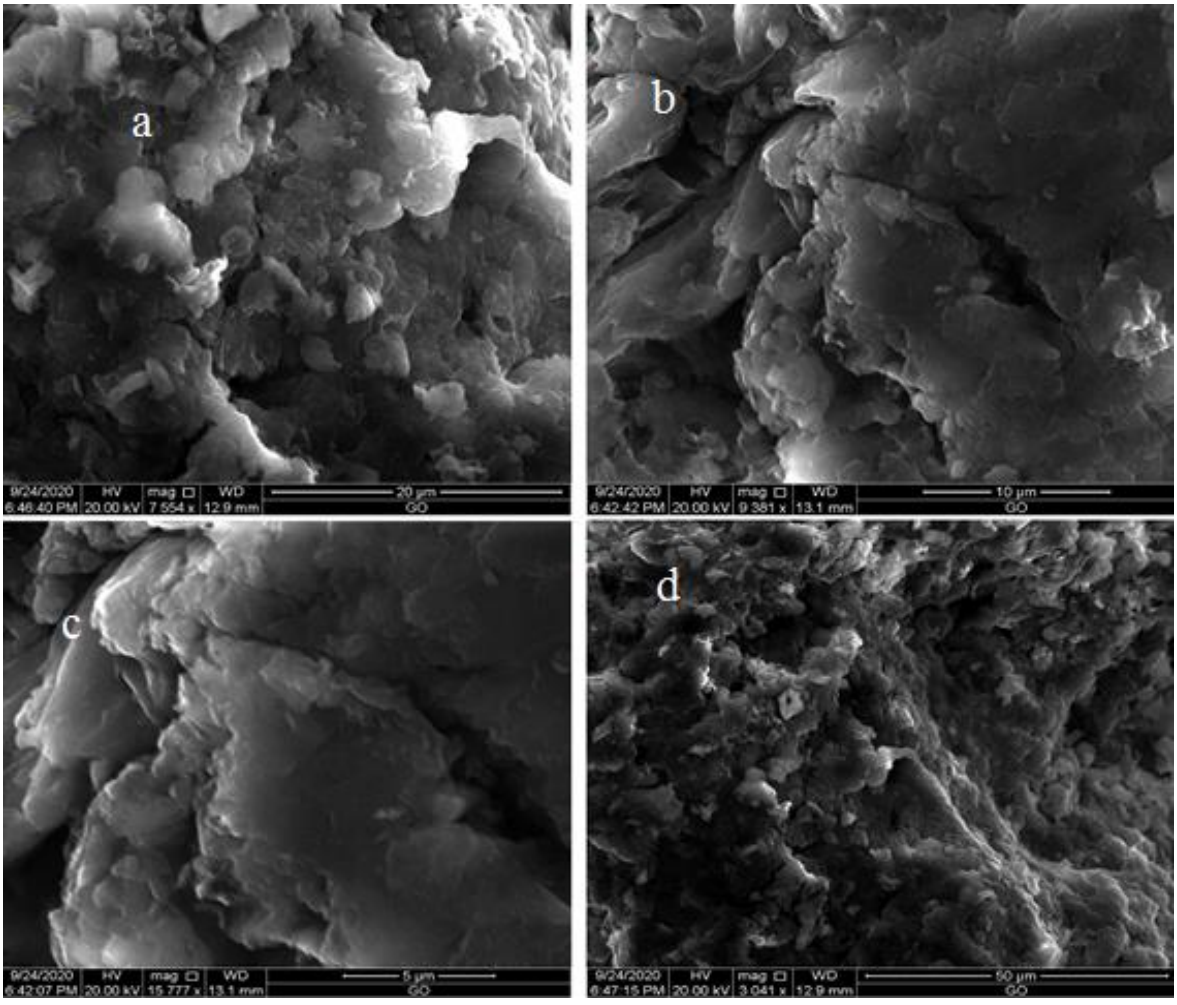

Figure 37: SEM image of GO at different magnification.

4.1.7 High resolution Transmission electron microscopy (HR-TEM)

HR-TEM was used to measure the particle size and investigate the morphology of the samples. Figure 38(a-d) and 40(f-i) show the TEM images recorded for GO and rGO

respectively. These materials were examined under HR-TEM to confirm the formation of GO and rGO and to determine their morphology and size.

The EDAX analysis was made to determine the elemental composition of GO and rGO. The EDAX result showed that C and O were the major components in addition to some impurities such as S from H_2SO_4, Na may be from plant extract, and Ca may also be from plant extract, Cl from HCl used for washing purpose, and K from the oxidizing agent $KMnO_4$; which must have completely removed during washing. As observed on the graph of EDAX, the percentages of oxygen were greatly reduced in the case of rGO and this is the indications of the reduction of GO to rGO.

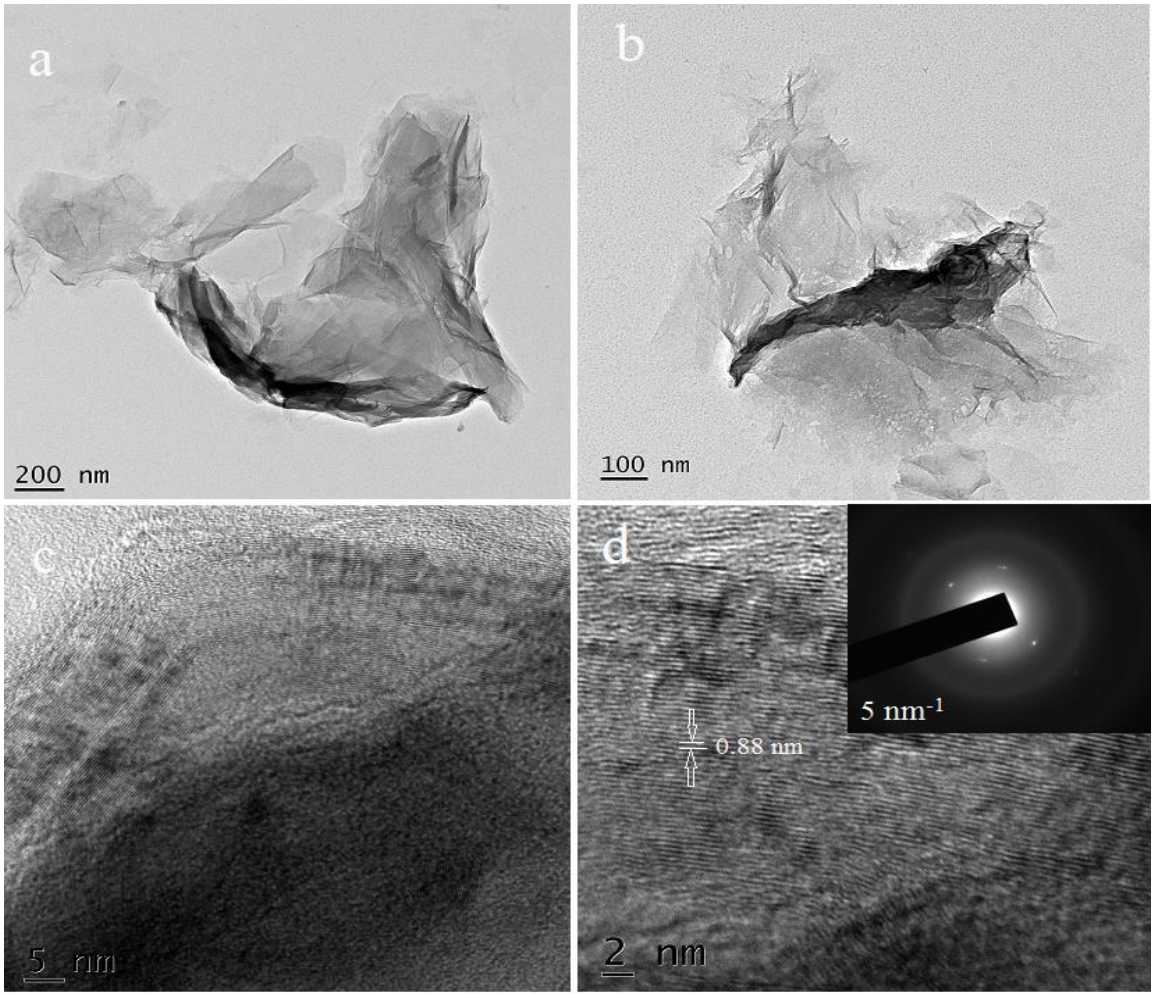

Figure 38: (a-d) HR-TEM image of GO and inset is SAED pattern of GO.

As it can also be seen from TEM image of Figure 38 (a and b), the highly electron transparent corrugated or wrinkled layered structure of GO was formed. It reveals a mixture of multi-layer graphene oxide (dark region) and few (single) layer of graphene oxide (transparent region). Even if the exact number of 2D nanosheet cannot be

determined, we can observe from the TEM and SEM image that there are no large graphitic aggregates present which indicate the formation of few layer of graphene. The folded edges observed on the TEM images of rGO were the indicators of the presence of the functional groups. The SAED pattern displayed the interlayer distance obtained by calculating the distance between two bright spot points around the core white spot were exactly match the values obtained from XRD analysis.

It can also be clearly seen that the rGO samples crippled and wrinkled structure which inhibits the restacking of the graphene sheets together. The TEM micrograph of rGO revealed that the edge of the sheets appeared to be smooth. The broad XRD peak and the diffused ring indicating the disordered structure and less crystallinity of materials were observed in SAED patterns of rGO.

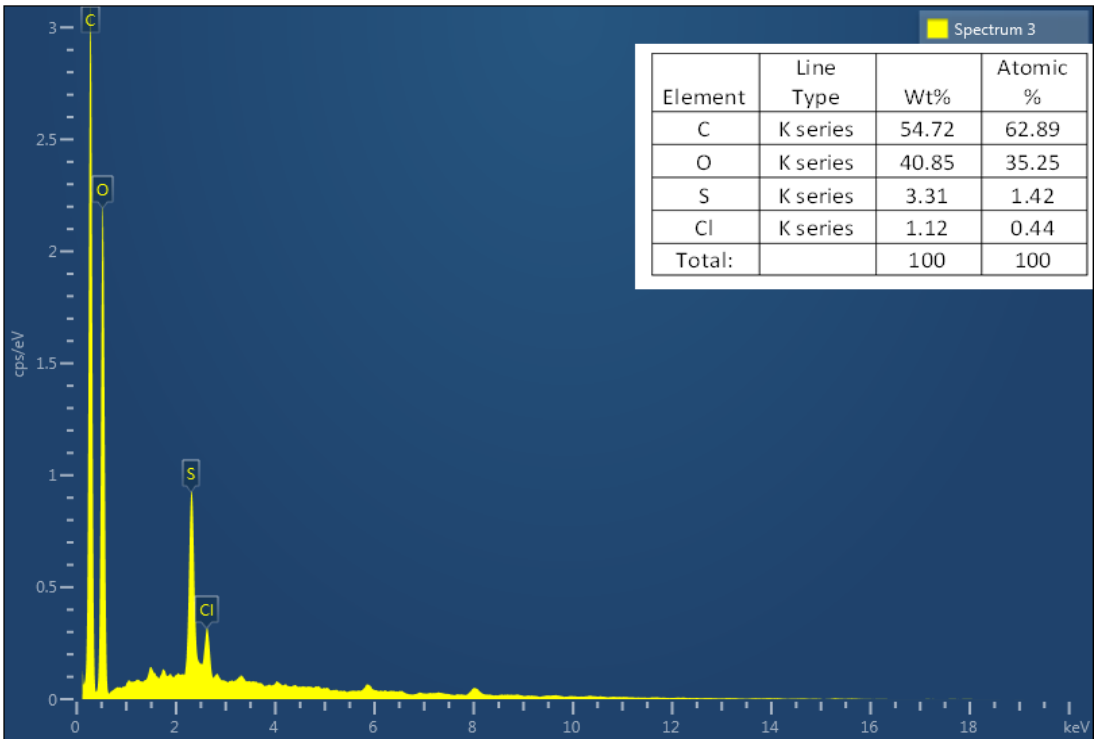

Element	Line Type	Wt%	Atomic %
C	K series	54.72	62.89
O	K series	40.85	35.25
S	K series	3.31	1.42
Cl	K series	1.12	0.44
Total:		100	100

Figure 39: Elemental composition of GO using EDAX.

Figure 41 (f-i) represents rGO micrograph which displayed plated rGO from a few layer to a single layer of graphene. This image depicted that the sample consists of scrolled, wrinkled and transparent which were often the indicators of few layers rGO sheets.

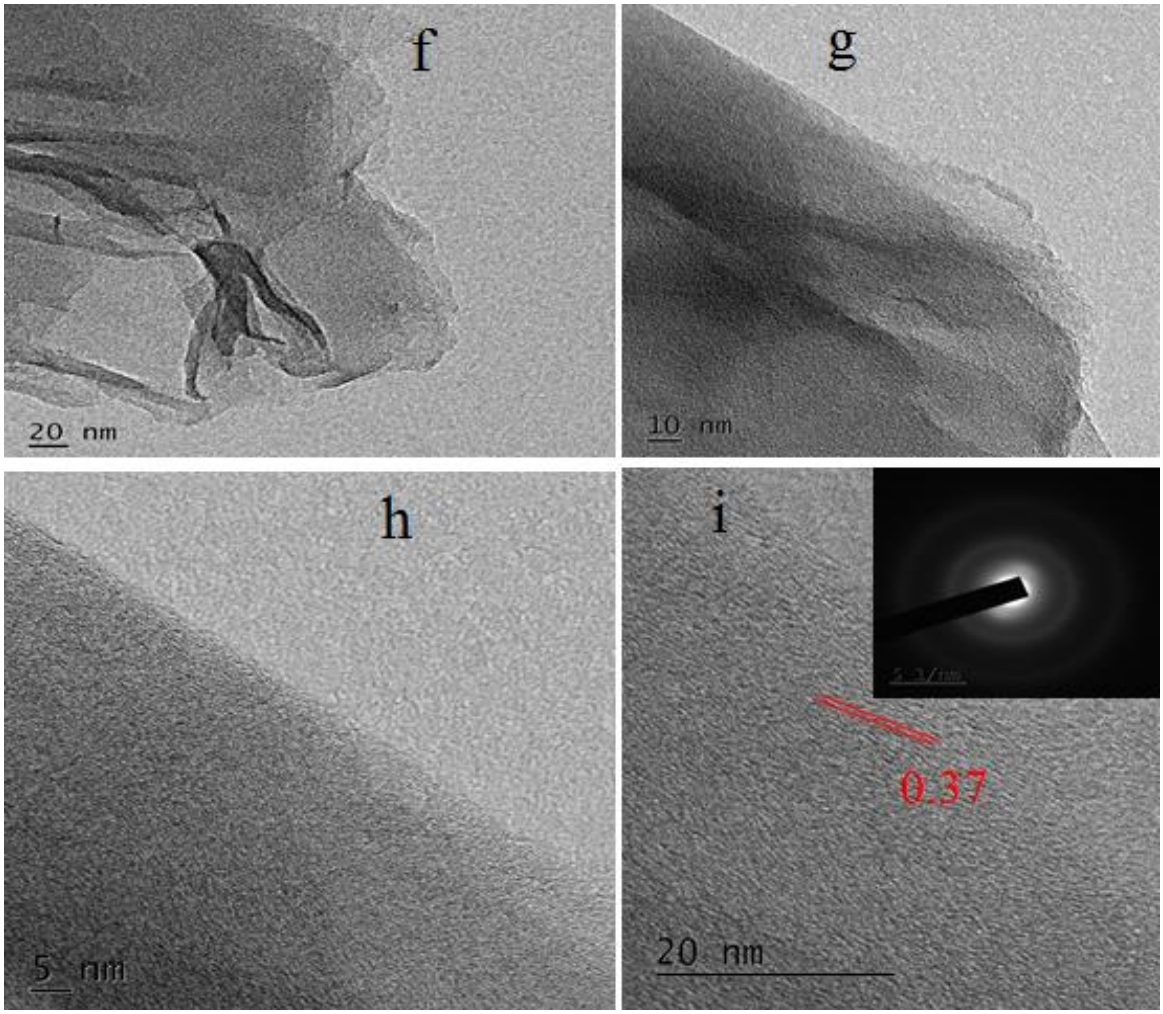

Figure 40: (f-i) HR-TEM image of rGO and inset is SAED pattern of rGO.

The Energy dispersive X-ray analysis (EDAX) obtained using K-series shown in Figure 39 and 41 for GO and rGO respectively revealed that the GO contains 62.89% of C, 35.25% of O and 1.42% of S. The EDAX analysis suggests that the rGO sheets contained 78.86% C, 20.30% of O, 0.17% of Si, 0.13% of S and 0.08% of Ca as reported by N. Rawal and S. Solanki (Rawal et al., 2020). The d-spacing of both GO and rGO was calculated to be 0.88 nm and 0.36 nm, respectively from the equation:

$$d - spacing = \frac{2}{distance\ between\ the\ two\ white\ spot}$$

As shown in Figure 39, the EDAX analysis is evidant that the GO contains a major parcentage of carbon and oxygen and small amount of sulfure and chloride which is possibly originated from H_2SO_4 and HCl, respectively.

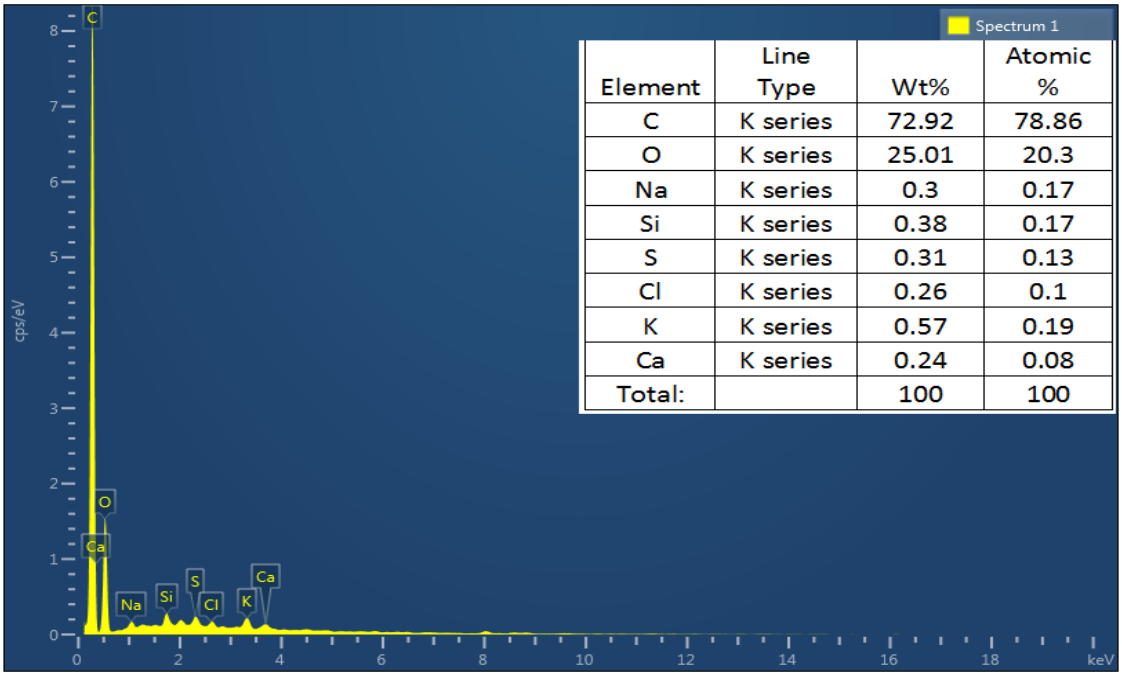

Element	Line Type	Wt%	Atomic %
C	K series	72.92	78.86
O	K series	25.01	20.3
Na	K series	0.3	0.17
Si	K series	0.38	0.17
S	K series	0.31	0.13
Cl	K series	0.26	0.1
K	K series	0.57	0.19
Ca	K series	0.24	0.08
Total:		100	100

Figure 41: Elemental composition of rGO using EDAX.

4.1.8 Thermal Stability Analysis

Figure 42 shows the DTA and TGA curves of Bi_2S_3 single crystal run from 0 to 1000 K under N_2 gas atmosphere. As it can be seen from the graph of TGA in Figure 42, the sample is slightly stable for the temperature range of 0 to 680 K with a weight loss of ~1-2% due to the decomposition of some compounds. The significant decomposition of the material with a severe weight loss was observed at around 700 K increasing continuously with rising temperature up to 1000K. The maximum weight loss recorded at 1000 K is 21% (Deshpande et al., 2015; Z. Ge et al., 2011). This weight loss is attributed to the decomposition of sulfur dioxide (SO_2) and the remaining product finally turns into Bi_2O_3 residue which is confirmed from DTA analysis Figure 42 that gives endothermic peak at around 910 K. Following with the severe weight loss at 700-1000 K, two exothermic peaks and two endothermic peaks were observed from the DTA curve. The maximum endothermic peak at around 910 K means that this temperature is the melting point of Bi_2S_3 which is supposed to be reduced from 1036 K due to the lowered particle size to the nanoscale.

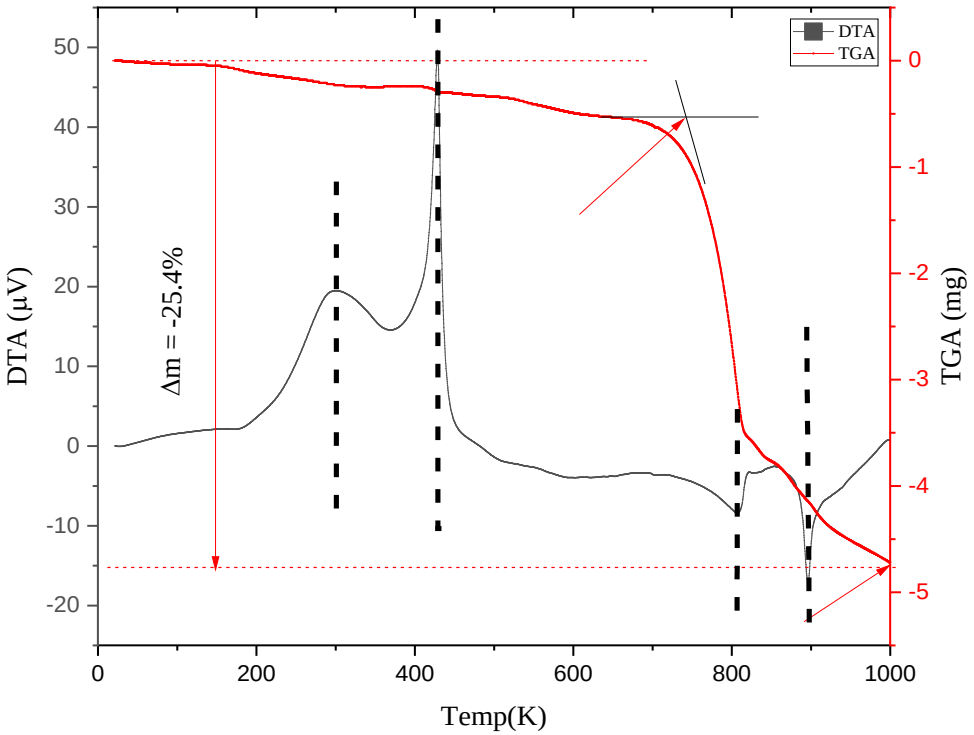

Figure 42: DTA and TGA curves of single crystal Bi_2S_3.

From the differential thermogravimetric analysis result shown in Figure 43, the oxidative decomposition temperature of rGO-Bi_2S_3 is 450 K. This value is less than the DTA value of pure rGO which is equal to 570 K (Hwang et al., 2020). The decomposition of rGO is enhanced when a metal sulfide is bonded to it because of the catalytic effects of the metal sulfide nanoparticles. Hence, the lower decomposition temperature of rGO in the composite is attributed to the catalytic effects of the Bi_2S_3 which confirms the anchoring of Bi_2S_3 to the surface of rGO to form the rGO-Bi_2S_3 composite. As it can be seen from the TGA analysis of Bi_2S_3 (Figure 43), maximum decomposition of the materials started at 700 K which is much greater than the value for the composite rGO-Bi_2S_3 which is equal to 430 K (Figure 43). The lowered decomposition temperature in the case of composite is attributed to the presence of oxygen that favors decomposition rate with low temperature.

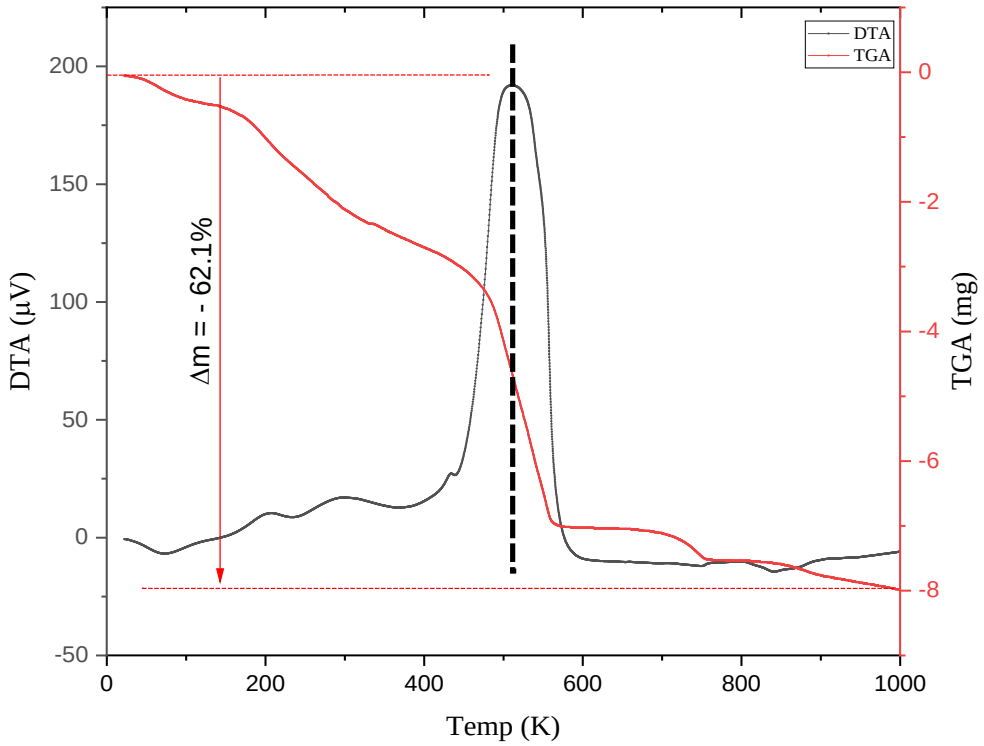

Figure 43: Thermal analysis results of rGO-Bi_2S_3 NSs composite.

4.3 Photocatalysis Study

4.3.1 Presumed Photocatalytic Degradation

As far as the mechanism of photocatalytic degradation is concern, the radical species that generated in the semiconductor photoexcitation play an important role for organic pollutant's degradation. The pictorial illustration of degradation using graphene/Bi_2S_3 as a photocatalyst in the presence of visible light is presented in Figure 44.

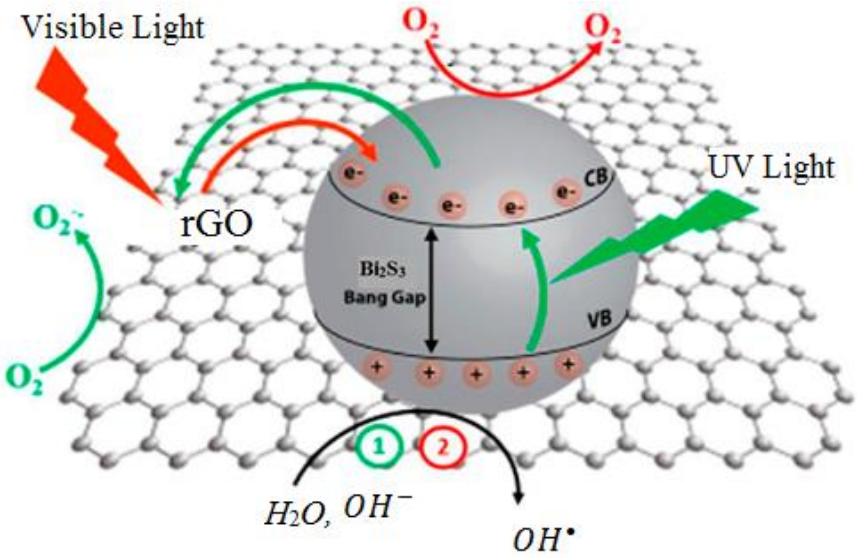

Figure 44: Mechanism of photodegradation by using rGO-Bi_2S_3 as a photocatalyst in the presence of visible light.

The most crucial steps which will involve in this degradation process can be pictured in the equations below.

$$\text{Photons } (h\nu) + \text{Semiconductor} \rightarrow h^+(VB) + e^-(CB)$$

$$h^+ + H_2O \rightarrow H^+ + OH^-$$

$$h^+ + OH^- \rightarrow OH^\bullet$$

$$e^- + O_2 \rightarrow O_2^\bullet$$

$$2e^- + O_2 + H_2O \rightarrow H_2O_2$$

$$e^- + H_2O_2 \rightarrow OH^\bullet + OH^-$$

$$\textit{Organic contaminant} + OH^\bullet + O_2 \rightarrow CO_2 + H_2O + \text{other } \textit{degraded products}$$

The mechanism also depends on certain conditions of experiment. The degradation mostly depends on the excited electron with hole inside the semiconductor. A variety of semiconductors are being employed with mostly nanosized state owing to the large surface area and effect of quantum size favorably. Different forms of Bi_2S_3 with either metal or non-metal doping can be applied in the various types of pollutant degradation due to stability, non-toxic properties and capability in degradation of dyes. Nevertheless, the application of this compound has been restricted for the degradation of organic pollutant commercially because of the possible variables related to experiment such as separation treatment technique. Bi_2S_3 has been attracting significant attention of researchers owing to its interesting band gap in the photocatalysis application for water purification. However, the small band gap of Bi_2S_3 is subjected to the risk of charge carrier recombination and its light response range but still very effective and efficient if composited with a platform which stabilize the band gap and optimize its light absorption range. The intensity of semiconductor scattering on the surface can vary and thus, the most variable is more accounted for the roughness factor value on the surfaces. Furthermore, the absorption coefficient value depends on different physical features such as roughness of surface, the size particle of inherent valence electrons occupancy added and the occupied wave functions.

4.3.2 Photocatalytic degradation of methylene blue

One of the organic dyes most extensively used in almost all textile industries is methylene blue (MB) and often pollutes the environment (Ya Liu et al., 2016). Thus, in this study we tried to examine the photocatalytic degradation performance of as-prepared rGO-Bi_2S_3 against this important as well as serious pollutant MB under simulated visible light

irradiation. The photocatalytic degradation of methylene blue (MB) was investigated in the absence and presence of as-synthesized rGO-Bi_2S_3 composite nanostructures (NSs) catalyst under visible light irradiation. As shown in Figure 45 in the photodegradation spectra of MB, there is no significant change observed in the intensity of MB in the absence of the catalyst. The maximum wavelength (λ_{max}) of the MB is 664 nm and the red and blue shift was not observed with the prolonged irradiation in the absence of rGO-Bi_2S_3 but there was insignificant intensity change (with a maximum decrease of 7%) at 20 minutes. Hence, the dye does not degrade when exposed to the light in the absence of catalyst. The decrease in the intensity of the spectra is not consistent with the time of irradiation in the absence of the catalyst as it can be observed in Figure 45. Hence, the use of a catalyst is mandatory to degrade dyes to prevent the environment from pollution.

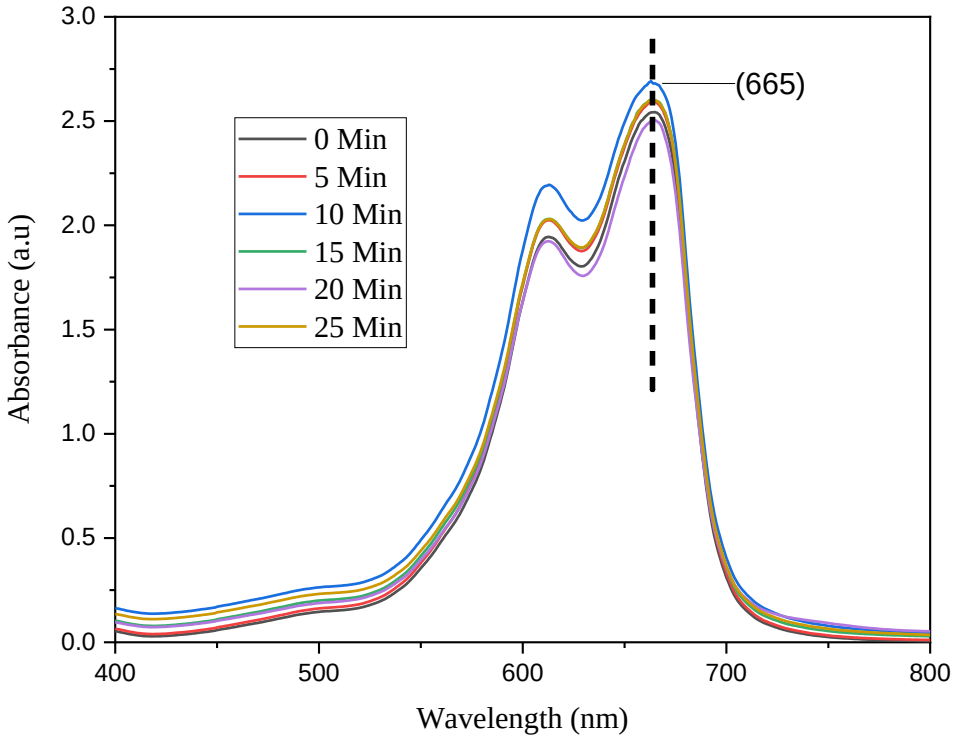

Figure 45: Degradation of MB in the absence of the catalyst under visible light at 5 minutes interval run.

It has been reported that graphene oxide (GO) significantly enhanced the efficiency of Bi_2S_3 in the degradation of dyes (methylene blue) (Ayodhya & Veerabhadram, 2018). As shown below in Figure 46, rGO displayed superior enhancement for the dyes degradation in this study. The degradations started immediately as a 1:25 ratio of catalyst to dye mixture was subjected to a visible radiation. The study was carried for a total of 25 minutes.

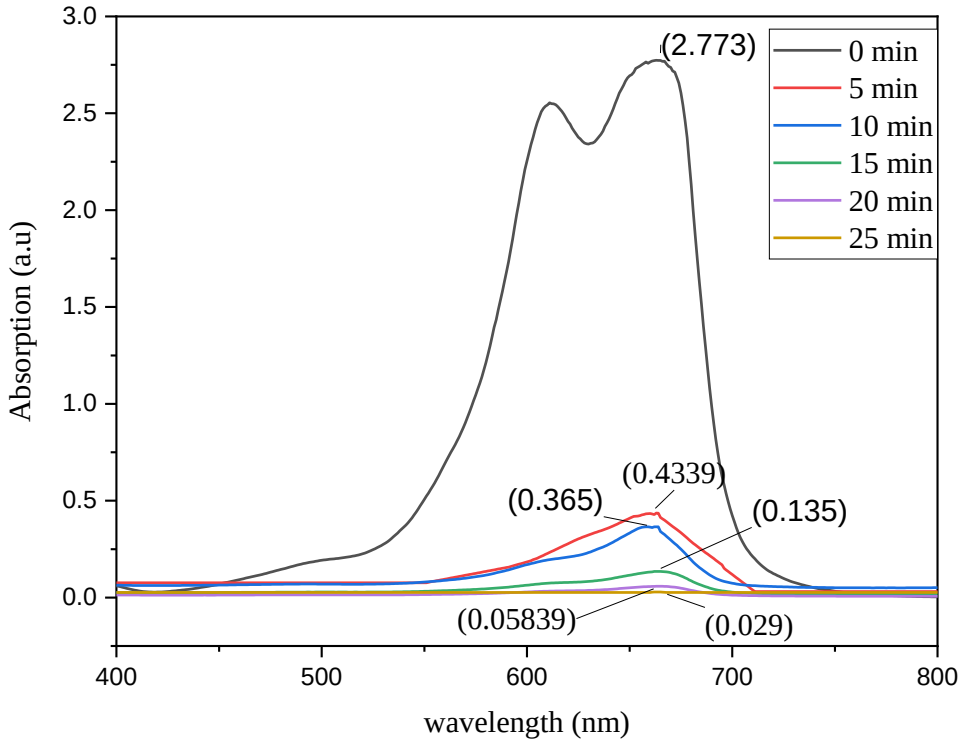

Figure 46: Degradation of MB in the presence of the catalyst under visible light at 5 minutes interval run.

The maximum intensity of MB after 5 minutes irradiation was decreased to 0.4339. The degradation efficiency was recorded to be 84%, 86%, 95%, 97% and 99% at 5, 10, 15, 20, and 25 minutes, respectively. Hence, rGO-Bi_2S_3 is the best composite with 99% degradation efficiency. Figure 47 shows the degradation percentage of the pollutant versus the time taken.

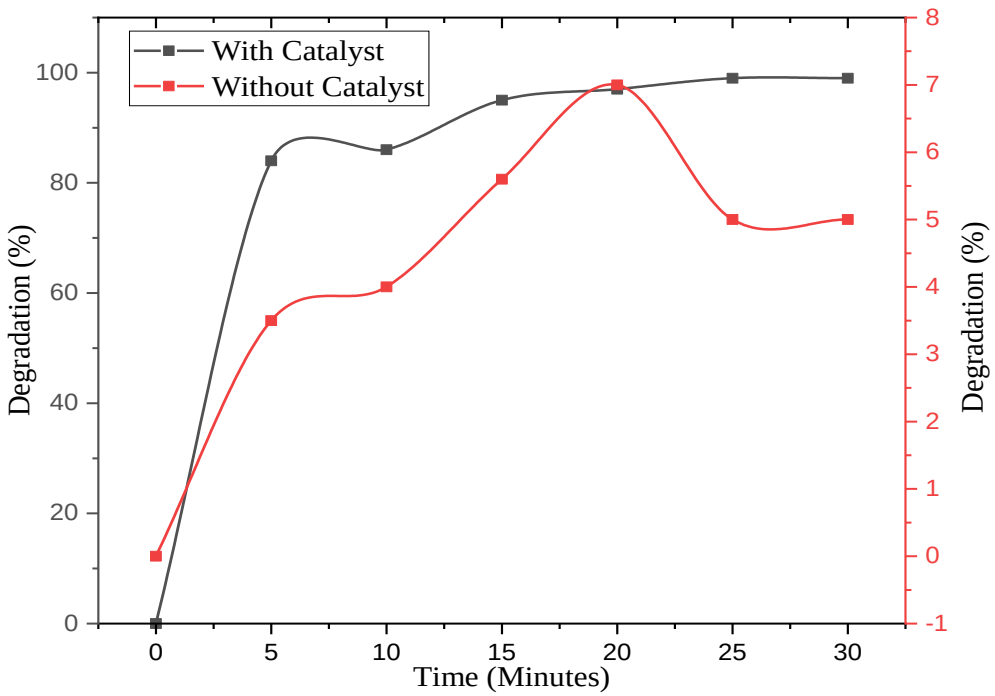

Figure 47: Degradation of methylene blue under visible light irradiation with and without a catalyst at different time interval.

The durability and reusability are also another way of measuring the performance of a catalyst Figure 48.

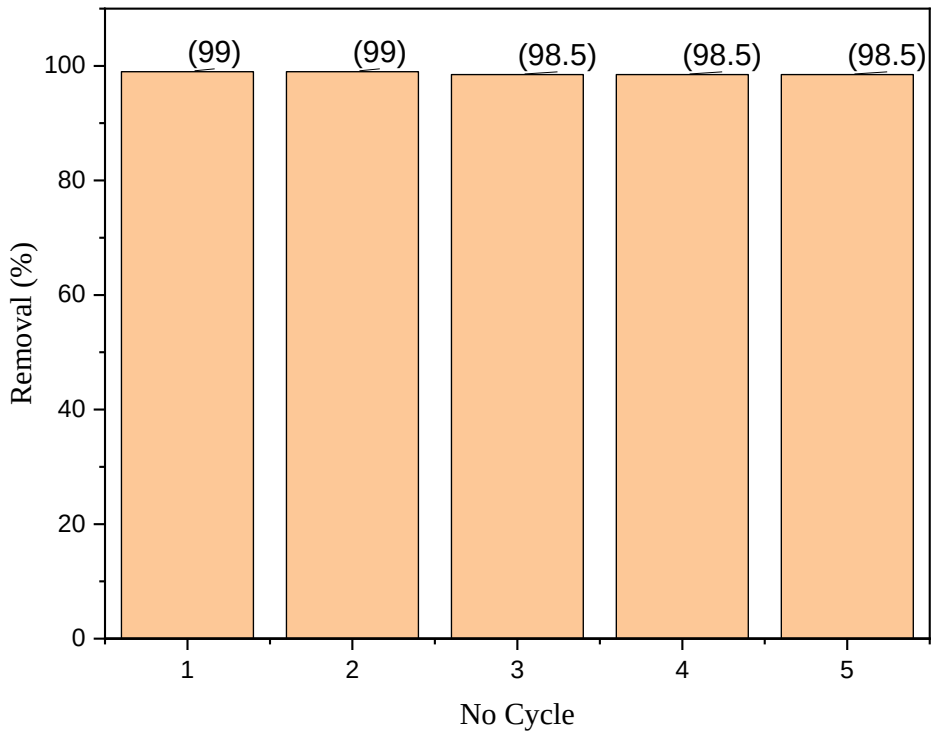

Figure 48: Cyclic degradation efficiency of rGO-Bi_2S_3 composite against MB.

The photocatalyst after each run were collected, washed with distilled water, dried at 80 ^{0}C and used for the successive new run. The photocatalytic activity of rGO-Bi_2S_3 nanostructure composites exhibited insignificant change (decrease) after running for five cycles as shown in Figure 48 for 25 minutes retention time, confirming that the potentials of rGO-Bi_2S_3 to be a stable catalyst to use it several times.

4.3.3 Mechanism of photodegradation of dyes

The generation of the charge carriers (electron-hole) by the semiconductor during irradiation by visible light was the initiator of the photodegradation reaction. The charge inter-transfer mechanism through rGO-Bi_2S_3 composite nanostructure during the degrradation of MB dye is shown in Figure 49. When the semiconductor is irradiated by sunlight, it generates e^--h^+ pair which was stablized by rGO. This graphene material provent the recombination of the charge carrier by optimizing the gap between the charge carreirs favoring them generate continously. Reduced graphene oxide stablize the semiconductor by two different ways unlike GO. One is by using its periferal residual oxygen and the second is by the polarity formed at its edges due to the delocalized electron on the materials.

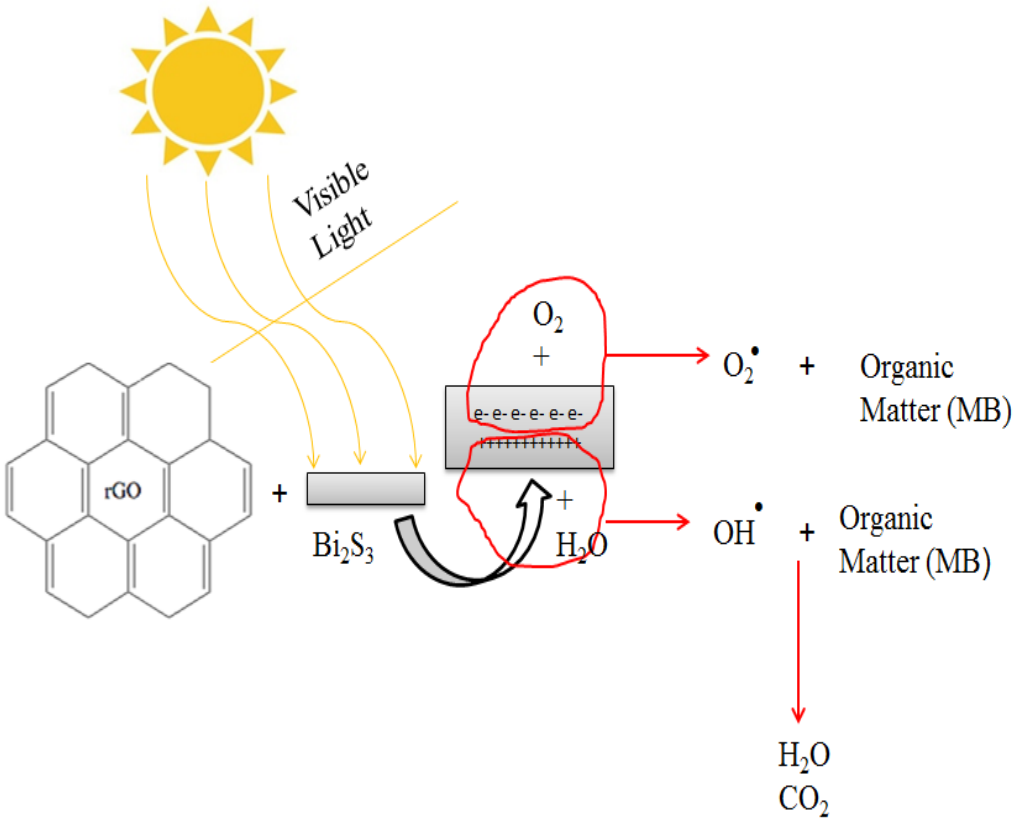

Figure 49: Mechanisms of photodegradation by rGO-Bi_2S_3 under visible light irradiation.

rGO inhibite charge carrier recombination by stablizing the band gap so that the energy absorption effeciency of rGO-Bi_2S_3 is increased which in turn resulted in accelerated generation of the e^--h^+ pair. Therefore, with the effective separation of charge carriers upon the irradiation of Bi_2S_3 with visible light, the continously generated electrons were participated in the activation of O_2 and H_2O_2 to generate the active species such as $O_2^{\bullet-}$, and •OH for the degradation of the dyes. Dye degradation detail is described as follows:

The MB solutions were treated by the rGO-Bi_2S_3 composite, and the color of the MB solution gradually faded as the reaction proceeded, which indicated that the MB concentration decreased obviously. This phenomenon can be ascribed to the destruction of the whole molecules or the chromophore destruction. In the MB degradation mechanism, intermediates and final products generated and the MB degradation pathway was proposed was shown in Figure 50. The S−Cl bond was the first broken in the MB degradation process and the MB molecule oxidized into NO_3^-, Cl^-, and SO_4^{2-} in the process. Hydroxyl radical was proved to generate on the surface of the catalyst thus, the process may be described as follows: H_2O_2 was catalyzed to decompose and hydroxyl radicals were generated on the surface of the catalyst and then transferred to the liquid phase to oxidize MB in solution. Most Cl^- may be ionized during the dissolution of MB and exist in the detached state. N−CH_3 with the lowest bond energy of 70.8 kcal/mol is first broken and the −CH_3 is oxidized to HCHO or HCOOH. C−S and C−N are broken in the following oxidization of the remaining structure; N−CH3 and C−N are broken after the oxidation of Cl−S to S=O, and the S−C bond in the remaining structure is broken to form phenol and aniline-2-sulfonic acid; some two-OH and -SO_3H connected to C2, C5, C8, and C11 in one MB molecules as the N−CH_3 bond is broken, and then -OH is derived. These organic intermediates in solution were further oxidized until finally transformed into CO_2, H_2O, Cl^-, SO_4^{2-}, and NO_3^-.

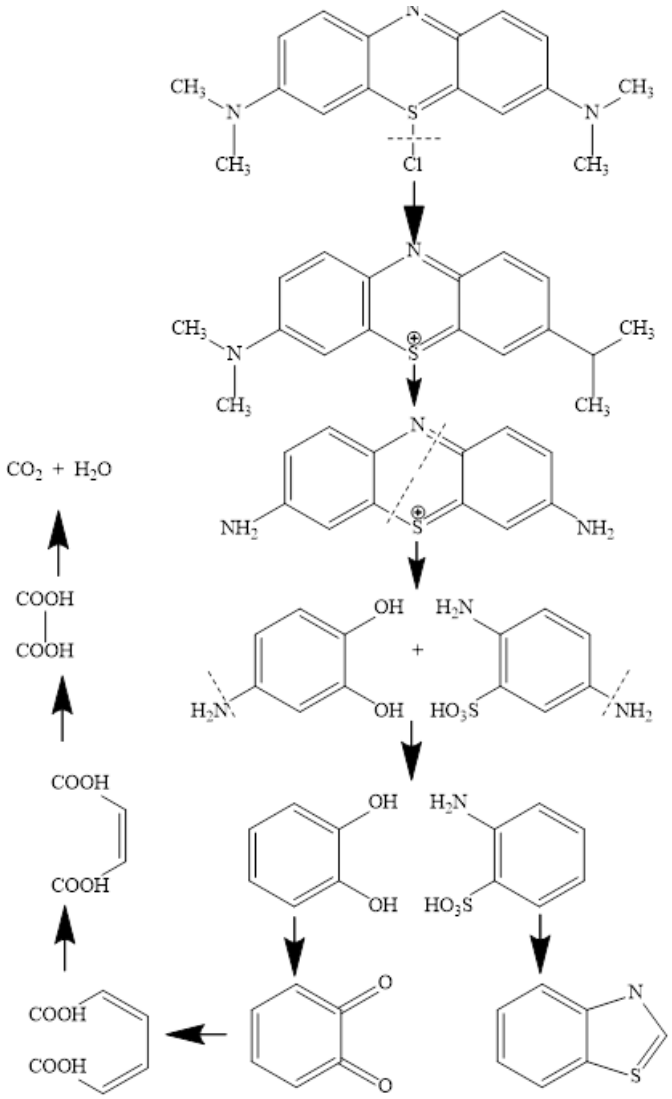

Figure 50: Proposed degradation pathway of MB (Q. Wang et al., 2014).

4.4 Adsorption Study

4.4.1 Physicochemical Properties of the Sample

The physicochemical properties of the Dugda-Bora ground water with maximum fluoride content were analyzed and the results were presented in Table 6.

Table 6: The physicochemical properties of Dugda-Bora ground water with maximum fluoride content

Parameter	Value
pH	8.5
Conductivity (µs/cm)	3000
Total hardness (mg/L)	108
F^-(mg/L)	37
SO_4^{2-}(mg/L)	7
Cl^-(mg/L)	4
PO_4^-(mg/L)	0.6
NO_3^-(mg/L)	14.7
HCO_3^-(mg/L)	371

4.5 Parameter Optimization

4.5.1 Effect of pH

The adsorption of anionic pollutants on the surface of GO is affected by pH, with the adsorption capacity increasing at lower pH (Perreault, Fonseca De Faria, et al., 2015). The behaviour of GO in aqueous solution is governed by its point of zero charge (pH_{pzc}). When solution pH is greater than pH_{pzc} then the GO surface is negatively charged because of the deprotonation of carboxyl and hydroxyl groups. On the other hand, when the solution pH is less than pH_{pzc}, GO surface becomes positively charged (Perreault, Faria, et al., 2015). Hence, this larger pH_{pzc} value than the media solution pH is the condition under the investigations was performed.

The adsorption of fluoride onto GO was determined by varying the pH values from 3 to 11.The hydrogen ion concentration plays a significant role in determining the fluoride ion adsorption capacity of graphene based nanomaterials. OH^- is the anion competing for the adsorption of F^- because of their similar lattice size and charge. The pH_{pzc} of the adsorbent and the pH of the stock solution were determined prior to carry out adsorption activity to be 4.5, and 8.5 respectively. The pH of the mixture solution became around 6.8. Hence

this is a favorable pH value where the GO is ready to adsorb the negatively charged anions. Figure 51 and 52 show the effect of pH on removal of fluoride from laboratory prepared stock solution and ground water, respectively.

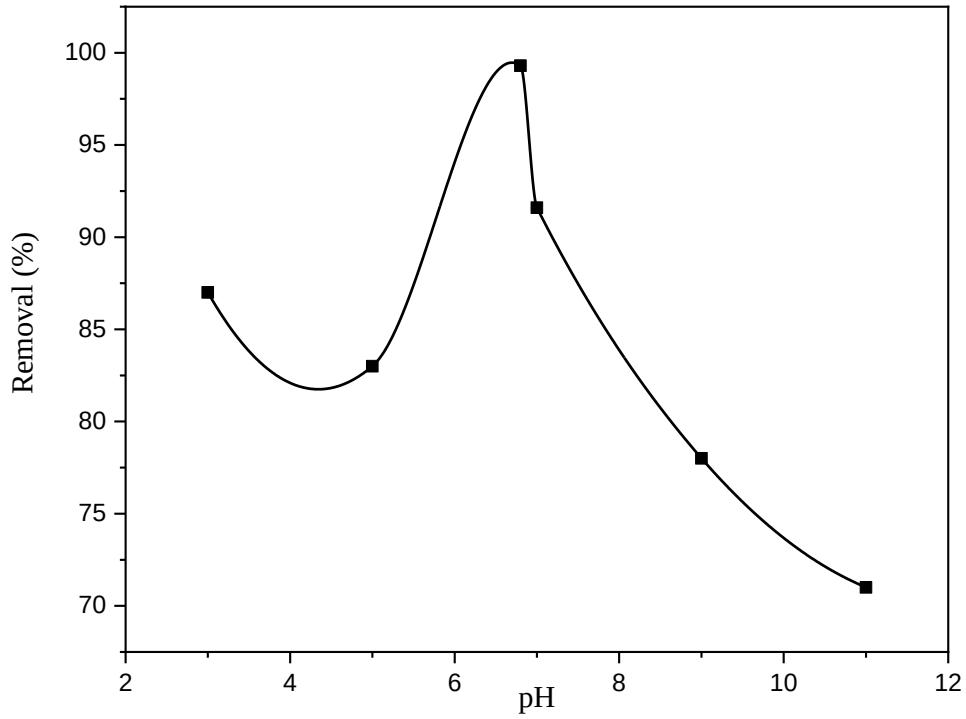

Figure 51: Effect of pH on removal of F^- obtained from NaF solution sample.

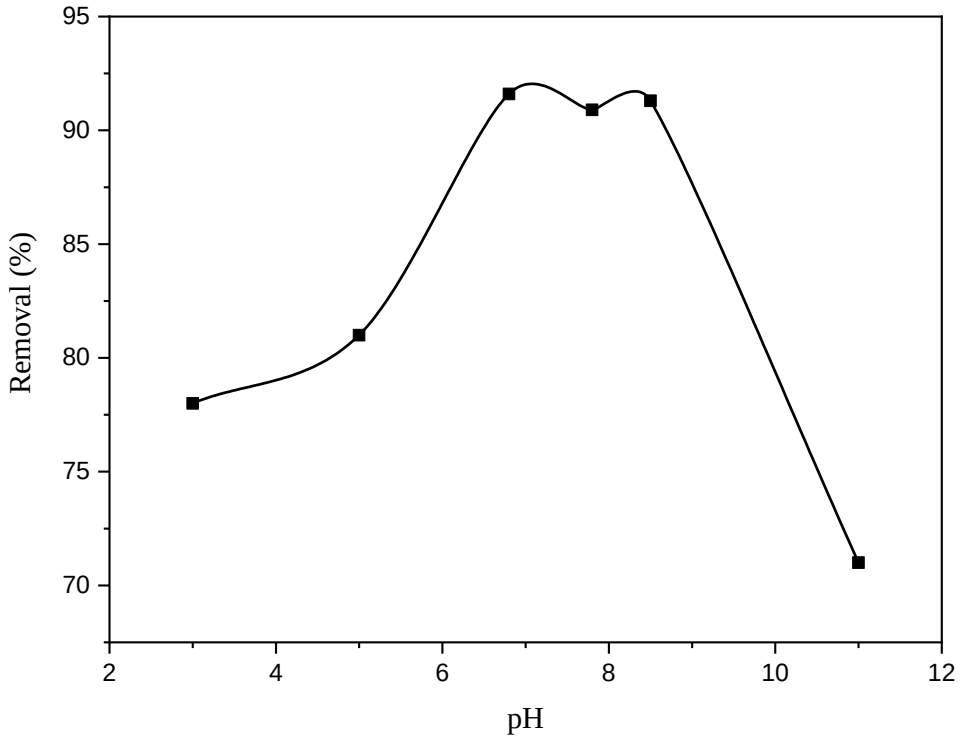

Figure 52: Effect of pH on removal of F^- obtained from ground water sample.

When pH_{pzc}> pH, the surface of GO is positively charged and ready to attract negatively charged particles. At this pH, the epoxides across the basal plane and carbonyl, and carboxyl at the edge of GO were highly protonated and the total surface of the adsorbent were positively charged. Hence this is the convenient condition for the fluoride ion to be adsorbed on the GO surfaces. The reusability and recyclability of the adsorbent was done by desorbing the F^- from the surfaces through acidulation of the solution. The optimum pH at which GO adsorbs fluoride ion was obtained to be 6.8. At this pH, 99.3% of F^- obtained from NaF solution and 91.6% of fluoride in the real sample were adsorbed by GO which is similar to previous reports (Fito et al., 2019; Karthikeyan, 2019; Ku et al., 2002; Malakootian et al., 2011).

The UV-Vis spectra of the mixture were taken at different pH values and the result showed that the UV-Vis absorption peak of a complex solution of fluoride ion formed at λ_{max} around 525 was completely removed after adsorption. The result also showed that the behaviour of GO on the absorption spectrum of UV-VIS record with the λ_{max} value 226 was retained unchanged as shown in Figure 53.

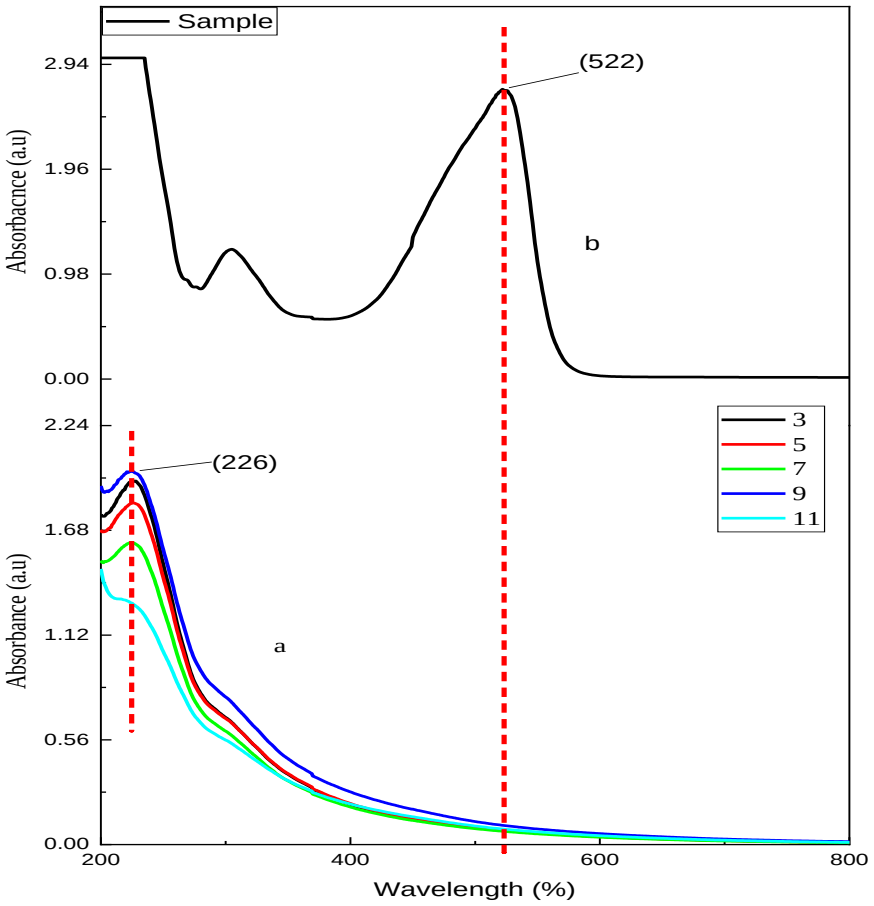

Figure 53: (a) UV-Vis absorbance spectra of adsorbent at pH (3-11) after F^- adsorption, (b) UV-Vis of the sample.

This depicted the adsorption process is physisorption so that the possibility of reusing the adsorbent is high. The intensity of the absorption peak of the adsorbent after the adsorption activity is not consistent. As shown in Figure 53, the intensity of UV-Vis absorbance spectrum for the solution at pH 9 is maximum but the adsorption capacity of the adsorbent at this pH is 78%. The exchange capacity of GO for fluoride decreased rapidly for solution at pH greater than 7 as shown in Figure 51 & 52. The adsorption rates were also found to decrease with increasing solution pH beyond 7.

4.5.2 Effects of contact time

By adding known amount of adsorbent dosage 0.42 mg to each of 50 mL fluoride solution in measuring flask containing 10 mg/L of initial fluoride concentration, agitated by digital shaker at 120 rpm and pH of 6.8 with varying contact time 50, 70, 90, 110 and 130; the effect of contact time on the adsorption of fluoride was studied. The influence of contact time on the fluoride removal efficiency is shown in Figure 54.

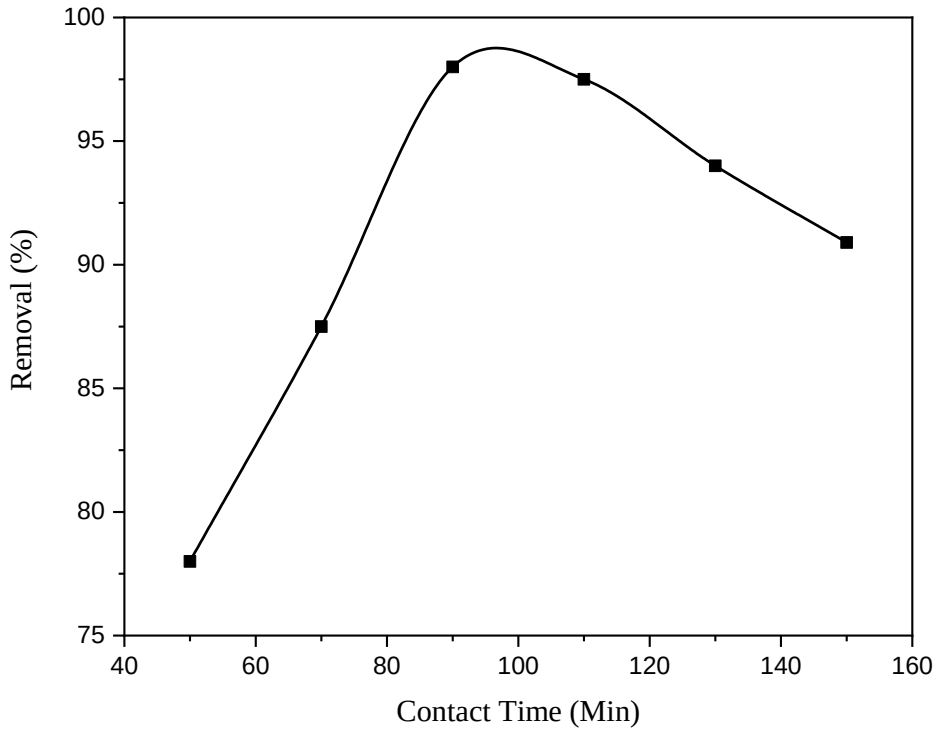

Figure 54: Effect of contact time on fluoride adsorption.

It was observed that with a constant dose of GO, the amount of fluoride adsorbed on the surface of the absorbent increases with time until the steady state was reached at 90 minutes. The maximum adsorption capacity recorded at the end of 90 minutes was found to be 98%.

4.5.3 Effect of adsorbent dosage

Figure 55 shows the effect of adsorbent dosage on at agitation rate of 120 rpm, agitation time of 90 minutes and pH of the solution was 6.8. The result depicted that the adsorption of fluoride by GO increases rapidly as the dosage increases up to the optimum value 0.42 mg. The adsorption capacity of GO at this dosage is 97%. The increase of the dosage beyond this value does not bring any change on the adsorption of fluoride ions.

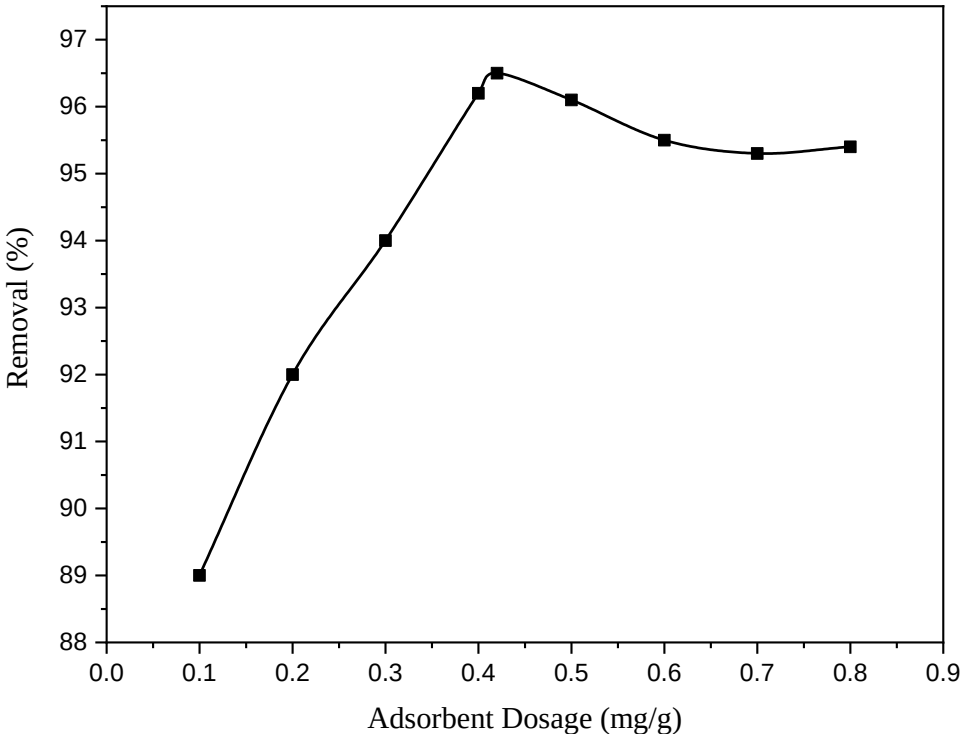

Figure 55: Effect of adsorbent dosage on fluoride ions adsorption.

4.5.4 Effect of Initial Concentration

The capacity of GO to adsorb fluoride was assessed by using the initial concentration of fluoride ranging from 1 to 40 mg/L while the other parameters were constant. The rate of adsorption of fluoride onto GO was so fast that most of the adsorption process was completed within 30 minutes. Fluoride adsorption increased with increasing initial concentration of fluoride and this is attributed to the diffusion of the adsorbate to the adsorbent surface as shown in Figure 56.

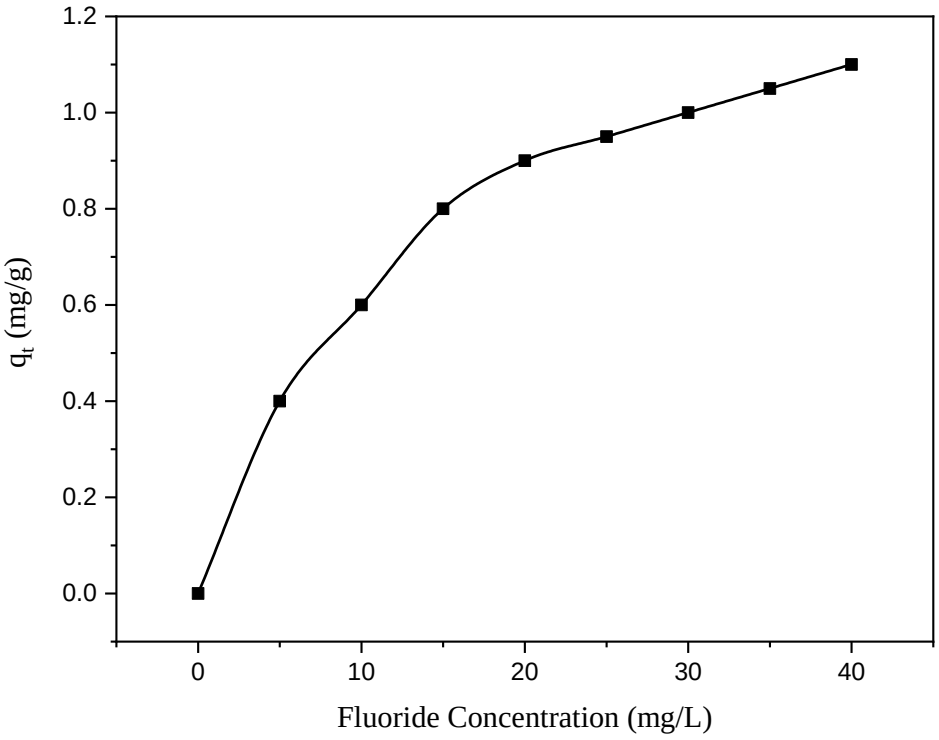

Figure 56: Effects of initial fluoride concentration**.**

4.6 Adsorption Kinetics

Figure 57 shows the pseudo-first-order and pseudo-second-order kinetics model of fluoride adsorption onto GO. The fluoride adsorption kinetics of GO at agitation speed of 120 rpm, adsorbent dosage of 0.42 mg/L, contact time of 90 minutes and pH of 6.8. Table 7 shows the values of K_f, K_s, K_d and K_p experimental adsorption capacity at equilibrium $q_{e,\,exp}$ and calculated adsorption capacity at equilibrium $q_{e,\,calc}$.

The adsorption kinetics of both pseudo-first-order (SFO) and pseudo-second order (SSO) reactions were determined. The adsorption kinetics for the SSO reactions was found to be 0.99 for the coefficient of determination (R^2) and the sum of square errors was 0.0002. R^2 and sum of square errors for the SFO reaction was 0.96 and 0.02, respectively as indicated in Table 7.

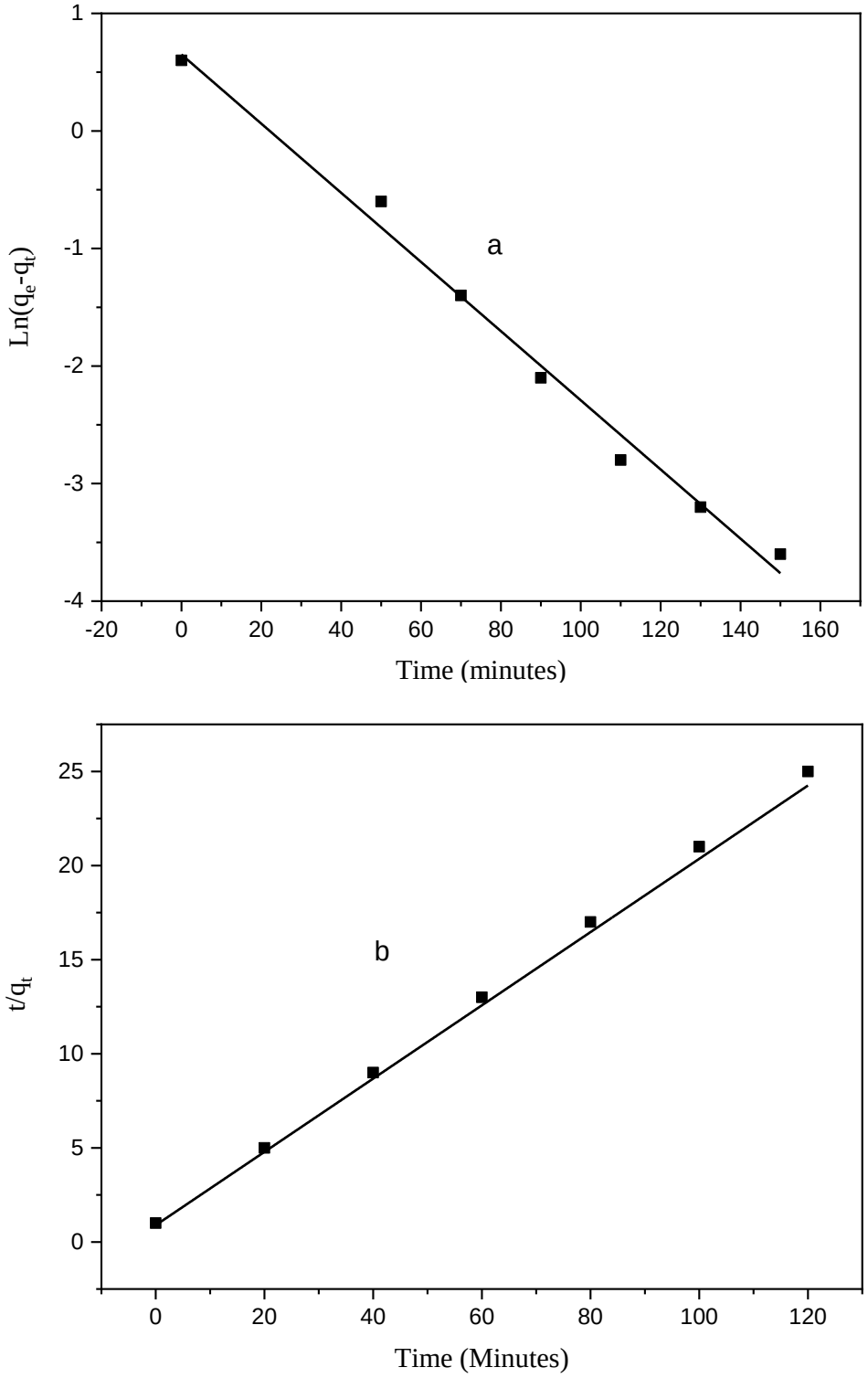

Figure 57: pseudo-first-order (a) and pseudo-second-order kinetics model of fluoride adsorption onto GO.

The R^2 value for the SSO kinetics is larger than the corresponding R^2 value for SFO reaction and the difference between $q_{e,\ calc}$ and $q_{e,\ exp}$ was insignificant so that the sum of

square error is very small. This shows that the SSO reaction is best describes the fluoride adsorption by GO.

Table 7: The kinetics parameter for the adsorption of fluoride ions by GO

SFO	Parameter	Value
	$q_{e,\ exp}$ (mg/g)	0.2263
	$q_{e,\ calc}$ (mg/g)	0.0920
	K_f (g/mg min)	0.0381
	R^2	0.96
SSO	Parameter	Value
	$q_{e,\ exp}$ (mg/g)	0.2263
	$q_{e,\ calc}$ (mg/g)	0.2533
	K_s (g/mg min)	0.739
	R^2	0.99
Intraparticle diffusion	Parameter	Value
	K_{id1} (mg/g $min^{0.5}$)	0.0086
	C_{i1} (mg/g)	0.161
	R_1^2	0.86
	K_{id2} (mg/g $min^{0.5}$)	11.1
	C_{i2} (mg/g)	89.72
	R_2^2	0.85
	K_{id3} (mg/g $min^{0.5}$)	0.061
	C_{i3} (mg/g)	109.3
	R_3^2	0.61
Particle diffusion	Parameter	Value
	k_p (mg/g min)	0.221

The absorption/diffusibility of the adsorbate into the adsorbent was determined from the intraparticle diffusion model. Using equation 15, the value of intraparticle diffusion rate constant k_p and the value of C were obtained from the slop (m) and intercept (C) of the plot of q_e versus square root of time as in Table 7. The plot of q_t versus $t^{0.5}$, Figure 58 (a) showed nonlinear dependency over the total range, with the line not passing through the origin.

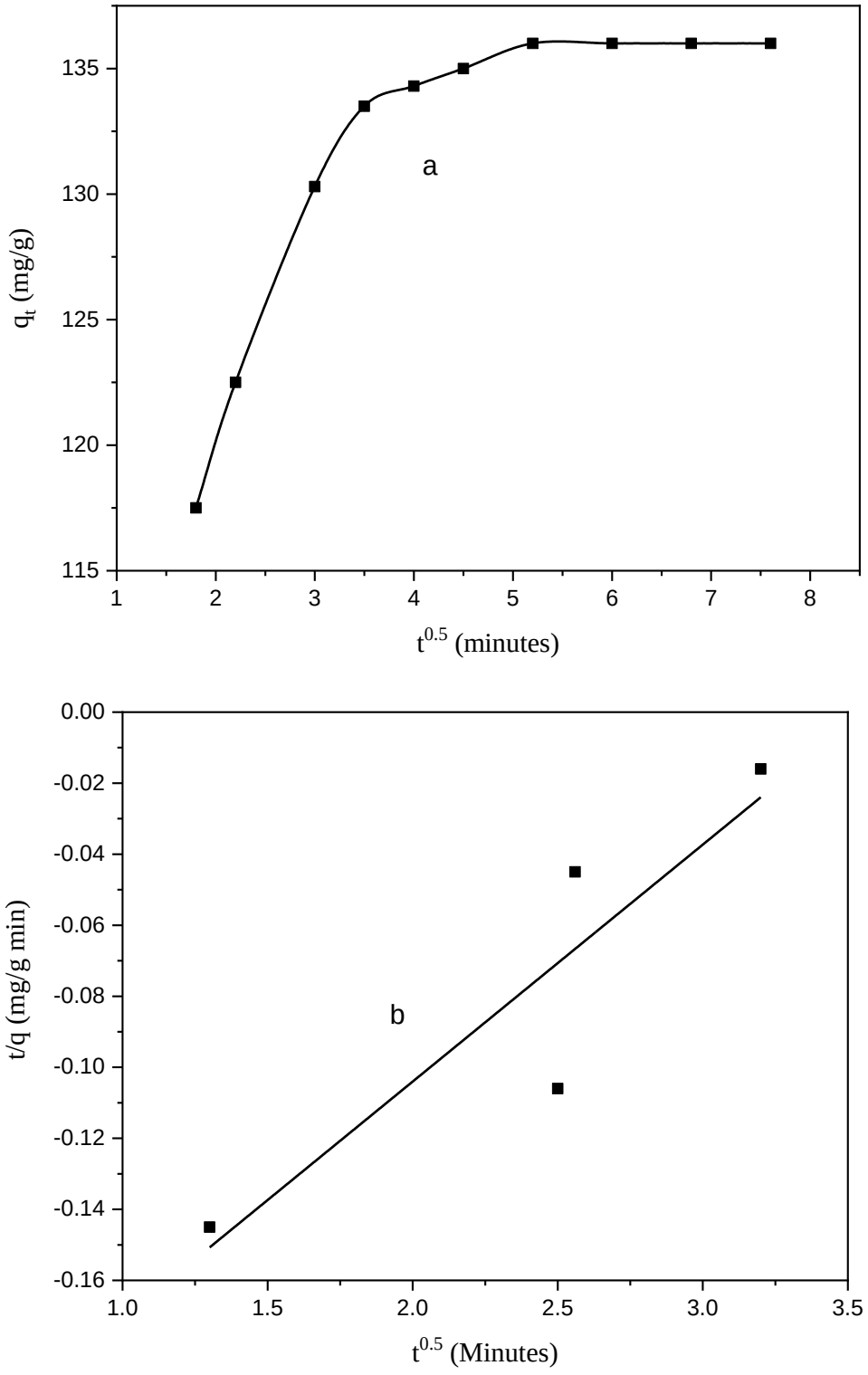

Figure 58: A plot for (a) Weber and Morris, (b) Chanda models

This indicates the rate limiting step is controlled by boundary layer diffusion. The sharp rapid increasing plot initially observed indicates the fast uptake of ions onto GO surface which is decreased gradually due to surface saturation at equilibrium. As shown in the upper region of Figure 58 (a), there is slow process which was involved in the

transportation of F^- into the adsorbent pores. Therefore the overall process is controlled by particles rather than pore diffusion, which is also supported by high value of R^2 shown in Table 7.

4.7 Adsorption Isotherms

Langmuir and Freundlich isotherms are the basic models which are employed to describe the adsorption isotherms using the experimentally obtained data (Tefera et al., 2020; Xu et al., 2020). The adsorption capacity of the GO was evaluated under the removal of fluoride from aqueous solution of NaF and a real sample taken from fluoride polluted ground water of Dugda-Bora.The Langmuir isotherm model is suitable for monolayer adsorption while the Freundlich isotherm model is applied for multilayer adsorption because of its heterogonous active surfaces which have different adsorption capacities. The Langmuir and Freundlich isotherm are expressed as given in equations 18 and 19 which are the simplified forms of equations 11 and 12, respectively.

$$\frac{C_e}{q_e} = \frac{C_e}{q_m} + \frac{1}{bq_m} \tag{18}$$

$$lnq_e = lnK_f + \frac{1}{n} lnc_e \tag{19}$$

Where c_e adsorbate concentration at equilibrium (mg/L), q_e amount of adsorbate adsorbed per unit mass of adsorbent at equilibrium (mg/g), q_m maximum adsorption capacity of adsorbate per unit mass of adsorbent (mg/g), b Langmuir constant related to energy adsorption (L/mg), k_f Freundlich constant (mg/g) which correlated to relative adsorption capacity of adsorbent, n is the Freundlich exponent which describes the intensity of adsorption. Figure 59 shows the isotherm modeling of Langmuir and Freundlich for fluoride Adsorption by GO and Figure 60 shows the plot of Temkin and D-R isotherm. Table 8 shows the parameters of the Langmuir, Freundlich and other models for the removal of fluoride by GO.

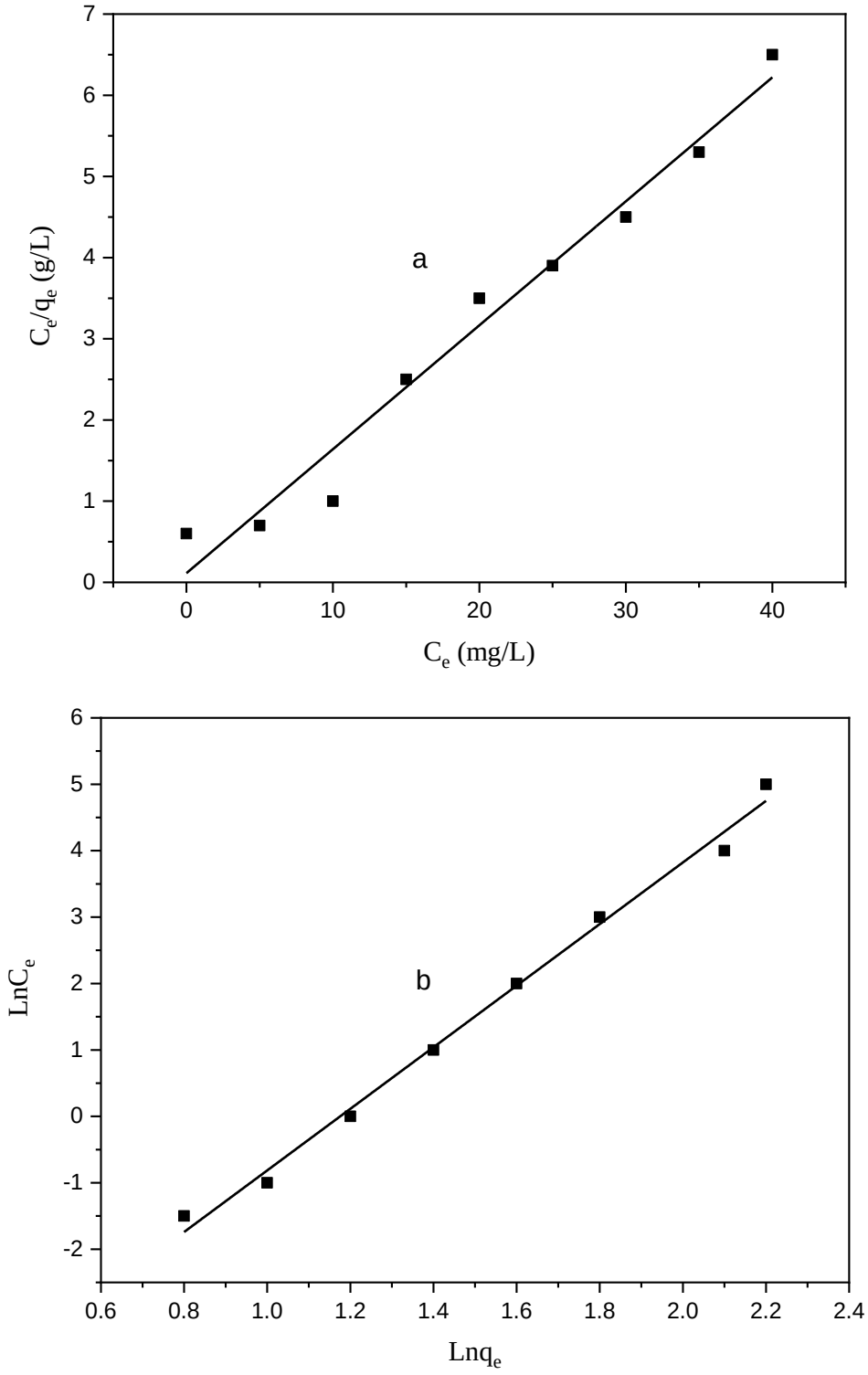

Figure 59: Langmuir (a) and Freundlich (b) isotherm modeling of fluoride adsorption onto GO.

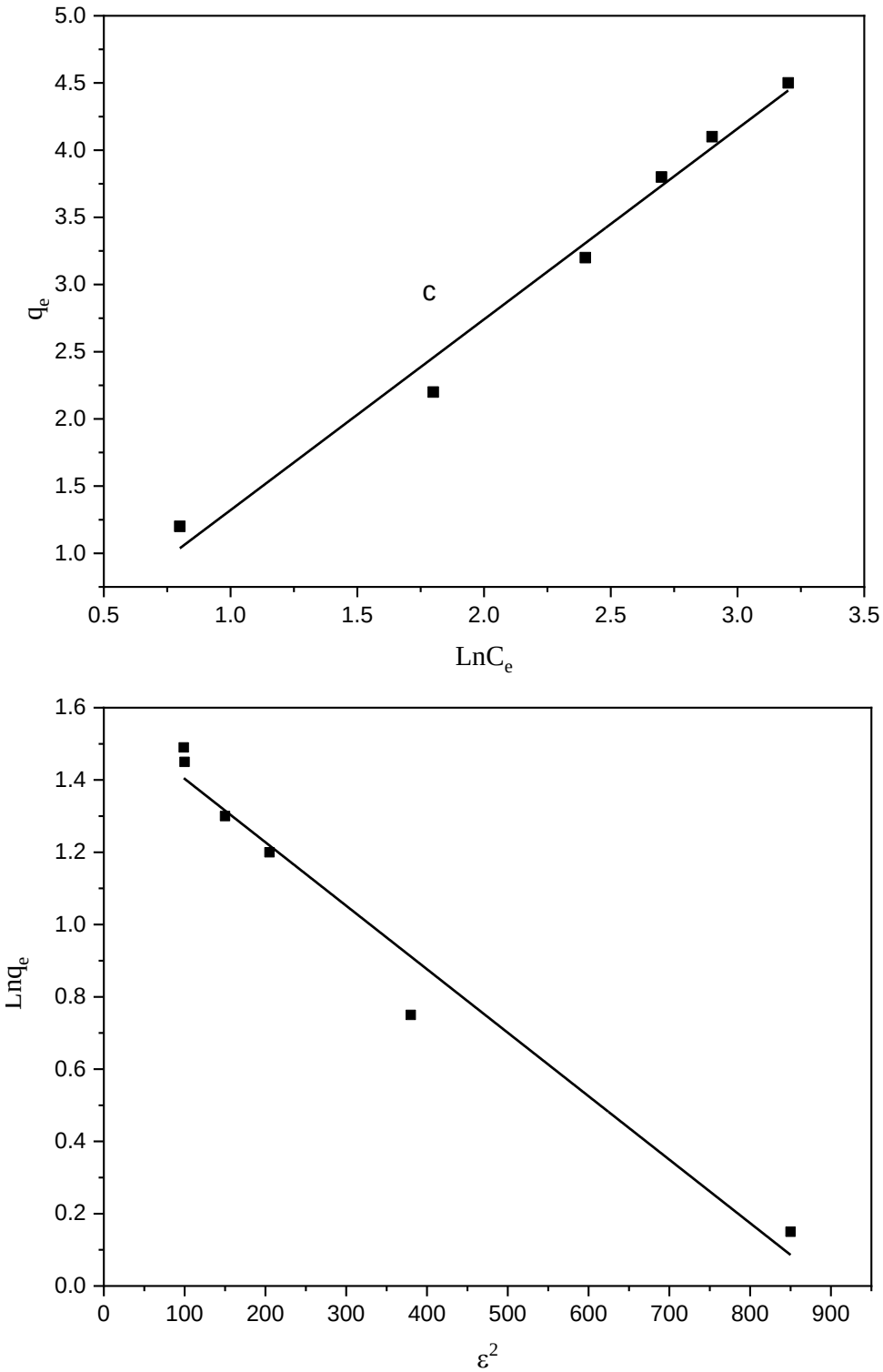

Figure 60: Temkin (c) and D-R (d) isotherm modeling of fluoride adsorption onto GO.

As shown in Table 9, the value of correlation coefficient (R^2) of Langmuir and Freundlich adsorption model was 0.96 and 0.99, respectively. Based on the data obtained from Table 8, the Freundlich isotherm depicted a good fit to the experimental data. The Freundlich constant K_f and Freundlich coefficient n were obtained from the slop and intercept as 4.61

and 4.05. The value of n shows the adsorption process is favorable. This is due to the presence of different functional group on the surface of GO having different active sites. The maximum adsorption capacity of GO was calculated to be 301.43 mg/g.

Table 8: The four isotherm models parameter values for fluoride adsorption by GO

Isotherms Model	Parameters	Values
Langmuir	R^2	0.96
	q_m (mgg-1)	6
	K_L (Lmg^{-1})	0.098
	ΔG ($KJmol^{-1}$)	-10.6
	R_L	0.5
Freundlich	R^2	0.99
	K_F (mgg^{-1})	4.61
	n	4.05
Tempkin	R^2	0.94
	K_T (Lg^{-1})	0.86
	b ($Jmol^{-1}$)	1760.4
D-R	R^2	0.92
	q_m (mgg^{-1})	5
	K_{D-R} (Lmg^{-1})	-0.001
	E ($KJmol^{-1}$)	17

Table 9 shows the comparative adsorption capacity of graphene oxide nanostructure with the previously reported works.

Table 9: Comparison of adsorption capacity of GO with literature values

S. No	Adsorbent	Adsorbate	Adsorption Capacity (qe) in mg/g	References
1	Graphene oxide NS	Fluoride	301.43	Present work
2	Modified lemna powder	Fluoride	41.76	(Zazouli, Belarak, et al., 2014)
3	Synthetic sodalite zeolite	Fluoride	315.82	(Balarak et al., 2017)
4	Modified azolla filiculoides	Fluoride	47.25	(Zazouli, Mahvi, et al., 2014b)
5	Sorghum and Canola	Fluoride	37.11, 43.19	(Zazouli et al., 2015)
6	Carbon nanotube	Fluoride	216.35	(Balarak et al., 2016)
7	Chitosan	Fluoride	62.73	(Akbari et al., 2018)
8	Cupricoxide NP	Fluoride	173.28	(Bazrafshan et al., 2016)
9	Eucalyptus bark	Fluoride	119.77	(Zazouli, Mahvi, et al., 2014a)
10	Chitosan/Zeolite composite	Fluoride	164.43	(Mahvi et al., 2019)

NS = Nanostructure, NP = Nanoparticles

4.8 Desorption Studies

Desorption studies aid in determining adsorbent reusability without compromising the adsorbent's efficiency. Therefore desorption and regeneration studies are important in adsorption. Desorption may occur either by thermal treatment or through suitable desorbing agents. Desorption of F^- ions were studied in HCl solution. The adsorbent with its adsorbed adsorbate were placed in this desorption medium and stirred continuously (at a stirring rate of 700 rpm) for 15 min at room temperature. Desorption ratio was calculated from the amount of F^- ions adsorbed on the nanostructure and the final concentration of F^- ions in the desorption medium. To test the reusability of the adsorbent, adsorption–desorption procedure of F^- ions was repeated 10 times using the same adsorbent. To regenerate after desorption, the adsorbent were washed with 0.1 M HCl and ethanol.

Figures 61 shows desorption of F^- and the maximum desorption efficiency was obtained in 0.05 M HCl solution as a good eluent for desorption of F^- loaded adsorbents.

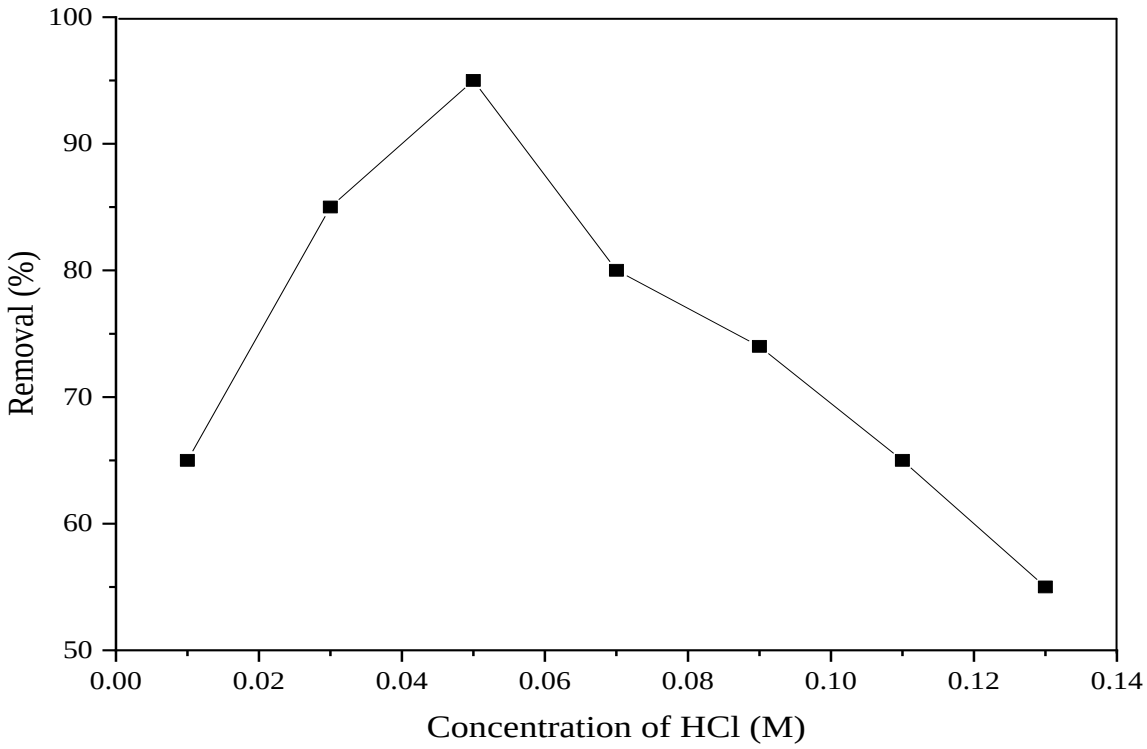

Figure 61: The cyclic adsorption performance of the adsorbent GO against F^-.

4.9 Recyclability study

The reusability of the adsorbent, GO nanostructure, in the adsorption of fluoride ion from ground water was explored. After washing repeatedly with doubly distilled water, the pH of the solution was adjusted to be around 6.8 where re-adsorption of fluoride from the solution was initiated. The adsorbent was filtered and collected to dry in the oven at 60 ^{0}C overnight. 0.42 mg of the powder of GO was used for the recyclability test as shown in Figure 62. The pH adjustment was done by HCl/H_2SO_4 and NaOH and the maximum adsorption capacity of GO were recovered and recorded to be 99%.

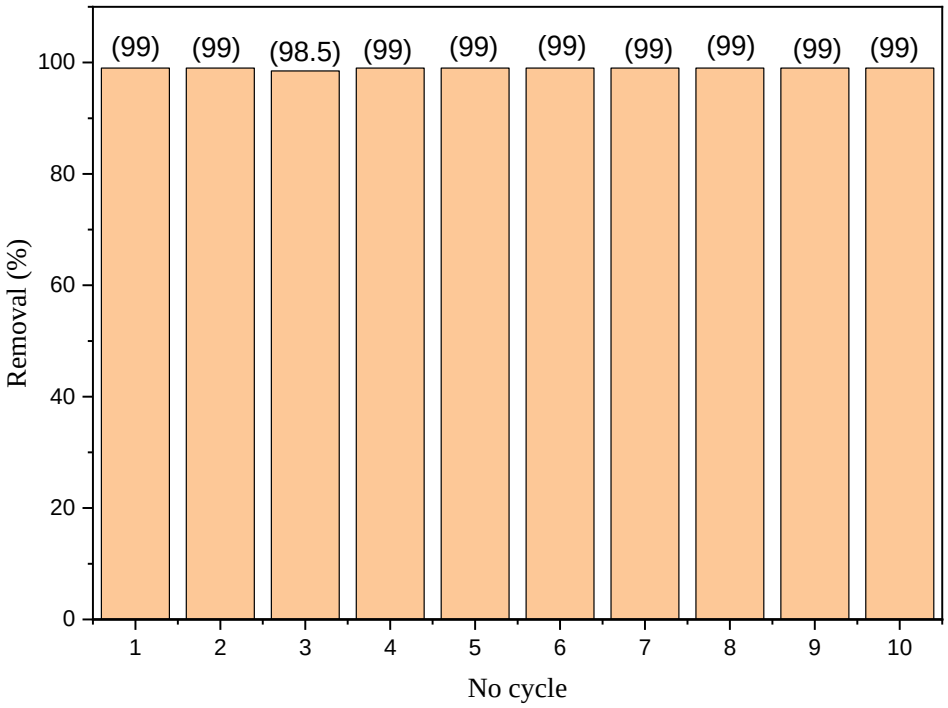

Figure 62: The cyclic adsorption performance of the adsorbent GO against F^-.

5. Conclusion and Recommendations

5.1 Conclusions

In this study, we have used the compounds *Vernonia Amygdalina* plant extract for the green synthesis of reduced graphene oxide. UV-Vis and GC-MS instruments were used to identify compounds in the plant extracts. These compounds were seen to be antioxidizing agent and capping agent in the synthesis of reduced graphene oxide from graphene oxide. UV-Vis spectroscopy and XRD were used to characterize VA leaf extract synthesized rGO with parametric properties exactly match the literature values.

Slightly modified non-explosive and time saving Tour method was used to synthesis GO. Easily available, cheap and green reducing agent as well as capping agent at the same time having a maximum capacity to reduce GO to graphene was discovered from *Vernonia Amygdalina*. The reducing capacity of *Vernonia Amygdalina* was attributed to the existence of large amount of terpenoids and polyphenols in its methanol extracts. Besides, they are capping agents due to their carbonyl and hydroxyl ends in the extracts to stabilize the nanoparticle synthesized.

The appropriate conditions identified for the optimum adsorption activity was 120 rpm agitation rate, 90 minutes contact time, 0.42 mg/L adsorbent dosage and 6.8 pH. Fluoride ion removal capacity of GO from aqueous solution of NaF and real sample was 99.3% and 89.6%, respectively. The kinetics model of adsorption of F^- onto GO was best described by pseudo-second-order kinetics. The research finding clearly indicated that the Freundlich isotherm is more suitable than Langmuir for the adsorption of fluoride in the ground water by GO. The 1/n value of the Freundlich isotherm is 0.25 which lie between 0.1 and 1 and this indicates the adsorption processes is favorable.

The heterogeneous photocatalyst, rGO-Bi_2S_3 was synthesized from Bi_2S_3 and rGO by a single step reflux method. Bi_2S_3 was synthesized from thiourea and bismuth chloride in the presence of methanol extracted VA. All the synthesized materials were characterized and their formations were confirmed. With two groups of samples, comparative studies were performed on the degradation rate of MB under visible light irradiation. Samples with and without the presence of the catalyst were considered. A group of sample with presence of a catalyst were prepared by adding 5 mg of rGO-Bi_2S_3 to 125 ml of MB (1:25) ratio and sonicated for 30 minutes to obtain adsorption desorption equilibrium. This degradation performance capacity is confirmed to be constant by repeating the test for five

times and the maximum average is 99% for 25 minutes retention time. The maximum degradation value recorded under visible light irradiation of MB in the absence of catalyst was 7%.

The reusability and durability test made confirmed that the catalyst can be reused continuously for several times without decrease in capacity. The catalyst regenerated from the solution by washing with distilled water several times was reused for catalysis of MB for five cycles with the insignificant decrease in the degradation capacity. From the result obtained, the maximum decrease in the degradation capacity by percent for 25 minutes retention time was 7%.

5.2 Recommendations

One of the main advantages possessed by graphene based materials is its biodegradability after it reaches its final stage of usefulness, but it is not yet studied thoroughly.

The toxicity of graphene oxide and graphene oxide materials was proved to depend highly on the shape and size of those materials, and through a carefully chosen shape the impact on the environment through subsequent disposal after the complete life cycle can be minimized sufficiently. Hence researchers should do research works intensively on that area.

The studied graphene oxide materials tested against all target pollutants which pose a great concern towards the environment and human health, being they are organic in nature or inorganic anions are confirmed to have good and very good sorption and photocatalysis capacities but the accessibility issue should be solved.

The only real challenge that may remain in the future is sending those materials to work, in the help of societies which still lack access to clean water, a challenge which can only be tackled globally, a challenge which is too great to be ascertained by one person or one research group alone.

Deep investigations on these new nanosystems are currently underway with increasing achievements for prototype applications. However, more intense research and funding are required for their industrial-scale applications.

In this way, these 2D materials are new challenges for the materials scientists and a great opportunity for further research and development.

6. References

Abdel Maksoud, M. I. A., Fahim, R. A., Shalan, A. E., Abd Elkodous, M., Olojede, S. O., Osman, A. I., Farrell, C., Al-Muhtaseb, A. H., Awed, A. S., Ashour, A. H., & Rooney, D. W. (2021). Advanced materials and technologies for supercapacitors used in energy conversion and storage: a review. In *Environmental Chemistry Letters* (Vol. 19, Issue 1). Springer International Publishing. https://doi.org/10.1007/s10311-020-01075-w

Abdelrasoul, A., Doan, H., & Lohi, A. (2013). Fouling in Membrane Filtration and Remediation Methods. *Mass Transfer - Advances in Sustainable Energy and Environment Oriented Numerical Modeling*, *120*(10). https://doi.org/10.5772/52370

Abirami, P., & Rajendran, A. (2012). *GC-MS analysis of methanol extracts of Vernonia cinerea*. *2*(1), 9–12.

Achuba, F. I. (2018). Role of bitter leaf (Vernonia amygdalina) extract in prevention of renal toxicity induced by crude petroleum contaminated diets in rats. *International Journal of Veterinary Science and Medicine*, *6*(2), 172–177. https://doi.org/10.1016/j.ijvsm.2018.07.002

Aggeborn, L., & Öhman, M. (2017). *The Effects of Fluoride in the Drinking Water*.

Ai, K., Liu, Y., Liu, J., Yuan, Q., He, Y., & Lu, L. (2011). Large-scale synthesis of Bi 2S 3 nanodots as a contrast agent for in vivo X-ray computed tomography imaging. *Advanced Materials*, *23*(42), 4886–4891. https://doi.org/10.1002/adma.201103289

Aigbe, U. O., & Onyancha, B. (2020). Removal of fl uoride ions using a polypyrrole magnetic nanocomposite in fl uenced by a rotating magnetic fi eld. *RSC Adv.*, *10*, 595–609. https://doi.org/10.1039/c9ra07379e

Ajani, O. O., Owoeye, F. T., Owolabi, F. E., Akinlabu, D. K., & Audu, O. Y. (2019). *Phytochemical screening and nutraceutical potential of sandbox tree (Hura crepitans L .) seed oil*. *7*(1), 143–150.

Akbari, H., Jorfi, S., Mahvi, A. H., Yousefi, M., & Balarake, D. (2018). Adsorption of fluoride on chitosan in aqueous solutions: Determination of adsorption kinetics. *Fluoride*, *51*(4), 319–327.

Alara, O. R., Abdurahman, N. H., Ishmael, C., & Kabbashi, N. A. (2019a). Extraction and characterization of bioactive compounds in Vernonia amygdalina leaf ethanolic extract comparing Soxhlet and microwave-assisted extraction techniques. *Journal of Taibah University for Science*, *13*(1), 414–422.

https://doi.org/10.1080/16583655.2019.1582460

Alara, O. R., Abdurahman, N. H., Ishmael, C., & Kabbashi, N. A. (2019b). *Extraction and characterization of bioactive compounds in Vernonia amygdalina leaf ethanolic extract comparing Soxhlet and microwave-assisted extraction techniques*. *3655*. https://doi.org/10.1080/16583655.2019.1582460

Alemu, Z. A., Mengesha, S. D., & Alemayehu, T. A. (2015). Retrospective Study of Fluoride Distribution in Ethiopian Drinking Water Sources. *Asian Journal of Applied Science and Engineering*, *4*(2), 127–136.

Ali, I., Basheer, A. A., Mbianda, X. Y., Burakov, A., Galunin, E., Burakova, I., Mkrtchyan, E., Tkachev, A., & Grachev, V. (2019). Graphene based adsorbents for remediation of noxious pollutants from wastewater. *Environment International*, *127*(January), 160–180. https://doi.org/10.1016/j.envint.2019.03.029

Aliyev, E., Filiz, V., Khan, M. M., Lee, Y. J., Abetz, C., & Abetz, V. (2019). Structural characterization of graphene oxide: Surface functional groups and fractionated oxidative debris. *Nanomaterials*, *9*(8). https://doi.org/10.3390/nano9081180

Allen, M. J., Tung, V. C., & Kaner, R. B. (2010). Honeycomb carbon: A review of graphene. *Chemical Reviews*, *110*(1), 132–145. https://doi.org/10.1021/cr900070d

Altemimi, A., Lakhssassi, N., Baharlouei, A., & Watson, D. G. (2017). *Phytochemicals: Extraction, Isolation, and Identification of Bioactive Compounds from Plant Extracts*. https://doi.org/10.3390/plants6040042

AMECHI, M. O. (2018). *GREEN SYNTHESIS OF SILVER NANOPARTICLES USING LEAF (Vernonia amygdalina) EXTRACTS IN SELECTED SOLVENTS AND IT'S CHARACTERIZATION BY SPECTROCOPIC METHODS AND SCANNING ELECTRON MICROSCOPY*.

Ansari, M., Kazemipour, M., Dehghani, M., & Kazemipour, M. (2011). The defluoridation of drinking water using multi-walled carbon nanotubes. *Journal of Fluorine Chemistry*, *132*(8), 516–520. https://doi.org/10.1016/j.jfluchem.2011.05.008

Ariffinisa Lintang Widyaningtyas, Yoki Yulizar, D. O. B. A. (2019). *Ag 2 O nanoparticles fabrication by Vernonia amygdalina Del . leaf extract : synthesis , characterization , and its photocatalytic activities Ag 2 O nanoparticles fabrication by Vernonia amygdalina Del . leaf extract : synthesis , characterization , and i*. https://doi.org/10.1088/1757-899X/509/1/012022

Assmuth, T., Häkkinen, P., & Heiskanen, J. (2011). Risk management and governance of chemicals in articles: Case study textiles. In *The Finnish Environment Institute*.

Ayalew, A. A. (2020). Development of Kaolin Clay as a Cost-Effective Technology for Defluoridation of Groundwater. *International Journal OfChemical Engineering*.

Ayodhya, D., & Veerabhadram, G. (2018). Highly efficient sunlight-driven photocatalytic degradation of organic pollutants and fluorescence detection of Hg2+ using multifunctional GO-Bi2S3 nanostructures. *Journal of Photochemistry and Photobiology A: Chemistry*, *356*, 545–555. https://doi.org/10.1016/j.jphotochem.2018.01.039

Azeez, F., Al-Hetlani, E., Arafa, M., Abdelmonem, Y., Nazeer, A. A., Amin, M. O., & Madkour, M. (2018). The effect of surface charge on photocatalytic degradation of methylene blue dye using chargeable titania nanoparticles. *Scientific Reports*, *8*(1), 1–9. https://doi.org/10.1038/s41598-018-25673-5

B.S. Audu, P.C. Ofojekwu, A. Ujah, M. N. O. A. (2014). *Phytochemical , proximate composition , amino acid profile and characterization of Marijuana (Cannabis sativa L .). January*.

Bafekrpour, E., Kafi, A. A., Simon, G. P., Yang, C., Habsuda, J., Naebe, M., & Fox, B. L. (2012). Preparation and properties of stepwise graded synthetic graphite/phenolic nanocomposites. *ECCM 2012 - Composites at Venice, Proceedings of the 15th European Conference on Composite Materials*, *February 2016*.

Balandin, A. A. (2011). Thermal properties of graphene and nanostructured carbon materials. *Nature Materials*, *10*(8), 569–581. https://doi.org/10.1038/nmat3064

Balarak, D., Mahdavi, Y., Bazrafshan, E., Mahvi, A. H., & Esfandyari, Y. (2016). *ADSORPTION OF FLUORIDE FROM AQUEOUS SOLUTIONS BY CARBON NANOTUBES: DETERMINATION OF EQUILIBRIUM, KINETIC, AND THERMODYNAMIC PARAMETERS*. *49*(March), 71–83.

Balarak, D., Mostafapour, F. K., Bazrafshan, E., & Mahvi, A. H. (2017). The equilibrium, kinetic, and thermodynamic parameters of the adsorption of the fluoride ion on to synthetic nano sodalite zeolite. *Fluoride*, *50*(2), 223–234.

Bazrafshan, E., Balarak, D., Panahi, A. H., & Kamani, H. (2016). *FLUORIDE REMOVAL FROM AQUEOUS SOLUTIONS BY CUPRICOXIDE NANOPARTICLES*. *January 2019*.

Bekyarova, E., Sarkar, S., Niyogi, S., Itkis, E., Haddon, C., Bekyarova, E., Sarkar, S., Niyogi, S., Itkis, M. E., & Haddon, R. C. (2012). Advances in the chemical modification of epitaxial graphene. *Journal of Physics D: Applied Physics*, *45*(15). https://doi.org/10.1088/0022-3727/45/15/154009

Bennaceur, K., Matter, C., & Paris, U. (2011). *Electronic transport in graphene To cite this version : Transport électronique dans le graphène*.

Bhatnagar, A., & Minocha, A. K. (2006). Conventional and non-conventional adsorbents for removal of pollutants from water - A review. *Indian Journal of Chemical Technology*, *13*(3), 203–217.

Bilalis, P., Katsigiannopoulos, D., Avgeropoulos, A., & Sakellariou, G. (2014). Non-covalent functionalization of carbon nanotubes with polymers. *RSC Advances*, *4*(6), 2911–2934. https://doi.org/10.1039/c3ra44906h

Bo, Z., Yang, Y., Chen, J., Yu, K., Yan, J., & Cen, K. (2013). Plasma-enhanced chemical vapor deposition synthesis of vertically oriented graphene nanosheets. *Nanoscale*, *5*(12), 5180–5204. https://doi.org/10.1039/c3nr33449j

Bottari, G., Ángeles Herranz, M., Wibmer, L., Volland, M., Rodríguez-Pérez, L., Guldi, D. M., Hirsch, A., Martín, N., D'Souza, F., & Torres, T. (2017). Chemical functionalization and characterization of graphene-based materials. *Chemical Society Reviews*, *46*(15), 4464–4500. https://doi.org/10.1039/c7cs00229g

Boulouz, A., Giani, A., Sorli, B., Koutti, L., Massaq, A., & Pascal-Delannoy, F. (2014). Fabrication of Thermoelectric Sensor and Cooling Devices Based on Elaborated Bismuth-Telluride Alloy Thin Films. *Journal of Materials*, *2014*, 1–8. https://doi.org/10.1155/2014/430410

Cai, M., Thorpe, D., Adamson, D. H., & Schniepp, H. C. (2012). Methods of graphite exfoliation. *Journal of Materials Chemistry*, *22*(48), 24992–25002. https://doi.org/10.1039/c2jm34517j

Cai, W., Piner, R. D., Stadermann, F. J., Park, S., Shaibat, M. A., Ishii, Y., Yang, D., Velamakanni, A., Sung, J. A., Stoller, M., An, J., Chen, D., & Ruoff, R. S. (2008). Synthesis and solid-state NMR structural characterization of 13C-labeled graphite oxide. *Science*, *321*(5897), 1815–1817. https://doi.org/10.1126/science.1162369

Carmen, Z., & Daniel, S. (2012a). Textile Organic Dyes – Characteristics, Polluting Effects and Separation/Elimination Procedures from Industrial Effluents – A Critical Overview. *Organic Pollutants Ten Years After the Stockholm Convention - Environmental and Analytical Update*. https://doi.org/10.5772/32373

Carmen, Z., & Daniel, S. (2012b). Textile Organic Dyes – Characteristics, Polluting Effects and Separation/Elimination Procedures from Industrial Effluents – A Critical Overview. *Organic Pollutants Ten Years After the Stockholm Convention - Environmental and Analytical Update*, *2741*(31). https://doi.org/10.5772/32373

Carmen, Z., & Daniela, S. (2016). *Textile Organic Dyes – Characteristics , Polluting Effects and Separation / Elimination Procedures from Industrial Effluents – A Critical Overview*. *October 2014*. https://doi.org/10.5772/32373

Casabianca, L. B., Shaibat, M. A., Cai, W. W., Park, S., Piner, R., Ruoff, R. S., & Ishii, Y. (2010). NMR-based structural modeling of graphite oxide using multidimensional 13C solid-state NMR and ab initio chemical shift calculations. *Journal of the American Chemical Society*, *132*(16), 5672–5676. https://doi.org/10.1021/ja9030243

Castro Neto, A. H., Guinea, F., Peres, N. M. R., Novoselov, K. S., & Geim, A. K. (2009). The electronic properties of graphene. *Reviews of Modern Physics*, *81*(1), 109–162. https://doi.org/10.1103/RevModPhys.81.109

Çelebi, C., Yanik, C., Demirkol, A. G., & Kaya, I. I. (2012). The effect of a SiC cap on the growth of epitaxial graphene on SiC in ultra high vacuum. *Carbon*, *50*(8), 3026–3031. https://doi.org/10.1016/j.carbon.2012.02.088

Chandrawat, P. S. (2020). ADSORPTION OF FLUORIDE IN SOILS OF RAJASTHAN. *Ijcrt.*, *8*(4), 3039–3046.

Chen, F., Cao, Y., & Jia, D. (2013). Facile synthesis of Bi2S3 hierarchical nanostructure with enhanced photocatalytic activity. *Journal of Colloid and Interface Science*, *404*, 110–116. https://doi.org/10.1016/j.jcis.2013.04.013

Chen, T., & Cheung, R. (2016a). Mechanical properties of graphene. *Graphene Science Handbook: Mechanical and Chemical Properties*, 3–15.

Chen, T., & Cheung, R. (2016b). Mechanical properties of graphene. *Graphene Science Handbook: Mechanical and Chemical Properties*, 3–15. https://doi.org/10.1201/b19642-19

Chiu, Y. H., Ou, Y. C., & Lin, M. F. (2016). Optical properties of graphene in external fields. *Graphene Science Handbook: Electrical and Optical Properties*, 469–488. https://doi.org/10.1201/b19642-29

Choudhary, O.P. and Choudhary, P. (2017). Scanning Electron Microscope: Advantages and Disadvantages in Imaging Components. *International Journal of Current Microbiology and Applied Sciences*, *6*(5), 1877–1882. https://doi.org/10.20546/ijcmas.2017.605.207

Chufa, B. M., Gonfa, B. A., Anshebo, T. Y., & Workneh, G. A. (2021). A Novel and Simplest Green Synthesis Method of Reduced Graphene Oxide Using Methanol Extracted Vernonia Amygdalina : Large-Scale Production. *Advances in Condensed Matter Physics*, *2021*, 1–10. https://doi.org/10.1155/2021/6681710

Çıplak, Z., Getiren, B., Gökalp, C., Yıldız, A., & Yıldız, N. (2020). Green synthesis of reduced graphene oxide-AgAu bimetallic nanocomposite: Catalytic performance. *Chemical Engineering Communications*, *207*(4), 559–573. https://doi.org/10.1080/00986445.2019.1613227

Collivignarelli, M. C., Abbà, A., Miino, M. C., Torretta, V., Rada, E. C., Caccamo, F. M., & Sorlini, S. (2020). Adsorption of fluorides in drinking water by palm residues. *Sustainability (Switzerland)*, *12*(9), 1–12. https://doi.org/10.3390/su12093786

da Silva Alves, D. C., Healy, B., Yu, T., & Breslin, C. B. (2021). Graphene-based materials immobilized within chitosan: Applications as adsorbents for the removal of aquatic pollutants. *Materials*, *14*(13). https://doi.org/10.3390/ma14133655

Das, R., Ali, M. E., Hamid, S. B. A., Ramakrishna, S., & Chowdhury, Z. Z. (2014). Carbon nanotube membranes for water purification: A bright future in water desalination. *Desalination*, *336*(1), 97–109. https://doi.org/10.1016/j.desal.2013.12.026

Datturi, S., Steenbergen, F. Van, Beusekom, M. Van, Kebede, S., & Ababa, A. (2015). COMPARING DEFLUORIDATION AND SAFE SOURCING FOR. *Fluoride*, *48*(4), 293–314.

De Heer, W. A., Berger, C., Ruan, M., Sprinkle, M., Li, X., Hu, Y., Zhang, B., Hankinson, J., & Conrad, E. (2011). Large area and structured epitaxial graphene produced by confinement controlled sublimation of silicon carbide. *Proceedings of the National Academy of Sciences of the United States of America*, *108*(41), 16900–16905. https://doi.org/10.1073/pnas.1105113108

De, M., & Mayado, T. (2016a). Graphene and Planar Dirac Equation. *Nanoscience*, *June*.

De, M., & Mayado, T. (2016b). *Graphene and Planar Dirac Equation*. *June*.

Demelash, H., Beyene, A., Abebe, Z., & Melese, A. (2019). Fluoride concentration in ground water and prevalence of dental fluorosis in Ethiopian Rift Valley: Systematic review and meta-analysis. *BMC Public Health*, *19*(1), 1–9. https://doi.org/10.1186/s12889-019-7646-8

Deng, B., Liu, Z., & Peng, H. (2019). Toward Mass Production of CVD Graphene Films. *Advanced Materials*, *31*(9), 1800996. https://doi.org/10.1002/adma.201800996

Desai, S., & Njuguna, J. (2012). Thermal properties of natural graphite flake composites. *International Review of Mechanical Engineering*, *6*(4), 923–926.

Description, I. (2007). *Dye Manufacturing*. *2*, 298–301.

Deshpande, M. P., Sakariya, P. N., Bhatt, S. V, Patel, N. H., Patel, K., & Chaki, S. H.

(2015). *Preparation and characterization of Bi 2 S 3 compound semiconductor*. *38*(1), 83–88.

Dideikin, A. T., & Vul', A. Y. (2019). Graphene oxide and derivatives: The place in graphene family. *Frontiers in Physics*, *6*(JAN). https://doi.org/10.3389/fphy.2018.00149

Diego, P. F. J. (2015). Influence of Graphite Properties on Tribological. *Conference Paper*, *3*.

Díez-Pascual, A. M. (2021). Development of graphene-based polymeric nanocomposites: A brief overview. *Polymers*, *13*(17). https://doi.org/10.3390/polym13172978

Dong, Y., Guo, S., Mao, H., Xu, C., Xie, Y., Cheng, C., Mao, X., Deng, J., Pan, G., & Sun, J. (2019). The growth of graphene on Ni–Cu alloy thin films at a low temperature and its carbon diffusion mechanism. *Nanomaterials*, *9*(11), 1–11. https://doi.org/10.3390/nano9111633

Dreyer, D. R., Park, S., Bielawski, C. W., & Ruoff, R. S. (2010). The chemistry of graphene oxide. *Chemical Society Reviews*, *39*(1), 228–240. https://doi.org/10.1039/b917103g

E. Sadurn´ı, E. Rivera-Moci˜nos, and A. R. (2015). Discrete symmetry in graphene : the Dirac equation and beyond. *RESEARCH*, *61*(June), 170–181.

Eigler, S., & Hirsch, A. (2014). Chemistry with graphene and graphene oxide - Challenges for synthetic chemists. *Angewandte Chemie - International Edition*, *53*(30), 7720–7738. https://doi.org/10.1002/anie.201402780

Ekaluo, U. B., Ikpeme, E. V., & Ekerette, E. (2015). *In vitro Antioxidant and Free Radical Activity of Some Nigerian Medicinal Plants : Bitter Leaf (Vernonia amygdalina L .) and Guava (Psidium guajava Del .)*. *October*. https://doi.org/10.3923/rjmp.2015.215.226

Ersan, G., Apul, O. G., Perreault, F., & Karanfil, T. (2017). Adsorption of organic contaminants by graphene nanosheets: A review. *Water Research*, *126*, 385–398. https://doi.org/10.1016/j.watres.2017.08.010

Etxebarria, N., Zuloaga, O., Olivares, M., Bartolomé, L. J., & Navarro, P. (2009). Retention-time locked methods in gas chromatography. *Journal of Chromatography A*, *1216*(10), 1624–1629. https://doi.org/10.1016/j.chroma.2008.12.038

Falkovsky, L. A. (2008). Optical properties of graphene. *Journal of Physics: Conference Series*, *129*. https://doi.org/10.1088/1742-6596/129/1/012004

Feicht, P., Biskupek, J., Gorelik, T. E., Renner, J., Halbig, C. E., Maranska, M., Puchtler,

F., Kaiser, U., & Eigler, S. (2019). Brodie's or Hummers' Method: Oxidation Conditions Determine the Structure of Graphene Oxide. *Chemistry - A European Journal*, *25*(38), 8955–8959. https://doi.org/10.1002/chem.201901499

Feng, J., Ye, Y., Xiao, M., Wu, G., & Ke, Y. (2020). Synthetic routes of the reduced graphene oxide. *Chemical Papers*, *74*(11), 3767–3783. https://doi.org/10.1007/s11696-020-01196-0

Fentaw, T., & Worku, D. (2017). Controlled synthesis , characterization and reduction of graphene oxide : A convenient method for large scale production. *Egyptian Journal of Basic and Applied Sciences*, *4*(1), 74–79. https://doi.org/10.1016/j.ejbas.2016.11.002

Fito, J., Said, H., Feleke, S., & Worku, A. (2019). Fluoride removal from aqueous solution onto activated carbon of Catha edulis through the adsorption treatment technology. *Environmental Systems Research*, 1–10. https://doi.org/10.1186/s40068-019-0153-1

Forrester, D. M., & Kusmartsev, F. V. (2014). Graphene levitons and anti-levitons in magnetic fields. *Nanoscale*, *6*(13), 7594–7603. https://doi.org/10.1039/c4nr00754a

Fu, Y., Hansson, J., Liu, Y., Chen, S., Zehri, A., Samani, M. K., Wang, N., Ni, Y., Zhang, Y., Zhang, Z. Bin, Wang, Q., Li, M., Lu, H., Sledzinska, M., Torres, C. M. S., Volz, S., Balandin, A. A., Xu, X., & Liu, J. (2020). Graphene related materials for thermal management. *2D Materials*, *7*(1). https://doi.org/10.1088/2053-1583/ab48d9

Fuchs, J.-N. (2013). *Dirac fermions in graphene and analogues: magnetic field and topological properties*. http://arxiv.org/abs/1306.0380

Ge, Z. H., Qin, P., He, D., Chong, X., Feng, D., Ji, Y. H., Feng, J., & He, J. (2017). Highly Enhanced Thermoelectric Properties of Bi/Bi2S3 Nanocomposites. *ACS Applied Materials and Interfaces*, *9*(5), 4828–4834. https://doi.org/10.1021/acsami.6b14803

Ge, Z., Zhang, B., & Yu, Z. (2011). *Effect of spark plasma sintering temperature on thermoelectric properties of Bi2S3 polycrystal Effect of spark plasma sintering temperature on thermoelectric properties of Bi 2 S 3 polycrystal*. *November*. https://doi.org/10.1557/jmr.2011.273

Geim, A. K. (2011). Nobel Lecture: Random walk to graphene. *Reviews of Modern Physics*, *83*(3), 851–862. https://doi.org/10.1103/RevModPhys.83.851

Ghanbari, D., Salavati-Niasari, M., Karimzadeh, S., & Gholamrezaei, S. (2014). Hydrothermal Synthesis of Bi2S3 Nanostructures and ABS-Based Polymeric Nanocomposite. *Journal of NanoStructures*, *4*(2), 227–232.

Ghanbarian, M., Ghanbarian, M., Hossein, A., & Tabatabaie, T. (2020). Enhanced fl

uoride removal over MgFe 2 O 4 – chitosan – CaAl nanohybrid : Response surface optimization , kinetic and isotherm study. *International Journal of Biological Macromolecules*, *148*, 574–590. https://doi.org/10.1016/j.ijbiomac.2020.01.143

Ghanem, A. F., & Rehim, M. A. (2018). Assisted Tip Sonication Approach for Graphene Synthesis in Aqueous Dispersion. *Biomedicines*, *6*(63), 1–15. https://doi.org/10.3390/biomedicines6020063

Ghori, S. W., Siakeng, R., Rasheed, M., Saba, N., & Jawaid, M. (2018). The role of advanced polymer materials in aerospace. *Sustainable Composites for Aerospace Applications*, 19–34. https://doi.org/10.1016/B978-0-08-102131-6.00002-5

Gupta, K. M., & Gupta, N. (2015). Advanced semiconducting materials and devices. In *Advanced Semiconducting Materials and Devices*. https://doi.org/10.1007/978-3-319-19758-6

Gürünlü, B., Taşdelen Yücedağ, Ç., & Bayramoğlu, M. R. (2020). Green Synthesis of Graphene from Graphite in Molten Salt Medium. *Journal of Nanomaterials*, *2020*. https://doi.org/10.1155/2020/7029601

Habte, A. T., Ayele, D. W., & Hu, M. (2019). Synthesis and Characterization of Reduced Graphene Oxide (rGO) Started from Graphene Oxide (GO) Using the Tour Method with Different Parameters. *Advances in Materials Science and Engineering*, *2019*(Vc). https://doi.org/10.1155/2019/5058163

Hacker, P. J., Neighbour, G. B., & Mcenaney, B. (2013). *The coefficient of thermal expansion of nuclear graphite with increasing thermal oxidation*. *December*. https://doi.org/10.1088/0022-3727/33/8/316

Haghighi, B., & Tabrizi, M. A. (2013). Green-synthesis of reduced graphene oxide nanosheets using rose water and a survey on their characteristics and applications. *RSC Advances*, *3*(32), 13365–13371. https://doi.org/10.1039/c3ra40856f

Hakimi, M., & Alimard, P. (2012). Graphene : Synthesis and Applications in Biotechnology - A Review. *World Applied Programming*, *2*(June), 377–388.

Handayani, M., Nafi, N., Nugroho, A., Rasyida, A., Prasetyo, A. B., & Febriana, E. (2021). *The Development of Graphene / Silica Hybrid Composites : A Review for Their Applications and Challenges*. 1–28.

Hessain, H. A., & Hassan, J. J. (2020). Green synthesis of reduced graphene oxide using ascorbic acid. *Iraqi Journal of Science*, *61*(6), 1313–1319. https://doi.org/10.24996/ijs.2020.61.6.9

Hidayah, N. M. S., Liu, W. W., Lai, C. W., Noriman, N. Z., Khe, C. S., Hashim, U., &

Lee, H. C. (2017). Comparison on graphite, graphene oxide and reduced graphene oxide: Synthesis and characterization. *AIP Conference Proceedings*, *1892*(October). https://doi.org/10.1063/1.5005764

Hu, E., Gao, X., Etogo, A., Xie, Y., Zhong, Y., & Hu, Y. (2014). Controllable one-pot synthesis of various one-dimensional Bi 2S3 nanostructures and their enhanced visible-light-driven photocatalytic reduction of Cr(VI). *Journal of Alloys and Compounds*, *611*, 335–340. https://doi.org/10.1016/j.jallcom.2014.05.075

Huang, H. H., Chen, J., Meng, Y. Z., Yang, X. Q., Zhang, M. Z., Yu, Y., Ma, Z. Y., & Zhao, Y. Di. (2013). Synthesis and characterization of Bi2S3 composite nanoparticles with high X-ray absorption. *Materials Research Bulletin*, *48*(10), 3800–3804. https://doi.org/10.1016/j.materresbull.2013.05.091

HUANG, X. (2016). *Electromagnetic Applications of Graphene and Graphene Oxide A thesis submitted for the degree of PhD at the*.

Huber, A. C., & Mosler, H. J. (2013). Determining behavioral factors for interventions to increase safe water consumption: A cross-sectional field study in rural Ethiopia. *International Journal of Environmental Health Research*, *23*(2), 96–107. https://doi.org/10.1080/09603123.2012.699032

Hwang, J., Park, J., Yoon, K., & Kim, J. (2020). One-pot synthesis of Bi-reduced graphene oxide composite using supercritical acetone as anode for Na-ion batteries. *Chemical Engineering Journal*, *387*(October 2019), 124111. https://doi.org/10.1016/j.cej.2020.124111

Igwe, K. K., & Ijeh, P. N. O. I. I. (2015). *GC-MS analysis of phytocomponents in Vernonia amygdalina . Del leaves and its contractile potential in mammary tissue in female albino Wistar rats*. *8*(11), 25–30. https://doi.org/10.9790/2380-081112530

Ilondu, E. M. (2010). *Antifungal activities of three Vernonia spp. Phytochemical composition and efficacy of ethanolic leaf extracts of some*.

Iwuozor, K. O. (2019). *Prospects and Challenges of Using Coagulation-Flocculation Method in the Treatment of Effluents*. *2*(2), 105–127.

Jane Ogoamaka Okwuzu, Peter Odeiga, Olubunmi AdetoroOtubanjo, O. C. E. (n.d.). *Cytotoxicity testing of aqueous extract of bitter leaf (Vernonia amygdalina Del) and sniper 1000EC (2,3 dichlorovinyl dimethyl phosphate) using the Alium cepa test.* 147–153.

Ji, D. K., Reina, G., Guo, S., Eredia, M., Samorì, P., Ménard-Moyon, C., & Bianco, A. (2020). Controlled functionalization of carbon nanodots for targeted intracellular

production of reactive oxygen species. *Nanoscale Horizons*, *5*(8), 1240–1249. https://doi.org/10.1039/d0nh00300j

Ji, G., & Zhao, M. (2017). Membrane Separation Technology in Carbon Capture. *Recent Advances in Carbon Capture and Storage, March*. https://doi.org/10.5772/65723

Jilani, A., Hafiz, M., Othman, D., Ansari, M. O., & Hussain, S. Z. (2018). Graphene and its derivatives : synthesis , modifications , and applications in wastewater treatment. *Environmental Chemistry Letters, 0123456789*. https://doi.org/10.1007/s10311-018-0755-2

Jilani, A., Othman, M. H. D., Ansari, M. O., Hussain, S. Z., Ismail, A. F., Khan, I. U., & Inamuddin. (2018). Graphene and its derivatives: synthesis, modifications, and applications in wastewater treatment. *Environmental Chemistry Letters*, *16*(4), 1301–1323. https://doi.org/10.1007/s10311-018-0755-2

Jin, X., Adpakpang, K., Young Kim, I., Mi Oh, S., Lee, N. S., & Hwang, S. J. (2015). An effective way to optimize the functionality of graphene-based nanocomposite: Use of the colloidal mixture of graphene and inorganic nanosheets. *Scientific Reports*, *5*(May), 1–13. https://doi.org/10.1038/srep11057

Jing, C. (2014). La3 + -modified activated alumina for fluoride removal from water. *Journal of Hazardous Materials J*, *278*, 343–349 Contents.

Joshi, S., Siddiqui, R., Sharma, P., Kumar, R., Verma, G., & Saini, A. (2020). Green synthesis of peptide functionalized reduced graphene oxide (rGO) nano bioconjugate with enhanced antibacterial activity. *Scientific Reports*, *10*(1), 1–11. https://doi.org/10.1038/s41598-020-66230-3

Kair, G. S., & Faj, C. R. S. (2014). Effect of fluoride in the human body. *World Scientific News*, *5*, 12–16.

Kariuki, S. M., Ngari, M. S., Mavura, W. J., Ollengo, M. S., & Ongoma, P. O. (2015). Effect of Essential Mineral Ions from Aqueous Media on Adsorption of Fluoride by Bone Char. *IOSR Journal of Environmental Science Ver. II*, *9*(5), 2319–2399. https://doi.org/10.9790/2402-09520917

Karthikeyan, B. (2019). Fluoride removal from aqueous solution using Psidium guajava and Mimosa pudica Leaves. *International Journal of Advanced Research Trends in Engineering and Technology*, *5*(5).

Kavitha, M. K., & Jaiswal, M. (2016). Graphene : A review of optical properties and photonic applications. *Asian Journal of Physics*, *25*(7), 809–831.

Kebede, S. (2013). Groundwater in Ethiopia: Features, numbers and opportunities. In

Groundwater in Ethiopia: Features, Numbers and Opportunities. https://doi.org/10.1007/978-3-642-30391-3

Keeling, J. (2017). Graphite: properties, uses and South Australian resources. *MESA Journal*, *84*(3), 28–41.

Khan, I., Saeed, K., & Khan, I. (2019). Nanoparticles: Properties, applications and toxicities. *Arabian Journal of Chemistry*, *12*(7), 908–931. https://doi.org/10.1016/j.arabjc.2017.05.011

Ki, W., Si, R., & James, A. S. (2020). *Modified Crushed Oyster Shells for Fluoride Removal from Water*. https://doi.org/10.1038/s41598-020-60743-7

Kianpour, B., Ebrahimi, A., Salehi, Z., & Fatemi, S. (2017). Evaluating the Effect of Graphite Source and Operating Conditions on the Synthesis of Graphene Oxide. *Journal of Chemical and Petroleum Engineering*, *50*(2), 37–45.

Kocsis, M., & Hideg, E. (2013). *On the spectrophotometric determination of total phenolic and flavonoid contents on the spectrophotometric determination of total phenolic and flavonoid contents*. *December*. https://doi.org/10.1556/ABiol.64.2013.4.10

Kopelevich, Y., & Luk'yanchuk, I. A. (2010). Graphite vs graphene: scientific background. *Noble Prize*, *50005*(October), 0–10. http://arxiv.org/abs/1011.4680

Kosik-bogacka, D. I., Lebiotkowski, M., Baranowska-bosiacka, I., Gutowska, I., & Chlubek, D. (2015). BONE FLUORIDE CONTENT IN PATIENTS AFTER. In *Fluoride* (Vol. 48, Issue 3).

Kowalchuk, E. (2012). *Selective fluoride removal by aluminum precipitation & membrane filtration*.

Ku, Y., Chiou, H., & Wang, W. (2002). Separation Science and Technology The removal of fluoride ion from aqueous solution by a cation synthetic resin. *Separation Science and Technology*, *37*(1), 89–103. https://doi.org/10.1081/SS-120000323

Kumar, P., Kumar Singh, A., Hussain, S., Nam Hui, K., San Hui, K., Eom, J., Jung, J., & Singh, J. (2013). Graphene: Synthesis, Properties and Application in Transparent Electronic Devices. *Reviews in Advanced Sciences and Engineering*, *2*(4), 238–258. https://doi.org/10.1166/rase.2013.1043

Kumar, R. T., & Vijaya, J. J. (2017). Nanomaterials for photocatalysis and heavy metals removal R. *Catalysis and Nanomaterials*.

Le Marechal, A. M., Krianec, B., Vajnhandl, S., & Volmajer, J. (2012). Textile Finishing Industry as an Important Source of Organic Pollutants. *Organic Pollutants Ten Years*

After the Stockholm Convention - Environmental and Analytical Update. https://doi.org/10.5772/32272

Lee, A. Y. W., Lim, S. F., Chua, S. N. D., Sanaullah, K., Baini, R., & Abdullah, M. O. (2017). Adsorption Equilibrium for Heavy Metal Divalent Ions (Cu2+, Zn2+, and Cd2+) into Zirconium-Based Ferromagnetic Sorbent. *Advances in Materials Science and Engineering*, *2017*. https://doi.org/10.1155/2017/1210673

Lellis, B., Fávaro-polonio, C. Z., Pamphile, J. A., & Polonio, J. C. (2019). *Effects of textile dyes on health and the environment and bioremediation potential of living organisms*. https://doi.org/10.1016/j.biori.2019.09.001

Li, J., Zeng, X., Ren, T., & van der Heide, E. (2014). The preparation of graphene oxide and its derivatives and their application in bio-tribological systems. *Lubricants*, *2*(3), 137–161. https://doi.org/10.3390/lubricants2030137

Li, R., Zhang, L., & Wang, P. (2015). Rational design of nanomaterials for water treatment. *Nanoscale*, *October*. https://doi.org/10.1039/c5nr04870b

Li, Xiaolin, Zhang, G., Bai, X., Sun, X., Wang, X., Wang, E., & Dai, H. (2008). Highly conducting graphene sheets and Langmuir-Blodgett films. *Nature Nanotechnology*, *3*(9), 538–542. https://doi.org/10.1038/nnano.2008.210

Li, Xing, Chen, Y., Cheng, Z., Jia, L., Mo, S., & Liu, Z. (2014). Ultrahigh specific surface area of graphene for eliminating subcooling of water. *Applied Energy*, *130*, 824–829. https://doi.org/10.1016/j.apenergy.2014.02.032

Liao, X. H., Wang, H., Zhu, J. J., & Chen, H. Y. (2001). Preparation of Bi2S3 nanorods by microwave irradiation. *Materials Research Bulletin*, *36*(13–14), 2339–2346. https://doi.org/10.1016/S0025-5408(01)00734-6

Lin, J., Chen, Y., Hong, X., Huang, C., & Huang, C. P. (2020). The role of fluoroaluminate complexes on the adsorption of fluoride onto hydrous alumina in aqueous solutions. *Journal of Colloid And Interface Science*, *561*, 275–286. https://doi.org/10.1016/j.jcis.2019.10.085

Liu, P., Borrell, P. F., Božič, M., Kokol, V., Oksman, K., & Mathew, A. P. (2015). Nanocelluloses and their phosphorylated derivatives for selective adsorption of Ag+, Cu2+ and Fe3+ from industrial effluents. *Journal of Hazardous Materials*, *294*(April), 177–185. https://doi.org/10.1016/j.jhazmat.2015.04.001

Liu, W., Lukas, K. C., McEnaney, K., Lee, S., Zhang, Q., Opeil, C. P., Chen, G., & Ren, Z. (2013). Studies on the Bi2Te3-Bi2Se 3-Bi2S3 system for mid-temperature thermoelectric energy conversion. *Energy and Environmental Science*, *6*(2), 552–

560. https://doi.org/10.1039/c2ee23549h

Liu, Xiaofeng, Giordano, C., & Antonietti, M. (2014). A facile molten-salt route to graphene synthesis. *Small*, *10*(1), 193–200. https://doi.org/10.1002/smll.201300812

Liu, Xiaolu, Pang, H., Liu, X., Li, Q., Zhang, N., Mao, L., Qiu, M., Hu, B., Yang, H., & Wang, X. (2021). Orderly Porous Covalent Organic Frameworks-based Materials: Superior Adsorbents for Pollutants Removal from Aqueous Solutions. *The Innovation*, *2*(1), 100076. https://doi.org/10.1016/j.xinn.2021.100076

Liu, Ya, Shi, Y., Liu, X., & Li, H. (2016). A facile solvothermal approach of novel Bi2S3/TiO2/RGO composites with excellent visible light degradation activity for methylene blue. *Applied Surface Science*. https://doi.org/10.1016/j.apsusc.2016.11.028

Liu, Ying ying, Luo, S. hua, Yan, S. xue, Feng, J., & Yi, T. feng. (2020). Green synthesis of reduced graphene oxide as high-performance electrode materials for supercapacitors. *Ionics*, *26*(1), 415–422. https://doi.org/10.1007/s11581-019-03185-0

Liu, Zhang, Fang, J., Xu, W., Xu, X., Wu, S., & Zhu, X. (2012). Low temperature hydrothermal synthesis of Bi 2S 3 nanorods using BiOI nanosheets as self-sacrificing templates. *Materials Letters*, *88*, 82–85. https://doi.org/10.1016/j.matlet.2012.07.109

Liu, Zhenbao, Liu, B., Ding, J., & Liu, J. (2014). Fluorescent sensors using DNA-functionalized graphene oxide. In *Analytical and Bioanalytical Chemistry* (Vol. 406, Issue 27). https://doi.org/10.1007/s00216-014-7888-3

Lu, C. T., Weerasinghe, A., Maroudas, D., & Ramasubramaniam, A. (2016). A comparison of the elastic properties of graphene- and fullerene-reinforced polymer composites: The role of filler morphology and size. *Scientific Reports*, *6*(August), 1–9. https://doi.org/10.1038/srep31735

Luan, X., Wing, M. T. G., & Wang, Y. (2015). Enhanced photocatalytic activity of graphene oxide/titania nanosheets composites for methylene blue degradation. *Materials Science in Semiconductor Processing*, *30*, 592–598. https://doi.org/10.1016/j.mssp.2014.10.032

Luongo, G. (2015). Chemicals in textiles. In *Chemicals in textilies - A potential source for human exposure and environmental pollution*.

Lv, R., Chen, G., Li, Q., McCreary, A., Botello-Méndez, A., Morozov, S. V., Liang, L., Declerck, X., Perea-López, N., Cullen, D. A., Feng, S., Elías, A. L., Cruz-Silva, R., Fujisawa, K., Endo, M., Kang, F., Charlier, J. C., Meunier, V., Pan, M., … Terrones, M. (2015). Ultrasensitive gas detection of large-area boron-doped graphene.

Proceedings of the National Academy of Sciences of the United States of America, *112*(47), 14527–14532. https://doi.org/10.1073/pnas.1505993112

Ma, D., Zou, X., Li, R., Chen, P., Wang, Y., Chen, T., Zhang, Q., Liu, H., Chen, Y., Lv, W., Feng, Y., & Liu, G. (2020). Highly efficient adsorption of Pb(II) by cubic nanocrystals in aqueous solution: Behavior and mechanism. *Arabian Journal of Chemistry*, *13*(5), 5229–5240. https://doi.org/10.1016/j.arabjc.2020.02.022

Ma, L., Dong, X., Chen, M., Zhu, L., Wang, C., Yang, F., & Dong, Y. (2017). Fabrication and water treatment application of carbon nanotubes (CNTs)-based composite membranes: A review. *Membranes*, *7*(1). https://doi.org/10.3390/membranes7010016

Ma, W., Ya, F., Wang, R., & Zhao, Y. (2008). Fluoride removal from drinking water by adsorption using bone char as a biosorbent. *International Journal of Environmental Technology and Management*, *9*(1), 59–69. https://doi.org/10.1504/IJETM.2008.017860

Magampa, P. P., Manyala, N., & Focke, W. W. (2013). Properties of graphite composites based on natural and synthetic graphite powders and a phenolic novolac binder. *Journal of Nuclear Materials*, *436*(1–3), 76–83. https://doi.org/10.1016/j.jnucmat.2013.01.315

Mahendran, G. B., Ramalingam, S. J., Rayappan, J. B. B., Kesavan, S., Periathambi, T., & Nesakumar, N. (2020). Green preparation of reduced graphene oxide by Bougainvillea glabra flower extract and sensing application. *Journal of Materials Science: Materials in Electronics*, *31*(17), 14345–14356. https://doi.org/10.1007/s10854-020-03994-4

Mahvi, A. H., Mostafapour, F. K., Balarak, D., & Khatibi, A. D. (2019). Adsorption of fluoride from aqueous solutions by a chitosan/zeolite composite. *Fluoride*, *52*(4), 546–552.

Malakootian, M., Moosazadeh, M., Yousefi, N., & Fatehizadeh, A. (2011). Fluoride removal from aqueous solution by pumice : case study on Kuhbonan water. *African Journal of Environmental Science and Technology*, *5*(4), 299–306.

Malik, K., & Ahmed, M. (2018). *Identification of novel anticancer terpenoids from Prosopis juliflora (Sw) DC Identification of novel anticancer terpenoids from Prosopis juliflora (Sw) DC (Leguminosae) pods*. *April*. https://doi.org/10.4314/tjpr.v17i4.14

Manchala, S., Tandava, V. S. R. K., Jampaiah, D., Bhargava, S. K., & Shanker, V. (2019). Novel and Highly E ffi cient Strategy for the Green Synthesis of Soluble Graphene

by Aqueous Polyphenol Extracts of Eucalyptus Bark and Its Applications in High-Performance Supercapacitors. *ACS Sustainable Chem. Eng.*, *7*(13), 11612–11620. https://doi.org/10.1021/acssuschemeng.9b01506

Mandefro Ararso, M. S. (2017). Excessive fluoride concentration in the Ethiopian rift and the flowered project. *Geomatrix*, *20*(7), 1–72.

Mao, H. Y., Lu, Y. H., Lin, J. D., Zhong, S., Wee, A. T. S., & Chen, W. (2013). Manipulating the electronic and chemical properties of graphene via molecular functionalization. *Progress in Surface Science*, *88*(2), 132–159. https://doi.org/10.1016/j.progsurf.2013.02.001

Marcano, D. C., Kosynkin, D. V., Berlin, J. M., Sinitskii, A., Sun, Z., Slesarev, A., Alemany, L. B., Lu, W., & Tour, J. M. (2010). Improved synthesis of graphene oxide. *ACS Nano*, *4*(8), 4806–4814. https://doi.org/10.1021/nn1006368

März, B., Jolley, K., Marrow, T. J., Zhou, Z., Heggie, M., Smith, R., & Wu, H. (2018a). Mesoscopic structure features in synthetic graphite. *Materials and Design*, *142*(March), 268–278. https://doi.org/10.1016/j.matdes.2018.01.038

März, B., Jolley, K., Marrow, T. J., Zhou, Z., Heggie, M., Smith, R., & Wu, H. (2018b). Mesoscopic structure features in synthetic graphite. *Materials and Design*, *142*(May), 268–278. https://doi.org/10.1016/j.matdes.2018.01.038

Matte, H. S. S. R., Subrahmanyam, K. S., & Rao, C. N. R. (2011). Synthetic aspects and selected properties of graphene. *Nanomaterials and Nanotechnology*, *1*(1), 3–13. https://doi.org/10.5772/50945

Matyushkin, L. B., Ryzhov, O. A., Aleksandrova, O. A., & Moshnikov, V. A. (2016). Synthesis of metal and semiconductor nanoparticles in a flow of immiscible liquids. *Semiconductors*, *50*(6), 844–847. https://doi.org/10.1134/S1063782616060166

Medellin-castillo, N. A., Leyva-ramos, R., Ocampo-perez, R., Garcia, R. F., Cruz, D., Aragon-pin, A., & Martinez-rosales, J. M. (2007). Adsorption of Fluoride from Water Solution on Bone Char. *Ind. Eng. Chem. Res*, *46*, 9205–9212.

Meijiao, L. Ü., Jing, L. I., Xuyu, Y., Changan, Z., Jia, Y., Hao, H. U., & Xianbao, W. (2013). Applications of graphene-based materials in environmental protection and detection. *Chin Sci Bull*, *58*(22), 2698–2710. https://doi.org/10.1007/s11434-013-5887-y

Mikhailov, S., & L. Pietronero, S. Strassler, and H. R. Z. (2012). Physics and Applications of Graphene - Theory. In *Physics and Applications of Graphene - Theory*. Physics and Materials Science. https://doi.org/10.5772/1938

Milenov, T. I., Avramova, I., Valcheva, E., Avdeev, G. V., Rusev, S., Kolev, S., Balchev, I., Petrov, I., Pishinkov, D., & Popov, V. N. (2017). Deposition of defected graphene on (001) Si substrates by thermal decomposition of acetone. *Superlattices and Microstructures*, *111*(April), 45–56. https://doi.org/10.1016/j.spmi.2017.04.042

Mk, O., Oi, A., Bo, O., Ia, A., & Bi, O. (2019). *Identification and Quantification of Bioactive Compounds Present in the Plant Vernonia amygdalina Delile using GC-MS Technique*. *7*(1), 8–12. https://doi.org/10.4172/2329-6836.1000356

MM, M., SA Abo El, E., MY, H., MS, M., & MH, K. (2017). Thermally Reduced Graphene Oxide: Synthesis, Structural and Electrical Properties. *International Journal of Nanoparticles and Nanotechnology*, *3*(1). https://doi.org/10.35840/2631-5084/5508

Molitor, F., Güttinger, J., Stampfer, C., Dröscher, S., Jacobsen, A., Ihn, T., & Ensslin, K. (2011). Electronic properties of graphene nanostructures. *Journal of Physics Condensed Matter*, *23*(24). https://doi.org/10.1088/0953-8984/23/24/243201

Momoh, J., & Polytechnic, L. S. (2020). *PHYTOCOMPONENTS IN THE ROOT , STEM BARK AND LEAF OF VERNONIA*. *January 2017*. https://doi.org/10.20959/wjpr20172-7701

Morais, A., Alves, J. P. C., Lima, F. A. S., Lira-Cantu, M., & Nogueira, A. F. (2015). Enhanced photovoltaic performance of inverted hybrid bulk-heterojunction solar cells using TiO 2 /reduced graphene oxide films as electron transport layers. *Journal of Photonics for Energy*, *5*(1), 057408. https://doi.org/10.1117/1.jpe.5.057408

Morichi, S., Okahiro, Y., Komoda, Y., Inagaki, H., & Itami, H. (2008). Examination on the vertical normal strain observed at the grounds surface during earthquakes. *Doboku Gakkai Ronbunshuu A*, *64*(2), 452–457. https://doi.org/10.2208/jsceja.64.452

Mustereţ, C. P., & Teodosiu, C. (2007). Removal of persistent organic pollutants from textile wastewater by membrane processes. *Environmental Engineering and Management Journal*, *6*(3), 175–187. https://doi.org/10.30638/eemj.2007.022

N. G. Vinokurova, N. F. Zelenkova, B. P. Baskunov, and M. U. A. (2014). *Determination of Diketopiperazine Alkaloids of the Roquefortine Group by UV Spectroscopy, Thin-Layer Chromatography, and High-Performance Liquid Chromatography*. *January 2001*. https://doi.org/10.1023/A

Nabbou, N., Belhachemi, M., Boumelik, M., Merzougui, T., Lahcene, D., Harek, Y., Zorpas, A. A., & Jeguirim, M. (2019). Removal of fluoride from groundwater using natural clay (kaolinite): Optimization of adsorption conditions. *Comptes Rendus*

Chimie, *22*(2–3), 105–112. https://doi.org/10.1016/j.crci.2018.09.010

Naczk, M., Pink, J., Amarowicz, R., Pink, D., & Shahidi, F. (2001). *Multivariate Model for the Prediction of Soluble Condensed Tannins in Crude Extracts of Polyphenols from Canola and Rapeseed Hulls*. *April*. https://doi.org/10.1007/s11746-001-0276-1

Nassar, I., Osipova, V. V., Safiullin, G., Lobkov, V., & Galyametdinov, Y. (2011). Preparation of II-VI semiconductors nanoparticles and investigation of their photophysical properties. *International Journal of Green Nanotechnology: Biomedicine*, *3*(1), 22–36. https://doi.org/10.1080/19430892.2011.574509

Nazarpour, S., Hajian, R., & Sabzvari, M. H. (2020). A novel nanocomposite electrochemical sensor based on green synthesis of reduced graphene oxide/gold nanoparticles modified screen printed electrode for determination of tryptophan using response surface methodology approach. *Microchemical Journal*, *154*(January), 104634. https://doi.org/10.1016/j.microc.2020.104634

Neel, E. A. A., Aljabo, A., Strange, A., Ibrahim, S., Coathup, M., Young, A. M., Bozec, L., & Mudera, V. (2016). Demineralization–remineralization dynamics in teeth and bone. *International Journal of Nanomedicine*, *11*, 4743–4763. https://doi.org/10.2147/IJN.S107624

Nelson, K. G., & Higuchi, W. (1970). *Mechanism of Fluoride Uptake by Hydroxyapatite from Acidic Fluoride Solutions: Fig 2*, 1541–1548.

Nengjie Huo, Alberto Figueroba, Yujue Yang, Sotirios Christodoulou, Alexandros Stavrinadis, César Magén, G. K. (n.d.). *Engineering Vacancies in Bi2S3 yields sub-Bandgap Photoresponse and highly sensitive Short-Wave Infrared Photodetectors*.

Nyangiwe, N. N. (2012a). *GRAPHENE BASED NANO-COATINGS: SYNTHESIS AND PHYSICAL- CHEMICAL INVESTIGATIONS*.

Nyangiwe, N. N. (2012b). Synthesis and Physical- Chemical. *The Royal Society of Chemistry*.

NZEKEKWU, AK; ABOSEDE, O. (2019). *Green Synthesis and Characterization of Silver Nanoparticles Using Leaves Extracts of Neem (Azadirachta indica) and Bitter Leaf (Vernonia amygdalina)*. *23*(April), 695–699.

Oseni, L. A., Abugri, J., & Sumabe, B. K. (2014). *Leaf Extracts of Vernonia amygdalina Del . from Northern Ghana Contain Bioactive Agents that Inhibit the Growth of Some Beta-lactamase Producing Bacteria in vitro*. *July*. https://doi.org/10.9734/BJPR/2014/3200

Ouyang, D., Zhuo, Y., Hu, L., Zeng, Q., Hu, Y., & He, Z. (2019). Research on the

adsorption behavior of heavy metal ions by porous material prepared with silicate tailings. *Minerals*, *9*(5), 1–16. https://doi.org/10.3390/min9050291

Pachauri, N., Verma, S., Singh, P., & Singh, S. P. (2017). Few layered graphene oxide thin films: A potential matrix for immunosensors. *Integrated Ferroelectrics*, *184*(1), 85–91. https://doi.org/10.1080/10584587.2017.1368790

Pandurangan, P., Sahadeven, M., Sunkar, S., Krishna, S., & Mohana, N. (2018). *Comparative Analysis of Biochemical Compounds of Leaf, Flower and Fruit of Couroupita guianensis and Synthesis of Silver Nanoparticles*. *January*. https://doi.org/10.5530/pj.2018.2.55

Papageorgiou, D. G., Kinloch, I. A., & Young, R. J. (2017). Mechanical properties of graphene and graphene-based nanocomposites. *Progress in Materials Science*, *90*, 75–127. https://doi.org/10.1016/j.pmatsci.2017.07.004

Peccerillo, A., Donati, C., Santo, A. P., Orlando, A., Yirgu, G., & Ayalew, D. (2007). Petrogenesis of silicic peralkaline rocks in the Ethiopian rift: Geochemical evidence and volcanological implications. *Journal of African Earth Sciences*, *48*(2–3), 161–173. https://doi.org/10.1016/j.jafrearsci.2006.06.010

Pei, S., & Cheng, H. (2012). The reduction of graphene oxide The reduction of graphene oxide. *CARBON, October 2017*. https://doi.org/10.1016/j.carbon.2011.11.010

Pereira, L., & Alves, M. (2012). Dyes-environmental impact and remediation. *Environmental Protection Strategies for Sustainable Development*, 111–162. https://doi.org/10.1007/978-94-007-1591-2_4

Peres, M. A., & Cury, J. A. (2011). Drinking water quality and fl uoride concentration. *Rev Saúde Pública*, *45*(5).

Perreault, F., Faria, A. F. De, & Elimelech, M. (2015). Environmental applications of graphene-based nanomaterials. *The Royal Society of Chemistry*. https://doi.org/10.1039/c5cs00021a

Perreault, F., Fonseca De Faria, A., & Elimelech, M. (2015). Environmental applications of graphene-based nanomaterials. *Chemical Society Reviews*, *44*(16), 5861–5896. https://doi.org/10.1039/c5cs00021a

Petersen, R. (2015). Study of the π and π ∗ Electronic Bands in Graphene. *Thesis*.

Pietronero, L. (1980). *Electrical conductivity of a graphite layer*. *July*. https://doi.org/10.1103/PhysRevB.22.904

Pinto, J. (2020). Membrane Science & Technology Carbon Nanotubes Membrane for Water Filtration. *J Membr Sci Technol*, *10*(204), 1–2. https://doi.org/10.35248/2155-

9589.2020.10.204

Piras, R., Aresti, M., Saba, M., Marongiu, D., Mula, G., Quochi, F., Mura, A., Cannas, C., Mureddu, M., Ardu, A., Ennas, G., Calzia, V., Mattoni, A., Musinu, A., & Bongiovanni, G. (2014). Colloidal synthesis and characterization of Bi2S3 nanoparticles for photovoltaic applications. *Journal of Physics: Conference Series*, *566*(1). https://doi.org/10.1088/1742-6596/566/1/012017

Pratap, D., & Singh, D. (2013). IMPACT OF FLUORIDE ON ENVIRONMENT & HUMAN. *INTERNATIONAL JOURNAL OF SCIENCE, SPIRITUALITY, BUSINESS AND TECHNOLOGY*, *1*(2), 56–61.

Premathilaka, R. W., & Liyanagedera, N. D. (2019). Fluoride in drinking water and nanotechnological approaches for eliminating excess fluoride. *Journal of Nanotechnology*, *2019*. https://doi.org/10.1155/2019/2192383

Publishing, I. W. A., & Supply, W. (2020). Rapid de fl uoridation of drinking water by calcium carbonate nanoadsorbent : characterization , adsorption studies and application to real samples ' treatment Masooma Zawar , Rabia Nazir , Almas Hamid , Eder C . Lima. *Water Supply*, *20*(2), 667–678. https://doi.org/10.2166/ws.2019.196

Q Xiang, Y Liang, L Chen, C Wang, B Chen, X Chen, M. Z. (2003). Effect of fluoride in drinking water on children's intelligence. *Fluoride*, *36*(2), 84–94.

Raphael Mmaduka Obodo, I. A. and F. I. E. (n.d.). *Graphene and Its Applications*.

Rashid, M. H. O., & Ralph, S. F. (2017). Carbon nanotube membranes: Synthesis, properties, and future filtration applications. *Nanomaterials*, *7*(5), 1298–1299. https://doi.org/10.3390/nano7050099

Rawal, N., Solanki, S., & Shah, D. (2020). Green synthesis of reduced graphene oxide with in situ decoration of metal nanoparticles for charge storage application. *Materials Today: Proceedings*, *21*, 2066–2071. https://doi.org/10.1016/j.matpr.2020.01.325

Reeves, C. (2010). Graphene : Characterization After Mechanical Exfoliation. *Royal Society of Chemistry*, 1–23.

Rojas-Mayorga, C. K., Bonilla-Petriciolet, A., Aguayo-Villarreal, I. A., Hernández-Montoya, V., Moreno-Virgen, M. R., Tovar-Gómez, R., & Montes-Morán, M. A. (2013). Optimization of pyrolysis conditions and adsorption properties of bone char for fluoride removal from water. *Journal of Analytical and Applied Pyrolysis*, *104*, 10–18. https://doi.org/10.1016/j.jaap.2013.09.018

Romero, A., Lavin-lopez, M. P., Sanchez-silva, L., Valverde, J. L., & Paton-carrero, A.

(2018). Comparative study of different scalable routes to synthesize graphene oxide and reduced graphene oxide. *Materials Chemistry and Physics*, *203*, 284–292. https://doi.org/10.1016/j.matchemphys.2017.10.013

Sadurní, E., Rivera-Mociños, E., & Rosado, A. (2015). Discrete symmetry in graphene: The Dirac equation and beyond. *Revista Mexicana de Fisica*, *61*(3), 170–181.

Sahu, N., Bhan, C., & Singh, J. (2021). Removal of fluoride from an aqueous solution by batch and column process using activated carbon derived from iron infused. *Environ. Eng. Res.*, *26*(4), 0–3. https://doi.org/10.4491/eer.2020.241

Saini, R. D. (2017). Textile Organic Dyes: Polluting effects and Elimination Methods from Textile Waste Water. *International Journal of Chemical Engineering Research*, *9*(1), 975–6442. http://www.ripublication.com

Sandhya, S. (2010). *Biodegradation of Azo Dyes Under Anaerobic Condition: Role of Azoreductase* (Issue January 1970). https://doi.org/10.1007/698_2009_43

Sara Datturi, Assefa Kumsa, Seifu Kebede, F. van S. and M. van B. (2017). The Right to Smile: Fluoride and Fluorosis in Central Rift Valley (Ethiopia). *Groundwater Magazine*, *January*.

Saththasivam, J., Yiming, W., Wang, K., Jin, J., & Liu, Z. (2018). A Novel Architecture for Carbon Nanotube Membranes towards Fast and Efficient Oil/water Separation. *Scientific Reports*, *8*(1), 4–9. https://doi.org/10.1038/s41598-018-25788-9

Sciences, B. (2015). *AND POLYPYRROLE-REDUCED GRAPHENE OXIDE COMPOSITE FILMS AS A POTENTIAL Md Mominul Haque*. *November*.

Seah, C. M., Chai, S. P., & Mohamed, A. R. (2014). Mechanisms of graphene growth by chemical vapour deposition on transition metals. *Carbon*, *70*(November 2017), 1–21. https://doi.org/10.1016/j.carbon.2013.12.073

Seekaew, Y., Arayawut, O., & Timsorn, K. (2019). Applications of Graphene and Derivatives. In *Carbon-Based Nanofillers and Their Rubber Nanocomposites*. Elsevier Inc. https://doi.org/10.1016/B978-0-12-813248-7.00009-2

Seo, H. I., Cheon, Y. A., & Chung, B. G. (2016). Graphene and thermo-responsive polymeric nanocomposites for therapeutic applications. *Biomedical Engineering Letters*, *6*(1), 10–15. https://doi.org/10.1007/s13534-016-0214-6

Shabalin, I. L. (2014). Ultra-high temperature materials I: Carbon (graphene/graphite) and refractory metals. *Ultra-High Temperature Materials I: Carbon (Graphene/Graphite) and Refractory Metals*, *9789400775*(June), 1–794. https://doi.org/10.1007/978-94-007-7587-9

Sharma, S., & Khare, N. (2017). Synthesis of bismuth sulfide nanostructures for photodegradation of organic dye. *AIP Conference Proceedings*, *1832*(July 2018), 1–5. https://doi.org/10.1063/1.4980297

Simandl, G. J., Paradis, S., & Akam, C. (2015). Graphite deposit types , their origin , and economic significance. *British Columbia Geological Survey Paper*, *3*(Symposium on Strategic and Critical Materials Proceedings), 163–171.

Singh, K., & Arora, S. (2011). Removal of synthetic textile dyes from wastewaters: A critical review on present treatment technologies. *Critical Reviews in Environmental Science and Technology*, *41*(9), 807–878. https://doi.org/10.1080/10643380903218376

Singh, N., Siwatch, P., Kaushal, J., Sharma, J., & Tripathi, S. K. (2020). One-step green synthesis of reduced graphene oxide by electrochemical etching of carbon rods and effect of different bias voltages on the quality. *Journal of Solid State Chemistry*, *291*, 121537. https://doi.org/10.1016/j.jssc.2020.121537

Speranza, G. (2019). The Role of Functionalization in the Applications of Carbon Materials: An Overview. *C — Journal of Carbon Research*, *5*(4), 84. https://doi.org/10.3390/c5040084

Stavila, V., Whitmire, K. H., & Rusakova, I. (2009). Supporting Information: Synthesis of Bi 2 S 3 Nanostructures from Bismuth (III) Thiourea and Thiosemicarbazide Complexes. *Chemistry of Materials*, *21*(22), 1–10.

Suggs, J. A., & Neic, E. P. A. (2010). ENVIRONMENTAL CRIME. *16th International Forensic Science Symposium*.

Sun, J., Chen, Y., Cai, X., Ma, B., Chen, Z., Priydarshi, M. K., Chen, K., Gao, T., Song, X., Ji, Q., Guo, X., Zou, D., Zhang, Y., & Liu, Z. (2015). Direct low-temperature synthesis of graphene on various glasses by plasma-enhanced chemical vapor deposition for versatile, cost-effective electrodes. *Nano Research*, *8*(11), 3496–3504. https://doi.org/10.1007/s12274-015-0849-0

Sun, Y., Zhou, S., Chiang, P.-C., & Shah, K. J. (2019). Evaluation and optimization of enhanced coagulation process: Water and energy nexus. *Water-Energy Nexus*, *2*(1), 25–36. https://doi.org/10.1016/j.wen.2020.01.001

Sur, U. K., Saha, A., Datta, A., Ankamwar, B., Surti, F., Roy, S. D., & Roy, D. (2016). Synthesis and characterization of stable aqueous dispersions of graphene. *Bulletin of Materials Science*, *39*(1), 159–165. https://doi.org/10.1007/s12034-015-0893-0

susan n. J. martel, Cay Butler, tamara daWson. (2006). Fluoride in Drinking Water: A

Scientific Review of EPA's Standards. In *National Academy of Sciences* (p. 530). https://doi.org/10.17226/11571

Tan, T. L., Krusnamurthy, P. A. P., & Abdul, S. (2020). Adsorptive, kinetics and regeneration studies of fluoride removal from water using zirconium-based metal organic frameworks. *RSC Adv*, *10*, 18740–18752. https://doi.org/10.1039/d0ra01268h

Tefera, N., Mulualem, Y., & Fito, J. (2020). Adsorption of Fluoride from Aqueous Solution and Groundwater onto Activated Carbon of Avocado Seeds. *Water Conserv Sci Eng*. https://doi.org/10.1007/s41101-020-00093-7

Thakur, A., Kumar, S., & Rangra, V. S. (2015). Synthesis of reduced graphene oxide (rGO) via chemical reduction. *AIP Conference Proceedings*, *1661*(June). https://doi.org/10.1063/1.4915423

Thole, B. (2011). Defluoridation kinetics of 200 °c calcined bauxite, gypsum, and magnesite and breakthrough characteristics of their composite filter. *Journal of Fluorine Chemistry*, *132*(8), 529–535. https://doi.org/10.1016/j.jfluchem.2011.05.016

Thole, B. (2013). Ground Water Contamination with Fluoride and Potential Fluoride Removal Technologies for East and Southern Africa. In *Perspectives in Water Pollution fluorosis*. https://doi.org/10.5772/54985

Tian, W., Li, W., Yu, W., & Liu, X. (2017). A Review on Lattice Defects in Graphene : Types , Generation , Effects and Regulation. *Micromachines*. https://doi.org/10.3390/mi8050163

Torrisi, F., Hasan, T., Wu, W., Sun, Z., Lombardo, A., Kulmala, T. S., Hsieh, G. W., Jung, S., Bonaccorso, F., Paul, P. J., Chu, D., & Ferrari, A. C. (2012). Inkjet-printed graphene electronics. *ACS Nano*, *6*(4), 2992–3006. https://doi.org/10.1021/nn2044609

Trammell, M. P., & Pappano, P. J. (2011). *Analysis of Natural Graphite , Synthetic Graphite , and Thermosetting Resin Candidates for Use in Fuel Compact Matrix*. 1–66.

Tyagi, A., Tyagi, A., Mir, Z. A., & Ali, S. (2020). *Nano-materials for Wastewater Treatment*. 47–67.

Vajtai, R. (2013). Springer handbook of nanomaterials. In *Springer Handbook of Nanomaterials*. https://doi.org/10.1007/978-3-642-20595-8

Varghese, S. S., Varghese, S. H., Swaminathan, S., Singh, K. K., & Mittal, V. (2015). Two-Dimensional Materials for Sensing: Graphene and Beyond. *Electronics*, 651–687. https://doi.org/10.3390/electronics4030651

Veligura, A. (2007a). Graphene: relativistic physics in 2D. *Nanoscience, June*.

Veligura, A. (2007b). *Graphene: relativistic physics in 2D. June*.

Verma, S., & Kim, K.-H. (2022). Graphene-based materials for the adsorptive removal of uranium in aqueous solutions. *Environment International*, *158*, 106944. https://doi.org/10.1016/j.envint.2021.106944

Vinet, L., & Zhedanov, A. (2011). A "missing" family of classical orthogonal polynomials. *Journal of Physics A: Mathematical and Theoretical*, *44*(8), 61. https://doi.org/10.1088/1751-8113/44/8/085201

Vorrada, L., Krit, T., Passakorn, E., Wanchai, B., & Achanai, B. (2013). Preparation and Characterization of Reduced Graphene Oxide Sheets via Water-Based Exfoliation and Reduction Methods. *Advances in Materials Science and Engineering*, *2013*, 1–5.

Walker, D. G., Shaw, W. H. R., & Walker, D. G. (1956). *The Decomposition of Thiourea in Water Solutions*. *105*(1), 1954–1957. https://doi.org/10.1021/ja01603a014

Wang, G., Gao, Z., Wan, G., Lin, S., Yang, P., & Qin, Y. (2014). High densities of magnetic nanoparticles supported on graphene fabricated by atomic layer deposition and their use as efficient synergistic microwave absorbers. *Nano Research*, *7*(5), 704–716. https://doi.org/10.1007/s12274-014-0432-0

Wang, H., Zhu, J. J., Zhu, J. M., & Chen, H. Y. (2002). Sonochemical method for the preparation of bismuth sulfide nanorods. *Journal of Physical Chemistry B*, *106*(15), 3848–3854. https://doi.org/10.1021/jp0135003

Wang, Q., Tian, S., & Ning, P. (2014). *Degradation Mechanism of Methylene Blue in a Heterogeneous Fenton-like Reaction Catalyzed by Ferrocene.*

Wu, Q., Miao, W. S., Zhang, Y. Du, Gao, H. J., & Hui, D. (2020). Mechanical properties of nanomaterials: A review. *Nanotechnology Reviews*, *9*(1), 259–273. https://doi.org/10.1515/ntrev-2020-0021

Wu, T., Zhou, X., Zhang, H., & Zhong, X. (2010). Bi2S3 nanostructures: A new photocatalyst. *Nano Research*, *3*(5), 379–386. https://doi.org/10.1007/s12274-010-1042-0

Wu, X., Mu, F., Wang, Y., & Zhao, H. (2018). Graphene and graphene-based nanomaterials for DNA detection: A review. *Molecules*, *23*(8). https://doi.org/10.3390/molecules23082050

Xu, N., Li, S., Li, W., & Liu, Z. (2020). Removal of Fluoride by Graphene Oxide / Alumina Nanocomposite : Adsorbent Preparation , Characterization , Adsorption Performance and Mechanisms. *ChemistrySelect*, *5*, 1818–1828.

https://doi.org/10.1002/slct.201904867

Y. TRAVI, T. C. (1998). *FLUORIDE CONTAMINATION IN THE LAKES REGION OF THE ETHIOPIAN RIFT: Origin, mechanism and evolution*.

Yan, J. A., & Chou, M. Y. (2010). Oxidation functional groups on graphene: Structural and electronic properties. *Physical Review B - Condensed Matter and Materials Physics*, *82*(12). https://doi.org/10.1103/PhysRevB.82.125403

Yan, L., Zheng, Y. B., Zhao, F., Li, S., Gao, X., Xu, B., Weiss, P. S., & Zhao, Y. (2012). Chemistry and physics of a single atomic layer: Strategies and challenges for functionalization of graphene and graphene-based materials. *Chemical Society Reviews*, *41*(1), 97–114. https://doi.org/10.1039/c1cs15193b

Yang, K., Chen, B., & Zhu, L. (2015). Graphene-coated materials using silica particles as a framework for highly efficient removal of aromatic pollutants in water. In *Nature Publishing Group*. Nature Publishing Group. https://doi.org/10.1038/srep11641

Yao, M., Tijing, L. D., Naidu, G., Kim, S. H., Matsuyama, H., Fane, A. G., & Shon, H. K. (2020). A review of membrane wettability for the treatment of saline water deploying membrane distillation. *Desalination*, *479*(October 2019), 114312. https://doi.org/10.1016/j.desal.2020.114312

Yazdi, G. R., Iakimov, T., & Yakimova, R. (2016). Epitaxial graphene on SiC: A review of growth and characterization. *Crystals*, *6*(5). https://doi.org/10.3390/cryst6050053

Yenny Hernandez, Mustafa Lotya, Valeria Nicolosi, Fiona M Blighe Sukanta De, G., & Duesberg, and J. N. C. (2009). Liquid phase production of graphene by exfoliation of graphite in surfactant/water solutions Yenny. *American Chemical Society*. https://doi.org/10.1021/ja807449u

Yildirim, O. A., & Ozturk, T. (2018). Graphene-Semiconductor Composites as Visible Light-Induced Photocatalyst. *Visible-Light Photocatalysis of Carbon-Based Materials*. https://doi.org/10.5772/intechopen.70709

Yu, X. Z., Hwang, C. G., Jozwiak, C. M., Köhl, A., Schmid, A. K., & Lanzara, A. (2011). New synthesis method for the growth of epitaxial graphene. *Journal of Electron Spectroscopy and Related Phenomena*, *184*(3–6), 100–106. https://doi.org/10.1016/j.elspec.2010.12.034

Yuan, C., Li, Y., Li, Q., Jin, R., & Ren, L. (2018). *Purification of Tea saponins and Evaluation of its Effect on Alcohol Dehydrogenase Activity*. 56–63.

Yuan, X., Wu, X., Feng, Z., Jia, W., Zheng, X., & Li, C. (2019). Facile Synthesis of Heterojunctioned ZnO/Bi2S3 Nanocomposites for Enhanced Photocatalytic

Reduction of Aqueous Cr(VI) under Visible-Light Irradiation. *Catalysts*, *9*(7), 624. https://doi.org/10.3390/catal9070624

Zainuddin, M. F., Nik Raikhan, N. H., Othman, N. H., & Abdullah, W. F. H. (2018). Synthesis of reduced Graphene Oxide (rGO) using different treatments of Graphene Oxide (GO). *IOP Conference Series: Materials Science and Engineering*, *358*(1), 0–6. https://doi.org/10.1088/1757-899X/358/1/012046

Zazouli, M. A., Belarak, D., Karimnezhad, F., & Khosravi, F. (2014). Removal of Fluoride from Aqueous Solution by Using of Adsorption onto Modified Lemna Minor: Adsorption Isotherm and Kinetics Study. *Journal of Mazandaran University of Medical Sciences*, *24*(109), 195–204.

Zazouli, M. A., Mahvi, A. H., Dobaradaran, S., Barafrashtehpour, M., Mahdavi, Y., & Balarak, D. (2014a). ADSORPTION OF FLUORIDE FROM AQUEOUS SOLUTION BY EUCALYPTUS BARK ACTIVATED CARBON: THERMODYNAMIC ANALYSIS. *Fluoride*, *47*(4), 349–358.

Zazouli, M. A., Mahvi, A. H., Dobaradaran, S., Barafrashtehpour, M., Mahdavi, Y., & Balarak, D. (2014b). Adsorption of fluoride from aqueous solution by modified Azolla filiculoides. *Fluoride*, *47*(4), 349–358.

Zazouli, M. A., Mahvi, A. H., Mahdavi, Y., & Balarak, D. (2015). Isothermic and kinetic modeling of fluoride removal from water by means of the natural biosorbents sorghum and canola. *Fluoride*, *48*(1), 37–44.

Zhang, B., Tian, Y., Jin, X., Lo, T. Y., & Cui, H. (2018). Thermal and mechanical properties of expanded graphite/paraffin gypsum-based composite material reinforced by carbon fiber. *Materials*, *11*(11). https://doi.org/10.3390/ma11112205

Zhang, L., Li, N., Jiu, H., & Zhang, Q. (2015). *Solvothermal synthesis of reduced graphene oxide-Bi 2 S 3 nanorod composites with enhanced photocatalytic activity under visible light irradiation*. https://doi.org/10.1007/s10854-015-4086-9

Zhang, R. Q., & De, A. (2011). Theoretical Studies on Formation, Property Tuning and Adsorption of Graphene Segments. *Physics and Applications of Graphene - Theory*, *March*, 2–28. https://doi.org/10.5772/15896

Zhang, Z., Zhou, C., Huang, L., Wang, X., Qu, Y., Lai, Y., & Li, J. (2013). Synthesis of bismuth sulfide/reduced graphene oxide composites and their electrochemical properties for lithium ion batteries. *Electrochimica Acta*, *114*, 88–94. https://doi.org/10.1016/j.electacta.2013.09.174

Zhao, D., Wang, W., Zong, W., Xiong, S., Zhang, Q., Ji, F., & Xu, X. (2017). Synthesis of

Bi2 S3 /BiVO4 heterojunction with a one-step hydrothermal method based on pH control and the evaluation of visible-light photocatalytic performance. *Materials*, *10*(8), 1–15. https://doi.org/10.3390/ma10080891

Zhen, Z., & Zhu, H. (2018). Structure and Properties of Graphene. In *Graphene*. Elsevier Inc. https://doi.org/10.1016/B978-0-12-812651-6.00001-X

Zhu, G., & Liu, P. (2009). Low-temperature urea-assisted hydrothermal synthesis of Bi 2S3 nanostructures with different morphologies. *Crystal Research and Technology*, *44*(7), 713–720. https://doi.org/10.1002/crat.200900137

Zou, H., Rowe, D. M., & Williams, S. G. K. (2002). Peltier effect in a co-evaporated Sb2Te3(P)-Bi2Te3(N) thin film thermocouple. *Thin Solid Films*, *408*(1–2), 270–274. https://doi.org/10.1016/S0040-6090(02)00077-9

Indexes

Effects pH on the adsorption process (NaF complex solution, Real Sample)

pH	Initial Conc. (mg/L)	Final Conc. (mg/L)	Removal %
3	10	1.3	87
5	10	1.7	83
6.8	10	0.07	99.3
7	10	0.84	91.6
9	10	2.2	78
11	10	2.9	71

pH	Initial Conc. (mg/L)	Final Conc. (mg/L)	Removal %
3	10	2.2	78
5	10	1.9	81
6.8	10	0.84	91.6
7	10	1.77	82.3
8.5	10	2.2	90.2
11	10	2.9	71

Effects of initial concentration

q_t	0	0.4	0.6	0.8	0.9	0.95	1	1.05	1.1
F^- Con.	0	5	10	15	20	25	30	35	40

Effects of contact time

Contact time (min)	Initial Con. (mg/L)	Final Con. (mg/L)	Removal (%)
50	10	2.2	78
70	10	1.25	87.5
90	10	0.2	98
110	10	0.25	97.5
130	10	0.2	94
150	10	0.2	90.9

Effects of Adsorbent dosage

Adsorbent Dosage	Initial Con. (mg/L)	Final Con. (mg/L)	Removal (%)
0.10	10	1.4	86
0.20	10	1.0	90
0.30	10	0.7	93
0.40	10	0.5	95
0.42	10	0.3	97
0.50	10	0.4	96
0.60	10	0.3	96.5
0.70	10	0.3	96
0.80	10	0.3	95

Recyclability study (Adsorption)

Cycle	% removal
1	99
2	99
3	98.5
4	99
5	99
6	99

Recyclability study (Photocatalyst)

Cycle	% removal
1	99
2	99
3	98.5
4	98.5
5	98.5

Degradation of MB With/without catalyst

Time	% degradation with	% degradation without
0	0	0
5	84	3.5
10	86	4
15	95	5.6
20	97	7
25	99	5
30	99	5

Desorption

HCl con. (M)	% removal
0.01	65
0.03	85
0.05	95
0.07	80
0.09	75
0.11	65
0.13	55

Publications

Published and on Publication out of this dissertation:

1. A Novel and simplest green synthesis method of reduced graphene oxide using methanol extracted vernonia amygdalina: Large scale production

***Bayisa Meka Chufa**, Bedasa Abdisa Gonfa, Teketel Yohannes Anshebo, Getachew Adam Workneh*

J. Adv. Cond. Physic., 2021

Published

2. Enhanced Photocatalytic Activity of Reduced Graphene Oxide/Bismuth Sulfide Nanostructure Composites for the Degradation of Methylene Blue: Environmental protection

***Bayisa Meka Chufa**, Bedasa Abdisa Gonfa, Teketel Yohannes Anshebo*

J. Adv. Nano Tech., 2021

Published

3. Carbon nanotubes: a review on green synthesis, growth mechanism and application as a membrane filter for fluoride remediation

***Bayisa Meka Chufa**, H. C. Ananda Murthy, Bedasa Abdisa Gonfa & Teketel Yohannes Anshebo*

Green Chemistry Letters and Reviews, 2021

Published

4. Graphene Oxide Nanoadsorbent for the Removal of Fluoride Ion from Ground Water: Adsorbent performance and adsorption Mechanism

***Bayisa Meka Chufa**, Bedasa Abdisa Gonfa, Teketel Yohannes Anshebo*

Journal of Nanotechnology, 2021

Accepted

5. The Investigation to Determine Effect of Solvents in Extraction of Vernonia Amygdalina for the Green Synthesis of Reduced Graphene Oxide Nanomaterials

***Bayisa Meka Chufa**, Bedasa Abdisa Gonfa, Teketel Yohannes Anshebo*

J. Adv. Natur. Scie., 2021

Under Review

Total publication

1. Effect on Poly (C6H5NH2) Emeraldine Salt by FeCl3 and KMnO4 as Secondary Dopants

*Kedir Mamma, Kalid Siraj, **Nathan Meka***

American Journal of Polymer Science & Engineering 1 (1), 1-13, 2014

2. Kinetic, equilibrium and thermodynamic study of 2-chlorophenol adsorption onto Ricinus communis pericarp activated carbon from aqueous solutions

*Birtukan Adane, Kalid Siraj, **Nathan Meka***

Green Chemistry Letters and Reviews 8 (3-4), 1-12, 2014

3. Synthesis and effect of secondary dopant on the conductivity of conducting polymer polyaniline

*Kadir Mamma, Kalid Siraj, **Nathan Meka***

Journal of Polymer Engineering 33 (9), 785-792, 2013

4. Electron Donor-Acceptor Interaction of 8-Hydroxyquinoline with Citric Acid in Different Solvents: Spectroscopic Studies

*Demelash Jado, Kalid Siraj, **Nathan Meka***

Journal of Applied Chemistry 2014

5. Determination of Concentration Level of Tin (II) in Canned Juice Vended in Local Shop in Jimma Town using Cyclic Voltametry

***Meka Nathan**, Tesfaye Tilehun, Kalid Siraj*

An International Journal of Life Sciences and Chemistry 31 (1), 138-145, 2012

6. Quantitative Determination of Ascorbic Acid in Orange Collected from Kochi Local Market by Using Cyclic Voltammetry

***Nathan Meka**, Tsehaynew Kasaw*

An International Journal of Life Sciences and Chemistry 31 (1), 325-332, 2013

7. Electrochemical Determination of Effects of Difference in Concentration between Enamel Crown's Buccal Side and Tooth Root and the Role of Fluoride Ion

***Meka Nathan**, Kalid Siraj*

World Journal of Analytical Chemistry 1 (4), 63-68, 2009

8. The Study of the Electrochemical Deterioration of Human Teeth in Oral Cavity and the Role of Saliva

***Meka Nathan**, Sergawie Assefa, Kalid Siraj*

International Journal of Biological and Physical Sciences 1 (3), 45-50, 2008

9. Effect of reinforcement of reduced graphene oxide on Mechanical Properties of Concrete nanocomposite

***Bayisa Meka Chufa**, H. C. Ananda Murthy*

J. Mater. Environ. Sci., 2020, Volume 11, Issue 6, Page 844-855

10. A Novel and simplest green synthesis method of reduced graphene oxide using methanol extracted vernonia amygdalina: Large scale production

***Bayisa Meka Chufa**, Bedasa Abdisa Gonfa, Teketel Yohannes Anshebo, Getachew Adam Workneh*

J. Adv. Cond. Physic., 2021

11. Enhanced Photocatalytic Activity of Reduced Graphene Oxide/Bismuth Sulfide Nanostructure Composites for the Degradation of Methylene Blue: Environmental protection

***Bayisa Meka Chufa**, Bedasa Abdisa Gonfa, Teketel Yohannes Anshebo*

J. Adv. Nano Tech., 2021

12. Carbon nanotubes: a review on green synthesis, growth mechanism and application as a membrane filter for fluoride remediation

***Bayisa Meka Chufa**, H. C. Ananda Murthy, Bedasa Abdisa Gonfa & Teketel Yohannes Anshebo*

Green Chemistry Letters and Reviews, 2021

13. Graphene Oxide Nanoadsorbent for the Removal of Fluoride Ion from Ground Water: Adsorbent performance and adsorption Mechanism

***Bayisa Meka Chufa**, Bedasa Abdisa Gonfa, Teketel Yohannes Anshebo*

Journal of Nanotechnology, 2021

14. The Investigation to Determine Effect of Solvents in Extraction of Vernonia Amygdalina for the Green Synthesis of Reduced Graphene Oxide Nanomaterials

***Bayisa Meka Chufa**, Bedasa Abdisa Gonfa, Teketel Yohannes Anshebo*

J. Adv. Natur. Scie., 2021-Accepted